

**Multifunctional and Stimuli-Responsive Polymersomes
for Biomedical Applications**

DISSERTATION

zur Erlangung des akademischen Grades

Doctor rerum naturalium

(Dr.rer.nat.)

vorgelegt

der Fakultät Mathematik und Naturwissenschaften

der Technischen Universität Dresden

von

M.Sc. Banu Iyisan

geboren am 23.03.1985 in Adana, Türkei

Eingereicht am 23.08.2016

Die Dissertation wurde in der Zeit von September 2012 bis August 2016

im Leibniz-Institut für Polymerforschung Dresden e.V. angefertigt

Gutachter : **Prof. Dr. Brigitte Voit**
Technische Universität Dresden / Leibniz
Institut für Polymerforschung Dresden e.V.

Prof. Dr. Rainer Haag
Freie Universität Berlin

Tag der Verteidigung: 18.11.2016

To my beloved family

Acknowledgements

Every big journey in life requires lots of working time and patience as likely the realization of this thesis. But most importantly, none of these efforts would have been sufficient for the success without the support of many people. As I have come to the end of this big step in my life, I would like to express my deep appreciation and thanks to all people helped me not only for a better science but also for good and happy days in Germany.

First of all, I would like to express my sincere gratitude to my supervisor Prof. Dr. Brigitte Voit for giving me the opportunity to work in this very interesting and fascinating research field, “Polymersomes” during my PhD at IPF. I deeply appreciate her continuous support and guidance which helped me a lot to make this research more productive and innovative. She has been also a great example for me by being a very successful woman scientist and a professor in chemistry world. This indeed has motivated me not only for my PhD experience but also this is a big inspiration for the future steps of my research life. Besides, I would like to extend my deep appreciation to my co-supervisor Dr. Dietmar Appelhans for his support, guidance and encouragement in every stage of this work. I am also greatly thankful to him for the fruitful discussions we have made at any time I needed. I have learnt a lot from those insightful comments and ideas that motivated me to think and question more which in turn led to improve the quality of this research significantly.

Regarding the funding of this thesis, I would like to thank DFG and IPF for their great support not only granting my PhD scholarship but also enabling me to participate several worldwide conferences. In addition, my acknowledgements also go to the International Helmholtz Research School for Nanoelectronic Networks (IHRS NANONET) for a comprehensive training in the field of nanotechnology and for giving me the opportunity to participate different soft skill courses and workshops. In particular, I want to thank PD. Dr. Artur Erbe and PD. Dr. Peter Zahn for their help in many organizational works. In this manner, I am thankful to all colleagues in IHRS NANONET for various discussions and social activities that we have done together.

Furthermore, it is my great pleasure to thank Prof. Dr. Lukas Eng and Dr. Philipp Reichenbach from IAPP in TU Dresden for the fruitful collaboration in the scope of the SPP 1327 DFG Project. The efforts of Dr. Reichenbach on the laser irradiation experiments and further imaging with Fluorescence Microscope add another perspective to this work.

Besides, this interdisciplinary environment helped me to get new and exciting insights about the laser technology and photophysics which I am very much appreciated.

I also owe a deep thank to many people in IPF who supported me for various characterization techniques. It is therefore my pleasure to thank department of Analytics, in particular Dr. Hartmut Komber, Andreas Korwitz (both NMR); Petra Treppe, Christina Harnisch (both SEC); Dr. Mikhail Malanin (IR) and Liane Häussler (DSC). My further special thanks go to Dr. Peter Formanek (cryo-TEM) and Andreas Janke (AFM) for making my tiny polymersomes visible which helped me a lot to maintain a proper flow in my work. By their warm support and guidance, I have the opportunity to meet with the fascinating world of microscopy and I am very much appreciated for this. Another special thanks goes to Anja Caspari for introducing me the use of DLS which is undoubtedly my almost everyday tool for characterizing my polymersomes. I would like to thank also Stefan Michel for introducing me the contact angle device so that I could conduct many measurements on my coated surfaces.

In addition, I would like thank all my colleagues in the department of bioactive and responsive polymers as well as polymer structures for the pleasant working atmosphere. My special thanks goes to also Carmen Krause for her support and help in various administrative works related to IPF. I feel myself very lucky that I was surrounded so many kind and nice people whom I've worked with, had fun with and got help whenever I needed. Many thanks to Gözde Öktem, Sandra Tripp, Mohamed Yassin, Ulrike Georgi, Jörg Kluge, Bahar Baghaei, Jens Gaitzsch, Hannes Gumz, Mimi Hetti, Xiaoling Liu, Emrah Demir, Francesco Piana, Maria Riedel, Christin Striegler, Robert Pöttsch, Shruti Pattanaik, Sourav Chakraborty, Johannes Fingernagel, Christiane Effenberg, Burak Kutlu, Haiping Zhang, Monika Warena, David Gräfe, Anna Bauer, Qiang Wei and Bettina Mamitzsch. I want to say so many words for each of you but the long pages of thanksgiving avoided me to continue. In this manner, I want to particularly thank to Ulrike for her great support in the beginning of my life in Germany. Her kindness and patience towards all my questions related to everyday life and IPF environment make my start in a new country very easier. Also, thanks to Sandra for her friendship and so many fun activities that we have done together. She has been also very supportive to me for a smooth start in Dresden. Therefore, thanks for all the nice places I have learned from you and thanks for all your support. And Gözde, my coffee addicted friend like myself, our long talks with hard black coffees would have never been forgettable. Thank you for your great, endless friendship and support in all manners.

And many thanks to Mohamed for being a great lab mate and a friend to me. His huge support for a smooth start in our lab was very worthy to me. In this manner, thanks to him and also to Jens, Jörg and Hannes for many fruitful polymersome discussions and various helps which improved this work a lot.

Moreover, I am grateful to my friends in Turkey as being my second family. Many thanks to Şefik Elbeyli, Selin Erkişi, Ceren Meriç, Özge Uğur, Handan Bakalcı, Burcu Atalay, Deniz Kimya and many others that I could not name now, for their endless friendship and emotional support during this work.

Last but not least, I wish to express my special thanks to my family for their immeasurable love, encouragement and support throughout this work and my life in general. In particular, I am grateful to my sister, Burcu Iyisan-Ocakçı and my brother in law, Hasan Ocakçı for being with me whenever I needed. Special thanks go to my sweet niece, Nehir and my sweet nephew, Güney for making me always cheerful and happy even after long working hours during our skype talks. I also want to express my deepest love and thanks to my husband, Umut Karagüzel for sharing all aspects of life with me by being my forever love and best friend ever. There are no words that can truly describe his unconditional support and help in overcoming various difficulties during this work. I can just say thank you so much Umut for always being there for me. I would like to extend my heartfelt thanks to my dear parents Halide-Nihat Iyisan for always supporting me and believing in me. Thank you so much for raising me with a strong passion of learning and leading me to follow always wisdom and reasoning in life. I know that I could have never finalized this work without your endless support and love. You make me who I am and I can just say thank you for everything.

Abstract

The demand for multifunctional nanocontainers possessing both recognition ability and responsive nature is increasing greatly because of their high potential in various biomedical applications. The engineering of such smart nanovesicles is useful to enhance the efficiency of many therapeutic and diagnostic tools that have the applicability in targeted drug delivery systems as well as designing sensing devices or conducting selective reactions as nanoreactors in the scope of nanobiotechnology. For this purpose, this study demonstrates the formation of multifunctional and stimuli-responsive polymersomes comprising various abilities including pH and light sensitivity as well as many reactive groups with sufficient accessibility to be used as smart and recognitive nanocontainers.

The fabrication included several steps starting from the synthesis of azide and adamantane terminated block copolymers, which were then self-assembled to prepare the polymersomes with the corresponding functional groups for the subsequent post-conjugations at the vesicle periphery. The accessible and sufficiently reactive groups were quantitatively proven when UV and IR cleavable NVOC protected amino groups as well as β -cyclodextrin molecules were conjugated to the pre-formed polymersomes through click chemistry and strong host-guest complexations. The gained light responsivity with the aid of successful NVOC attachment enabled further selective photochemical reactions triggered either by UV or harmless NIR light leading to liberated amine groups on the polymersome surface. Therein, these released amino groups were further conjugated with a model fluorescent compound as mimicking the attachment of biorecognition elements to see the direct picture of the applicability. To realize this concept in a more localized and selective way as well as to avoid the possible side effects of UV light, the NIR-light induced photochemical reactions and further dye coupling were performed when polymersomes were immobilized onto solid substrates. This fixation was achieved by adapting the host-guest chemistry into this part and conjugating the adamantane decorated polymersomes onto β -cyclodextrin coated substrates. Several investigations including adhesion behavior, pH sensitivity and mechanical properties of the established multifunctional polymersomes under liquid phase have been performed. It has been found that the polymersome shape is highly dependent on the attractive forces of the substrate and needs to be optimized to avoid the flattening of the vesicles. For these optimization steps, different conditions were investigated including the decrease of cyclodextrin amount and additional surface passivation with PEG molecules on the solid substrates. Besides, the calculated Young's and bending modulus of

the polymersome membrane ($E=27\pm 17.5$ MPa, $k=19\pm 12.5 \cdot 10^{-18}$ J) from AFM measurements showed a robust but still flexible “breathable” membrane which is an important criterion for the applicability of these smart and stable vesicles. In addition, the hosting ability as well as diffusion limits and sufficient membrane permeability of the polymersomes were observed by encapsulating gold nanoparticles as a smart cargo and doxorubicin molecules as an anticancer drug.

In conclusion, the established multifunctional polymersomes are highly versatile and thus present new opportunities in the design of targeted and selective recognition systems which is highly interesting for various applications including development of microsystem devices, design of chemo/biosensors, and also for conducting enhanced, combined therapy in the field of drug delivery.

Table of Contents

Acknowledgements	vii
Abstract	xi
I Fundamentals	
1 Theoretical Background	3
1.1 Introduction	3
1.2 Synthetic Methods to Produce Amphiphilic Block Copolymers	4
1.2.1 Anionic Polymerization	4
1.2.2 Atom Transfer Radical Polymerization	6
1.3 Polymersome Formation	8
1.3.1 Self-Assembly Principles of Amphiphilic Block Copolymers	8
1.3.2 Preparation Techniques	9
1.4 Design of Multifunctional Polymersomes	11
1.4.1 Stimuli-Responsive Polymersomes	12
1.4.2 Functionalization of Polymersome Surface	19
1.5 Characterization Methods of Polymersomes	23
1.6 Biomedical Applications of Polymersomes	28
1.7 References	30
2 Motivation and Aim	43
II Results and Discussion	
3 Multifunctional and Dual-Responsive Polymersomes	51
3.1 Introduction	51
3.2 Block Copolymer Synthesis and Characterization	52
3.3 Polymersome Preparation and Characterization	61
3.4 Polymersome Surface Functionalization by Sequential Post-Conjugations	67
3.4.1 Covalent Conjugation of Photoactive Moieties and Photocleavage	67
3.4.2 Covalent Conjugation of a Fluorescent Dye as a Model Compound	75
3.4.3 Non-Covalent Conjugation of β -Cyclodextrin by Host-Guest Interactions	77
3.5 Reversible pH-switch of Light Responsive Polymersomes	79
3.6 Summary	80
3.7 References	81

4	Multifunctional Polymersomes as Nanocontainers	85
4.1	Introduction	85
4.2	Doxorubicin Encapsulation and pH-triggered Release	86
4.3	Polymersome/Gold Nanoparticle Assemblies.....	89
4.4	Summary	101
4.5	References	102
5	Immobilized-Multifunctional Polymersomes on Solid Surfaces	105
5.1	Introduction	105
5.2	Preparation of β -cyclodextrin Coated Substrates	107
5.3	Polymersome Immobilization	110
5.4	Tuning Adhesion Properties of the Immobilized Polymersomes.....	112
5.5	pH-Responsive Surface-Immobilized Polymersomes.....	117
5.6	Infrared Light Induced Photochemical Reactions	119
5.7	Summary	122
5.8	References	123
6	Probing Mechanical Properties of Polymersomes	127
6.1	Introduction	127
6.2	Selection of the Analytical Model.....	128
6.3	Prediction of the Young's and Bending Modulus	129
6.4	Summary	133
6.5	References	134
7	Conclusion and Outlook	137
III Experimental Part		
8	Materials and Methods	147
8.1	Materials.....	147
8.2	Analytical Methods	150
8.3	Imaging Techniques and Analysis	152
8.4	Synthetic Methods and Characterization.....	153
8.4.1	Synthesis of Alkyne Functionalized Adamantane Molecule	153
8.4.2	Synthesis of Adamantane Functionalized Poly(ethylene glycol).....	154
8.4.3	Synthesis of Poly(ethylene glycol) Macroinitiators	155
8.4.4	Synthesis of Block Copolymers	156

8.4.5	Synthesis of Photoactive Compounds	158
8.5	References	160
9	Polymersome Formation and Encapsulation Procedures.....	161
9.1	Preparation of Multi-functionalized Polymersomes.....	161
9.2	Preparation of Polymersomes from Single Block-Copolymer	161
9.3	Cross-linking of Polymersomes	161
9.4	Reversible Swelling and Shrinking of Crosslinked Polymersomes	161
9.5	Polymersome Surface Functionalization.....	162
9.5.1	NVOC Modification of Polymersomes	162
9.5.2	Photocleavage of NVOC groups via UV-irradiation.....	162
9.5.3	Rhodamine B NCS Modification of Polymersomes	163
9.5.4	β -Cyclodextrin Modification of Polymersomes	163
9.5.5	Predicting the Accessibility of the Functional Groups.....	163
9.6	Doxorubicin-Encapsulated Polymersomes.....	167
9.7	In Vitro Release of Doxorubicin	168
9.8	Preparation of Polymersome/Gold Nanoparticle Assemblies	169
9.8.1	Pre-loading Approach.....	169
9.8.2	Post-loading Approach	170
9.9	References	170
10	Polymersome Immobilization onto Solid Substrates.....	171
10.1	Epoxy silane Coating of Substrates	171
10.2	β -cyclodextrin Coating of Substrates	171
10.3	Passivation of β -Cyclodextrin Coated Substrates with PEG molecules.....	171
10.4	Polymersome Immobilization	172
10.5	Two Photon Absorption (TPA) Induced Photochemical Reactions.....	172
10.6	References	173
	Abbreviations and Symbols	175
	List of Tables.....	179
	List of Figures	181
	List of Publications	191

I. Fundamentals

1 Theoretical Background

1.1 Introduction

Humanity has been using the elements of nature to develop new technologies for a long time. Especially, in the last few decades, the biomimicry studies have increased significantly to prepare materials with extremely interesting properties such as superhydrophobicity inspired by the lotus leaves.¹⁻² Apart from this, scientists have a wide interest on biological cells by being the basic structural and functional unit of living organisms that can perform complex reactions and multiple functions within confined environments. In particular, the cell membrane consists of the phospholipid bilayer with the embedded proteins and serves important functions which inspires new materials and particles for various biomedical applications. For instance, the selective permeability of the cell membrane is a mimicking source for designing nanocarriers, e.g. for drug delivery systems. Besides, cell adhesion and signaling abilities lead to creative ideas for building up biorecognition platforms, e.g. for sensing devices.³⁻⁵ At this point, the inspiration of cell membrane led to the development of lipid based vesicles, so called liposomes by Bangham et al. in 1961.⁶ The vesicles are self-assembled from phospholipids having hydrophilic head and hydrophobic tails in water which can host many compounds either in their lumen or in the membrane. This was a big step forward for delivery purposes as well as many other biotechnological applications. However, the lack of stability and undesired permeability of liposomes led scientists towards further developments. In this regard, the knowledge of cell mimicking was translated into the polymeric analogous of the liposomes which was developed using synthetic amphiphilic block copolymers. These vesicles, named as polymersomes, have been firstly reported by Discher and coworkers in 1999.⁷ The similarities of liposomes and polymersomes are their encapsulation ability of both hydrophilic and hydrophobic molecules as well as their biocompatible property. However, the big difference is originated by the use of synthetic polymers that enable chemical versatility and also stability with the aid of a thicker membrane. This is basically due to the higher molecular weight of polymeric materials leading to enhanced robustness and less permeability which makes polymersomes more advantageous in various applications including drug delivery, synthetic biology and sensors in comparison to their lipid counterparts (Figure 1.1).⁸⁻¹⁰

Hence, this chapter describes the methods of polymersome formation starting from the synthetic mechanism for required self-assembling polymers and ending with the design of

multifunctional polymersomes with the focus on responsiveness and surface functionalization. Furthermore, the most widely used characterization tools and the possible applications for polymersomes are given by referring to previous studies in literature.

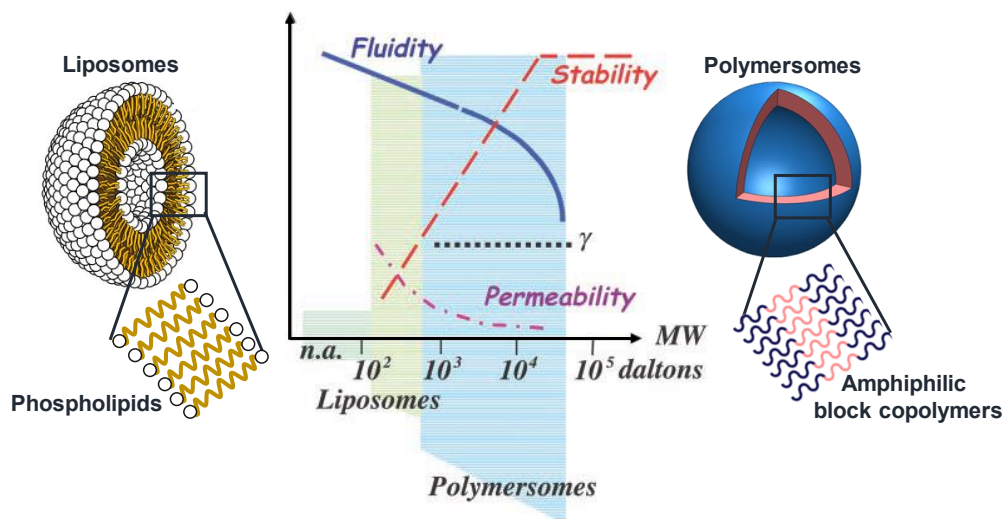


Figure 1.1 Illustration of liposome (adapted from Wikipedia) and polymersome structures. The graph represents the molecular weight dependent membrane properties of the corresponding self-assembled structures which show enhanced stability of polymersomes compared with liposomes.⁸

1.2 Synthetic Methods to Produce Amphiphilic Block Copolymers

The starting point of a polymersome formation is to produce amphiphilic block copolymers that consist of hydrophobic and hydrophilic segments. Depending on the ratio of these two blocks, the amphiphilic copolymers can self-assemble into variety of structures such as spherical micelles, rods and vesicles. Thus, a precise polymer structure is required to obtain the desired morphology that can be provided by applying controlled polymerization techniques. In the following section, the widely used synthetic methods to prepare polymersome-forming block copolymers are discussed.

1.2.1 Anionic Polymerization

This technique exemplifies the first polymersome forming block copolymer synthesis that is based on the poly(ethylene oxide)-b-poly-ethyl ethylene (PEO-b-PEE) structure.^{7, 11-12} Anionic polymerization is a type of chain growth polymerization that is carried out through a carbanion active species. The monomers having electrophile groups such as styrene, methacrylates, acrylates, butadiene, isoprene, acrylonitrile and ϵ -caprolactone can be

polymerized by this technique. In principle, the mechanism consists of three steps including initiation, propagation and termination. However, no chain termination occurs in living anionic polymerization systems in the case of strict reaction conditions like low temperature as well as devoid of any protonic impurities including water and oxygen. The initiation step may follow two different mechanisms as illustrated in Figure 1.2. The first way includes the initiators like n-butyl lithium or Grignard reagents in which their negatively-charged part is added to the monomers to form the anionic active center. In the second case, the use of alkali metals leads to a direct electron transfer to the monomer for the formation of a radical anion. Since the anionic centers of the resulting polymers stay reactive unless they are quenched, functional units can be added as a termination agent to stop the polymerization process. For instance, PEG oligomers having various functional end-groups such as azido and amino moieties can be prepared by using this approach that are also available in the polymer market.¹³ The commercial azido-terminated PEG molecules ($M_n=2700$ g/mol) used in this thesis was also synthesized by living anionic polymerization in which the initiation was performed through potassium salts of azido-ethoxy-ethanol.

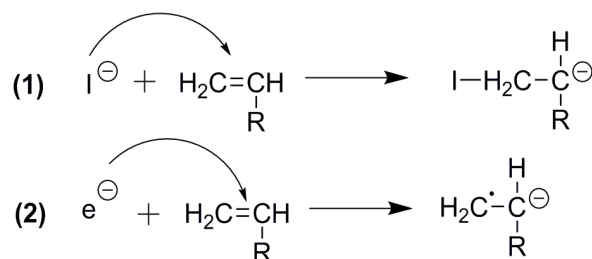


Figure 1.2 Illustration of different initiation mechanisms for anionic polymerization.

As an example for preparing a polymersome-forming block copolymers, the synthetic scheme of producing PEO-b-PEE block copolymer is given in Figure 1.3. Herein, anionic polymerization of butadiene is performed using alkyl lithium as an initiator which is followed by addition of ethylene oxide to obtain the monohydroxyl-terminated poly(butadiene) (PBD-OH). In the second step, this PBD-OH precursor is catalytically hydrogenated to synthesize the monohydroxyl-terminated poly(ethylethylene) (PEE-OH). Finally, the PEE-OH is turned into the corresponding potassium alkoxide (PEE-O-K⁺) as a macroinitiator to be used in the polymerization of ethylene oxide.¹¹⁻¹² The polymersomes prepared from the corresponding block copolymers is of great significance since they inspire many other investigations to form different polymersome systems for a broad spectrum of applications in the macromolecular nanotechnology.

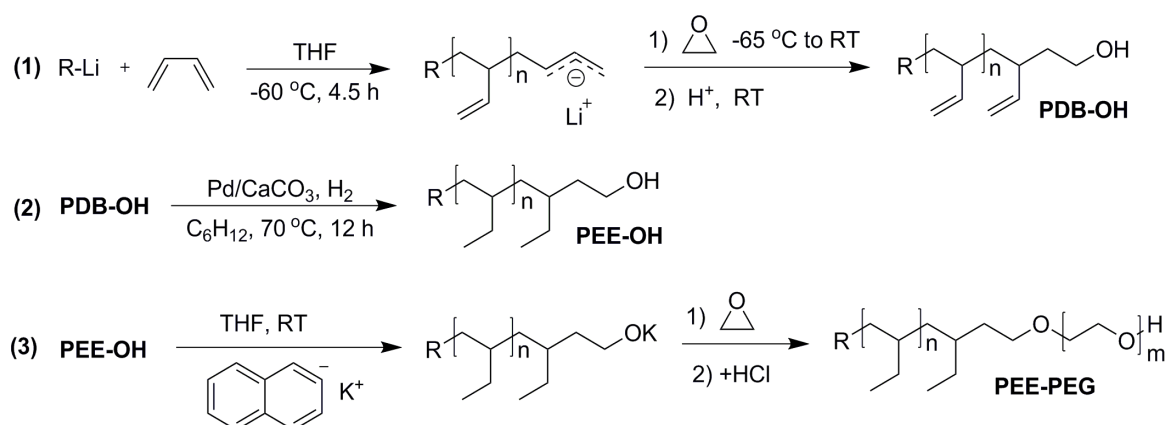


Figure 1.3 Synthetic mechanism for anionic polymerization of PEG-PEE block copolymer¹¹

1.2.2 Atom Transfer Radical Polymerization

Atom transfer radical polymerization (ATRP) is a controlled radical polymerization (CRP) technique which is very efficient to design multifunctional and nanostructured materials in the scope of biomedical applications.¹⁴ Among the available CRP techniques like reversible addition-fragmentation chain transfer (RAFT) and nitroxide-mediated radical polymerization (NMRP), ATRP is widely used in polymersome forming block copolymer synthesis as listed in Table 1.1.¹⁵⁻²⁰ This high attention is simply based on various advantages such as commercially available initiators and precise control over macromolecular structure. In addition, several monomers including styrene, methacrylate and acrylate can be polymerized in a controlled manner with this technique.²¹

Table 1.1 Polymersome forming block copolymers produced by ATRP

Block Copolymers	Functionality	Reference
PEG ₄₃ - <i>block</i> -P(DEA ₄₀ - <i>stat</i> -TMSPMA ₄₀)	pH sensitive	15
PMPC ₂₅ - <i>block</i> -PDPA ₁₂₀	pH sensitive	16
PS ₁₅₀ - <i>block</i> -PAA ₂₀	pH sensitive	17
PMPC ₂₅ - <i>block</i> -PDPA ₇₀	pH sensitive	18, 19
PEG ₄₅ - <i>block</i> -PS ₁₃₀ - <i>block</i> -PDEA ₁₂₀	pH sensitive	20

PEG: polyethylene glycol, DEA: 2-(diethylamino)ethyl methacrylate, TMSPMA: 3-(trimethoxy-silyl)propyl methacrylate, MPC: 2-(methacryloyloxy)ethyl phosphorylcholine, DPA: 2-(diisopropylamino)ethyl methacrylate, PS: polystyrene, PAA: polyacrylic acid.

1.3 Polymersome Formation

1.3.1 Self-Assembly Principles of Amphiphilic Block Copolymers

The self-assembly of amphiphilic block copolymers may result in different morphologies including planar bilayers, micelles and vesicles depending on the relative size of hydrophilic to hydrophobic segments. The curvature of the hydrophobic-hydrophilic interface is described by its mean (H) and Gaussian (K) curvature as shown in Figure 1.5.²²

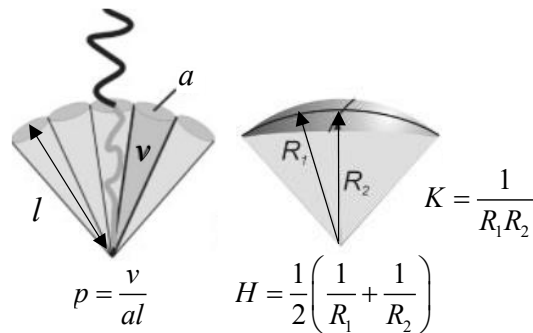


Figure 1.5 Description of amphiphile shape in terms of molecular packing parameter (p) and its relation to the to the interfacial mean curvature (H) and Gaussian curvature (K).²²

In this regard, a model developed by Israelachvili et al. is used to define the shape of the self-assembled structures by linking the curvature with the molecular packing parameter (p) (equation 2.1) where v denotes the hydrophobic volume, a is the interfacial area and l represents the hydrophobic chain length.²³ By calculating the p values, the resulting shape of the self-assembled structures can be predicted as seen in Table 1.2.²⁴

$$p = \frac{v}{al} = 1 - Hl + \frac{Kl^2}{3} \quad (1.1)$$

However, it should be noted that the packing parameter is defined by means of geometrical aspects and therefore it is not adequate to fully explain the self-assembly of amphiphilic block copolymers. The free energy of the system, which is the combination of the interfacial energy of the hydrophobic-hydrophilic interface and the entropy loss of the polymer chains during vesicle formation, have a considerable effect on the resulting morphologies. In this manner, Disher and Eisenberg reported another parameter known as mass or volume fraction of hydrophilic part of the block copolymer (f) to predict the morphology of the self-assembled structures (Table 1.2).^{8, 25-26}

Table 1.2 Packing parameter and hydrophilic fraction of different self-assemblies^{8, 24-26}

Shape of the assemblies	Packing parameter (p)	^a Hydrophilic Fraction (f)
Spherical Micelle	$p < 1/3$	$f = 0.55 - 0.70$
Cylindrical Micelle	$1/3 < p < 1/2$	$f = 0.45 - 0.55$
Vesicle	$1/2 < p < 1$	$f = 0.10 - 0.40$

^aHydrophilic fraction of the block copolymers either mass or volume ratios

Apart from the above-mentioned parameters, several other factors can also influence the shape of the self-assembled block copolymers. For instance, the nature of the solvent, temperature, amount of water in the medium and the presence of salts, acids or bases may also have an effect on the final morphologies.²⁷ It has been reported that PS-PAA copolymer self-assembled into spheres when DMF was used as the dissolution solvent, whereas vesicles can be obtained in the case of THF usage.²⁸ Another example is that the addition of hydrochloric acid (HCl) to PS-PAA spheres led to a decrease in the volume of the corona which resulted in a morphological change into rods and vesicles.²⁹ Thus, self-assembly of the block copolymers should be always investigated by taking into account all these factors in combination with the preparation method.

1.3.2 Preparation Techniques

Numerous techniques exist for preparing polymersomes from the self-assembly of amphiphilic block copolymers. These can be classified into five groups including solvent-switch, film rehydration, electroformation, microfluidic technology and direct dissolution like the pH switch method which is indeed utilized in this study. The selection of the convenient method is highly dependent on the copolymer structure and the application needs. It should be also noted that the resulting polymersome size can be varied significantly from nanometer to micrometer scale by using different techniques. Therefore, this is also an essential criterion for choosing the most suitable preparation method.

The solvent-switch method, also termed as co-solvent method, is a common polymersome preparation technique for the block copolymers that are not soluble in water. The procedure requires an organic solvent such as THF, chloroform, dichloromethane or ethanol for dissolving all block copolymers which are then gradually mixed with water under vigorous stirring. Subsequently, the organic phase is separated from the mixture by using

dialysis against water or ultrafiltration. During this procedure, the hydrophobic blocks of the copolymer are assembled together in the aqueous solution that form the membrane whereas the solvated hydrophilic blocks create the polymersome corona.^{27,30} Although this technique is a simple way of polymersome preparation, the use of organic solvent includes some drawbacks. For instance, the variation of the solvent behavior during the prolonged dialysis period may affect the morphology of the resulting self-assembled structures.³¹⁻³² In addition, use of fully water miscible solvents like acetone and THF led to smaller polymersomes in comparison to the chloroform/water systems when biodegradable PEG-PDLLA polymersomes were formed. A broad size distribution of the resulting polymersomes within the range of 70 nm to 50 μm was also reported which points out another drawback of this technique.³³

The film rehydration method starts with the dissolution of the block copolymers in an organic solvent such as chloroform and ethanol. Then the solvent is evaporated under reduced pressure to form the polymeric film on a solid surface like glass or roughened Teflon. Afterwards, the addition of the aqueous buffer solution enables the hydration of the copolymer film and thus, the polymersomes are formed. To support this process, gentle methods such as stirring, sonication or mechanical agitation may be utilized.³⁰ This method is generally combined with an extrusion step to obtain polymersomes with a narrow size distribution like it was applied for poly(dimethylsiloxane)-block-poly(2-methyloxazoline) based polymersomes reported by Meier et.al.³⁴

Electroformation is similar to the film hydration method which results in micrometer-sized giant polymersomes. Therein, the copolymers are spread onto an electrode surface followed by the addition of a buffer solution and finally the rehydration process is facilitated by applying the electric current.²⁷ The used electrodes can be made of indium-tin oxide (ITO) coated glass plates,³⁵ platinum wires³⁶ or gold wires³⁷ which have been already applied to form liposomes or polymersomes.

The microfluidic technology is utilized recently to prepare polymersomes in a controllable and reproducible way. This technique is based on two approaches including the formation of a double emulsion template in microchannels³⁸⁻⁴⁰ or the hydrodynamic flow-focusing in microfluidics.⁴¹⁻⁴² In the former approach, the amphiphilic block copolymers are carried in an organic solvent which is then removed in the case of double emulsion formation at the microchannels to produce the polymersomes. This way of production enables larger polymersomes in the range of micrometer size. An example for the latter approach is the

preparation of poly-2-vinylpyridine-b-poly(ethylene oxide) based polymersomes in which the block copolymers were dissolved in ethanol and flowed through the main channel of the microfluidic device. The side channel of the microfluidic device was also filled with Millipore water that was flowing in the perpendicular direction to the block copolymer side. Eventually, these two solutions mixed through diffusion that led to the polymersomes with a controllable size range of 40 nm to 2 μm .⁴¹ This result showed that the hydrodynamic-flow based microfluidic production is a feasible preparation technique for nanometer-sized polymersomes as well. However, Braun et. al has shown that there was no difference in the size distribution of pH sensitive poly(2-(methacryloyloxy) ethyl phosphorylcholine)-b-poly(2-(diisopropylamino) ethyl methacrylate) based polymersomes formed either using microfluidics or direct bulk production.⁴²

The direct dissolution method is carried out without the need of an organic solvent. The block copolymers are directly self-assembled in water or aqueous buffer solutions under vigorous stirring. For instance, the poly(ϵ -caprolactone)-b-poly(2-aminoethyl-methacrylate) and poly(ϵ -caprolactone)-b-poly[2-(methacryloyloxy)ethyl phosphorylcholine] based polymeromes have been successfully prepared in pure water within this technique.⁴³⁻⁴⁴ In addition, the self-assembly of pH-responsive block copolymers can be easily performed by adjusting the pH of the corresponding polymer solution. The pH-sensitive groups such as 2-(diisopropylamino)ethyl methacrylate enables the direct dissolution of the copolymer in an acidic water by means of protonation. This is followed by adding a base to deprotonate the amino groups that triggers the self-assembly process for polymersome formation. Nano-sized range polymersomes can be obtained using this technique which is advantageous by being practical, clean and fast.¹⁶ In this context, the polymersomes established in this thesis are also prepared through the direct dissolution of pH-sensitive block copolymers.

1.4 Design of Multifunctional Polymersomes

Multifunctionality of polymersomes is described as the combination of two or more abilities of a single polymersome system that can act either simultaneously or separately. The design of such structures can be performed within two ways. First, stimuli-responsive polymersomes can be formed using triggers like pH,⁴⁵⁻⁴⁶ temperature,⁴⁷⁻⁴⁸ redox,⁴⁹⁻⁵⁰ light⁵¹ and magnetic fields.⁵²⁻⁵³ Second, several useful functionalities including amino groups, photoactive moieties, or guest molecules for supramolecular complexes can be inserted to the polymersome surface using -pre/-post functionalization methods.⁵⁴⁻⁵⁵ In this regard, this

section emphasizes the design of multifunctional polymersomes with the focus on stimuli-responsive systems and polymersome surface functionalization.

1.4.1 Stimuli-Responsive Polymersomes

Stimuli-responsive polymersomes are able to sense small variations in their environment and converted these signals into physical or chemical structural changes such as morphological transitions, membrane permeability and reactivity of the functionalities. Different external or internal stimuli can be applied for controlling the uptake of drugs and various particles to be favored in different areas of biomedical applications. In the scope of this thesis, some of these stimuli including pH and light responsiveness are discussed in the following.

The pH-responsive polymersomes are of great interest due to the high tendency of pH variation in biological and physiological systems. Nature itself contains a wide range of pH gradients especially in the cellular compartments like decrease of pH values in the endosomes and lysosomes to trigger the degradation of biomacromolecules.⁵⁶ In addition, the healthy (pH 7.4) and the inflamed or wound tissue (between pH 7.4-5.4) show different pH values. Similarly, cancerous cells also exhibit acidic condition having the value up to pH 5 in the late endosome.⁵⁷ Therefore, pH-responsivity is widely used to deliver drugs in a controlled manner by various scientists. It is indeed not only favorable in controlled delivery of drugs but also very useful to deliver genes, proteins, diagnostic probes and various other chemical compounds depending on the needs.⁵⁸

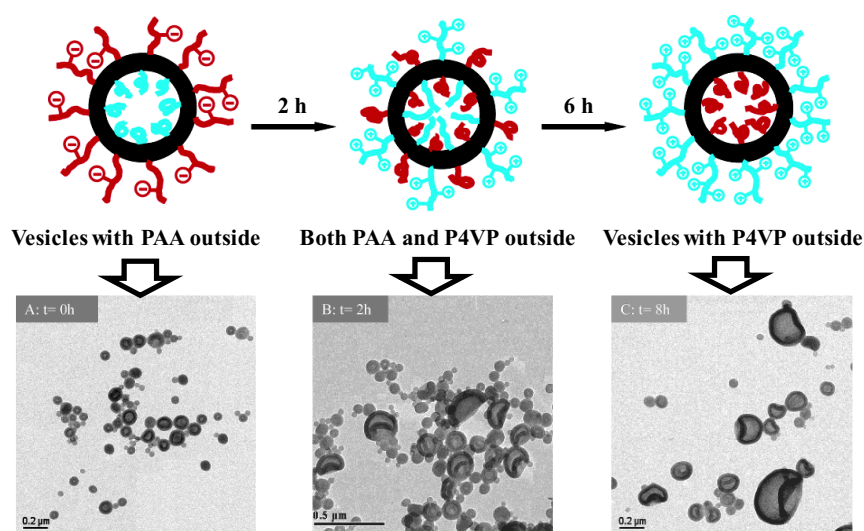


Figure 1.6 Schematic representation and corresponding TEM micrographs of pH-induced inversion of vesicles based on poly(acrylic acid)-b-polystyrene-b-poly(4-vinylpyridine) (PAA-b-PS-P4VP) vesicles. Adapted from Eisenberg et al.⁵⁹

The Eisenberg group has started early studies in this field by producing pH-sensitive vesicles based on a triblock copolymer, poly(acrylic acid)-*b*-polystyrene-*b*-poly(4-vinylpyridine) (PAA-*b*-PS-*b*-P4VP). In this work, the vesicle morphology (pH 1) was inverted into solid spherical or ellipsoidal aggregates (pH 3-11) and switched back to vesicle shape at pH 14 in the period of gradual pH increase. The former case of the vesicles (pH 1) have the P4VP chains at the exterior corona and PAA chains at the interior part whereas the latter case at pH 14 was the opposite which was believed to be sourced by the difference in repulsive interactions within PAA or P4VP corona at varied pH states. (Figure 1.6).⁵⁹

Furthermore, Armes et al. has reported pH-responsive polymersomes based on poly(ethylene oxide)-*b*-poly[2-(diethylamino)ethyl methacrylate-*stat*-3-(trimethoxysilyl)propyl methacrylate] (PEO-*b*-P[DEA-*stat*-TMSMA]) copolymers in which DEA residues function as the pH-sensitive segment and TMSMA residues are the hydrolytically self-crosslinking units. Therein, the polymersome membrane was able to switch from hydrophobic to hydrophilic states when pH was decreased into acidic conditions. The principle behind this concept was that the DEA groups were protonated at low pH which were then deprotonated at the basic state leading to swelling-shrinking of the membrane. With the help of cross-linking, the disassembly of the vesicles was avoided and finally tunable pH responsivity was achieved which is usable for controlled release systems (Figure 1.7a).¹⁵ Another example of pH responsive polymersomes was prepared from PMPC-*b*-PDPA block copolymers which contain a highly biocompatible 2-(methacryloyloxy)ethyl phosphorylcholine (MPC) and the pH sensitive 2-(diisopropylamino)ethyl methacrylate (pKa of DPA~5.8-6.6) (Figure 1.7b). Therein, the polymersomes were formed when the pH was above 6 but they are completely disassembled in the case of acidification. This is simply based on the same logic as the previous DEA based polymersomes in which the DPA is protonated below its pKa leading the dissolution of the corresponding block copolymers. These polymersomes were also utilized to assess the loading of doxorubicin molecules which are used as anticancer drug in the pharmaceutical market.¹⁶ Besides, DNA plasmid encapsulation was also carried out within these polymersomes in another study of the group.⁴⁶

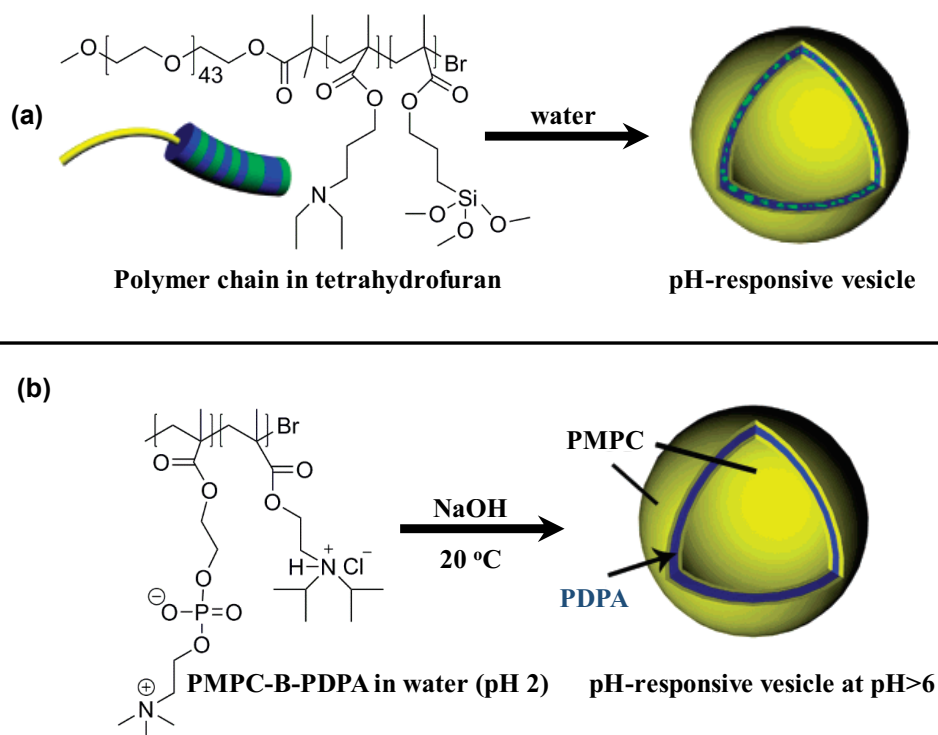


Figure 1.7 (a) Formation of pH-responsive polymersomes from PEO-*b*-P[DEA-*stat*-TMSPMA]) block copolymers. Adapted from Armes et al.¹⁵ (b) Formation of pH-responsive polymersomes from PMPC-*b*-PDPA block copolymers. Adapted from Armes et al.¹⁶

Moreover, photo-crosslinked polymersomes were successfully developed in the group of Voit et al. The block copolymers based on poly(ethylene glycol)-*b*-[2-(diethylamino) ethyl methacrylate-*stat*-3,4-dimethyl maleic imidoethyl methacrylate]⁶⁰ or poly(ethylene glycol)-*b*-[2-(diethylamino) ethyl methacrylate-*stat*-2-hydroxy-4-(methacryloyloxy) benzophenone]⁶¹ were self-assembled into pH-responsive polymersomes having the corresponding cross-linker units in their membrane. In this regard, the further membrane cross-linking was triggered through a UV-irradiation that prevented the polymersome disassembly at acidic condition (< pH 7). In addition to the tunable membrane permeability, this way of cross-linking also offers a clean process which is advantageous for using these polymersomes in biomedical science.

The light-responsive polymersomes are promising and convenient vesicles for biomedical applications since light is a rapid and clean external stimulus which does not require any additional chemicals to be triggered. The light response is usually obtained by incorporating photo-cleavable groups leading to light-triggered cleavage reactions or other photoactive molecules like azobenzene (AZO) resulting in light-induced conformational changes, into the vesicle structure.⁶² For photocleavage reactions, *o*-nitrobenzyl (NB)

derivatives can be utilized to realize the UV or NIR responsiveness.⁶³⁻⁶⁴ It should be also noted that several studies on light responsive systems based on liposomes⁶⁵⁻⁶⁸ or micelles⁶⁹⁻⁷² are inspiring guides to develop analogous light-sensitive polymersomes which draw more attention in the recent years.

In this regard, Meier et al. have reported light-responsive polymersomes self-assembled from a photocleavable amphiphilic block copolymer, poly(methyl caprolactone)-*O*-nitrobenzyl-polyacrylic acid (PMCL-ONB-PAA). The photocleavable group (ONB) was placed between the hydrophobic and hydrophilic blocks leading to PAA chains with the photodegraded linker and PMCL chains with carboxyl end groups after the UV exposure (Figure 1.8). In order to utilize these polymersomes as intelligent drug delivery systems, different cargos including fluorescein, ATTO 655 dye and enhanced green fluorescent protein were encapsulated and they were further released upon UV trigger. Therein, the broken polymersomes evolved into micellar structures to minimize the charge interactions that were induced by the formation of negatively charged PMCL chains (Figure 1.9).⁵¹ Besides, Katz and coworkers have developed biocompatible and photocleavable polymersomes prepared from poly(ϵ -caprolactone)-block-poly(ethylene glycol) having a 2-nitrophenylalanine (2NPA) group between the block junction. The photocleavage of 2NPA molecules upon UV-exposure led to a morphological transition that was utilized to release the encapsulated biocytin.⁷³

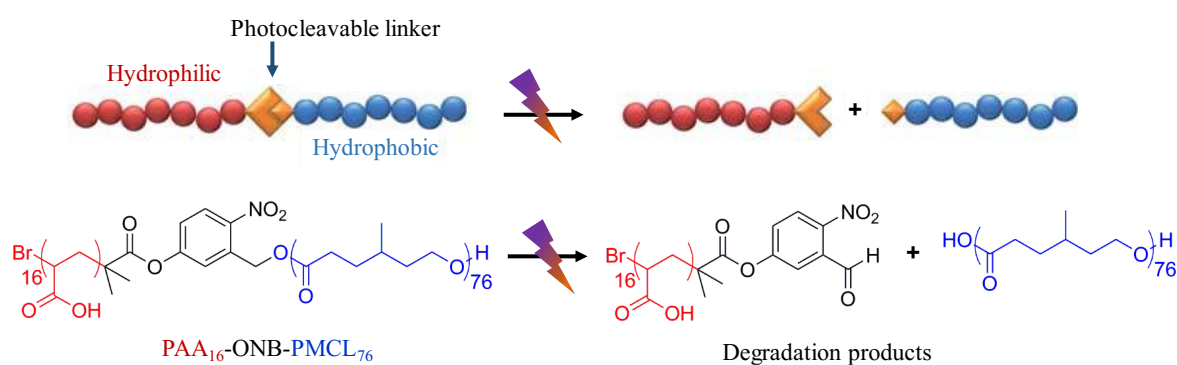


Figure 1.8 Schematic view and chemical structure of the poly(methyl caprolactone)-*O*-nitrobenzyl-poly(acrylic acid) diblock copolymer and its degradation products after UV exposure.⁵¹

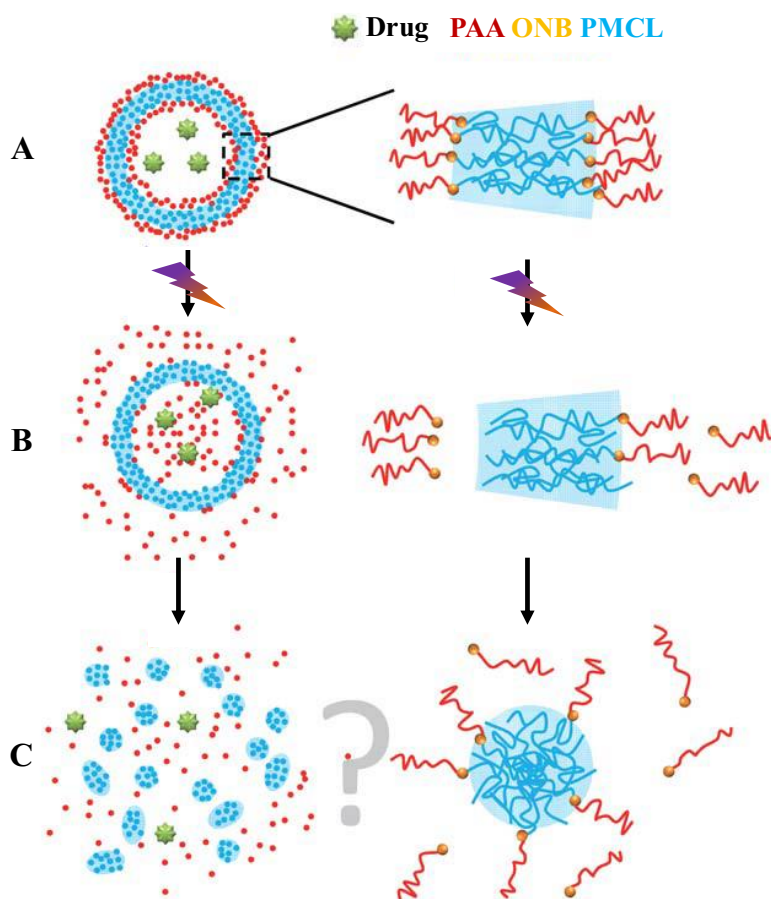


Figure 1.9 Scheme showing the polymersomes, and the conformation of the assembled polymer chains forming the membrane (A). The corona containing the PAA chains cleaved upon UV-trigger and separated from the PMCL chains (B). Finally, polymersome membrane was destroyed and the cargo released (C).⁵¹

In addition to the photocleavage reactions, Zhao et al. have shown azobenzene containing block copolymer vesicles that could be reversibly dissociated and reformed by light trigger through trans-cis photoisomerization of the azobenzene molecules. The block copolymer used in this study consisted of a methacrylate-based azobenzene containing side chain liquid crystalline polymer as the hydrophobic block (PAzo) and poly(tert-butyl acrylate-co-acrylic acid) (tBA-AA) as the hydrophilic block. This switchable morphology was monitored in-situ by tracking the variations in the optical transmittance of the vesicle solutions under UV or visible light exposure. Therein, the thermodynamic instability led to UV-triggered dissociation of the vesicles which was caused by the shift of hydrophilic/hydrophobic balance originating from the trans-cis isomerization of the azobenzene molecules. In the reverse case, the vesicles recovered their morphology upon visible light illumination in which the hydrophilic/hydrophobic balance was shifted in the

opposite direction (Figure 1.10).^{58, 74-75} Another interesting example of light-induced morphological changes is polymersomes self-assembled from azopyridine-based block copolymers that showed reversible photo-controlled swelling and shrinking behavior. These polymersomes were in micron size-range and the structure of the self-assembling block copolymer was poly(N-isopropylacrylamide)-block-poly[6-[4-(4-pyridyazo) phenoxy] hexylmethacrylate] (PNIPAM-b-PAzPy). The principle of light response was arising from the reversible isomerization of the azopyridine units upon UV and visible light illumination. The change from trans-to cis isomerization under UV-exposure ($\lambda=365$ nm) caused an increase in the diameter of the vesicles from 7.86 μm to 8.16 μm whereas the visible light-trigger led to the shrinking back to the original size due to the opposite isomerization behavior. The swelling power could be also regulated by changing the power density of the UV-light. For instance, the diameter has increased of about 17% at UV-exposure having the power as 150 mW/cm^2 whereas no swelling occurred when the power decreased to the 20 mW/cm^2 .⁷⁶

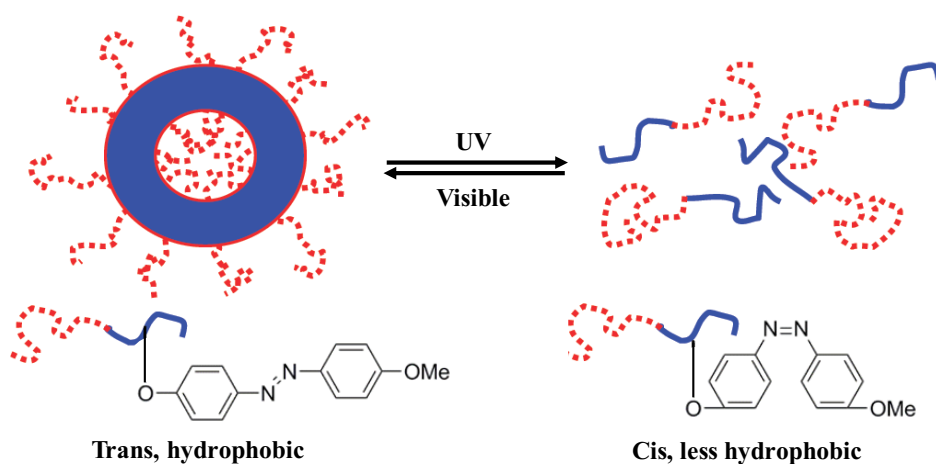


Figure 1.10 Reversible polymersome formation through UV/visible light irradiation.^{58, 75}

Moreover, near-infrared light responsivity is particularly interesting since the IR light provides deep penetration into organic materials and shows minimal harm to the tissues that leads to a safer applicability in biological environments. In this context, one way of replacing UV light source by NIR laser (700-1000 nm range) was to utilize two-photon absorption (TPA) processes in combination with the photosensitive groups. The principle of this technology is based on the simultaneous absorption of two photons with the aid of a femtosecond pulsed laser having a high power density. TPA enables to access the target excited state by using photons of half the energy or double the wavelength in comparison to

the one photon absorption processes triggered by UV light (Figure 1.11). The excitation probability is proportional to the square of light intensity and the two-photon absorption cross section quoted as Göppert-Mayer unit ($1 \text{ GM} = 10^{-50} \text{ cm}^4 \text{ s/photon}$) since this phenomenon was first described theoretically by the Nobel Prize winner, Maria Göppert-Mayer in the 1930s. In this regard, an additional advantageous of TPA technology arises in which the excitation of photons is confined to a very small volume leading to a very localized and focused photoactive area.^{62-63, 77-79} The polymersomes related studies exploiting this technology have been limited in the literature. However, there are examples of peptides⁸⁰ and hydrogel systems⁸¹ showing the successful cleavage of nitroveratryloxycarbonyl (NVOC) groups, a NB derivative, via IR light through TPA mechanism.

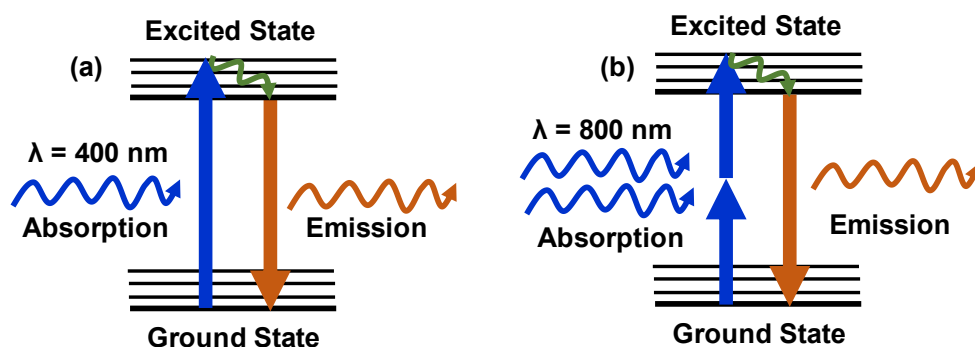


Figure 1.11 Principle of (a) one photon absorption (OPA) and (b) two photon absorption (TPA) optical processes

Another way of providing NIR sensitivity is to link polymersomes and gold nanoparticles (AuNPs) that have unique optical properties like surface plasmon resonance (SPR) as well as second harmonic generation (SHG) leading to frequency doubling. With the help of these optical features, AuNPs are able to absorb visible light and have the ability to convert it into heat energy.⁸²⁻⁸⁴ In this respect, Weitz et al. have developed photo and thermo-responsive polymersomes self-assembled from the mixture of gold nanoparticle incorporated PEG-b-PLA and 5 wt% PNIPAM-b-PLGA block copolymers. As shown in Figure 1.12, the encapsulation of a green dye was performed to monitor the release after irradiation with a mixture of three laser sources having wavelengths of 488, 532 and 633 nm, respectively. As a negative control, polymersomes without gold NPs were also prepared and a red dye was loaded into them which was subjected to the same laser irradiation at room temperature. Thus, the polymersomes having the AuNPs ruptured and the green dye was released due to the photo-responsive behavior within 20 minutes.⁸⁵ One another example

was the doxorubicin/gold nanorod-loaded polymersomes that was utilized as heat generator by the trigger of NIR light ($\lambda=808$ nm). Therein, polymersomes that were made of poly(ethylene glycol)-block-poly(ϵ -caprolactone) applied as delivery vehicle to release doxorubicin molecules.⁸⁶

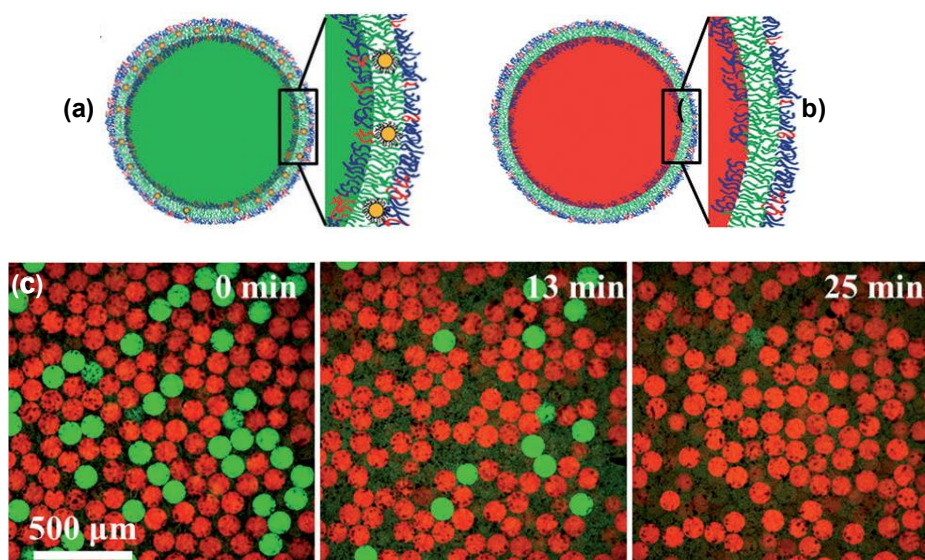


Figure 1.12 Scheme showing (a) the polymersomes with gold nanoparticles loaded with a green dye and (b) the polymersomes without gold nanoparticles loaded with a red dye. (c) A series of confocal microscope images of the mixture of corresponding polymersomes irradiated with lasers at room temperature. Adapted from Weitz et al.⁸⁵

1.4.2 Functionalization of Polymersome Surface

Polymersome functionalization is useful to develop active targeting via specific receptor-ligand interaction for enhanced therapeutic efficiency as well as a diagnostic ability for especially drug delivery purposes.⁵⁵ In addition, the integrated functional moieties can be favored in specific immobilization of the polymersomes onto solid substrates^{19, 87-88} which is important for designing microfluidic devices, e.g biosensors. In this respect, two common routes are available to incorporate functional groups to the polymersome surface. The first approach is the pre-functionalization method in which the desired molecules are incorporated to the block copolymer structures before the self-assembly process. Herein, the functional groups are equally placed at both inner and outer region of the bilayer membrane after the polymersome formation. In the second approach named as post-functionalization method, the functional moieties are conjugated to the polymersome surface after their formation (Figure 1.13).^{17, 54-55, 89-90} Depending on the polymersome structure, functionality

can be integrated either inside or outside within this method, e.g. when stimuli-responsive vesicles are used.

In this regard, attachment of many recognitive ligands such as antibodies,⁹¹⁻⁹³ peptides,⁹⁴⁻⁹⁵ folic acids,^{90, 96} and sugars^{89, 97} have been studied by using either pre-functionalization or post-functionalization methods. It is possible to conjugate the functionalities through covalent binding approaches like azide-alkyne click chemistry,^{17, 89, 98-99} and attachment via bis-aryl hydrazine bond.³⁴ Another way of conjugation is using non-covalent binding approaches including biotin-streptavidin binding,¹⁰⁰⁻¹⁰² adamantane-cyclodextrin binding,¹⁰³⁻¹⁰⁴ and nitrilotriacetic acid (NTA) metal complexations.¹⁰⁵⁻¹⁰⁶

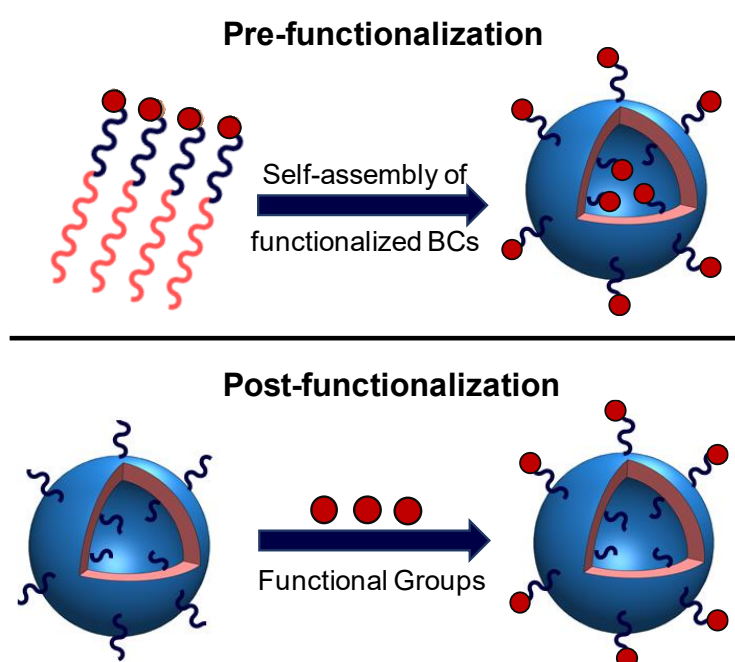


Figure 1.13 Scheme showing the principle of pre/post-functionalization routes

The group of van Hest has shown the use of click chemistry in polymersome field that illustrated both pre- and post- functionalization routes. In this study, azido terminated poly(styrene)-b-poly(acrylic acid) block copolymers were self-assembled to form the corresponding polymersomes. The further surface functionalization was carried out by conjugating different alkyne-modified ligands such as fluorescent dansyl probe, biotin, and enhanced green fluorescent protein (EGFP) in the presence of a copper catalyst ($\text{CuSO}_4 \cdot 5\text{H}_2\text{O}$), sodium ascorbate and tris-(benzyltriazolymethyl) amine (TBTA) as a stabilization ligand for copper species (Figure 1.14).¹⁷ The same group has also developed alkyne-functionalized polymersomes self-assembled from the mixture of polystyrene-b-

poly(ethylene glycol) (PS-b-PEG) bearing an acetylene moiety and polystyrene-b-poly[L-isocyanoalanine(2-thiophen-3-yl-ethyl) amide] (PS-b-PIAT) block copolymers. The conjugation of azido-modified Candida Antarctica Lipase B (CalB) was subsequently performed which retained its activity while attached on this hybrid polymersomes.⁹⁸

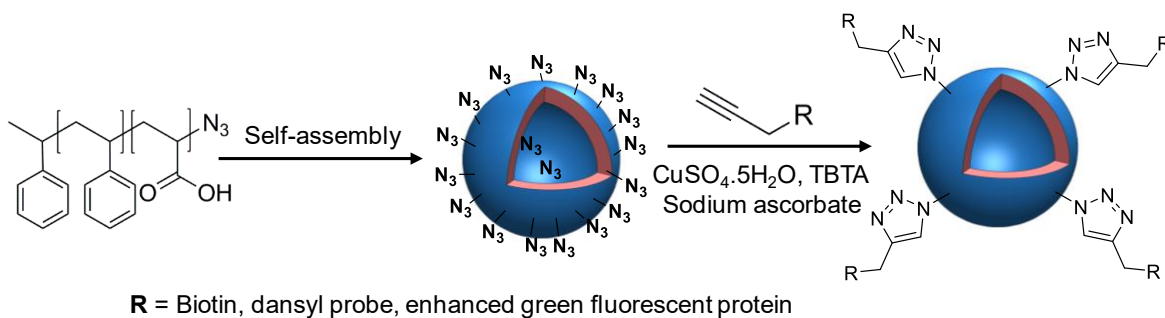


Figure 1.14 Clickable polymersomes self-assembled from azido-terminated PS-b-PAA block copolymers (pre-functionalization) and further post-functionalization with different molecules.¹⁷

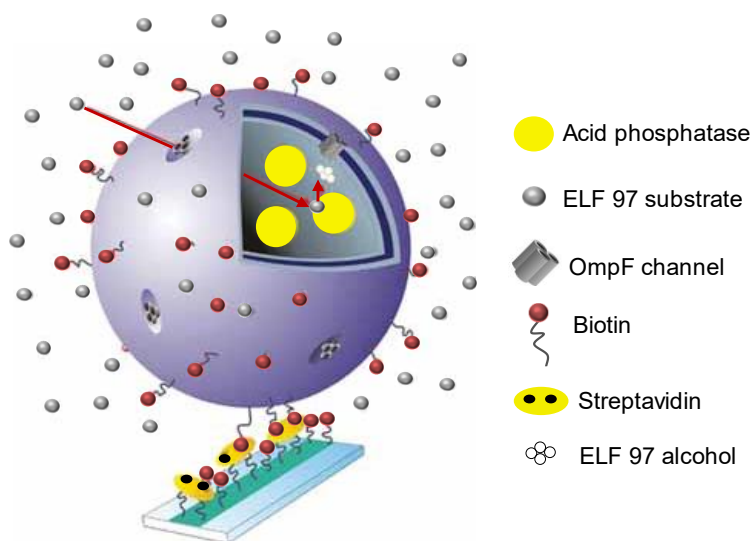


Figure 1.15 Scheme illustrating the immobilization of biotin-functionalized PMOXA-b-PDMS-b-PMOXA based polymersomes onto a glass substrate through streptavidin binding for realizing a nanoreactor platform.⁸⁷

As an example of non-covalent conjugation approaches, Hunziker and Meier et al. have reported biotin-functionalized triblock copolymers having the structure of [poly(2-methyloxazoline)-b-poly(dimethylsiloxane)-b-poly(2-methyloxazoline)] (PMOXA-b-PDMS-b-PMOXA) which was then self-assembled to form the respective polymersomes. In

this study they also linked the biotinylated ligands to these functionalized polymersomes through streptavidin coupling for cell-targeting purposes.¹⁰⁰ In another study, the same conjugation chemistry was utilized to immobilize the biotin-possessing polymersomes onto glass substrates to realize a nanoreactor platform by performing enzymatic conversions for applications in the field of analytics like sensors. The glass surface was modified with biotin bearing bovine serum albumin (BSA) through microcontact printing followed by exposure with streptavidin to prepare the relevant conjugation platform for biotinylated polymersomes. As a model enzymatic reaction, acid phosphatase was encapsulated within the polymersomes to trigger the dephosphorylation of the fluorogenic substrate ELF 97. The enzyme was able to access the substrate through the protein F channels (OmpF) embedded in the polymersome membrane that became permeable afterwards (Figure 1.15).⁸⁷

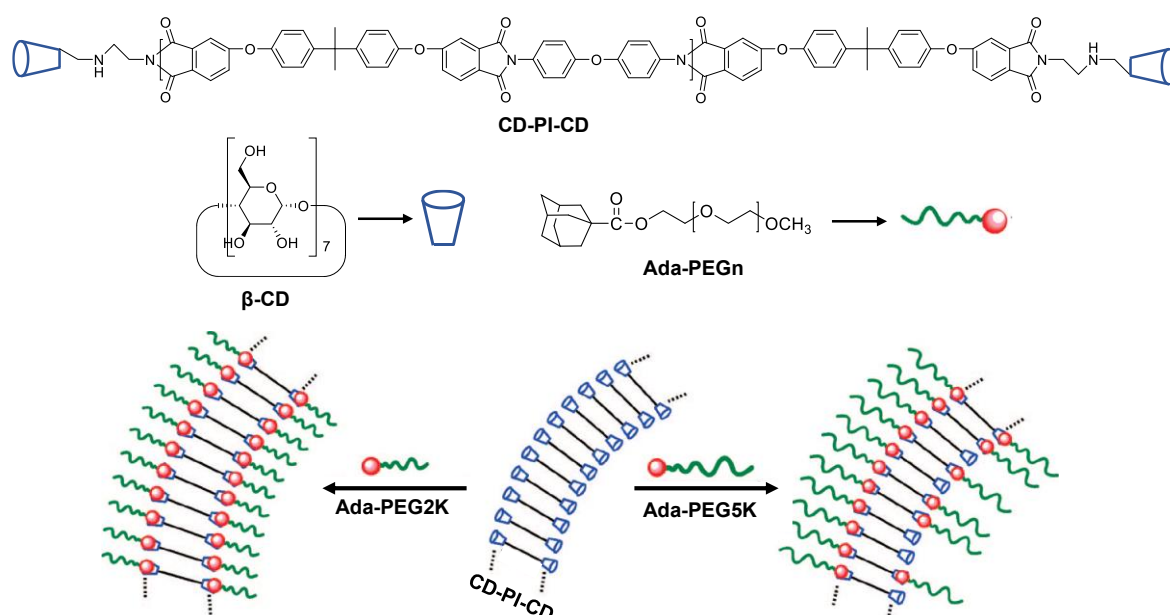


Figure 1.16 Surface modification of polymersomes with β -cyclodextrin molecules by pre-functionalization and further post-conjugation of adamantane-modified PEG having different molecular weights.¹⁰⁴

Another type of non-covalent conjugation is the host-guest complexation of adamantane and β -cyclodextrin (β -CD) molecules. This type of binding has been widely used in polymer chemistry since adamantane groups tightly fit into the cavity of β -CD molecules with a high association constant between 10^4 to 10^5 M^{-1} leading to a strong host-guest interaction.¹⁰⁷⁻¹⁰⁹ In this regard, Felici et al. has reported polymersomes decorated with β -cyclodextrin which was further conjugated to an adamantane modified enzyme, horseradish peroxidase (HRP),

through the host-guest interaction mechanism. Although the non-modified enzyme was also able to interact with polymersomes, the adamantane bearing HRP showed increased affinity and retained its activity while conjugated to the polymersomes. In this study, the vesicle formation was performed by the self-assembly of polystyrene having the permethylated β -cyclodextrin compounds.¹⁰³ Similar approach was also applied by Guo et al. by preparing a cyclodextrin-capped polyether imide (CD-PI-CD) that was self-assembled into polymersomes in water. As a guest molecule, polyethylene glycol with adamantane groups was utilized for conjugation to the CD-functionalized polymersomes. The successful host-guest complexation at both inner and outer region of polymersome corona was proven by using isothermal titration calorimetry (ITC) as well as static light scattering (SLS) measurements (Figure 1.16).¹⁰⁴

1.5 Characterization Methods of Polymersomes

Several characterization tools exist to investigate the polymersomes including light scattering methods, imaging techniques as well as spectroscopic methods. The selection of the relevant technique is highly dependent on the physicochemical properties and the size range of the analyzed polymersomes. Although the common essential characteristics are size, shape and membrane properties, the surface charge as well as topography on solid surfaces become significant when pH responsive or surface-immobilized polymersomes are investigated. In this context, the most frequent techniques such as dynamic light scattering for size determination, transmission electron microscopy for shape visualization and atomic force microscopy for probing topography and mechanical properties are highlighted in this section. In addition, the availability of light-absorbing molecules as functional groups or encapsulated cargos lead to the use of ultraviolet visible spectroscopy for quantitative and qualitative analysis which is emphasized in this part as well.

Dynamic light scattering (DLS) is a widely used technique to determine size and size distribution of the vesicles dispersed in a liquid through noninvasive measurements. The principle of the technique is relying on the measurement of translational diffusion coefficient which is then related to the size by using relevant theoretical relations. In brief, the sample is illuminated by a laser beam at a fixed angle and use of photodetector enables to detect the fluctuations of the scattered light which reflects the Brownian motion of the particles. In order to obtain a meaningful information from the collected signal, the correlation function

is computed by using an autocorrelator which is shown in below along with the exponential fitting expression (equation 1.2).

$$G(\tau) = \langle I(t) \cdot I(t + \tau) \rangle = A[1 + B \exp(-2Dq^2\tau)] \quad (1.2)$$

In the above equation, I is the scattering intensity, t is the initial time, τ represents the delay time, A is the intercept and B is the baseline of the correlation function. Additionally, D represents the diffusion coefficient, an important parameter to define the size. The scattering vector (q) is also included in this equation and it is defined by the following relation where n is the refractive index of the medium, Θ is the scattering angle and λ_0 is the wavelength of the laser (equation 1.3).

$$q = (4\pi n / \lambda_0) \sin(\Theta / 2) \quad (1.3)$$

By following this, a common theoretical approach named as Cumulants analysis is used to determine the mean size and polydispersity index of the particles. The principle of this analysis is basically fitting a single exponential to the correlation function to compute the diffusion coefficient (D) from equation 1.2 which is then related to the radius of diffusing particles by Stokes Einstein equation where R_H is the z-average hydrodynamic radius, T is temperature, k_B is the Boltzmann constant and η is the viscosity of the solvent.¹¹⁰⁻¹¹³

$$D = \frac{k_B T}{6\pi\eta R_H} \quad (1.4)$$

In addition to the size information, the zeta potential of the polymersomes can be determined through DLS by measuring the electrophoretic mobility of the particles in a capillary cell containing two electrodes. In brief, an electrical field is applied to the electrodes and the charged particles move towards the oppositely charged electrode with a velocity known as the electrophoretic mobility (U_E) which is then related to the zeta potential (ζ) by the Henry equation shown in below. Herein, the parameters like viscosity (η) and dielectric constant (ϵ) is already known whereas the Henry's function, $f(\kappa a)$, is assumed as 1.5 for the aqueous solutions of moderate electrolyte concentration. This is known as the Smoluchowski approximation which can be applicable to polymersomes as well.¹¹⁴ As can be inferred, information about zeta potential is specifically important for pH responsive polymersomes where charge of the particles is highly dependent on the working pH value.

$$U_E = \frac{2\epsilon\zeta f(\kappa a)}{3\eta} \quad (1.5)$$

Ultraviolet visible spectroscopy (UV-Vis) is another efficient method for polymersome characterization when they are tagged with fluorescent compounds. For instance, the encapsulation and further release of a light absorbing cargo such as doxorubicin molecules^{96, 115} or enzymatic reactions within the polymersomes¹¹⁶⁻¹¹⁷ can be monitored easily by using this technique. Indeed, the method is useful naturally for light-responsive polymersomes which can be simply tracked through the chromophore in their structure. The theory of UV-Vis spectroscopy is based on the light absorbing capability of the molecules. In principle, the molecules having valence electrons of low excitation energy can absorb UV or visible light through the electronic transitions (Figure 1.11a). The possible transitions involving π , σ and n electrons with the required energy levels can be seen in Figure 1.17. Among them, $n-\pi^*$ and $\pi-\pi^*$ transitions are frequently observed since absorption peaks for these transitions lay in the experimentally relevant region of the spectrum which is ranging between 200 to 700 nm. However, the required energy to excite an electron in a bonding σ orbital into the corresponding antibonding σ^* orbital ($\sigma-\sigma^*$ transition) is higher, therefore absorption sourced by this kind of transition is not seen in the UV-Vis spectrum. Similar case is also valid for $n-\sigma^*$ transitions despite of the lesser energy requirement in comparison to the $\sigma-\sigma^*$ transition in which the absorption range can be only in the region of 150 to 250 nm.

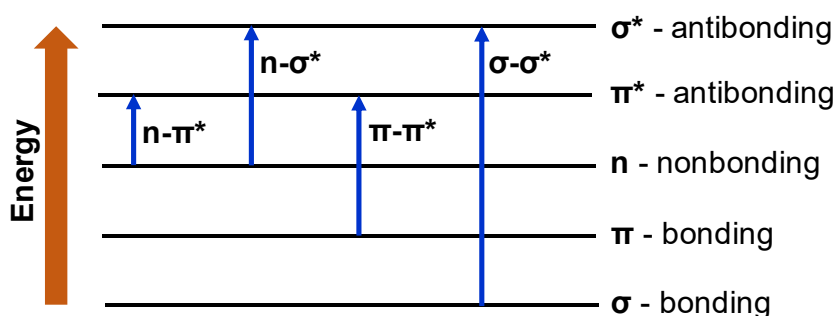


Figure 1.17 Electronic transitions and corresponding energy levels for bonding (σ , π) and nonbonding (n) orbitals

In this context, the absorbance spectra of a material can be recorded through an optical spectrometer in which the light passes through the sample solution relating the decrease of transmitted light with the material characteristics. This phenomenon is described by Lambert-Beer Law (equation 1.6) where A is the absorbance I_0 and I are the initial and outgoing intensities whereas c is the sample concentration, L is the optical path length and $\epsilon(\lambda)$ is the wavelength dependent molar absorption coefficient having the units of $M^{-1}cm^{-1}$.

This relationship enables to perform quantitative analysis for a particular material by determining either the concentration or molar absorption coefficient depending on the known quantity.¹¹⁸

$$A = \log \frac{I_0}{I} = \varepsilon(\lambda).c.L \quad (1.6)$$

Atomic Force Microscopy (AFM) is another tool to characterize polymersome topology particularly for the immobilized cases on solid substrates.^{19, 88, 119} Indeed, fixation onto convenient substrate is the precondition for the analysis with AFM. Basically, this technique allows to measure the interactions between the sample and the sharp tip attached to the cantilever in which the surface is scanned by moving either the tip or the sample. Figure 1.18 shows the components of an AFM when the sample is stationary and the tip is moved over the surface with the aid of a connected piezo scanner. The topography of the sample surface leads to a deflection of the cantilever which is detected through the reflected laser light onto a split photodiode. The converted electrical signal is evaluated by a feedback control system through a given set point. The tapping and non-contact mode of AFM enables a constant cantilever vibration amplitude whereas in contact mode, the cantilever deflection is maintained by moving the piezo scanner at the vertical position. The data at each (x, y) position for any chosen modes of AFM are then stored by the computer software to obtain a three-dimensional surface topography. This operation can take place in both ambient and liquid environments. For the latter case, special cantilever holders are available which is very advantageous to image the vesicles under liquid phase.¹²⁰⁻¹²¹

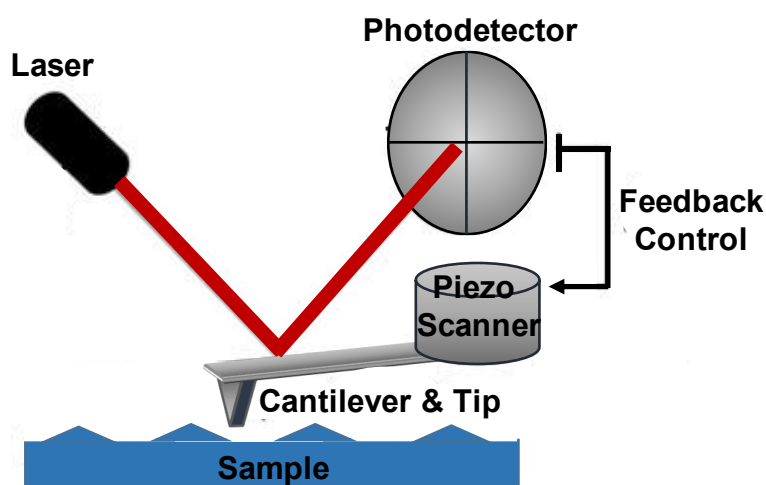


Figure 1.18 Scheme of the Atomic Force Microscopy setup. Adapted from Averett et al.¹²²

Among the different AFM modes, tapping mode is widely used for soft materials due to the lower applied forces on the sample. As can be inferred, polymersomes are also in the class of relatively soft particles and therefore possible deformation during the tip interaction has to be kept to a minimum. In this context, the AFM technology provides peak force tapping mode which enables precise control over the probe sample interaction with the lowest available forces and highest resolution imaging. Within this technique, feedback loop controls the maximum force on the tip that helps to avoid any possible damage on the sample surface while enabling a minimized contact area between tip and the sample. In addition to the topography images, the mechanical properties can be also probed within AFM through individual force curves by monitoring approaching, contacting and withdrawal of tip from the sample surface. In this regard, the measured cantilever deflection versus piezo scanner extension is converted into the force versus tip-sample separation curves.¹²³⁻¹²⁵ A basic idea of this operation can be seen in Figure 1.19 in which different analytical models such as Hertz¹²⁶ or Reissner Thin Shell Theory¹²⁷ are used to evaluate the measured data for acquiring elastic modulus values. Apart from polymersomes,¹²⁸⁻¹³⁰ several other soft materials such as liposomes,¹³¹⁻¹³² micelles,¹³³ polyelectrolyte multilayer capsules,¹³⁴ and natural membrane nanovesicles¹³⁵ are monitored within AFM for obtaining the information about their mechanical properties.

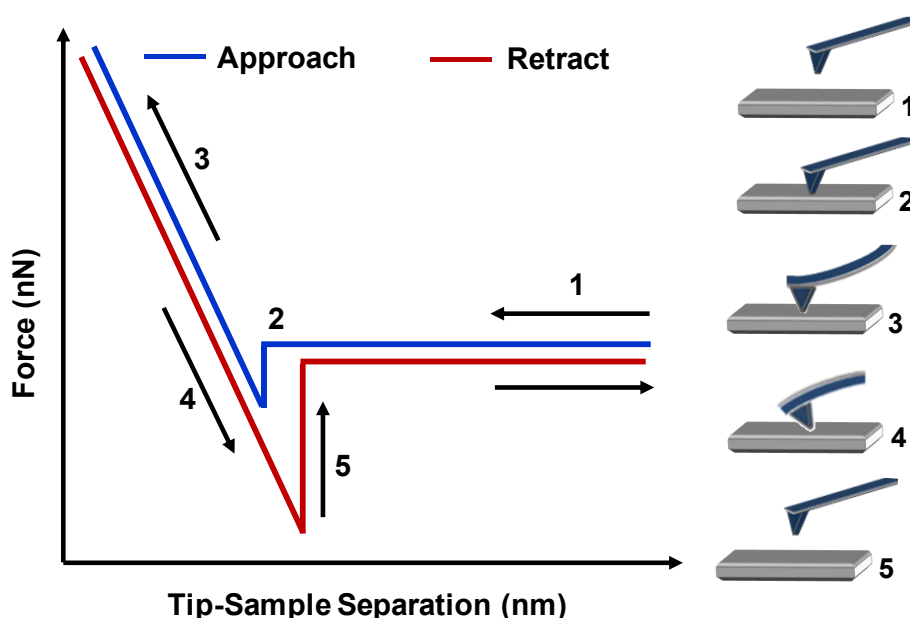


Figure 1.19 Scheme of ideal force-distance curves of AFM, eg. on a hard surface, where tip is approaching (1), contacting (2) and deflecting (3) respectively whereas the set point leads to the retraction of the tip from the sample surface (4) and further jump out occurs showing the complete retraction of the tip. Adapted from Leggett et al.¹²¹

Transmission electron microscopy (TEM) is widely used for imaging the nano-sized polymersomes to observe their morphology and size.¹³⁶⁻¹³⁷ Indeed, visualization is the most feasible way to understand the shape of the self-assembled structures whether they are in the form of vesicles, micelles or other morphologies. The driving force of TEM utilization is their resolution enabling to image smaller particles in the sub-nano range which is not possible with conventional optical microscopes. This is described through a mathematical expression by Abbe's equation where d is the resolution, λ is the wavelength and α is the aperture angle. For optical microscopes containing ideal lenses, the resolution (d) can be 200 nm whereas for TEM it is possible to decrease the wavelength several orders of magnitude leading to a decreased resolution of about 0.3 nm.¹³⁸

$$d = \frac{0.6\lambda}{\sin \alpha} \quad (1.7)$$

Since the specimen preparation of TEM requires the drying of the sample by dropping them onto a thin carbon film stretched over fine-meshed metal grid, some artifacts can occur especially for soft colloidal particles like polymersomes. To avoid such artifacts based on drying as well as the interactions of sample with the film support, one can use cryo-TEM which enables to visualize the polymersomes in their native hydrated state. This is basically sourced by the rapid cooling (1000 K/s) of the sample solution through vitrification but avoiding crystallization to form a frozen thin film. In this case, the morphological changes caused by different stimuli, e.g pH can be also observed as vitrifying the samples in acidic and basic aqueous solutions.¹³⁹⁻¹⁴²

1.6 Biomedical Applications of Polymersomes

The driving force of polymersome applicability is their inherent ability to encapsulate variety of organic and inorganic molecules. Unlike micelles, polymersomes are able to host both hydrophilic and hydrophobic compounds either in their aqueous lumen or in the membrane. Besides, the synthetic polymer chemistry provides flexible structure design which enables to prepare controlled membrane permeability through stimuli-responsive segments and selective recognition by integrating functional groups before or after the polymersome formation. In this respect they can act as nanocontainers^{78, 143} for storage, transport and release of drugs, enzymes, proteins, gold or magnetic nanoparticles by using the hosting ability either individually or in combination with responsiveness and functionality. From the terminology, nanocontainers can be defined as nanocarriers when the vesicles are used in

delivery purposes. In addition, they can have the task of nanoreactors¹⁴⁴⁻¹⁴⁶ to mimic the cell functions through metabolic reactions as well as to be used in various other reaction platforms such as enzymatic catalysis. Both of these duties widen the application areas of polymersomes, particularly in biomedical science including drug delivery systems^{55, 58, 90, 147-149}, synthetic biology^{116, 150} in combination with multicompartimentalization to form artificial organelles and therapeutic delivery carriers.^{5, 151} In addition, despite of the few studies on using polymersomes in microsystem devices, e.g. for building chemo/biosensors,^{87, 152} their phospholipid analogous, liposomes, have been widely applied for designing such microsystem devices.¹⁵³⁻¹⁵⁸ For this purpose, the future applications of polymersomes will be in this direction by being more stable than the liposomes and having the ability of hosting signal amplifiers like gold nanoparticles¹⁵⁹ as well as allowing conjugation of biorecognition elements to their surface.

As an example of drug delivery applications, the group of Lecommandoux has prepared doxorubicin (Dox) loaded polymersomes (PolyDox) self-assembled from poly(γ -benzyl L-glutamate)-*b*-hyaluronan (PBLG₂₃-*b*-HYA₁₀) block copolymers. In this study, the PolyDox showed an enhanced circulation time in comparison to free Dox molecules by targeting the cancer cells overexpressed with CD44 receptors. Besides, PolyDox also increased life span of the mouse having the Ehrlich ascites tumor (EAT) by six times than the ones treated with free Dox.¹⁴⁹ It should be also noted that doxorubicin is one of the most common anticancer drugs used in the nanomedicine market and therefore it is highly investigated in polymersome field as well.^{90, 148, 160} As already mentioned in the previous sections, gold nanoparticles can be also combined with polymersomes to realize photodynamic therapy as well as diagnostic purposes.^{82, 161} This was shown by using Dox and gold nanorod-loaded poly(ethylene glycol)-block-poly(ϵ -caprolactone) based polymersomes which increased the therapeutic efficiency in the treatment of solid tumors through combined chemophotothermal therapy.⁸⁶

Use of enzymes either attached to the surface or encapsulated within the polymersomes enables three enzyme cascade reactions as reported by van Hest group. Therein, polystyrene-*b*-poly(L-isocyanoalanine(2-thiophen-3-yl-ethyl) amide) (PS₄₀-PIAT₅₀) block copolymers were self-assembled to form porous polymersomes that showed a relatively high diffusion towards small molecules whereas proteins as being larger molecules cannot move across the membrane. The enzymes used in this study were positioned at different regions of the polymersomes in which glucose oxidase (GOx) was in their lumen, candida antartica lipase

B (CalB) was in the bilayer membrane and horseradish peroxidase (HRP) was conjugated to the surface by using click chemistry. The multi-step reactions within polymersomes was started with the conversion of glucose acetate into glucose by CalB which was then oxidized into gluconolactone by GOx enzyme. The third step of the reaction was to oxidize 2,2'-azinobis (3-ethylbenzothiazoline-6-sulfonic acid) (ABTS) using the hydrogen peroxide from the previous reaction by HRP on the surface.¹⁶² Although this porous polymersome enabled efficient cascade reactions, the permeability and thus the activity of the enzymes were not tunable. In this context, pH-responsive polymersomes having controlled membrane permeability were used to perform enzymatic reactions by Voit group. In this study, myoglobin was encapsulated into the lumen of the photo-crosslinked PDEAEM based polymersomes which catalyzed the reaction of hydrogen peroxide and guaiacol. The reaction activity was significantly enhanced in the case of acidic condition (pH 6) whereas relatively low activity was observed at basic state since the substrate cannot diffuse inside the polymersome to reach the myoglobin enzyme.^{116, 150}

In the study of Egli and Meier, targeting antibodies including antibiotin IgG and trastuzumab were conjugated to the polymersomes through bis-aryl hydrazine bonds for specific binding towards biotin patterned solid surfaces and breast cancer cells. The polymersomes structure was based on poly(dimethylsiloxane)-b-poly(2-methylloxazoline) block copolymers and functionalized with succinimidyl 4-formylbenzoate (NHS-4FB) groups after the self-assembly. Since the antibodies as well as enhanced yellow fluorescent protein (eYFP) were modified with 6-hydrazinonicotinate acetone hydrazone (HyNic), the next step was to attach them to the surface of the polymersomes. The special attention here was that the selective recognition of the antibiotin IgG on the polymersome surface led to a specific binding to the biotinylated pattern on the glass slide. This was one example of potential biosensor applications to be utilized in enzyme-linked immunosorbent assays (ELISA) that can show enhanced sensitivity in comparison to the conventional ELISA tests.¹⁵²

1.7 References

- [1] Aizenberg, J.; Fratzl, P., Biological and Biomimetic Materials. *Adv. Mater.* **2009**, *21*, 387-388.
- [2] Fratzl, P., Biomimetic Materials Research: What Can We Really Learn from Nature's Structural Materials? *Journal of The Royal Society Interface* **2007**, *4*, 637-642.

- [3] Marguet, M.; Bonduelle, C.; Lecommandoux, S., Multicompartmentalized Polymeric Systems: Towards Biomimetic Cellular Structure and Function. *Chem. Soc. Rev.* **2013**, *42*, 512-529.
- [4] Himmelein, S.; Ravoo, B. J., In *Bioinspiration and Biomimicry in Chemistry*, John Wiley & Sons, Inc.: **2012**, pp 209-249.
- [5] Chandrawati, R.; Caruso, F., Biomimetic Liposome- and Polymersome-Based Multicompartmentalized Assemblies. *Langmuir* **2012**, *28*, 13798-13807.
- [6] Bangham, A. D.; Horne, R. W., Negative Staining of Phospholipids and Their Structural Modification by Surface-Active Agents as Observed in the Electron Microscope. *J. Mol. Biol.* **1964**, *8*, 660-1010.
- [7] Discher, B. M.; Won, Y.-Y.; Ege, D. S.; Lee, J. C.-M.; Bates, F. S.; Discher, D. E.; Hammer, D. A., Polymersomes: Tough Vesicles Made from Diblock Copolymers. *Science* **1999**, *284*, 1143-1146.
- [8] Discher, D. E.; Eisenberg, A., Polymer Vesicles. *Science* **2002**, *297*, 967-973.
- [9] Messenger, L.; Gaitzsch, J.; Chierico, L.; Battaglia, G., Novel Aspects of Encapsulation and Delivery Using Polymersomes. *Curr. Opin. Pharmacol.* **2014**, *18*, 104-111.
- [10] Discher, D. E.; Ahmed, F., Polymersomes. *Annu. Rev. Biomed. Eng.* **2006**, *8*, 323-341.
- [11] Hillmyer, M. A.; Bates, F. S., Synthesis and Characterization of Model Polyalkane-Poly(Ethylene Oxide) Block Copolymers. *Macromolecules* **1996**, *29*, 6994-7002.
- [12] Hillmyer, M. A.; Bates, F. S.; Almdal, K.; Mortensen, K.; Ryan, A. J.; Fairclough, J. P. A., Complex Phase Behavior in Solvent-Free Nonionic Surfactants. *Science* **1996**, *271*, 976-978.
- [13] Voit, B.; Haag, R.; Appelhans, D.; Welzel, P. B., In *Bio- and Multifunctional Polymer Architectures*, John Wiley & Sons, Inc: **2016**, pp 19-111.
- [14] Siegwart, D. J.; Oh, J. K.; Matyjaszewski, K., Atrp in the Design of Functional Materials for Biomedical Applications. *Prog. Polym. Sci.* **2012**, *37*, 18-37.
- [15] Du, J.; Armes, S. P., Ph-Responsive Vesicles Based on a Hydrolytically Self-Cross-Linkable Copolymer. *J. Am. Chem. Soc.* **2005**, *127*, 12800-12801.
- [16] Du, J.; Tang, Y.; Lewis, A. L.; Armes, S. P., Ph-Sensitive Vesicles Based on a Biocompatible Zwitterionic Diblock Copolymer. *J. Am. Chem. Soc.* **2005**, *127*, 17982-17983.
- [17] Opsteen, J. A.; Brinkhuis, R. P.; Teeuwen, R. L. M.; Lowik, D. W. P. M.; van Hest, J. C. M., "Clickable" Polymersomes. *Chem. Commun.* **2007**, 3136-3138.
- [18] Massignani, M.; LoPresti, C.; Blanz, A.; Madsen, J.; Armes, S. P.; Lewis, A. L.; Battaglia, G., Controlling Cellular Uptake by Surface Chemistry, Size, and Surface Topology at the Nanoscale. *Small* **2009**, *5*, 2424-2432.
- [19] Battaglia, G.; LoPresti, C.; Massignani, M.; Warren, N. J.; Madsen, J.; Forster, S.; Vasilev, C.; Hobbs, J. K.; Armes, S. P.; Chirasatitsin, S.; Engler, A. J., Wet Nanoscale Imaging and Testing of Polymersomes. *Small* **2011**, *7*, 2010-2015.

- [20] Yu, S.; Azzam, T.; Rouiller, I.; Eisenberg, A., “Breathing” Vesicles. *J. Am. Chem. Soc.* **2009**, *131*, 10557-10566.
- [21] Braunecker, W. A.; Matyjaszewski, K., Controlled/Living Radical Polymerization: Features, Developments, and Perspectives. *Prog. Polym. Sci.* **2007**, *32*, 93-146.
- [22] Antonietti, M.; Förster, S., Vesicles and Liposomes: A Self-Assembly Principle Beyond Lipids. *Adv. Mater.* **2003**, *15*, 1323-1333.
- [23] Israelachvili, J. N.; Mitchell, D. J.; Ninham, B. W., Theory of Self-Assembly of Hydrocarbon Amphiphiles into Micelles and Bilayers. *Journal of the Chemical Society, Faraday Transactions 2: Molecular and Chemical Physics* **1976**, *72*, 1525-1568.
- [24] Zhang, J.; Li, X.; Li, X., Stimuli-Triggered Structural Engineering of Synthetic and Biological Polymeric Assemblies. *Prog. Polym. Sci.* **2012**, *37*, 1130-1176.
- [25] Le Meins, J. F.; Sandre, O.; Lecommandoux, S., Recent Trends in the Tuning of Polymersomes’ Membrane Properties. *The European Physical Journal E* **2011**, *34*, 1-17.
- [26] Lee, J. S.; Feijen, J., Polymersomes for Drug Delivery: Design, Formation and Characterization. *J. Controlled Release* **2012**, *161*, 473-483.
- [27] Balasubramanian, V.; Herranz-Blanco, B.; Almeida, P. V.; Hirvonen, J.; Santos, H. A., Multifaceted Polymersome Platforms: Spanning from Self-Assembly to Drug Delivery and Protocells. *Prog. Polym. Sci.*
- [28] Yu, Y.; Eisenberg, A., Control of Morphology through Polymer–Solvent Interactions in Crew-Cut Aggregates of Amphiphilic Block Copolymers. *J. Am. Chem. Soc.* **1997**, *119*, 8383-8384.
- [29] Zhang, L.; Eisenberg, A., Morphogenic Effect of Added Ions on Crew-Cut Aggregates of Polystyrene-B-Poly(Acrylic Acid) Block Copolymers in Solutions. *Macromolecules* **1996**, *29*, 8805-8815.
- [30] Kita-Tokarczyk, K.; Grumelard, J.; Haeefe, T.; Meier, W., Block Copolymer Vesicles—Using Concepts from Polymer Chemistry to Mimic Biomembranes. *Polymer* **2005**, *46*, 3540-3563.
- [31] Zhang, L.; Eisenberg, A., Multiple Morphologies and Characteristics of “Crew-Cut” Micelle-Like Aggregates of Polystyrene-B-Poly(Acrylic Acid) Diblock Copolymers in Aqueous Solutions. *J. Am. Chem. Soc.* **1996**, *118*, 3168-3181.
- [32] Won, Y.-Y.; Davis, H. T.; Bates, F. S., Giant Wormlike Rubber Micelles. *Science* **1999**, *283*, 960-963.
- [33] Meng, F.; Hiemstra, C.; Engbers, G. H. M.; Feijen, J., Biodegradable Polymersomes. *Macromolecules* **2003**, *36*, 3004-3006.
- [34] Egli, S.; Nussbaumer, M. G.; Balasubramanian, V.; Chami, M.; Bruns, N.; Palivan, C.; Meier, W., Biocompatible Functionalization of Polymersome Surfaces: A New Approach to Surface Immobilization and Cell Targeting Using Polymersomes. *J. Am. Chem. Soc.* **2011**, *133*, 4476-4483.
- [35] Dimitrov, D. S.; Angelova, M. I., In *New Trends in Colloid Science*, Hoffmann, H., Ed. Steinkopff: Darmstadt, **1987**, pp 48-56.

- [36] Bucher, P.; Fischer, A.; Luisi, P. L.; Oberholzer, T.; Walde, P., Giant Vesicles as Biochemical Compartments: The Use of Microinjection Techniques. *Langmuir* **1998**, *14*, 2712-2721.
- [37] Sauer, M.; Haefele, T.; Graff, A.; Nardin, C.; Meier, W., Ion-Carrier Controlled Precipitation of Calcium Phosphate in Giant ABA Triblock Copolymer Vesicles. *Chem. Commun.* **2001**, 2452-2453.
- [38] Shum, H. C.; Kim, J.-W.; Weitz, D. A., Microfluidic Fabrication of Monodisperse Biocompatible and Biodegradable Polymersomes with Controlled Permeability. *J. Am. Chem. Soc.* **2008**, *130*, 9543-9549.
- [39] Perro, A.; Nicolet, C.; Angly, J.; Lecommandoux, S.; Le Meins, J.-F.; Colin, A., Mastering a Double Emulsion in a Simple Co-Flow Microfluidic to Generate Complex Polymersomes. *Langmuir* **2011**, *27*, 9034-9042.
- [40] Shum, H. C.; Zhao, Y.-j.; Kim, S.-H.; Weitz, D. A., Multicompartment Polymersomes from Double Emulsions. *Angew. Chem.* **2011**, *123*, 1686-1689.
- [41] Thiele, J.; Steinhauser, D.; Pfohl, T.; Förster, S., Preparation of Monodisperse Block Copolymer Vesicles Via Flow Focusing in Microfluidics. *Langmuir* **2010**, *26*, 6860-6863.
- [42] Brown, L.; McArthur, S. L.; Wright, P. C.; Lewis, A.; Battaglia, G., Polymersome Production on a Microfluidic Platform Using Ph Sensitive Block Copolymers. *Lab on a Chip* **2010**, *10*, 1922-1928.
- [43] Du, J.; Armes, S. P., Preparation of Primary Amine-Based Block Copolymer Vesicles by Direct Dissolution in Water and Subsequent Stabilization by Sol[^]Gel Chemistry. *Langmuir* **2008**, *24*, 13710-13716.
- [44] Du, J.; Armes, S. P., Preparation of Biocompatible Zwitterionic Block Copolymer Vesicles by Direct Dissolution in Water and Subsequent Silicification within Their Membranes. *Langmuir* **2009**, *25*, 9564-9570.
- [45] Blanz, A.; Massignani, M.; Battaglia, G.; Armes, S. P.; Ryan, A. J., Tailoring Macromolecular Expression at Polymersome Surfaces. *Adv. Funct. Mater.* **2009**, *19*, 2906-2914.
- [46] Lomas, H.; Canton, I.; MacNeil, S.; Du, J.; Armes, S. P.; Ryan, A. J.; Lewis, A. L.; Battaglia, G., Biomimetic Ph Sensitive Polymersomes for Efficient DNA Encapsulation and Delivery. *Adv. Mater.* **2007**, *19*, 4238-4243.
- [47] Qin, S.; Geng, Y.; Discher, D. E.; Yang, S., Temperature-Controlled Assembly and Release from Polymer Vesicles of Poly(Ethylene Oxide)-Block- Poly(N-Isopropylacrylamide). *Adv. Mater.* **2006**, *18*, 2905-2909.
- [48] Xu, H.; Meng, F.; Zhong, Z., Reversibly Crosslinked Temperature-Responsive Nano-Sized Polymersomes: Synthesis and Triggered Drug Release. *J. Mater. Chem.* **2009**, *19*, 4183-4190.
- [49] Napoli, A.; Valentini, M.; Tirelli, N.; Muller, M.; Hubbell, J. A., Oxidation-Responsive Polymeric Vesicles. *Nat Mater* **2004**, *3*, 183-189.
- [50] Cerritelli, S.; Velluto, D.; Hubbell, J. A., Peg-Ss-Pps: Reduction-Sensitive Disulfide Block Copolymer Vesicles for Intracellular Drug Delivery. *Biomacromolecules* **2007**, *8*, 1966-1972.

- [51] Cabane, E.; Malinova, V.; Menon, S.; Palivan, C. G.; Meier, W., Photoresponsive Polymersomes as Smart, Triggerable Nanocarriers. *Soft Matter* **2011**, *7*, 9167-9176.
- [52] Krack, M.; Hohenberg, H.; Kornowski, A.; Lindner, P.; Weller, H.; Förster, S., Nanoparticle-Loaded Magnetophoretic Vesicles. *J. Am. Chem. Soc.* **2008**, *130*, 7315-7320.
- [53] Sanson, C.; Diou, O.; Thévenot, J.; Ibarboure, E.; Soum, A.; Brûlet, A.; Miraux, S.; Thiaudière, E.; Tan, S.; Brisson, A.; Dupuis, V.; Sandre, O.; Lecommandoux, S., Doxorubicin Loaded Magnetic Polymersomes: Theranostic Nanocarriers for Mr Imaging and Magneto-Chemotherapy. *ACS Nano* **2011**, *5*, 1122-1140.
- [54] Egli, S.; Schlaad, H.; Bruns, N.; Meier, W., Functionalization of Block Copolymer Vesicle Surfaces. *Polymers* **2011**, *3*, 252-280.
- [55] Pawar, P. V.; Gohil, S. V.; Jain, J. P.; Kumar, N., Functionalized Polymersomes for Biomedical Applications. *Polymer Chemistry* **2013**, *4*, 3160-3176.
- [56] Che, H.; van Hest, J. C. M., Stimuli-Responsive Polymersomes and Nanoreactors. *Journal of Materials Chemistry B* **2016**.
- [57] Schmaljohann, D., Thermo- and Ph-Responsive Polymers in Drug Delivery. *Adv. Drug Del. Rev.* **2006**, *58*, 1655-1670.
- [58] Meng, F.; Zhong, Z.; Feijen, J., Stimuli-Responsive Polymersomes for Programmed Drug Delivery. *Biomacromolecules* **2009**, *10*, 197-209.
- [59] Liu, F.; Eisenberg, A., Preparation and Ph Triggered Inversion of Vesicles from Poly(Acrylic Acid)-Block-Polystyrene-Block-Poly(4-Vinyl Pyridine). *J. Am. Chem. Soc.* **2003**, *125*, 15059-15064.
- [60] Gaitzsch, J.; Appelhans, D.; Gräfe, D.; Schwille, P.; Voit, B., Photo-Crosslinked and Ph Sensitive Polymersomes for Triggering the Loading and Release of Cargo. *Chem. Commun.* **2011**, *47*, 3466-3468.
- [61] Yassin, M. A.; Appelhans, D.; Mendes, R. G.; Rummeli, M. H.; Voit, B., pH-Dependent Release of Doxorubicin from Fast Photo-Cross-Linkable Polymersomes Based on Benzophenone Units. *Chemistry – A European Journal* **2012**, *18*, 12227-12231.
- [62] Liu, G.; Liu, W.; Dong, C.-M., Uv- and Nir-Responsive Polymeric Nanomedicines for on-Demand Drug Delivery. *Polymer Chemistry* **2013**, *4*, 3431-3443.
- [63] Pelliccioli, A. P.; Wirz, J., Photoremovable Protecting Groups: Reaction Mechanisms and Applications. *Photochemical & Photobiological Sciences* **2002**, *1*, 441-458.
- [64] Zhao, H.; Sterner, E. S.; Coughlin, E. B.; Theato, P., O-Nitrobenzyl Alcohol Derivatives: Opportunities in Polymer and Materials Science. *Macromolecules* **2012**, *45*, 1723-1736.
- [65] Bisby, R. H.; Mead, C.; Morgan, C. G., Wavelength-Programmed Solute Release from Photosensitive Liposomes. *Biochem. Biophys. Res. Commun.* **2000**, *276*, 169-173.
- [66] Bisby, R. H.; Mead, C.; Morgan, C. G., Active Uptake of Drugs into Photosensitive Liposomes and Rapid Release on Uv Photolysis. *Photochem. Photobiol.* **2000**, *72*, 57-61.

- [67] Troutman, T. S.; Leung, S. J.; Romanowski, M., Light-Induced Content Release from Plasmon-Resonant Liposomes. *Adv. Mater.* **2009**, *21*, 2334-2338.
- [68] Chandra, B.; Subramaniam, R.; Mallik, S.; Srivastava, D. K., Formulation of Photocleavable Liposomes and the Mechanism of Their Content Release. *Organic & Biomolecular Chemistry* **2006**, *4*, 1730-1740.
- [69] Feng, Z.; Lin, L.; Yan, Z.; Yu, Y., Dual Responsive Block Copolymer Micelles Functionalized by Nipam and Azobenzene. *Macromol. Rapid Commun.* **2010**, *31*, 640-644.
- [70] Yan, B.; Boyer, J.-C.; Branda, N. R.; Zhao, Y., Near-Infrared Light-Triggered Dissociation of Block Copolymer Micelles Using Upconverting Nanoparticles. *J. Am. Chem. Soc.* **2011**, *133*, 19714-19717.
- [71] Cao, J.; Huang, S.; Chen, Y.; Li, S.; Li, X.; Deng, D.; Qian, Z.; Tang, L.; Gu, Y., Near-Infrared Light-Triggered Micelles for Fast Controlled Drug Release in Deep Tissue. *Biomaterials* **2013**, *34*, 6272-6283.
- [72] Liu, X.; Jiang, M., Optical Switching of Self-Assembly: Micellization and Micelle–Hollow-Sphere Transition of Hydrogen-Bonded Polymers. *Angew. Chem.* **2006**, *118*, 3930-3934.
- [73] Katz, J. S.; Zhong, S.; Ricart, B. G.; Pochan, D. J.; Hammer, D. A.; Burdick, J. A., Modular Synthesis of Biodegradable Diblock Copolymers for Designing Functional Polymersomes. *J. Am. Chem. Soc.* **2010**, *132*, 3654-3655.
- [74] Tong, X.; Wang, G.; Soldera, A.; Zhao, Y., How Can Azobenzene Block Copolymer Vesicles Be Dissociated and Reformed by Light? *The Journal of Physical Chemistry B* **2005**, *109*, 20281-20287.
- [75] Wang, G.; Tong, X.; Zhao, Y., Preparation of Azobenzene-Containing Amphiphilic Diblock Copolymers for Light-Responsive Micellar Aggregates. *Macromolecules* **2004**, *37*, 8911-8917.
- [76] Han, K.; Su, W.; Zhong, M.; Yan, Q.; Luo, Y.; Zhang, Q.; Li, Y., Reversible Photocontrolled Swelling-Shrinking Behavior of Micron Vesicles Self-Assembled from Azopyridine-Containing Diblock Copolymer. *Macromol. Rapid Commun.* **2008**, *29*, 1866-1870.
- [77] Smith, A. M.; Mancini, M. C.; Nie, S., Bioimaging: Second Window for in Vivo Imaging. *Nat Nano* **2009**, *4*, 710-711.
- [78] Feng, A.; Yuan, J., Smart Nanocontainers: Progress on Novel Stimuli-Responsive Polymer Vesicles. *Macromol. Rapid Commun.* **2014**, *35*, 767-779.
- [79] Pawlicki, M.; Collins, H. A.; Denning, R. G.; Anderson, H. L., Two-Photon Absorption and the Design of Two-Photon Dyes. *Angew. Chem. Int. Ed.* **2009**, *48*, 3244-3266.
- [80] Shigenaga, A.; Yamamoto, J.; Sumikawa, Y.; Furuta, T.; Otaka, A., Development and Photo-Responsive Peptide Bond Cleavage Reaction of Two-Photon Near-Infrared Excitation-Responsive Peptide. *Tetrahedron Lett.* **2010**, *51*, 2868-2871.
- [81] Peng, K.; Tomatsu, I.; van den Broek, B.; Cui, C.; Korobko, A. V.; van Noort, J.; Meijer, A. H.; Spink, H. P.; Kros, A., Dextran Based Photodegradable Hydrogels Formed Via a Michael Addition. *Soft Matter* **2011**, *7*, 4881-4887.

- [82] Huang, X.; El-Sayed, M. A., Gold Nanoparticles: Optical Properties and Implementations in Cancer Diagnosis and Photothermal Therapy. *Journal of Advanced Research* **2010**, *1*, 13-28.
- [83] Daniel, M.-C.; Astruc, D., Gold Nanoparticles: Assembly, Supramolecular Chemistry, Quantum-Size-Related Properties, and Applications toward Biology, Catalysis, and Nanotechnology. *Chem. Rev.* **2004**, *104*, 293-346.
- [84] Clark, H. A.; Campagnola, P. J.; Wuskell, J. P.; Lewis, A.; Loew, L. M., Second Harmonic Generation Properties of Fluorescent Polymer-Encapsulated Gold Nanoparticles. *J. Am. Chem. Soc.* **2000**, *122*, 10234-10235.
- [85] Amstad, E.; Kim, S.-H.; Weitz, D. A., Photo- and Thermoresponsive Polymersomes for Triggered Release. *Angew. Chem. Int. Ed.* **2012**, *51*, 12499-12503.
- [86] Liao, J.; Li, W.; Peng, J.; Yang, Q.; Li, H.; Wei, Y.; Zhang, X.; Qian, Z., Combined Cancer Photothermal-Chemotherapy Based on Doxorubicin/Gold Nanorod-Loaded Polymersomes. *Theranostics* **2015**, *5*, 345-356.
- [87] Grzelakowski, M.; Onaca, O.; Rigler, P.; Kumar, M.; Meier, W., Immobilized Protein-Polymer Nanoreactors. *Small* **2009**, *5*, 2545-2548.
- [88] Domes, S.; Filiz, V.; Nitsche, J.; Frömsdorf, A.; Förster, S., Covalent Attachment of Polymersomes to Surfaces. *Langmuir* **2010**, *26*, 6927-6931.
- [89] Martin, A. L.; Li, B.; Gillies, E. R., Surface Functionalization of Nanomaterials with Dendritic Groups: Toward Enhanced Binding to Biological Targets. *J. Am. Chem. Soc.* **2008**, *131*, 734-741.
- [90] Yassin, M. A.; Appelhans, D.; Wiedemuth, R.; Formanek, P.; Boye, S.; Lederer, A.; Temme, A.; Voit, B., Overcoming Concealment Effects of Targeting Moieties in the Peg Corona: Controlled Permeable Polymersomes Decorated with Folate-Antennae for Selective Targeting of Tumor Cells. *Small* **2015**, *11*, 1580-1591.
- [91] Lee, J. S.; Groothuis, T.; Cusan, C.; Mink, D.; Feijen, J., Lysosomally Cleavable Peptide-Containing Polymersomes Modified with Anti-Egfr Antibody for Systemic Cancer Chemotherapy. *Biomaterials* **2011**, *32*, 9144-9153.
- [92] Lin, J. J.; Ghoroghchian, P. P.; Zhang, Y.; Hammer, D. A., Adhesion of Antibody-Functionalized Polymersomes. *Langmuir* **2006**, *22*, 3975-3979.
- [93] Robbins, G. P.; Saunders, R. L.; Haun, J. B.; Rawson, J.; Therien, M. J.; Hammer, D. A., Tunable Leuko-Polymersomes That Adhere Specifically to Inflammatory Markers. *Langmuir* **2010**, *26*, 14089-14096.
- [94] Georgieva, J. V.; Brinkhuis, R. P.; Stojanov, K.; Weijers, C. A. G. M.; Zuilhof, H.; Rutjes, F. P. J. T.; Hoekstra, D.; van Hest, J. C. M.; Zuhorn, I. S., Peptide-Mediated Blood-Brain Barrier Transport of Polymersomes. *Angew. Chem.* **2012**, *124*, 8464-8467.
- [95] Klermund, L.; Poschenrieder, S. T.; Castiglione, K., Simple Surface Functionalization of Polymersomes Using Non-Antibacterial Peptide Anchors. *Journal of Nanobiotechnology* **2016**, *14*, 1-12.
- [96] Yang, X.; Grailer, J. J.; Rowland, I. J.; Javadi, A.; Hurley, S. A.; Matson, V. Z.; Steeber, D. A.; Gong, S., Multifunctional Stable and Ph-Responsive Polymer Vesicles Formed by Heterofunctional Triblock Copolymer for Targeted Anticancer Drug Delivery and Ultrasensitive Mr Imaging. *ACS Nano* **2010**, *4*, 6805-6817.

- [97] You, L.; Schlaad, H., An Easy Way to Sugar-Containing Polymer Vesicles or Glycosomes. *J. Am. Chem. Soc.* **2006**, *128*, 13336-13337.
- [98] van Dongen, S. F. M.; Nallani, M.; Schoffelen, S.; Cornelissen, J. J. L. M.; Nolte, R. J. M.; van Hest, J. C. M., A Block Copolymer for Functionalisation of Polymersome Surfaces. *Macromol. Rapid Commun.* **2008**, *29*, 321-325.
- [99] Li, B.; Martin, A. L.; Gillies, E. R., Multivalent Polymer Vesicles Via Surface Functionalization. *Chem. Commun.* **2007**, 5217-5219.
- [100] Brož, P.; Benito, S. M.; Saw, C.; Burger, P.; Heider, H.; Pfisterer, M.; Marsch, S.; Meier, W.; Hunziker, P., Cell Targeting by a Generic Receptor-Targeted Polymer Nanocontainer Platform. *J. Controlled Release* **2005**, *102*, 475-488.
- [101] Lin, J. J.; Silas, J. A.; Bermudez, H.; Milam, V. T.; Bates, F. S.; Hammer, D. A., The Effect of Polymer Chain Length and Surface Density on the Adhesiveness of Functionalized Polymersomes. *Langmuir* **2004**, *20*, 5493-5500.
- [102] Rigler, P.; Meier, W., Encapsulation of Fluorescent Molecules by Functionalized Polymeric Nanocontainers: Investigation by Confocal Fluorescence Imaging and Fluorescence Correlation Spectroscopy. *J. Am. Chem. Soc.* **2006**, *128*, 367-373.
- [103] Felici, M.; Marzá-Pérez, M.; Hatzakis, N. S.; Nolte, R. J. M.; Feiters, M. C., B-Cyclodextrin-Appended Giant Amphiphile: Aggregation to Vesicle Polymersomes and Immobilisation of Enzymes. *Chemistry – A European Journal* **2008**, *14*, 9914-9920.
- [104] Guo, M.; Jiang, M.; Zhang, G., Surface Modification of Polymeric Vesicles Via Host–Guest Inclusion Complexation. *Langmuir* **2008**, *24*, 10583-10586.
- [105] Nehring, R.; Palivan, C. G.; Casse, O.; Tanner, P.; Tüxen, J.; Meier, W., Amphiphilic Diblock Copolymers for Molecular Recognition: Metal–Nitrilotriacetic Acid Functionalized Vesicles. *Langmuir* **2009**, *25*, 1122-1130.
- [106] Nehring, R.; Palivan, C. G.; Moreno-Flores, S.; Manton, A.; Tanner, P.; Toca-Herrera, J. L.; Thunemann, A.; Meier, W., Protein Decorated Membranes by Specific Molecular Interactions. *Soft Matter* **2010**, *6*, 2815-2824.
- [107] Paolino, M.; Ennen, F.; Lamponi, S.; Cernescu, M.; Voit, B.; Cappelli, A.; Appelhans, D.; Komber, H., Cyclodextrin-Adamantane Host–Guest Interactions on the Surface of Biocompatible Adamantyl-Modified Glycodendrimers. *Macromolecules* **2013**, *46*, 3215-3227.
- [108] Böhm, I.; Isenbügel, K.; Ritter, H.; Branscheid, R.; Kolb, U., Cyclodextrin and Adamantane Host–Guest Interactions of Modified Hyperbranched Poly(Ethylene Imine) as Mimetics for Biological Membranes. *Angew. Chem.* **2011**, *123*, 8042-8045.
- [109] Granadero, D.; Bordello, J.; Pérez-Alvite, M. J.; Novo, M.; Al-Soufi, W., Host-Guest Complexation Studied by Fluorescence Correlation Spectroscopy: Adamantane–Cyclodextrin Inclusion. *International Journal of Molecular Sciences* **2010**, *11*, 173-188.
- [110] Hallett, F. R.; Watton, J.; Krygsman, P., Vesicle Sizing. *Biophys. J.* **59**, 357-362.
- [111] Pencer, J.; Hallett, F. R., Effects of Vesicle Size and Shape on Static and Dynamic Light Scattering Measurements. *Langmuir* **2003**, *19*, 7488-7497.
- [112] Pecora, R., Dynamic Light Scattering Measurement of Nanometer Particles in Liquids. *J. Nanopart. Res.* **2000**, *2*, 123-131.

- [113] Standart, I., Particle Size Analysis, Dynamic Light Scattering (DLS). **2008**.
- [114] Schmitz, K. S., In *Introduction to Dynamic Light Scattering by Macromolecules*, Academic Press: Oxford, **1990**, pp 319-376.
- [115] Nahire, R.; Haldar, M. K.; Paul, S.; Ambre, A. H.; Meghnani, V.; Layek, B.; Katti, K. S.; Gange, K. N.; Singh, J.; Sarkar, K.; Mallik, S., Multifunctional Polymersomes for Cytosolic Delivery of Gemcitabine and Doxorubicin to Cancer Cells. *Biomaterials* **2014**, *35*, 6482-6497.
- [116] Gräfe, D.; Gaitzsch, J.; Appelhans, D.; Voit, B., Cross-Linked Polymersomes as Nanoreactors for Controlled and Stabilized Single and Cascade Enzymatic Reactions. *Nanoscale* **2014**, *6*, 10752-10761.
- [117] Kuiper, S. M.; Nallani, M.; Vriezema, D. M.; Cornelissen, J. J. L. M.; van Hest, J. C. M.; Nolte, R. J. M.; Rowan, A. E., Enzymes Containing Porous Polymersomes as Nano Reaction Vessels for Cascade Reactions. *Organic & Biomolecular Chemistry* **2008**, *6*, 4315-4318.
- [118] Förster, H., In *Characterization I*, Karge, H. G.; Weitkamp, J., Eds. Springer Berlin Heidelberg: Berlin, Heidelberg, **2004**, pp 337-426.
- [119] Li, F.; Ketelaar, T.; Cohen Stuart, M. A.; Sudhölter, E. J. R.; Leermakers, F. A. M.; Marcelis, A. T. M., Gentle Immobilization of Nonionic Polymersomes on Solid Substrates. *Langmuir* **2007**, *24*, 76-82.
- [120] Shan, Y.; Wang, H., The Structure and Function of Cell Membranes Examined by Atomic Force Microscopy and Single-Molecule Force Spectroscopy. *Chem. Soc. Rev.* **2015**, *44*, 3617-3638.
- [121] Leggett, G. J., In *Surface Analysis – the Principal Techniques*, John Wiley & Sons, Ltd: **2009**, pp 479-562.
- [122] Averett, L. E.; Schoenfish, M. H., Atomic Force Microscope Studies of Fibrinogen Adsorption. *Analyst* **2010**, *135*, 1201-1209.
- [123] Alsteens, D.; Dupres, V.; Yunus, S.; Latgé, J.-P.; Heinisch, J. J.; Dufrière, Y. F., High-Resolution Imaging of Chemical and Biological Sites on Living Cells Using Peak Force Tapping Atomic Force Microscopy. *Langmuir* **2012**, *28*, 16738-16744.
- [124] Heu, C.; Berquand, A.; Elie-Caille, C.; Nicod, L., Glyphosate-Induced Stiffening of Hacat Keratinocytes, a Peak Force Tapping Study on Living Cells. *J. Struct. Biol.* **2012**, *178*, 1-7.
- [125] Foster, B., New Atomic Force Microscopy (AFM) Approaches Life Sciences Gently, Quantitatively, and Correlatively. *Am. Lab* **2012**, *44*, 24.
- [126] Hertz, H., On the Contact of Elastic Solids. *J. reine angew. Math* **1881**, *92*, 156-171.
- [127] Taber, L. A., Large Deflection of a Fluid-Filled Spherical Shell under a Point Load. *Journal of Applied Mechanics* **1982**, *49*, 121-128.
- [128] Jaskiewicz, K.; Makowski, M.; Kappl, M.; Landfester, K.; Kroeger, A., Mechanical Properties of Poly(Dimethylsiloxane)-Block-Poly(2-Methyloxazoline) Polymersomes Probed by Atomic Force Microscopy. *Langmuir* **2012**, *28*, 12629-12636.
- [129] Chen, Q.; Schonherr, H.; Vancso, G. J., Mechanical Properties of Block Copolymer Vesicle Membranes by Atomic Force Microscopy. *Soft Matter* **2009**, *5*, 4944-4950.

- [130] Gaitzsch, J.; Appelhans, D.; Janke, A.; Stempel, M.; Schwille, P.; Voit, B., Cross-Linked and Ph Sensitive Supported Polymer Bilayers from Polymersomes - Studies Concerning Thickness, Rigidity and Fluidity. *Soft Matter* **2014**, *10*, 75-82.
- [131] Delorme, N.; Fery, A., Direct Method to Study Membrane Rigidity of Small Vesicles Based on Atomic Force Microscope Force Spectroscopy. *Physical Review E* **2006**, *74*, 030901.
- [132] Liang, X.; Mao, G.; Ng, K. Y. S., Mechanical Properties and Stability Measurement of Cholesterol-Containing Liposome on Mica by Atomic Force Microscopy. *J. Colloid Interface Sci.* **2004**, *278*, 53-62.
- [133] Li, S.; Palmer, A. F., Structure and Mechanical Response of Self-Assembled Poly(Butadiene)-B-Poly(Ethylene Oxide) Colloids Probed by Atomic Force Microscopy. *Macromolecules* **2005**, *38*, 5686-5698.
- [134] Fery, A.; Weinkamer, R., Mechanical Properties of Micro- and Nanocapsules: Single-Capsule Measurements. *Polymer* **2007**, *48*, 7221-7235.
- [135] Calo, A.; Reguera, D.; Oncins, G.; Persuy, M.-A.; Sanz, G.; Lobasso, S.; Corcelli, A.; Pajot-Augy, E.; Gomila, G., Force Measurements on Natural Membrane Nanovesicles Reveal a Composition-Independent, High Young's Modulus. *Nanoscale* **2014**, *6*, 2275-2285.
- [136] Nardin, C.; Hirt, T.; Leukel, J.; Meier, W., Polymerized ABA Triblock Copolymer Vesicles. *Langmuir* **2000**, *16*, 1035-1041.
- [137] Cabane, E.; Malinova, V.; Meier, W., Synthesis of Photocleavable Amphiphilic Block Copolymers: Toward the Design of Photosensitive Nanocarriers. *Macromol. Chem. Phys.* **2010**, *211*, 1847-1856.
- [138] Williams, D. B.; Carter, C. B., In *Transmission Electron Microscopy: A Textbook for Materials Science*, Springer US: Boston, MA, **1996**, pp 3-17.
- [139] Almgren, M.; Edwards, K.; Karlsson, G., Cryo Transmission Electron Microscopy of Liposomes and Related Structures. *Colloids Surf. Physicochem. Eng. Aspects* **2000**, *174*, 3-21.
- [140] Kuntsche, J.; Horst, J. C.; Bunjes, H., Cryogenic Transmission Electron Microscopy (Cryo-Tem) for Studying the Morphology of Colloidal Drug Delivery Systems. *Int. J. Pharm.* **2011**, *417*, 120-137.
- [141] Voit, B.; Haag, R.; Appelhans, D.; Welzel, P. B., In *Bio- and Multifunctional Polymer Architectures*, John Wiley & Sons, Inc: **2016**, pp 113-186.
- [142] Won, Y.-Y.; Brannan, A. K.; Davis, H. T.; Bates, F. S., Cryogenic Transmission Electron Microscopy (Cryo-Tem) of Micelles and Vesicles Formed in Water by Poly(Ethylene Oxide)-Based Block Copolymers. *The Journal of Physical Chemistry B* **2002**, *106*, 3354-3364.
- [143] Kim, K. T.; Meeuwissen, S. A.; Nolte, R. J. M.; van Hest, J. C. M., Smart Nanocontainers and Nanoreactors. *Nanoscale* **2010**, *2*, 844-858.
- [144] Renggli, K.; Baumann, P.; Langowska, K.; Onaca, O.; Bruns, N.; Meier, W., Selective and Responsive Nanoreactors. *Adv. Funct. Mater.* **2011**, *21*, 1241-1259.
- [145] Gaitzsch, J.; Huang, X.; Voit, B., Engineering Functional Polymer Capsules toward Smart Nanoreactors. *Chem. Rev.* **2016**, *116*, 1053-1093.

- [146] Vriezema, D. M.; Comellas Aragonès, M.; Elemans, J. A. A. W.; Cornelissen, J. J. L. M.; Rowan, A. E.; Nolte, R. J. M., Self-Assembled Nanoreactors. *Chem. Rev.* **2005**, *105*, 1445-1490.
- [147] Ahmed, F.; Pakunlu, R. I.; Brannan, A.; Bates, F.; Minko, T.; Discher, D. E., Biodegradable Polymersomes Loaded with Both Paclitaxel and Doxorubicin Permeate and Shrink Tumors, Inducing Apoptosis in Proportion to Accumulated Drug. *J. Controlled Release* **2006**, *116*, 150-158.
- [148] Onaca, O.; Enea, R.; Hughes, D. W.; Meier, W., Stimuli-Responsive Polymersomes as Nanocarriers for Drug and Gene Delivery. *Macromol. Biosci.* **2009**, *9*, 129-139.
- [149] Upadhyay, K. K.; Mishra, A. K.; Chuttani, K.; Kaul, A.; Schatz, C.; Le Meins, J.-F.; Misra, A.; Lecommandoux, S., The in Vivo Behavior and Antitumor Activity of Doxorubicin-Loaded Poly(Γ -Benzyl L-Glutamate)-Block-Hyaluronan Polymersomes in Ehrlich Ascites Tumor-Bearing Balb/C Mice. *Nanomed. Nanotechnol. Biol. Med.* **2012**, *8*, 71-80.
- [150] Gaitzsch, J.; Appelhans, D.; Wang, L.; Battaglia, G.; Voit, B., Synthetic Bio-Nanoreactor: Mechanical and Chemical Control of Polymersome Membrane Permeability. *Angew. Chem. Int. Ed.* **2012**, *51*, 4448-4451.
- [151] Schoonen, L.; van Hest, J. C. M., Compartmentalization Approaches in Soft Matter Science: From Nanoreactor Development to Organelle Mimics. *Adv. Mater.* **2016**, *28*, 1109-1128.
- [152] Egli, S.; Nussbaumer, M. G.; Balasubramanian, V.; Chami, M.; Bruns, N.; Palivan, C., Biocompatible Functionalization of Polymersome Surfaces: A New Approach to Surface Immobilization and Cell Targeting Using Polymersomes. *J. Am. Chem. Soc.* **2011**, *133*.
- [153] Liu, Q.; Boyd, B. J., Liposomes in Biosensors. *Analyst* **2013**, *138*, 391-409.
- [154] Goral, V. N.; Zaytseva, N. V.; Baeumner, A. J., Electrochemical Microfluidic Biosensor for the Detection of Nucleic Acid Sequences. *Lab on a Chip* **2006**, *6*, 414-421.
- [155] Katoh, S.; Sohma, Y.; Mori, Y.; Fujita, R.; Sada, E.; Kishimura, M.; Fukuda, H., Homogeneous Immunoassay of Polyclonal Antibodies by Use of Antigen-Coupled Liposomes. *Biotechnol. Bioeng.* **1993**, *41*, 862-867.
- [156] Ho, J.-a. A.; Zeng, S.-C.; Huang, M.-R.; Kuo, H.-Y., Development of Liposomal Immunosensor for the Measurement of Insulin with Femtomole Detection. *Anal. Chim. Acta* **2006**, *556*, 127-132.
- [157] Sasaki, Y.; Shioyama, Y.; Tian, W.-J.; Kikuchi, J.-i.; Hiyama, S.; Moritani, Y.; Suda, T., A Nanosensory Device Fabricated on a Liposome for Detection of Chemical Signals. *Biotechnol. Bioeng.* **2010**, *105*, 37-43.
- [158] Yoshimoto, M.; Iida, C.; Kariya, A.; Takaki, N.; Nakayama, M., A Biosensor Composed of Glucose Oxidase-Containing Liposomes and MnO₂-Based Layered Nanocomposite. *Electroanalysis* **2010**, *22*, 653-659.
- [159] Cao, X.; Ye, Y.; Liu, S., Gold Nanoparticle-Based Signal Amplification for Biosensing. *Anal. Biochem.* **2011**, *417*, 1-16.

- [160] Wang, R.; Billone, P. S.; Mullett, W. M., Nanomedicine in Action: An Overview of Cancer Nanomedicine on the Market and in Clinical Trials. *J. Nanomaterials* **2013**, *2013*, 1-1.
- [161] Tiwari, P.; Vig, K.; Dennis, V.; Singh, S., Functionalized Gold Nanoparticles and Their Biomedical Applications. *Nanomaterials* **2011**, *1*, 31-63.
- [162] van Dongen, S. F. M.; Nallani, M.; Cornelissen, J. J. L. M.; Nolte, R. J. M.; van Hest, J. C. M., A Three-Enzyme Cascade Reaction through Positional Assembly of Enzymes in a Polymersome Nanoreactor. *Chemistry – A European Journal* **2009**, *15*, 1107-1114.

2 Motivation and Aim

Nature has been always served as an inspiration tool for humans to create new scientific approaches in order to develop novel materials and devices. Indeed, learning from the largest laboratory as being the life itself, has led to an increased number of interdisciplinary studies in the last few decades.¹⁻² In this context, a special interest among scientists is to adapt the knowledge of biological cellular compartments in developing various nanoparticles by mimicking the phospholipid based cell membrane. One of the noteworthy attempts is the invention of liposomes self-assembled in water from analogous phospholipids having hydrophilic head and hydrophobic tails.³ Although these nanoparticles have been very attractive in many biotechnological applications, they lack stability, show undesired permeability and allow limited chemical versatility.⁴ Therefore, the mimicking approach has been taken one step further and polymersomes that are wholly synthetic counterparts of liposomes have been developed. These vesicles are formed by the self-assembly process of amphiphilic block copolymers leading to a bilayer membrane enclosing an aqueous interior phase.⁵⁻⁶ Similarly as liposomes, polymersomes can host both hydrophilic and hydrophobic compounds which is very useful for delivery purposes.⁷⁻⁸ In addition, the artificial nature of these vesicles provides high flexibility in chemical design of the structures which makes them promising nanoparticles in many biomedical applications including drug delivery,⁹⁻¹⁴ synthetic biology¹⁵⁻¹⁹ and usage in microsystem devices such as chemo/biosensors.²⁰⁻²¹ Besides they also show an enhanced stability and reduced permeability²² so that the demand for polymersomes is increasing greatly especially in the field of material science and biotechnology.

Nevertheless, the key challenge to enhance the efficiency in the mentioned application areas is to fabricate robust polymersomes that possess both selective recognition and responsive nature. The responsiveness is necessary for the cargos to be released in a controlled way when polymersomes are used as nanocontainers or nanoreactors. Among the external stimulus, pH and light triggers are one of the cleanest and feasible ways for designing smart polymersomes. The biological and physiological systems are naturally prone to pH variation, like having more acidic environment for inflamed tissue or cancerous cells.²³⁻²⁴ Besides, light is already very convenient for biomedical applications since it does not even require any additional chemicals to be triggered.²⁵ Although such triggers can provide controlled release of the cargos, e.g. drugs, they are still inadequate for specific targeting to certain disease sites or ligands in the scope of the application. To solve this

problem, selective recognition has arisen as the second tool by providing specific receptor-ligand interactions to the nanocarriers which are active solely for confined and targeted regions. For instance, it is useful to increase the therapeutic efficiency of drug delivery systems by enabling the release of the drugs only at the certain diseased cells through recognitive molecules. Besides, specific recognition is also very beneficial for sensing devices as well as to perform selective reactions in the scope of synthetic biology. In order to realize this property, polymersome surface functionalization can be used to conjugate desired reactive groups as well as targeting ligands to the vesicle periphery.¹⁴ Apart from that, polymersome stability is another concern since they can encounter disassembly problems due to shear forces or dilution effects either in the blood circulation system or in the manufacturing steps. To overcome this problem, cross-linking the membrane^{12,15} is a promising way to have enhanced mechanical and chemical strength. In this point, gathering information about the mechanical properties of the polymersomes is of significant importance to know the limits of the applicability of these soft particles.

As seen, all these above-mentioned abilities are fulfilling some functions in the varied biomedical applications. Although some of them have already been introduced individually to polymersomes, it is rare to combine all these properties into one single system having the simultaneous recognition and delivery capability for intelligent nanocontainers and nanoreactors. The term multifunctionality is coined in this point meaning that the single polymersome system possess more than one property which can function either simultaneously or separately. As stated above, these properties are responsiveness and/or functional groups. The latter ability can open up new opportunities in the case of sufficient reactivity and accessibility to increase their use in microsystem technology for designing specific compartments as well as building sensing devices. Such kind of devices can be used for different purposes like creating cell-mimicking platforms to study the complex biomacromolecule functions and interactions. Indeed, this is possible if the polymersomes are connected to a solid surface or to other systems like hydrogels or polymeric microchannel. When they are immobilized onto a solid surface, this also enables to perform deeper analysis and characterization of the polymersomes with advanced microscopy techniques like AFM. This field is quite less investigated in comparison to the delivery applications and therefore the number of studies concerning surface immobilization and probing the various functions of polymersomes in these confined states have to be increased.

In this regard, the overall goal of this study is to develop multifunctional and stimuli-responsive polymersomes possessing various abilities including pH, UV and IR light sensitivity as well as many sequentially accessible reactive groups for selective recognition systems in the scope of biomedical applications, e.g. designing sensing devices. In the way of reaching this goal, the following objectives are also addressed in this thesis:

- (i) The synthesis of polymersome forming amphiphilic, photocrosslinkable and pH sensitive block copolymers comprising azide and adamantane groups is aimed for further post-functionalization steps through click chemistry and host-guest interaction.
- (ii) Sequential post-conjugation is the second objective to evaluate the accessibility and reactivity of the functional groups on polymersome surface. In this stage, photo active groups as nitroveratryloxycarbonyl (NVOC) protected amine molecules are also integrated as IR or UV cleavable moieties.
- (iii) The immobilization of the developed polymersomes onto solid substrates is another target to perform infrared light induced selective photochemical reactions as well as probing pH response and mechanical properties through AFM under wet state. Herein, the attachment of model fluorescent compounds mimicking biorecognition molecules, onto locally released amine groups on polymersome surface by IR trigger is also aimed to fulfill the selective recognition concept for biomedical applications.
- (iv) Lastly, to assess the hosting ability and membrane permeability limits of the established polymersomes as nanocontainers, incorporation of 5 to 10 nm sized gold nanoparticles as well as doxorubicin molecules as an anticancer drug is performed.

Each of the above-mentioned sub-objectives are discussed in detail starting from the design and formation in chapter 3 and continued with the capability as nanocontainers in chapter 4. The last two chapters of results and discussion are devoted to immobilized multifunctional polymersomes focusing on firstly photoreactivity and pH responsivity at confined states in chapter 5 and lastly probing mechanical properties in chapter 6.

References

- [1] Aizenberg, J.; Fratzl, P., Biological and Biomimetic Materials. *Adv. Mater.* **2009**, *21*, 387-388.
- [2] Fratzl, P., Biomimetic Materials Research: What Can We Really Learn from Nature's Structural Materials? *Journal of The Royal Society Interface* **2007**, *4*, 637-642.

- [3] Bangham, A. D.; Horne, R. W., Negative Staining of Phospholipids and Their Structural Modification by Surface-Active Agents as Observed in the Electron Microscope. *J. Mol. Biol.* **1964**, *8*, 660-110.
- [4] Antonietti, M.; Förster, S., Vesicles and Liposomes: A Self-Assembly Principle Beyond Lipids. *Adv. Mater.* **2003**, *15*, 1323-1333.
- [5] Discher, B. M.; Won, Y.-Y.; Ege, D. S.; Lee, J. C.-M.; Bates, F. S.; Discher, D. E.; Hammer, D. A., Polymersomes: Tough Vesicles Made from Diblock Copolymers. *Science* **1999**, *284*, 1143-1146.
- [6] Discher, D. E.; Eisenberg, A., Polymer Vesicles. *Science* **2002**, *297*, 967-973.
- [7] Messenger, L.; Gaitzsch, J.; Chierico, L.; Battaglia, G., Novel Aspects of Encapsulation and Delivery Using Polymersomes. *Curr. Opin. Pharmacol.* **2014**, *18*, 104-111.
- [8] Chandrawati, R.; Caruso, F., Biomimetic Liposome- and Polymersome-Based Multicompartmentalized Assemblies. *Langmuir* **2012**, *28*, 13798-13807.
- [9] Ahmed, F.; Pakunlu, R. I.; Brannan, A.; Bates, F.; Minko, T.; Discher, D. E., Biodegradable Polymersomes Loaded with Both Paclitaxel and Doxorubicin Permeate and Shrink Tumors, Inducing Apoptosis in Proportion to Accumulated Drug. *J. Controlled Release* **2006**, *116*, 150-158.
- [10] Onaca, O.; Enea, R.; Hughes, D. W.; Meier, W., Stimuli-Responsive Polymersomes as Nanocarriers for Drug and Gene Delivery. *Macromol. Biosci.* **2009**, *9*, 129-139.
- [11] Upadhyay, K. K.; Mishra, A. K.; Chuttani, K.; Kaul, A.; Schatz, C.; Le Meins, J.-F.; Misra, A.; Lecommandoux, S., The in Vivo Behavior and Antitumor Activity of Doxorubicin-Loaded Poly(Γ -Benzyl L-Glutamate)-Block-Hyaluronan Polymersomes in Ehrlich Ascites Tumor-Bearing Balb/C Mice. *Nanomed. Nanotechnol. Biol. Med.* **2012**, *8*, 71-80.
- [12] Yassin, M. A.; Appelhans, D.; Wiedemuth, R.; Formanek, P.; Boye, S.; Lederer, A.; Temme, A.; Voit, B., Overcoming Concealment Effects of Targeting Moieties in the Peg Corona: Controlled Permeable Polymersomes Decorated with Folate-Antennae for Selective Targeting of Tumor Cells. *Small* **2015**, *11*, 1580-1591.
- [13] Meng, F.; Zhong, Z.; Feijen, J., Stimuli-Responsive Polymersomes for Programmed Drug Delivery. *Biomacromolecules* **2009**, *10*, 197-209.
- [14] Pawar, P. V.; Gohil, S. V.; Jain, J. P.; Kumar, N., Functionalized Polymersomes for Biomedical Applications. *Polymer Chemistry* **2013**, *4*, 3160-3176.
- [15] Gräfe, D.; Gaitzsch, J.; Appelhans, D.; Voit, B., Cross-Linked Polymersomes as Nanoreactors for Controlled and Stabilized Single and Cascade Enzymatic Reactions. *Nanoscale* **2014**, *6*, 10752-10761.
- [16] Renggli, K.; Baumann, P.; Langowska, K.; Onaca, O.; Bruns, N.; Meier, W., Selective and Responsive Nanoreactors. *Adv. Funct. Mater.* **2011**, *21*, 1241-1259.
- [17] Gaitzsch, J.; Huang, X.; Voit, B., Engineering Functional Polymer Capsules toward Smart Nanoreactors. *Chem. Rev.* **2016**, *116*, 1053-1093.
- [18] Vriezema, D. M.; Comellas Aragonès, M.; Elemans, J. A. A. W.; Cornelissen, J. J. L. M.; Rowan, A. E.; Nolte, R. J. M., Self-Assembled Nanoreactors. *Chem. Rev.* **2005**, *105*, 1445-1490.

- [19] Schoonen, L.; van Hest, J. C. M., Compartmentalization Approaches in Soft Matter Science: From Nanoreactor Development to Organelle Mimics. *Adv. Mater.* **2016**, *28*, 1109-1128.
- [20] Egly, S.; Nussbaumer, M. G.; Balasubramanian, V.; Chami, M.; Bruns, N.; Palivan, C.; Meier, W., Biocompatible Functionalization of Polymersome Surfaces: A New Approach to Surface Immobilization and Cell Targeting Using Polymersomes. *J. Am. Chem. Soc.* **2011**, *133*, 4476-4483.
- [21] Grzelakowski, M.; Onaca, O.; Rigler, P.; Kumar, M.; Meier, W., Immobilized Protein-Polymer Nanoreactors. *Small* **2009**, *5*.
- [22] Discher, D. E.; Ahmed, F., Polymersomes. *Annu. Rev. Biomed. Eng.* **2006**, *8*, 323-341.
- [23] Che, H.; van Hest, J. C. M., Stimuli-Responsive Polymersomes and Nanoreactors. *Journal of Materials Chemistry B* **2016**.
- [24] Schmaljohann, D., Thermo- and pH-Responsive Polymers in Drug Delivery. *Adv. Drug Del. Rev.* **2006**, *58*, 1655-1670.
- [25] Liu, G.; Liu, W.; Dong, C.-M., UV- and NIR-Responsive Polymeric Nanomedicines for on-Demand Drug Delivery. *Polymer Chemistry* **2013**, *4*, 3431-3443.

II. Results and Discussion

3 Multifunctional and Dual-Responsive Polymersomes

3.1 Introduction

It has been already emphasized that multifunctionality in polymersomes is highly demanded in various fields of biomedical applications which enables to fabricate smart nanocontainers that possess both selective recognition and responsive nature. To design and establish such polymersomes, some concerns have to be taken into account. Obviously, the first issue is that the polymersomes should have effective reactive groups attached to their membrane whether before or after the self-assembly process. Herein, both approaches are favored starting with the functional block copolymers synthesis having adamantane and azide end groups in their structure and proceeded by post-modification of the preformed polymersome surface with photoactive groups. As can be inferred, polymersomes should show a stable and robust behavior without facing any disassembly problems within these whole applied fabrication steps. In addition, shear forces or dilution effects during blood circulation when used as drug carriers,¹⁻² and also possible stability problems during manufacturing steps when commercializing these particles are another issue in the scope of the design parameters. In order to solve this problem, 2-hydroxy-4-(methacryloyloxy) benzophenone (BMA) units are integrated to the block copolymer structure for photo-crosslinking the membrane by UV-irradiation which is aimed to have enhanced robustness.³ This photo-crosslinking in combination with the pH responsive segments in the block copolymer structure provides tunable membrane permeability which is very favorable in many biomedical applications.

Thus, this chapter describes the fabrication of robust, multifunctional and dual-responsive polymersomes as the basis of this study and it has been already published.⁴ Figure 3.1 outlines the discussed points by starting with the formation of pH responsive and photo-crosslinked polymersomes decorated with adamantane and azide groups in combination with the synthesis of suitably end-modified block copolymers. In addition, the sequential post-modifications steps including the conjugation of nitroveratryloxycarbonyl protected amine (NVOC) molecules as light responsive moieties and further photocleavage step to assess the potential of dual-responsivity is discussed. In the scope of responsiveness, reversible pH dependent swelling/shrinking ability of the polymersomes at different conjugation steps is also analyzed. Eventually, the subsequent β -cyclodextrin attachment to the adamantane groups of the polymersomes is investigated to gain information about the accessibility and reactivity of the functional groups within these sequential post-modification steps.

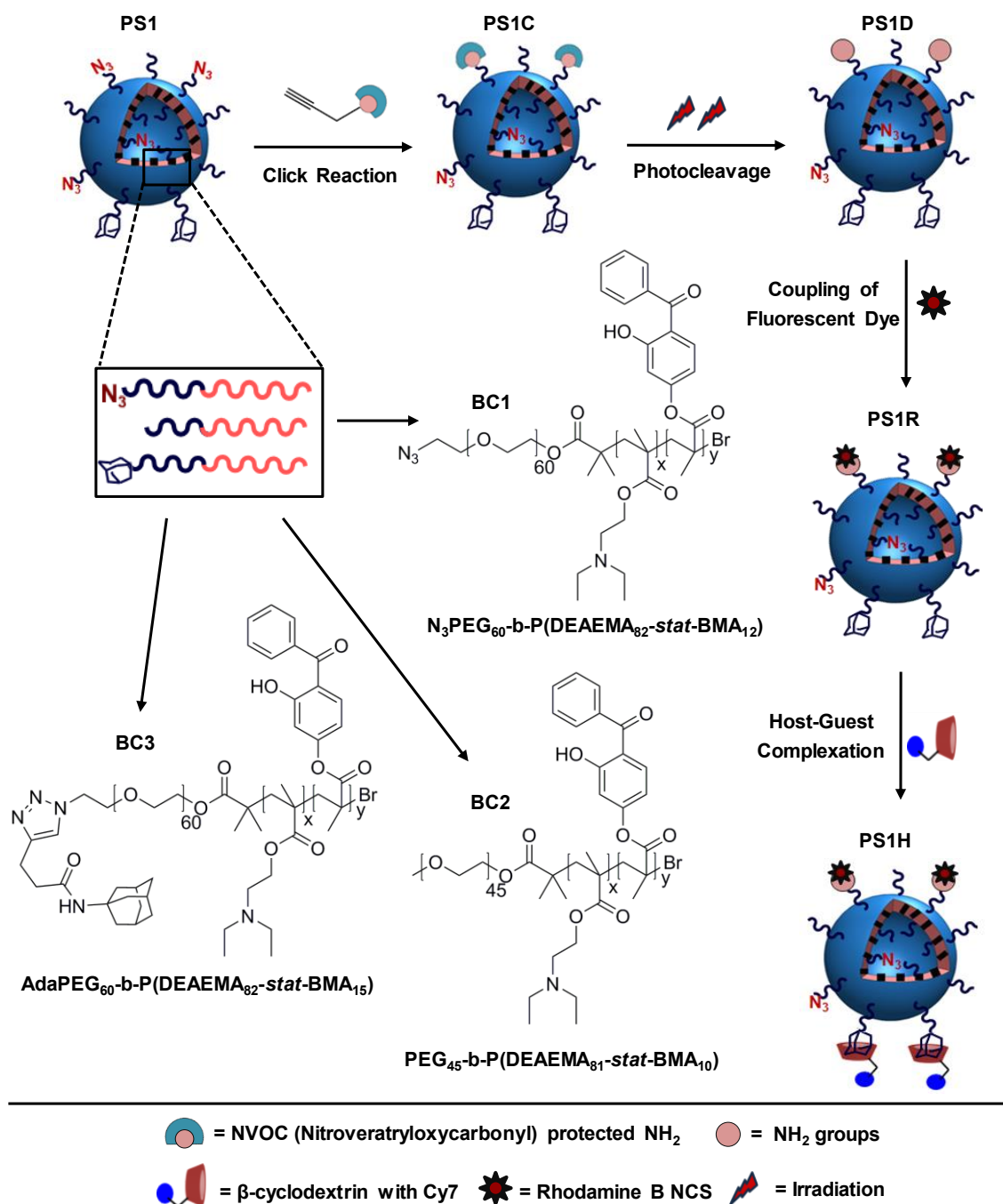


Figure 3.1 Overview of the multifunctional polymersome formation by sequential post-conjugations starting from the self-assembly of block copolymers having azide (BC1), methoxy (BC2) and adamantane (BC3) functionalities

3.2 Block Copolymer Synthesis and Characterization

One of the common methods to prepare multifunctional polymersomes is to conjugate desired functional moieties to the block copolymer structure before starting the self-assembly process. This approach was taken as the basis of this study and required block

copolymers were synthesized with some key features. One essential basis was to ensure the polymersome formation upon self-assembly by assigning the hydrophilic fraction of the block copolymers as the first key feature.⁵ Because it is known that depending on the hydrophilic to hydrophobic ratio together with the balance of all free energy during the self-assembly of copolymers, various morphologies such as micelles, macroscopic aggregates or vesicles may be formed.⁶ Therefore, it is important to produce the block copolymers with a fixed length and having a desired structure. For this purpose, atom transfer radical polymerization (ATRP) was chosen as a controlled polymerization technique to synthesize three block copolymers having azide, adamantane and methoxy end groups at their hydrophilic segment (Figure 3.1, Figure 3.2). Here, azide and adamantane functionalities were the second key features which were chosen to favor ease of click chemistry and host-guest interactions for further post-functionalization steps. The structures of the block copolymers are based on poly(ethylene glycol)-*b*-poly[2-(diethylamino) ethyl methacrylate-*stat*-2-hydroxy-4-(methacryloyloxy) benzophenone] (BC2).³ Herein, poly(ethylene glycol) (PEG) is the hydrophilic segment of the amphiphilic block copolymer whereas pH sensitive 2-(diethylamino)ethyl methacrylate (DEAEM) and a photo cross-linker benzophenone (BMA) groups form together the hydrophobic part. Each block of the polymer was chosen by a purpose to fulfill some essential key properties in biomedical applications. PEG was selected due to its biocompatibility as well as the ability of in-vivo protein resistance that enables long circulation times.⁷ DEAEM was chosen to impart pH responsivity to the polymersome structure and finally BMA was selected to provide robustness as well as tuned membrane permeability. Since the selected approach to form multi-functionalized polymersomes was to mix three block copolymers having different end groups, another issue concerning the homogeneity of the resulting polymersomes was taken into account. Firstly, to induce a homogenous formation for the polymersome membrane (hydrophobic part) from the tertiary system, the hydrophobic block length of the polymers was kept almost equal. However, the hydrophilic length of the azide- and adamantane-functionalized block copolymers (BC1, BC3) was designed to be longer than the non-functional methoxy terminated block copolymer (BC2) to increase the accessibility of the reactive groups on the polymersome surface. This strategy has been successfully applied in the Voit group to conjugate folate molecules to the polymersome system which showed remarkable specificity towards cancer cells.⁸ Therefore, it was also assigned as the last key feature to establish multifunctional polymersomes in the scope of this study.

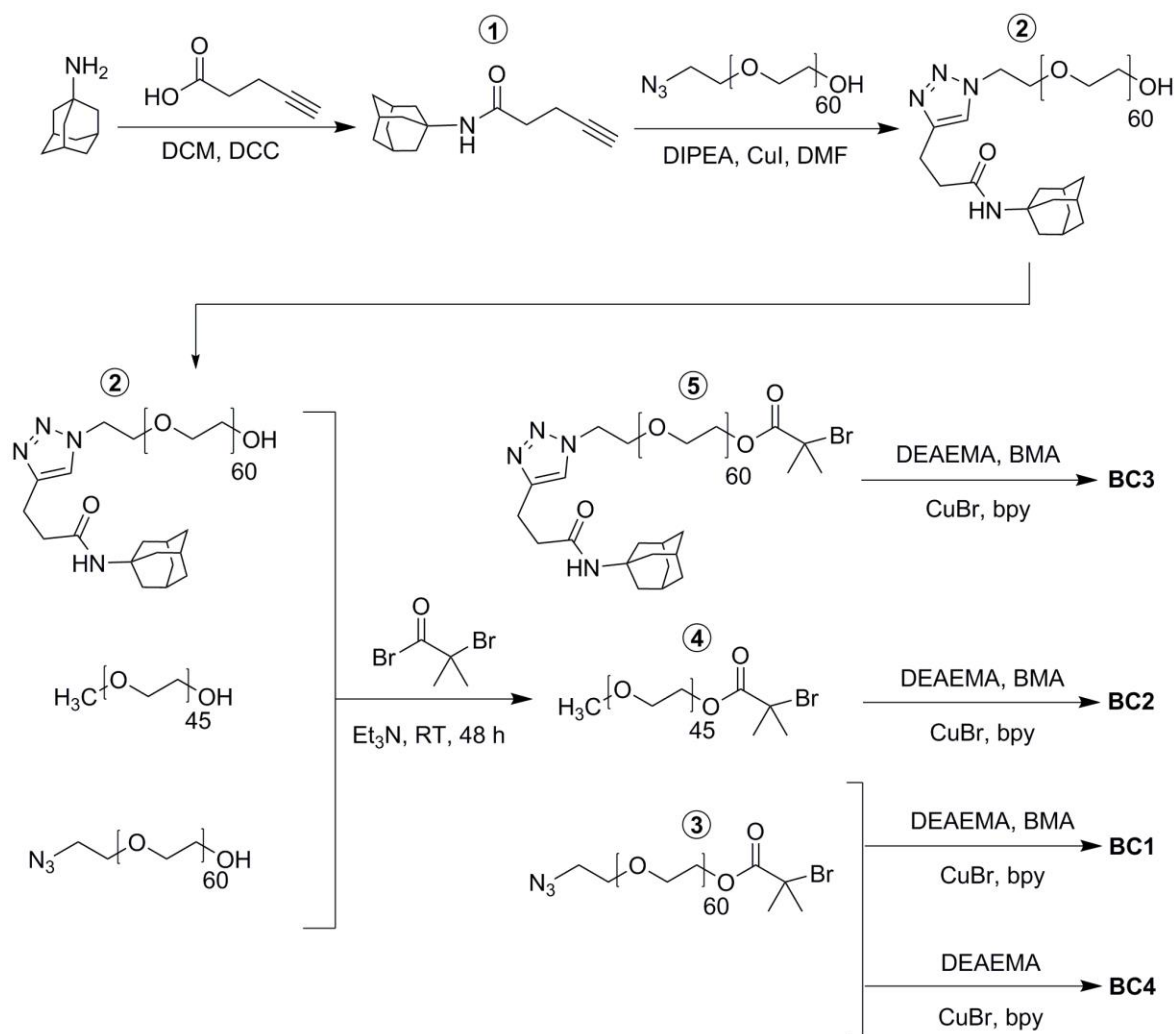


Figure 3.2 Overall synthetic pathway of block copolymers (BC1, BC2, BC3, BC4)

To establish such functional block copolymers, a multi-step synthetic approach was performed as seen in Figure 3.2. The first attempt was to prepare the suitably end-modified PEG molecules for further ATRP process. Although azide and methoxy terminated PEG can be provided commercially, adamantane functionalized PEG was prepared by utilizing copper (I) catalyzed azide/alkyne click chemistry (CuAAC) to provide a high degree of functionalization at moderate reaction conditions.⁹ Thus, the adamantane molecules were firstly modified with alkyne moieties for the click chemistry requirements by reacting carboxylic acid groups of 4-pentynoic acid with the amine moieties of the adamantane molecules. The simple amidation reaction through DCC activation of carboxylic acid results in a successful conjugation which is confirmed by ¹H NMR spectroscopy as shown in Figure 3.3. The next step was to react this purified (see experimental part) yne-modified molecule with commercially available azide-terminated poly(ethylene glycol) (Mn=2700 g/mol). The

confirmation of the conjugation was carried out by ^1H NMR spectroscopy and IR spectroscopy. From ^1H NMR spectrum, all peaks of the adamantane protons and the triazole proton (at 7.52 ppm in CDCl_3 , at 7.74 ppm in DMSO-d_6) were clearly detected (Figure 3.4). Additionally, the disappearance of the azide characteristic peaks at 2104 cm^{-1} after the reaction in IR spectra supported this successful conjugation as well (Figure 3.5). Thus, it is concluded that the ease of click reaction enables to convert all available azide groups in the commercial PEG molecules into adamantane moieties.

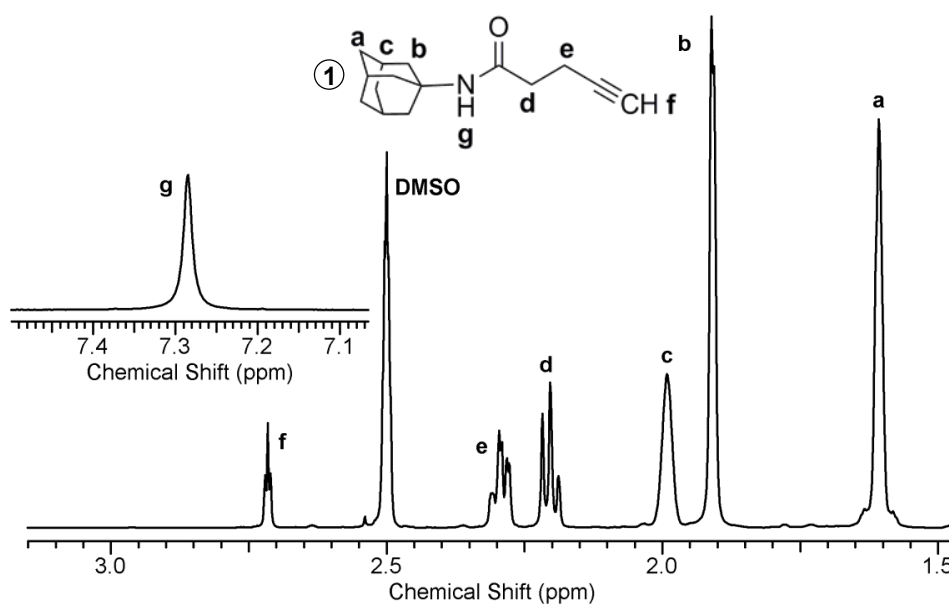


Figure 3.3 ^1H -NMR spectrum of alkyne functionalized adamantane in DMSO-d_6

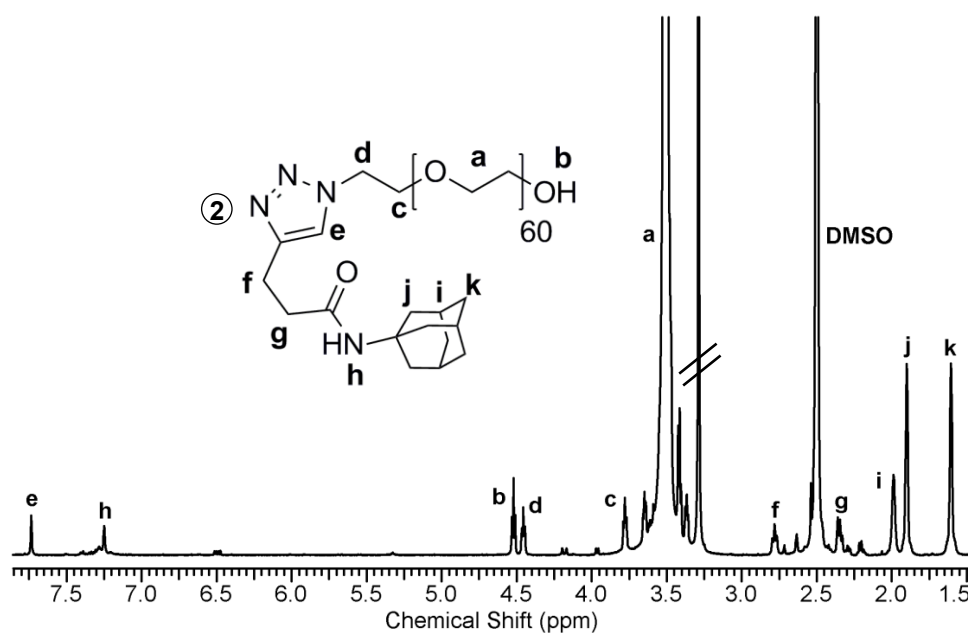


Figure 3.4 ^1H NMR spectrum of adamantane functionalized PEG in DMSO-d_6

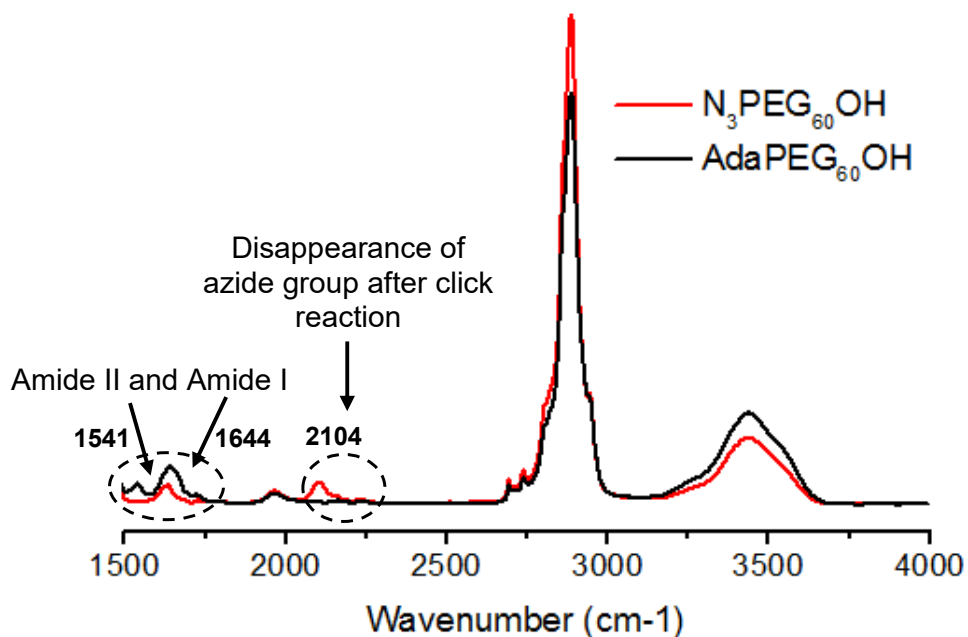


Figure 3.5 IR spectrum of azide/adamantane functionalized poly(ethylene glycol)

Afterwards, the PEG macroinitiators with azide ($N_3PEG_{60}Br$), adamantane ($AdaPEG_{60}Br$) and methoxy ($PEG_{45}Br$) end groups were synthesized for the next polymerization step. The successful coupling of 2-bromoisobutyryl bromide to the hydroxyl groups of PEG molecules was verified by 1H NMR spectroscopy from the appearance of the new signal at 1.95 ppm that corresponds to the six protons of the macroinitiator end group (Figure 3.6, 3.7, and 3.8).

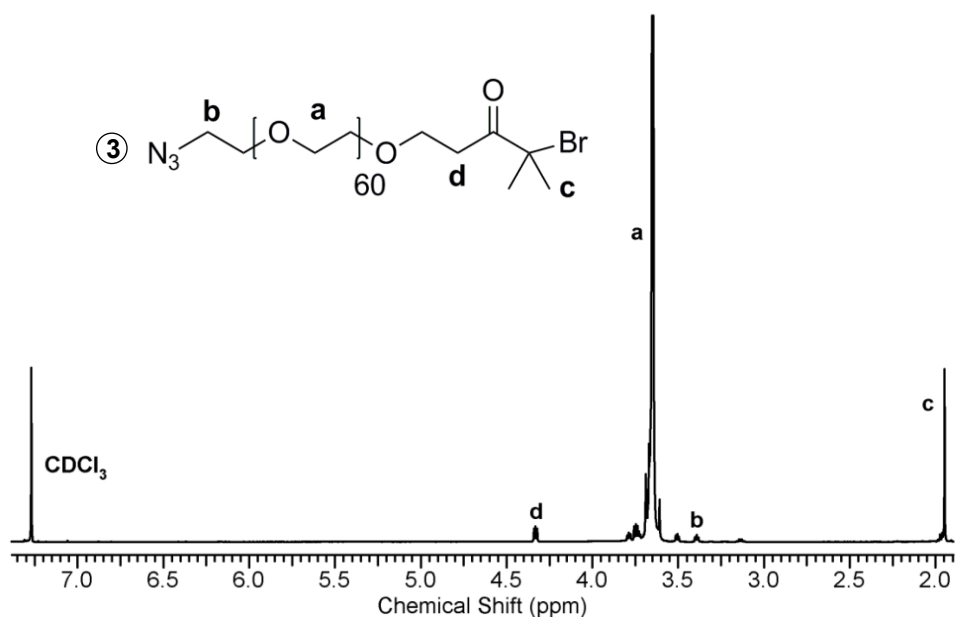


Figure 3.6 1H -NMR spectrum of poly(ethylene glycol) with azide end groups in $CDCl_3$

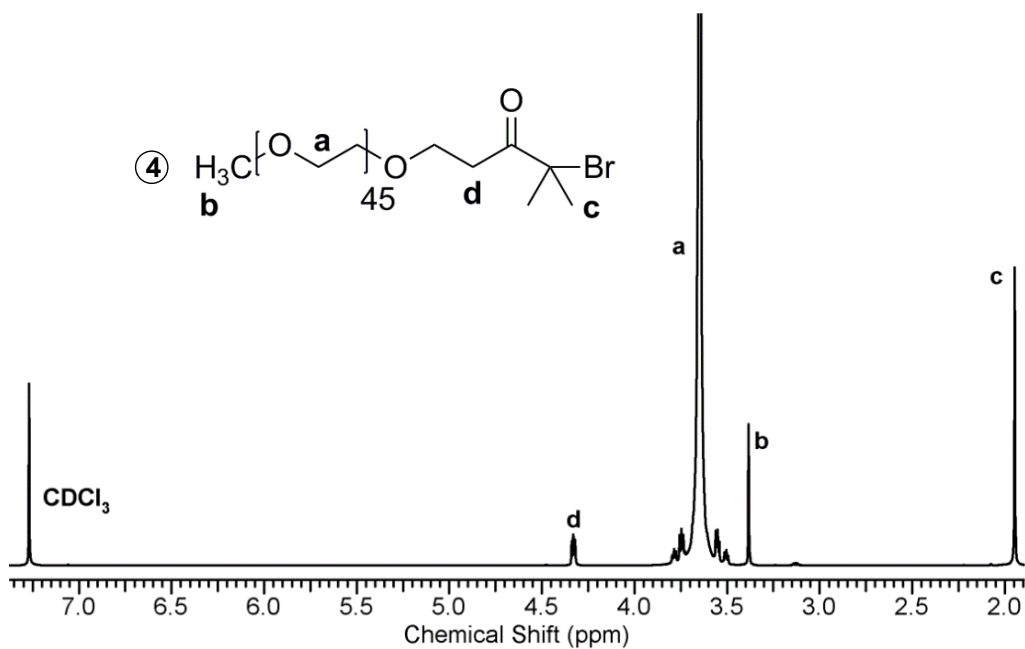


Figure 3.7 $^1\text{H-NMR}$ spectrum of poly(ethylene glycol) with methoxy end groups in CDCl_3

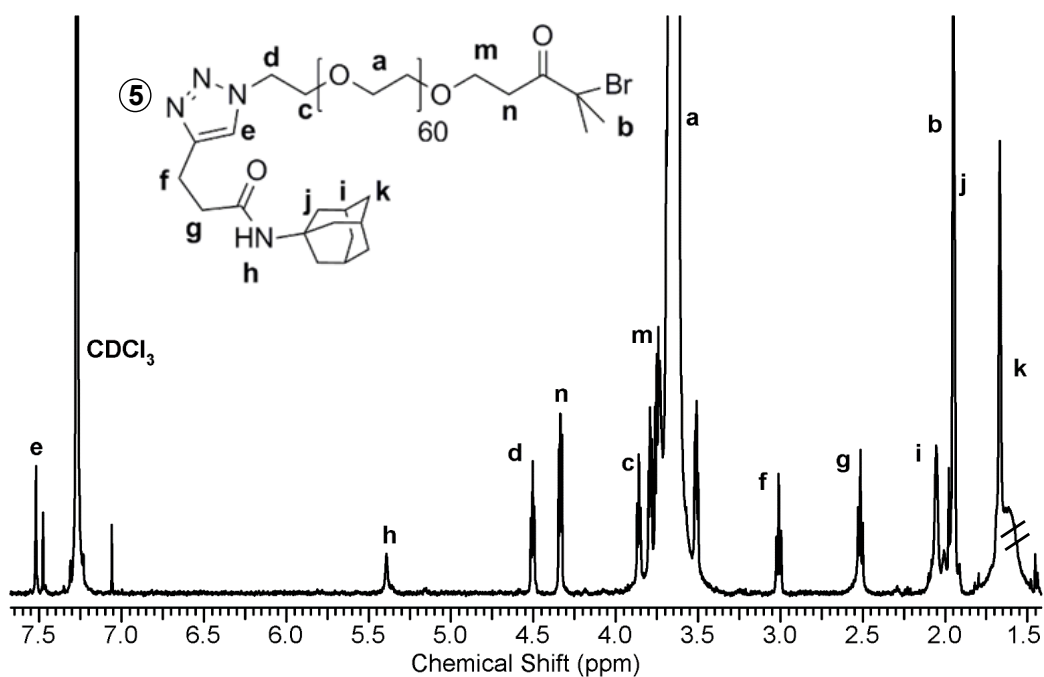


Figure 3.8 $^1\text{H-NMR}$ spectrum of poly(ethylene glycol) with adamantane end groups in CDCl_3

Finally, PEG macroinitiators terminated with corresponding end groups were statistically copolymerized with pH sensitive DEAEM units and photo-crosslinker BMA monomers to establish the desired block copolymers, named as BC1 – BC3. The BMA unit was not used for BC4 synthesis to obtain an azide functionalized polymer without cross-

linker. This polymer was required for the supporting proof approach of photoactive polymersome formation in further steps to distinguish the contributions of two photoactive species. The composition and the number average molecular weight (M_n) of the block copolymers were determined with ^1H NMR spectroscopy from the peak integrals of PEG (signal a, 3.6 ppm), DEAEMA (signal b, 4.2 ppm) and BMA (signal c, 6.6-7.7 ppm) by taking the PEG block as an internal standard (Figure 3.9-3.12, Table 3.1). Herein, the total number of protons of each monomer units has taken into account and related with the equation 3.1 to determine the repeating units of each block of the copolymer. Therein, the analyzed signal of the PEG unit has four protons whereas the DEAEMA and BMA monomers have two and eight protons respectively.

$$PEG : DEAEMA : BMA = \frac{\int sig.a}{4} : \frac{\int sig.b}{2} : \frac{\int sig.c}{8} \quad (3.1)$$

Thus, the length of the hydrophobic block was calculated as about 91 to 97 monomer units using the above equation whereas the photo-crosslinker (BMA) content was found about 10 to 15 repeating units. It should be noted that the feed ratios between the monomers during polymerization reaction are (1: 90: 10) for (PEG: DEAEMA: BMA) respectively (more information is available in section 8.4 of experimental part). The consistence of the feeding molar ratios and the resulted repeating units confirms the controlled nature of the polymerization reaction. Apart from that, in the ^1H NMR spectrum of BC3 polymer, six protons of the adamantane groups could be clearly observed at 1.66 ppm. However, the other two characteristics ^1H NMR signals of the adamantane groups (1.94 ppm, 2.05 ppm) are overlapped by DEAEM signals. Although other signals of adamantane groups are detectable in the spectra, a lower intensity of the corresponding peaks is observed because of the relatively high molar mass of the copolymer (Figure 3.11). This was an expected situation and therefore, the integration of the adamantane group to PEG segment was performed before the polymerization process for monitoring and proving the functionalization step clearly.

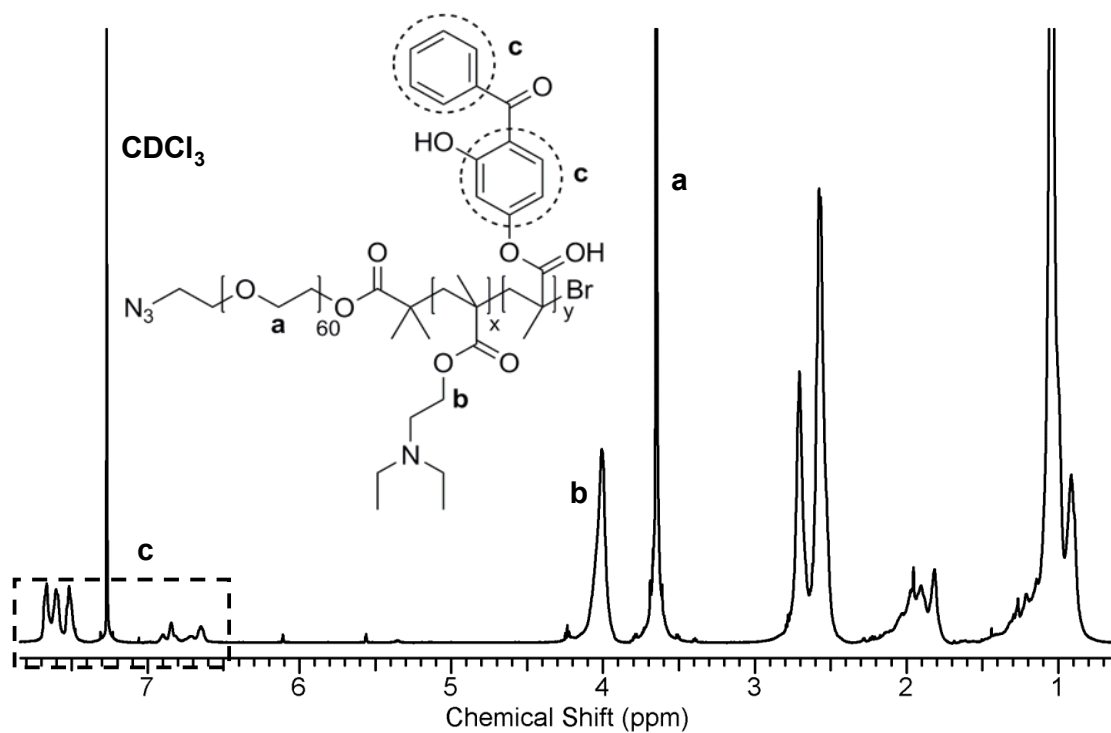


Figure 3.9 $^1\text{H-NMR}$ spectrum of $\text{N}_3\text{PEG}_{60}\text{-b-P}(\text{DEAEMA}_{82}\text{-stat-BMA}_{10})$ (BC1) block copolymer in CDCl_3

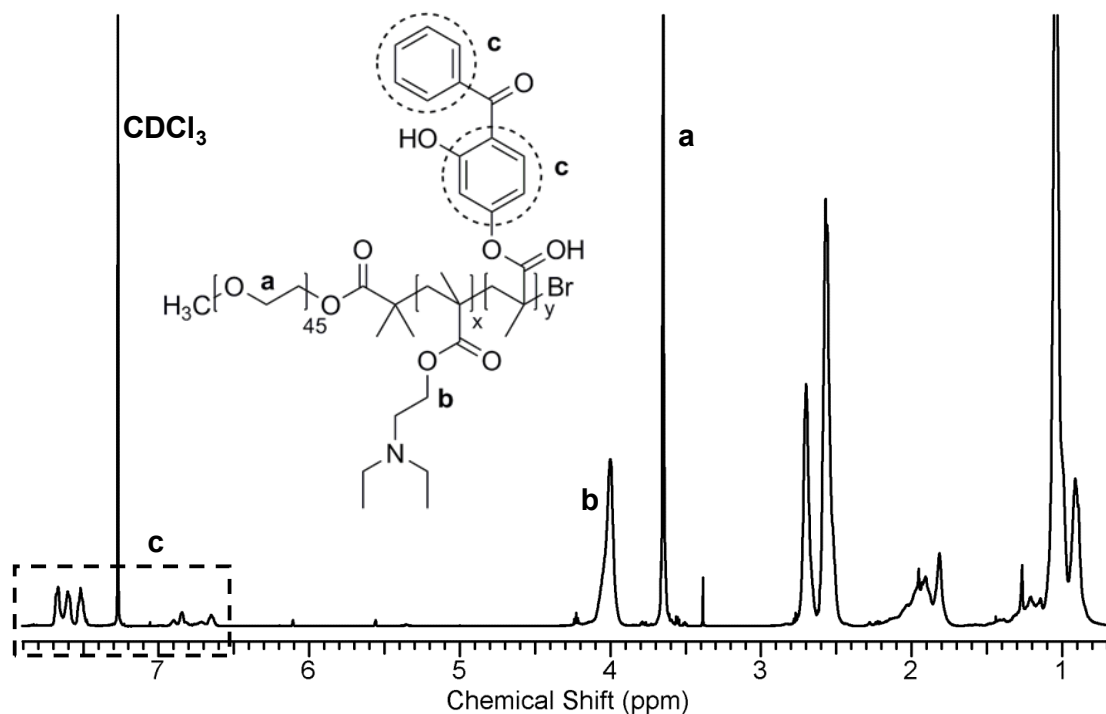


Figure 3.10 $^1\text{H-NMR}$ spectrum of $\text{PEG}_{45}\text{-b-P}(\text{DEAEMA}_{81}\text{-stat-BMA}_{10})$ (BC2) block copolymer in CDCl_3

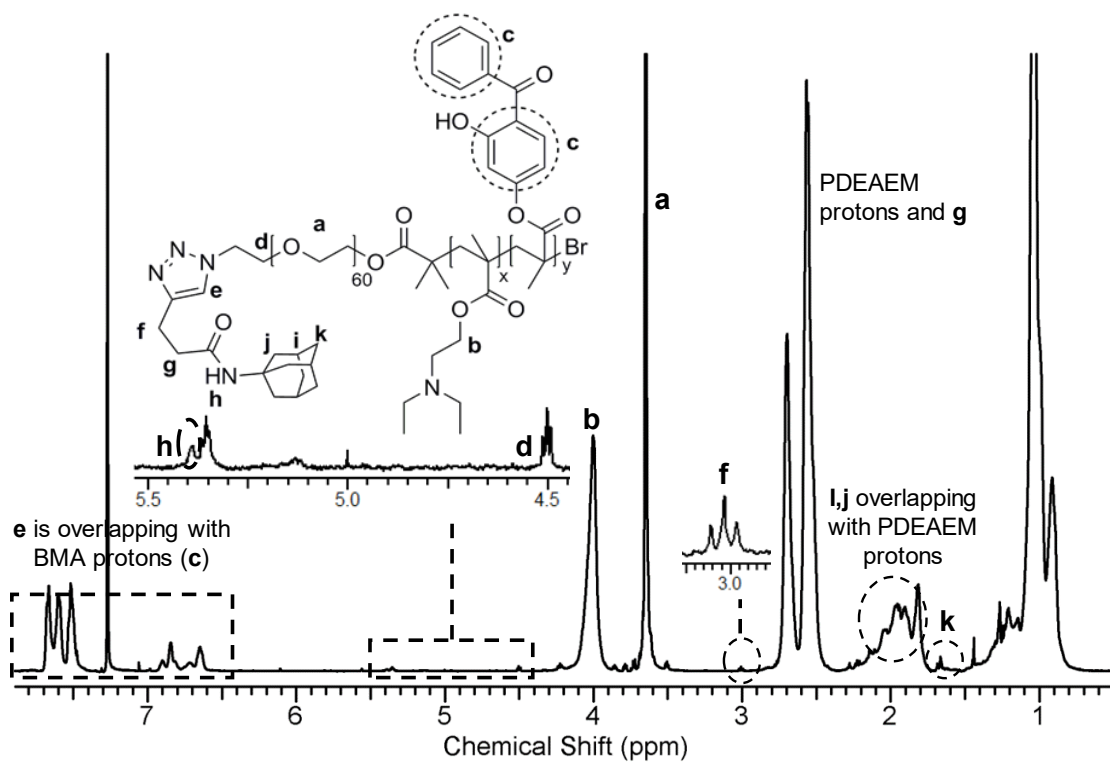


Figure 3.11 $^1\text{H-NMR}$ spectrum of AdaPEG₆₀-b-P(DEAEMA₈₂-*stat*-BMA₁₅) (BC3) block copolymer in CDCl₃

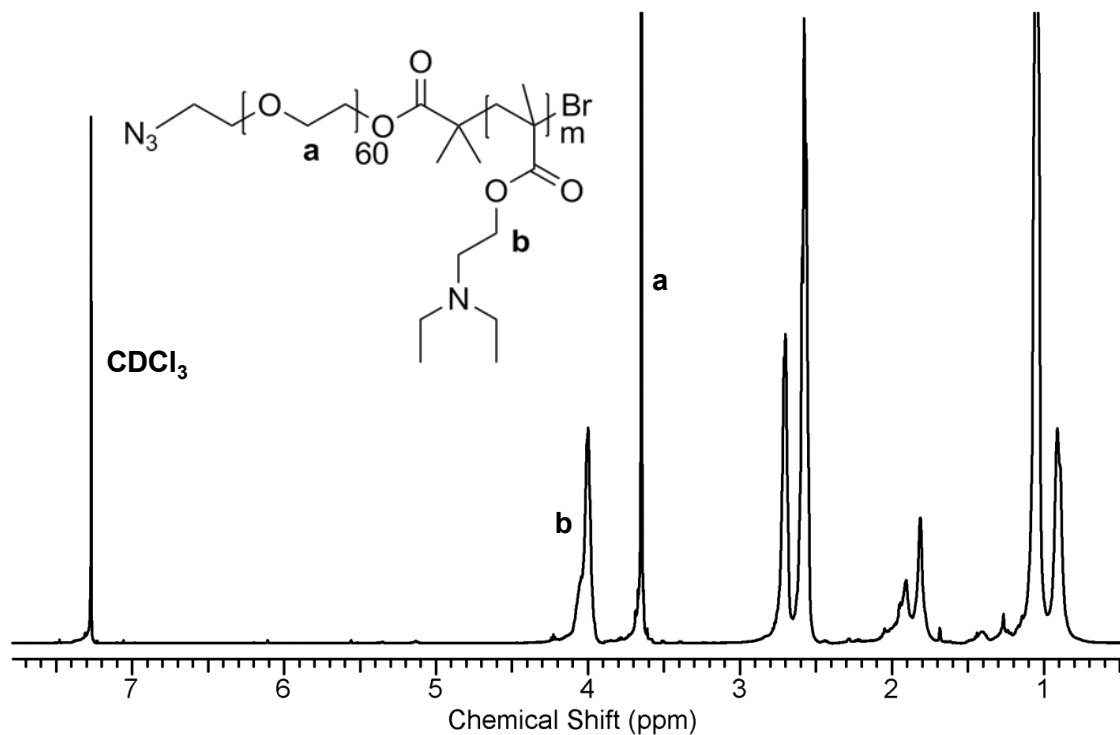


Figure 3.12 $^1\text{H-NMR}$ spectrum of N₃PEG₆₀-b-P(DEAEMA₁₅₀) (BC4) block copolymer in CDCl₃

Additionally, size exclusion chromatography (SEC) analyses showed narrow molar mass distributions (\bar{D}) of the block copolymers in the range of 1.3 to 1.4 which is in agreement with the characteristics of controlled polymerization systems. Herein, the SEC of the block copolymers were performed using DMAC as an eluent in order to avoid the interactions of the polymers with the SEC column. The use of a more polar solvent, like DMAC, in the SEC analysis of charged polymers is a favorable approach which prevents retaining the macromolecules in the column and give a logic result with respect to molecular weight and dispersity. Thus, the synthesized block copolymers with well-defined chemical composition as well as monomodal distribution fulfills the required design criteria for a narrow-dispersed polymersome formation.

Table 3.1 Molecular parameters of polymers synthesized by ATRP

Code	Polymer Chemical Composition	M_n^a (g/mol)	\bar{D}^b (M_w/M_n)	f_{PEG}^c
PEG-Br	PEG ₄₅ -Br	2150	1.07	-
N ₃ PEG-Br	N ₃ PEG ₆₀ -Br	2850	1.23	-
AdaPEG-Br	AdaPEG ₆₀ -Br	3080	1.30	-
BC1	N ₃ PEG ₆₀ -b-P(DEAEMA ₈₂ - <i>stat</i> -BMA ₁₀)	21400	1.35	0.13
BC2	PEG ₄₅ -b-P(DEAEMA ₈₁ - <i>stat</i> -BMA ₁₀)	20000	1.31	0.10
BC3	AdaPEG ₆₀ -b-P(DEAEMA ₈₂ - <i>stat</i> -BMA ₁₅)	22400	1.41	0.13
BC4	N ₃ PEG ₆₀ -b-P(DEAEMA ₁₅₀)	30600	1.17	0.09

^acalculated by ¹H NMR; ^bdetermined by SEC and ^chydrophilic mass fraction is calculated by dividing the PEG molar mass by the total block copolymer mass

3.3 Polymersome Preparation and Characterization

3.3.1 Preparation of Surface-Functionalized Polymersomes

Polymersomes were formed by using the pH switch method in which the mixture of the polymers was self-assembled in aqueous media without the aid of any organic solvent.¹⁰ In brief, tertiary amine groups of the PDEAEM segment are protonated in acidic conditions which enables to dissolve desired polymers in acidic water (pH 2). To obtain multi-functionalized polymersomes, the aqueous (pH 2) mixture of BC1, BC2 and BC3 block

copolymers was prepared. Then, to induce the self-assembly process, deprotonation of the tertiary amine moieties is performed by simply increasing the pH to a basic state (>pH 7). After 4 days of stirring, the final polymersome structure is formed with a bilayer membrane having a central hydrophobic part based on PDEAEM and BMA segments and a hydrophilic inner and outer PEG corona with azide and adamantane functionalities. The specifically designed hydrophilic fraction of about 0.1 enabled to form polymersomes through the self-assembly which is consistent with a previous report on polymersomes based on PEG-PDEAEMA block copolymers having hydrophilic volume fraction of about 0.11.¹¹

Table 3.2 Specifications of unfunctional and multifunctional polymersomes

Polymersome Code	Functional Groups [mol %]		Diameter ^a [nm]		PDI ^b	
	N ₃	Ada	pH 10	pH 5	pH 10	pH 5
PS0	-	-	116±0.4	161±1.5	0.20±0.01	0.18±0.03
PS1	29	9.2	120±1.0	173±1.1	0.20±0.02	0.18±0.01
PS1-2	9.5	9.2	122±1.0	172±1.7	0.19±0.01	0.20±0.01
PS1-3	29	18.4	119±0.3	172±1.9	0.17±0.01	0.14±0.02

^a The pH values were adjusted by 1 M NaOH or 1 M HCl solution to determine the diameter at basic or acidic state. ^bPDI=polydispersity index of polymersomes that shows the size variation.

As a next step, the BMA moieties were used for crosslinking the membrane of the polymersomes by UV irradiation with measured intensity of 80 mW/cm² for 30 minutes. This is another key feature of the multi-functionalized polymersomes to obtain robust and mechanically stable vesicles at different pH values. Since, it is aimed to apply several reaction sequences to a single polymersome system (Figure 3.1), it is essential to avoid any disassembly problems during the whole post-conjugation steps. Therefore, the photo cross-linking is supposed to favor the stability of the vesicles as previously shown by Yassin et al.³ and Gaitzsch et al.¹² In this manner, the prepared polymersomes were firstly characterized by dynamic light scattering (DLS) to determine the size distributions. Table 3.2 shows the hydrodynamic diameter as well as polydispersity index of the unfunctional and multi-functional polymersomes at different pH values. Herein, DLS results show that integrating functional moieties on polymersome surface by the co-assembly process of differently end-functionalized block copolymers has no significant effect on the average

diameter of the vesicles. Additionally, low PDI values in the range of 0.14 to 0.20 demonstrate the monodisperse polymersomes, even when tertiary mixtures of polymers with different end groups were used for the formation of the vesicles. Although it is possible to alter these block copolymer ratios according to the needs, one has to consider the challenges that can be encountered during the self-assembly process. Therefore, among the tested variations of different functionalization degrees (Table 3.2), only a maximum of 18.4 mol% of BC3 were incorporated due to the hydrophobic nature of adamantane groups. The assessed block copolymer ratios do not induce any undesired side effects like individual self-assembly or aggregation problems. In addition, the azide and adamantane functional groups are assumed to be placed homogeneously in the interior and outer region of the bilayer membrane during the formation of surface-functionalized polymersomes as indicated in previous studies.^{8, 13-15} Having sufficient functional groups on the outer region of the polymersomes is a well-known prerequisite for the further step to start a post-conjugation process on polymersome surface as observed in previous studies such as targeted drug delivery systems.^{13-14, 16-20}

3.3.2 pH Responsivity of the Surface-Functionalized Polymersomes

To assess the pH responsive behavior of the cross-linked polymersomes, the stability of the polymersomes was investigated at various pH conditions. Firstly, the size of the PS1 polymersomes in the range of pH 10.1 to pH 3.3 were obtained using DLS equipped with an autotitrator. As seen in Figure 3.13, polymersomes preserve their shape without disassembly at acidic conditions with the aid of the crosslinked membrane. It has been already proven that the vesicles without photo-crosslinking disassembled at acidic state because the polymer chains become hydrophilic due to the protonation of the tertiary amine groups in DEAEM groups and fully dissolved in water.³ However, in the case of cross-linking, the protonated polymer chains at acidic condition repel each other to reach the equilibrium state which in turn leads to an increase in the size of polymersomes. This indeed enables to release any hosted cargo through the pores formed during this swelling condition. Another important investigation from this experiment was that the expected size change of the polymersomes was seen at about pH 7 and this value roughly corresponds to the pKa of the DEAEM groups.²¹ As can be observed, the diameter of the polymersomes are constant before (>pH7-basic) and after (<pH7-acidic) the swelling point. In addition, the mixed block copolymers to form PS1 polymersomes did not make any alteration in the pKa of the resulting vesicles which is supported by zeta potential measurements (Figure 3.14). This was an expected

result since the mixed block copolymers was designed to have relatively equal hydrophobic block lengths that supports also the homogeneous membrane formation. Lastly, the zeta potential values at different pH values revealed that the membrane is almost unprotonated at physiological condition which is favorable for biomedical applications.

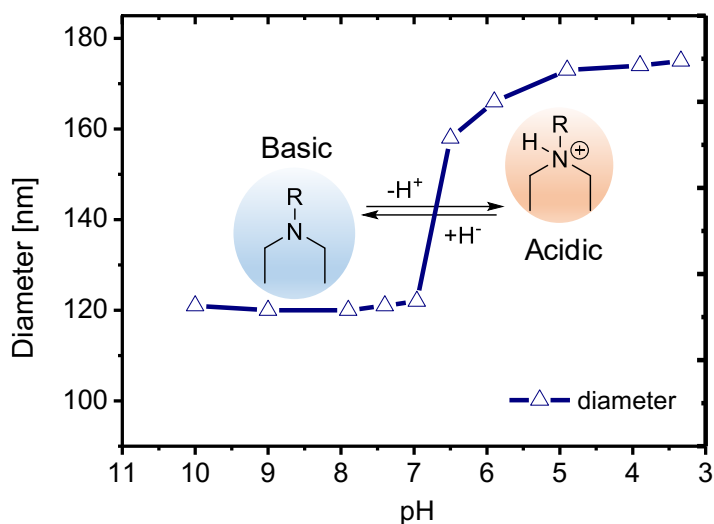


Figure 3.13 pH-dependent diameter variation of multifunctional polymersomes (PS1)

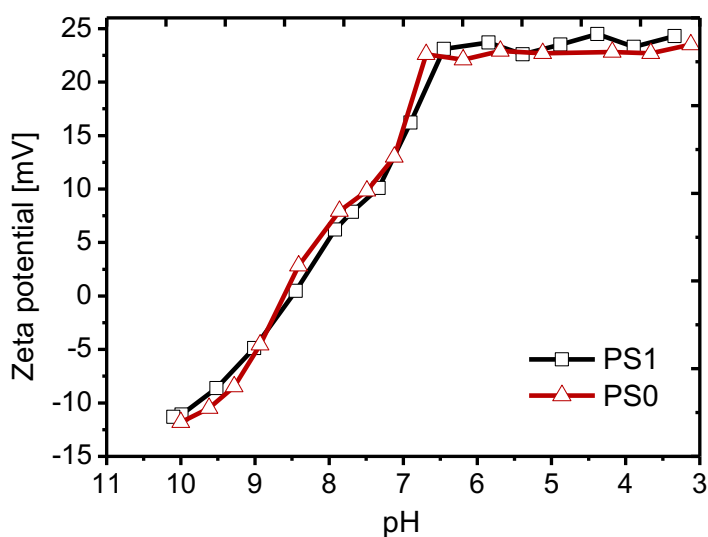


Figure 3.14 Zeta potential variation of multifunctional (PS1) and unfunctional (PS0) polymersomes at different pH values

Further investigation concerning the stability issue was to assess how PS1 polymersomes act upon reversible pH switch for several cycles. This helps to gain information about the tunable membrane permeability which is provided by the cross-linking

process. Thus, this phenomenon was explored by monitoring the size change of the polymersomes upon changes in pH value from basic to acidic state for 5 cycles. The intensity average hydrodynamic diameters measured by DLS at each cycle showed that the multifunctional polymersome was able to swell and shrink reversibly at acidic and basic conditions because of the protonation/deprotonation of the PDEAEM groups in the membrane (Figure 3.15). Here, the size of the vesicles increases about 44.2% in the swollen state and return back to the original diameter in each cycle. In this regard, it is clear that the cross-linking time was sufficient and the polymersomes are thoroughly cross-linked. Otherwise, some polymer chains would have been disassembled due to the leakage of cross-linking and this would result in a size decrease in the cycles of pH switch. Thus, this pH-controlled size alteration allowed considering the permeable polymersome membrane like a gate that can be opened or closed by the trigger of pH stimulus. This is useful in hosting and releasing several biological molecules such as drugs, enzymes and proteins to create intelligent nanocarriers or nanoreactors for various biomedical applications.²²⁻²⁵

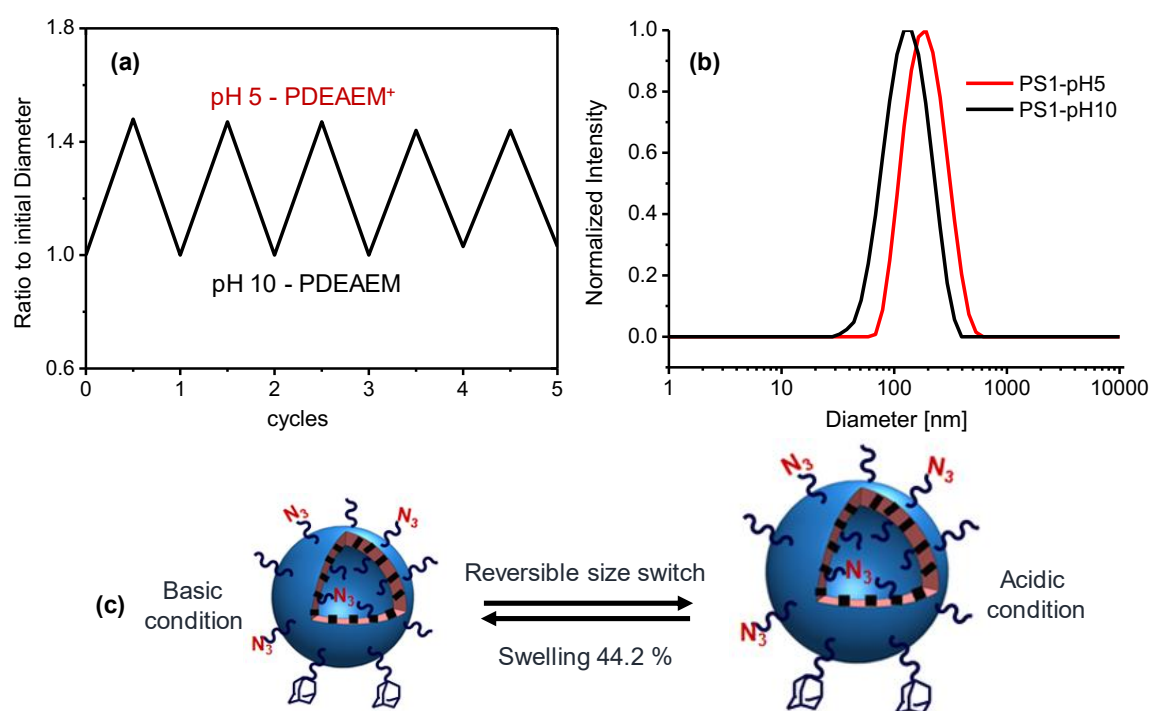


Figure 3.15 (a) Reversible swelling-shrinking of polymersomes (PS1) upon changes in pH value. (b) Intensity size distribution of PS1 polymersomes at pH 5 and pH 10 with average hydrodynamic diameter of 173 nm and 120 nm, respectively. (c) Schematic illustration of reversible size switch at basic and acidic condition.

3.3.3 Shape Visualization and Membrane Thickness

Cryo-TEM investigation was conducted to confirm the vesicular structure of the polymersomes at both acidic and basic conditions (Figure 3.16). Polymersome visualization by cryo-TEM has a great advantage over conventional TEM methods because the native vesicle structure can be imaged in the frozen hydrated state without the aid of sample staining. Sufficient contrast between the polymeric membrane and the vesicle interior filled with water leads to a clear identification of the structure. This enabled to determine the membrane thickness of polymersomes at high and low pH value by analyzing several cryo-TEM micrographs (Figure 3.16). The average membrane thickness increases from 18.6 ± 1.7 nm to 26.8 ± 3.8 nm when changing pH from a basic state (pH 9) to an acidic value (pH 5). This impressively implies that the repelling of polymer chains by protonation of DEAEM segments at acidic condition causes the state of a permeable membrane in polymersome PS1 with azide and adamantane surface groups (Figure 3.16b). The increase of the membrane thickness was calculated to be 44.1%. This is in a perfect agreement with the previous swelling/shrinking experiments as stated above (Figure 3.15). Thus, the cryo-TEM study not only approves the vesicular shape of the polymersomes but also supports the porous membrane formation at acidic condition to enable the pH controlled permeability. Additionally, it was proven that the average thickness of the polymersome membrane was almost 3.5 times thicker than the phospholipid membrane of liposomes which in turn leads to more stable, tougher and, in the collapsed state, tighter polymeric vesicles.²⁶⁻²⁸ Such thick membrane is also useful to avoid undesired leakage of the encapsulated molecules at basic state by providing impermeable polymersomes.

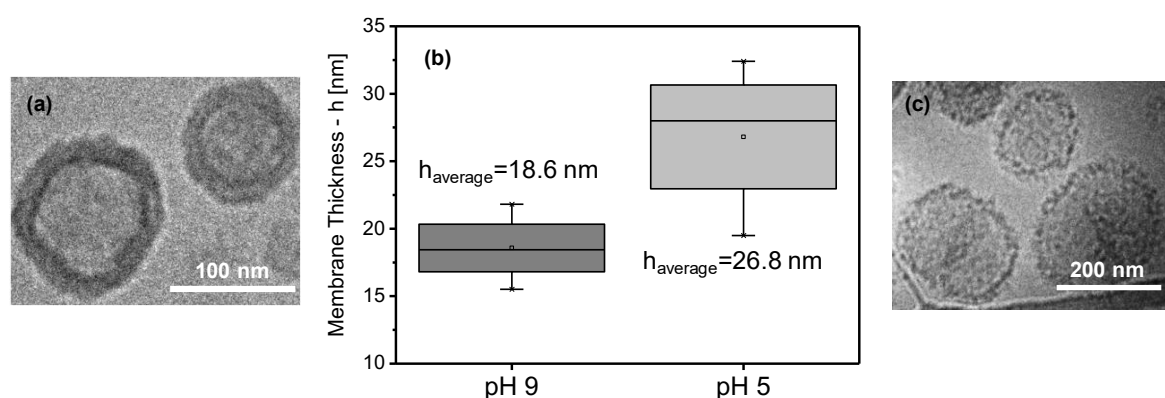


Figure 3.16 cryo-TEM micrographs of polymersomes (PS1) at pH 9 (a) and pH 5 (c). (b) Membrane thickness distribution of polymersomes (PS1) determined from corresponding cryo-TEM micrographs by analyzing 57 particles at pH 9 and 42 particles pH 5.

3.4 Polymersome Surface Functionalization by Sequential Post-Conjugations

3.4.1 Covalent Conjugation of Photoactive Moieties and the Successive Photocleavage

A second way to functionalize a polymersome surface is the introduction of functional moieties to the preformed vesicles after the block copolymer assembly. Herein, this technique was applied for further post-functionalization of pH sensitive polymersomes with photoactive moieties to obtain a dual-responsive structure (Figure 3.1: from PS1 up to PS1R). The aim was to perform a photocleavage reaction on polymersome surface to have additional functionalities in a controlled way which offers the potential to bind selectively biological entities afterwards. For this purpose, the released functions are chosen as amino groups which are protected by the well-known photolabile nitroveratryloxycarbonyl (NVOC) group for selective cleavage by UV irradiation. An important advantage of these groups are that they allow reactions at longer wavelengths up to 410 nm²⁹ meaning that the possibility to trigger the cleavage also in the IR range with the half energy through two photon absorption mechanism. Therefore, the post-modification process of photo-crosslinked polymersomes, PS1, was started with the synthesis of NVOC protected amine molecules possessing an alkyne moiety as confirmed by ¹H NMR spectrum (Figure 3.17).

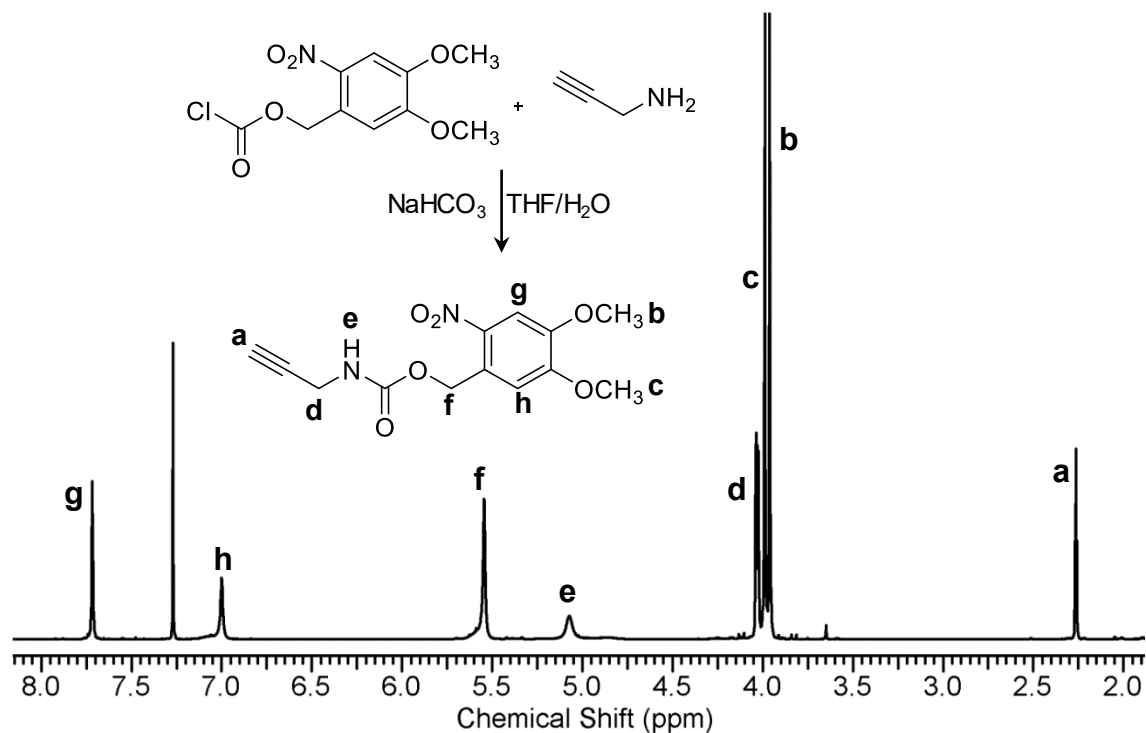


Figure 3.17 The synthetic scheme and ¹H-NMR spectrum of NVOC protected amine groups in CDCl₃

Afterwards, as seen in Figure 3.18a, this molecule was conjugated to the azido groups on polymersome surface of PS1 in the presence of a copper catalyst and tris-(benzyltriazolylmethyl) amine (TBTA) as a ligand, using slightly modified literature procedures.³⁰⁻³¹ After 2 days of reaction time, unbound NVOC groups and the copper catalyst were removed by extensive dialysis. To guarantee that the purification was efficient, the same amount of NVOC molecules without polymersomes was dialyzed under identical conditions and there was no sign of NVOC absorption in UV-Vis spectra (Figure 9.1, in experimental part). It should be noted that the working pH of whole conjugation steps including this one was kept as pH 8 to perform the reactions where the membrane of the vesicles is impermeable. Although the size of the polymersomes at basic state is constant (>pH 7, Figure 3.13), the surface charge is minimized at this state which is close to the isoelectric point of the polymersomes (Figure 3.14). In this context, selection of pH 8 as reaction parameter would not only avoid diffusion of the reactants into the lumen of the polymersomes but also decrease the possible electrostatic interaction of the reagents on the membrane periphery.

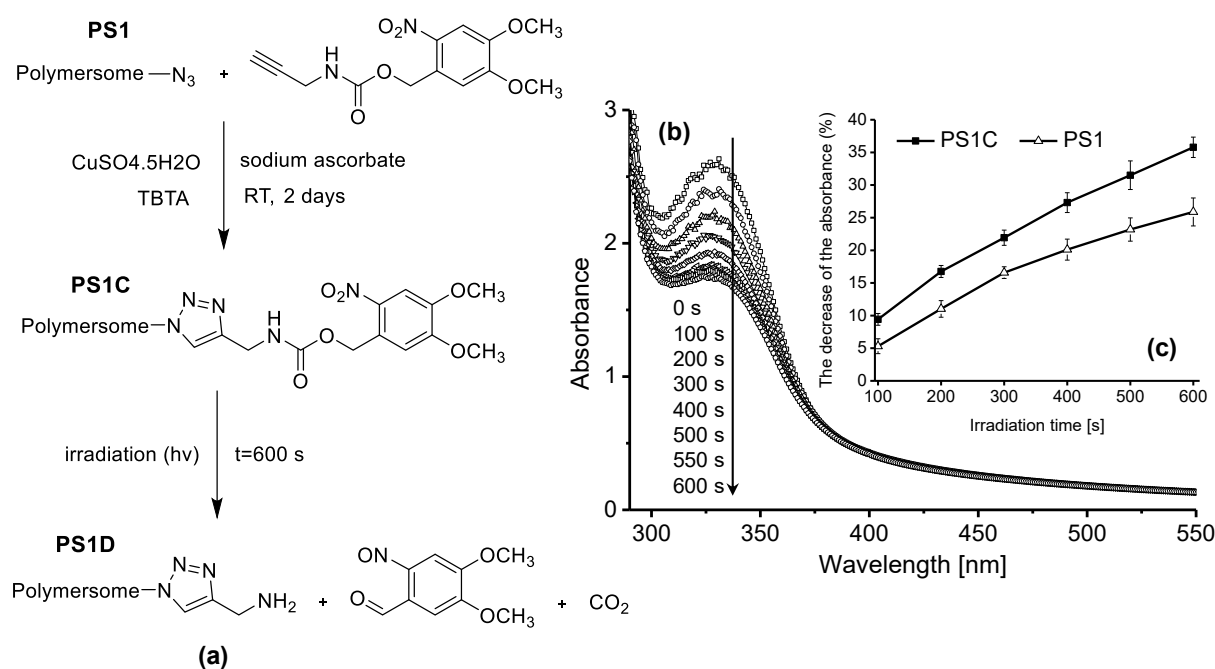


Figure 3.18 (a) Reaction scheme of NVOC conjugation and cleavage process on PS1 polymersomes. (b) UV-vis spectra of PS1C polymersomes upon UV exposure up to 600s showing the decrease of absorption bands due to NVOC cleavage. (c) The absorbance change (%) of PS1 and PS1C at $\lambda=345$ nm versus irradiation time under identical UV exposure.

After verification of the successful purification, the resulting polymersomes (PS1C) were exposed to UV light (320-500 nm) for up to 600 seconds to trigger the photocleavage reaction. The chemistry of this reaction sequence (PS1 over PS1C to PS1D) is outlined in Figure 3.18a. Thus, the photocleavage of the NVOC chromophore in PS1C resulted in the formation of free amine moieties on the polymersome surface of PS1D. Although the chemistry is straightforward, confirmation of this conjugation step as well as the cleavage process required multiple characterization efforts and model studies. Thus, the first inspection was realized by the time-dependent UV-vis study of the NVOC conjugated polymersomes (PS1C) (Figure 3.18b). The characteristic chromophore absorption of NVOC groups is seen in the wavelength range between 260 to 400 nm where the maximum absorption is at around $\lambda_{\text{max}} = 345 \text{ nm}$.³²⁻³³ As illustrated in Figure 3.18b, UV-vis spectra recorded during the irradiation process show a sharp decrease of the corresponding absorption bands. Although this is a strong evidence for the cleavage of NVOC chromophore and its conjugation to the vesicle, the effects of photo-crosslinker (BMA) units in the polymersome membrane has to be considered due to similar absorption maxima of BMA compared to NVOC. The UV-vis spectra of PS1C (Figure 3.18b) clearly indicates that there was no significant absorbance change after 500 seconds and the absorption bands between 300 to 400 nm did not fully disappear. This remaining absorbance can be caused to some extent by residual photocleavage products such as nitrosobenzaldehyde.³² However a significant contribution originated from BMA units because of the higher molar ratios compared with the possible side products. Thus, this clearly implies that BMA units show overlapping absorption bands with NVOC groups in the region of 250 and 330 nm due to their $\pi\text{-}\pi^*$ transition and $n\text{-}\pi^*$ transition, respectively.³⁴ In addition, photoreduction of the carbonyl groups in BMA units upon UV exposure could also lead to a decrease in the absorption spectra.³⁴⁻³⁵ To distinguish the effects of these two photoactive species in the same absorption wavelengths range, the same irradiation process to polymersomes without NVOC groups (PS1) was applied. As expected, the absorbance decrease ($\lambda=345 \text{ nm}$) of NVOC-conjugated polymersomes (PS1C) is about 1.5 times higher than that of those without NVOC groups (PS1) (Figure 3.18c). The small deviation of three repeated irradiation processes from different batches of PS1 and PS1C polymersomes supports the reproducible nature of photocleavage reaction as well as the NVOC conjugation (Figure 3.1, Figure 3.18c).

Furthermore, the shape persistence and stability of polymersomes during this whole reaction sequence was investigated by DLS and cryo-TEM visualization (Figure 3.19a, Table 3.3 and Figure 3.19b,c). This is an important prerequisite to use those polymeric vesicles as stable nanocontainers for various applications. Table 3.3 summarizes size distribution as well as portion of integrated functional moieties on polymersome surface in each post conjugation step. Here, results from DLS study show that the average diameter and the monodisperse nature of the polymersomes is not altered during these reaction steps. The size distribution seen in Figure 3.19a supports the stable behavior of polymersomes during the post-conjugation of the light sensitive group (NVOC) and the further photocleavage step. Additionally, cryo-TEM images of PS1D polymersomes at basic (pH8) and acidic state (pH5) confirm this claim by showing the preserved vesicular structure of the polymersomes as seen in Figure 3.19b, and c.

Table 3.3 Specification of the polymersomes with different functional groups

Polymersome	Functional groups [mol%]				Photo-crosslinked	Diameter ^c [nm]	PDI ^d
	N ₃ ^a	NVOC ^b	NH ₂ ^b	Ada ^a			
PS0	-	-	-	-	yes	117±1.1	0.19±0.03
PS1	29.0	-	-	9.2	yes	120±1.6	0.20±0.03
PS1C	21.3	7.7	-	9.2	yes	117±0.2	0.20±0.01
PS1D	21.3	3.2	4.5	9.2	yes	119±0.3	0.20±0.01
PS2	100	-	-	-	no	88.0±0.2	0.15±0.02
PS2C	73.5	26.5	-	-	no	84.5±0.5	0.18±0.02
PS2D	73.5	11	15.5	-	no	93.5±0.1	0.14±0.02

^a Azide and adamantane functionalities are placed equally both outer and inner part of the polymersome bilayer membrane and therefore only half of them is available for further outer surface functionalization. ^bThese values are the estimates of functionalities only at the outer surface of the polymersomes since the modification reaction was performed at basic condition meaning the impermeable state of the membrane. ^cDiameter is measured by DLS at pH8. ^dPDI=polydispersity index of polymersomes that shows the size variation.

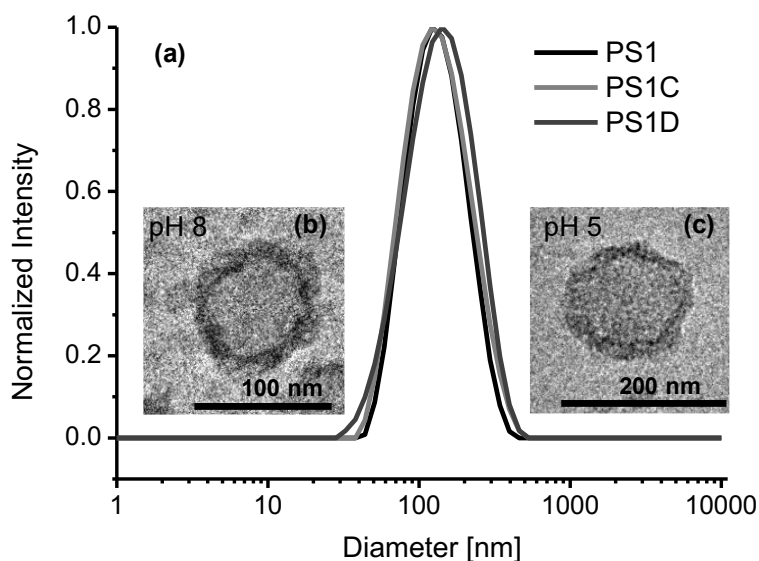


Figure 3.19 (a) Intensity size distribution of crosslinked polymersomes PS1, PS1C and PS1D (b,c) cryo-TEM micrographs of PS1D polymersomes at pH 8 and pH 5

Although the conjugation of photoactive groups has been proven with different ways so far, the covalent binding of the NVOC molecule has to be supported with alternative methods not to leave any questions behind. In this respect, two model reactions under identical conditions were performed (Figure 3.20a, Figure 3.22a) for further proof of this conjugation step (Figure 3.1: from PS1 to PS1C). Firstly, the azide terminated block copolymer without BMA groups was synthesized (BC4, see section 3.2) to form the corresponding polymersomes (PS2). By following this, the same click conditions were conducted to obtain NVOC-conjugated polymersomes devoid of the cross-linker unit (PS2C). Comparing the UV-vis spectra of polymersomes PS2 and PS2C (Figure 3.20b), absorption bands in the region of $\lambda=260-400$ nm after click reaction are a clear evidence of NVOC conjugation on the surface of PS2. In addition, the characterization of the freeze dried and disassembled PS2C polymersomes by ^1H NMR spectroscopy supports the successful conjugation of NVOC on PS2 surface through attributed ^1H NMR signals between 4.5 to 7.75 ppm (Figure 3.21). However, the relatively high molecular weight of the copolymer leads to low intensities of NVOC protons in ^1H NMR spectrum which is in agreement with previous studies.^{8, 36} Therefore, the conjugation yield cannot be quantified precisely with this approach. Thus, another model study was conducted by applying the same aqueous click conditions to a short azide terminated PEG molecule ($\text{N}_3\text{-PEG}_{60}\text{-OH}$, Figure 3.22a). As expected, ^1H NMR spectrum of the final product (M1C) enables a more precise detection of the NVOC groups using the relatively low molecular weight of the PEG molecule. The

successful synthesis as well as the conversion data of NVOC-PEG₆₀OH (M1C) were verified by ¹H NMR spectroscopy as shown in Figure 3.23. Furthermore, the UV-vis spectrum of M1C (Figure 3.22b) supports the conjugation clearly by the apparent absorption of the NVOC chromophore.

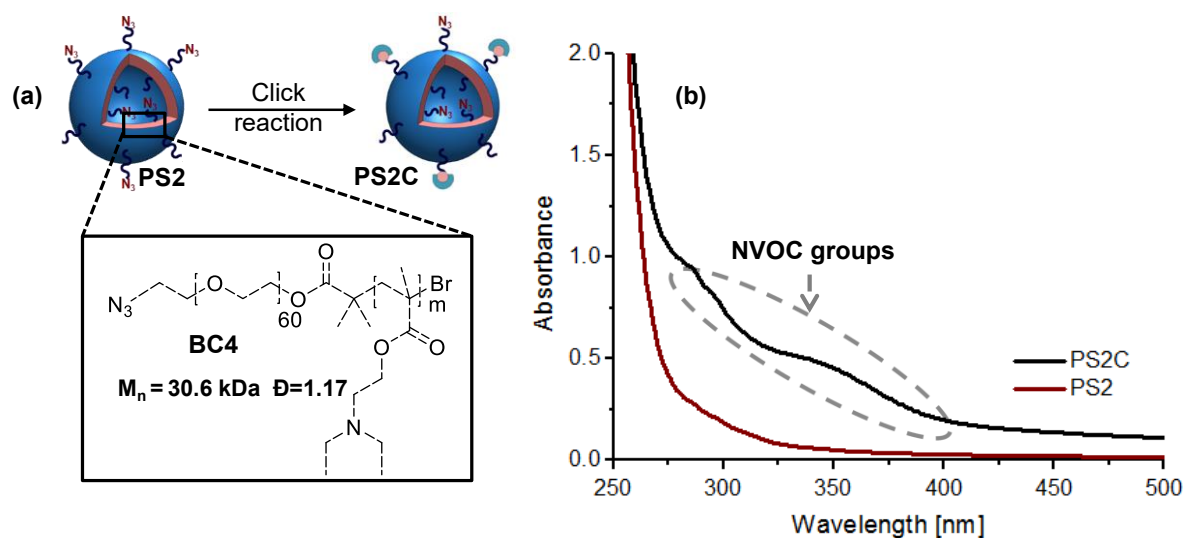


Figure 3.20 (a) Reaction Scheme of NVOC conjugation on PS2 polymersomes via identical click modification as done for PS1 polymersomes (b) UV-vis spectra of freeze dried PS2 and PS2C in CHCl₃

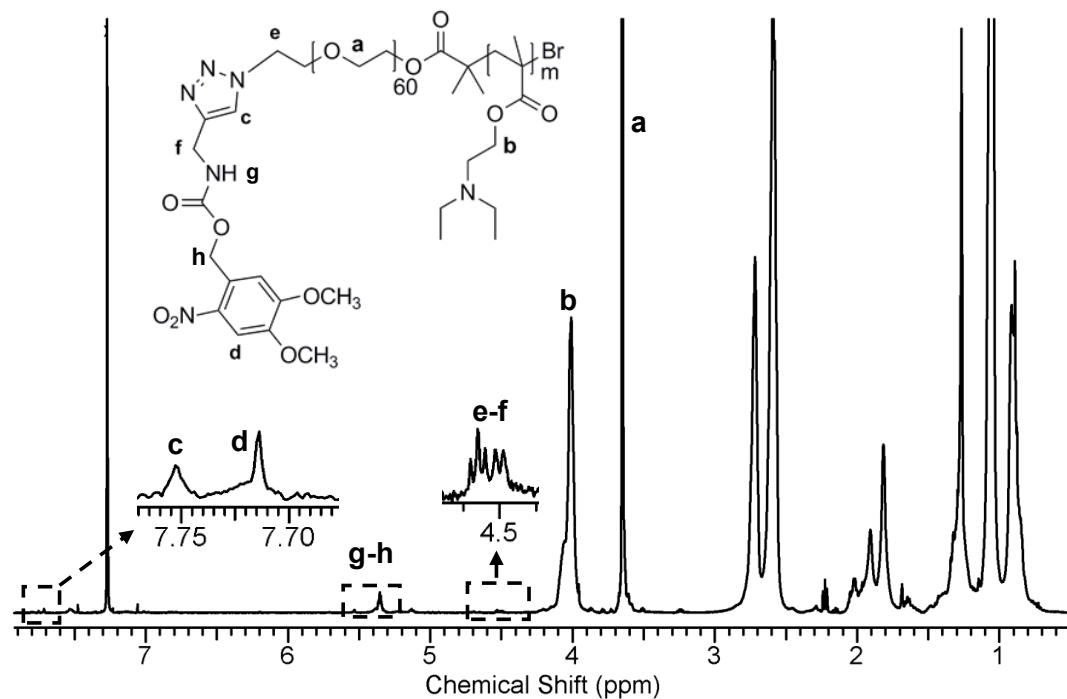


Figure 3.21 ¹H-NMR spectrum of freeze dried PS2C polymersome in CDCl₃

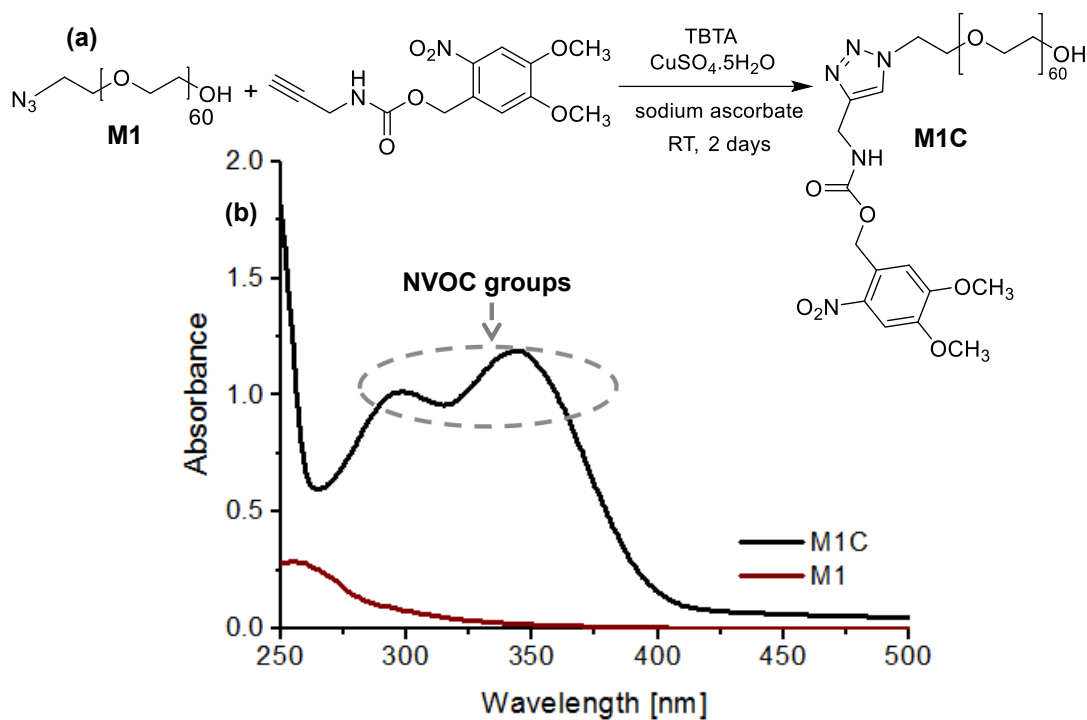


Figure 3.22 (a) Reaction Scheme of NVOC conjugation on short PEG molecule via identical aqueous click modification as a supporting model study (b) UV-vis spectra of M1 (before click) and M1C (after click) in CHCl₃

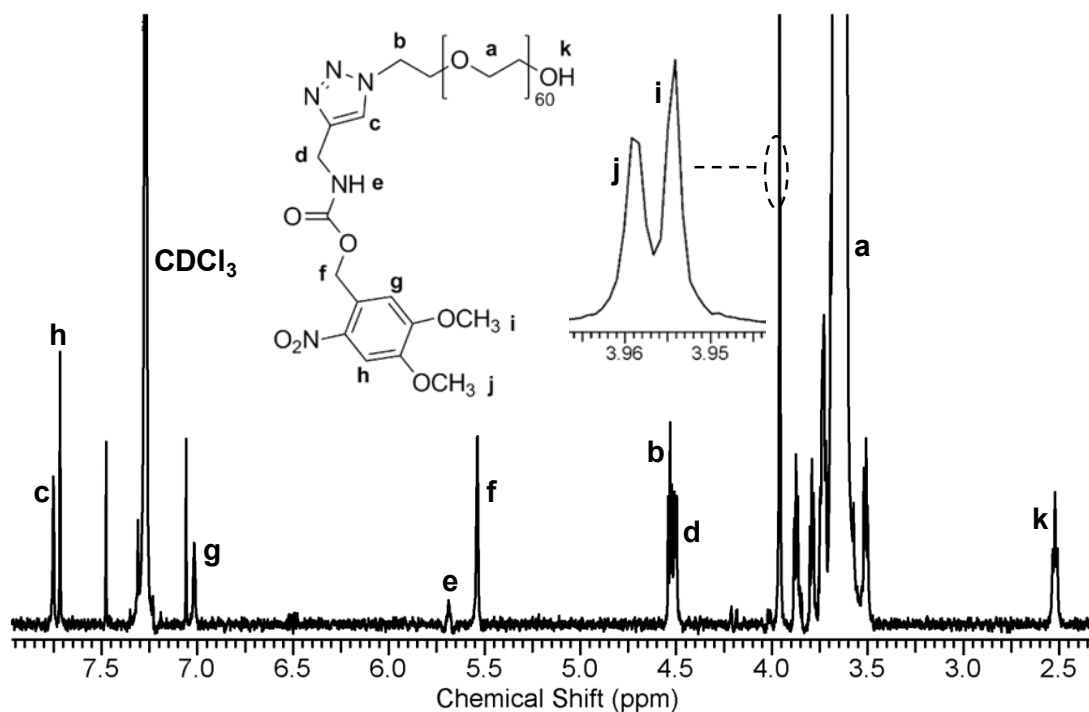


Figure 3.23 ¹H-NMR spectrum of NVOC-PEG₆₀-OH (M1C) in CDCl₃

After successful covalent attachment of the photoactive groups to the polymersomes, the conjugation yield (conversion of PS2 into PS2C) was estimated as 26.5% by comparing the molar extinction coefficients (ϵ) of PS2C polymersomes with MIC molecule (Figure 9.2, 9.3 experimental part). PS2C polymersomes were used here rather than PS1C polymersomes to obtain a more precise value by excluding the BMA contribution to the absorbance spectra. At first glance, this conjugation efficiency might be considered poor. However, about half of the azide moieties are placed in the interior of the bilayer membrane and not available for the reaction.^{8, 30, 37} This implies that about 53% of azide moieties on the outer surface of polymersomes were converted into NVOC groups. By assuming the same conversion behavior also for the conjugation step of PS1 into PS1C polymersomes, the starting point for all further covalent conjugation steps (Figure 3.1: PS1C to PS1D and PS1D to PS1R) can be clarified. Thus, from this postulation the resulting multifunctional polymersome system PS1C consist of about 7.7 mol% of NVOC, 9.2 mol% of adamantane and 21.3 mol% of azide functionalities as shown in Table 3.3. A noteworthy point here is that the 7.7 mol% of NVOC value depicts the modification only at the outer surface of PS1C polymersomes whereas the other two values represent the functionalities at both interior and exterior of the polymersome bilayer membrane.

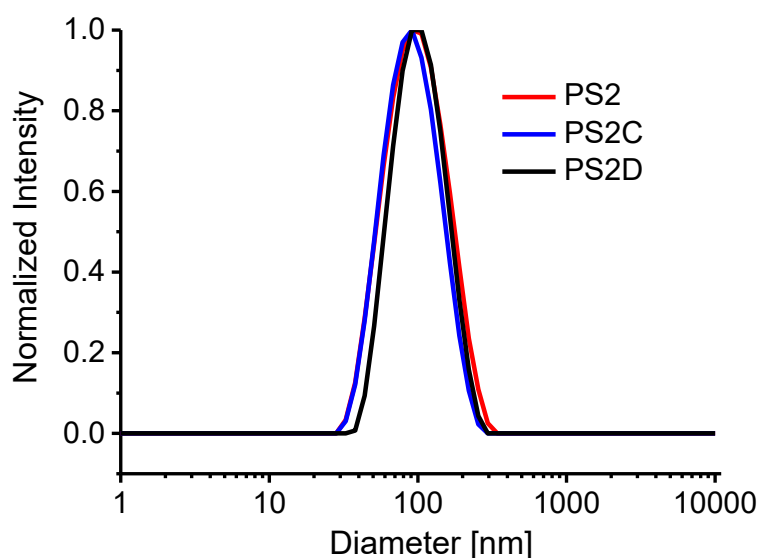


Figure 3.24 Intensity size distribution of non-cross-linked polymersomes before (PS2) and after click reaction (PS2C) and after photodeprotection (PS2D) at pH 8

As a next step, the photocleavage efficiency was determined as $58.4 \pm 2.3\%$ by calculating the NVOC chromophore cleavage from UV-vis analysis using PS2C

polymersomes (Figure 9.4, experimental part). This incomplete conversion behavior might be explained by an imine formation resulting from a reaction of nitroso benzaldehyde with amine groups released on the polymersome surface. To avoid this condition, the polymersomes were immediately dialyzed after UV exposure. However, dialysis required a certain time. Thus, this side reaction could occur before all aldehyde products were removed. The outcome is also in agreement with previously published results where del Campo et al. obtained 40-50% deprotection efficiency even in the presence of carbonyl scavenger.²⁹ It should be also noted that PS2C polymersomes showed a narrow size distribution (Figure 3.24, Table 3.3) during the whole reaction sequences as similarly observed for PS1C polymersomes. This ensured-stability without any disassembled polymer chains was important to simulate the PS1C formation thoroughly. In this manner, from the theoretical point of view, when transferring results from PS2D to PS1D, the final content of various functional groups in polymersomes is presented in Table 3.3. Thus, PS1D may have about 4.5 mol% of free NH₂ groups on the surface as an additional functionality for the next conversion step (Figure 3.1: PS1D into PS1R).

3.4.2 Covalent Conjugation of a Fluorescent Dye as a Model Compound

Gathering information about the accessibility of converted functional groups at each conjugation step on the polymersome surface is of great significance to use them as efficient nanocontainers for various applications. For this purpose, a final covalent conjugation step (Figure 1: PS1D to PS1R) was carried out to evaluate the accessibility of amino groups on the polymersome surface of PS1D. Thus, rhodamine B isothiocyanate (RhB-NCS) was selected as photo-stable and high quantum yielding fluorescent dye over a broad pH range³⁸ to be reacted with the released NH₂ groups of PS1D vesicles after UV exposure (Figure 3.25a). Herein, the fluorescent dye acts as a model compound to mimic a possible binding of bio/chemo molecules to the polymersome surface. Although isothiocyanate groups are highly reactive towards primary amines, their susceptibility to hydrolysis in water at higher pH values should be considered.³⁹ Therefore, excess amount of RhB-NCS dye was used to ensure its reactivity in polymersome solutions at pH 8 within an appropriate time. Next, an extensive purification step by dialysis was carried out to remove the unreacted reagent. As shown in Figure 3.25b, there is no change in the characteristic absorption bands of RhB-NCS dye ($\lambda_{\text{max}}=555$ nm) after 3 days of dialysis at basic conditions. This clearly indicates the successful conjugation of RhB-NCS molecules on polymersome surface of PS1D. However, a possible physical interaction between RhB-NCS dye and the vesicle membrane

might also contribute to the observed absorption band.⁴⁰ To investigate this possibility, the same process under identical conditions was applied to PS1 polymersomes. As shown in Figure 3.25c, about 1.4 times higher amount of RhB-NCS molecules conjugated to NH₂ functionalized polymersomes (PS1D) than to the ones without NH₂ groups (PS1, control). This difference clearly confirms the successful covalent conjugation as well as the availability of the amine groups on the polymersome surface liberated after photocleavage process of PS1C. The absorbance difference of PS1R and the control experiment at $\lambda_{\text{max}}=555$ nm was defined as measure for the covalent attachment of the RhB-NCS dye (Figure 3.25b, A₅₅₅ of PS1R=0.893, A₅₅₅ of PS1=0.655). This value was used in further calculations together with the measured molar extinction coefficient of RhB-NCS (Figure 9.6, experimental part) to estimate the conjugation efficiency of amino groups in polymersome PS1D (Table 3.3). This leads to a value of about 57% of amino groups on the surface of PS1R which reacted with RhB-NCS dye.

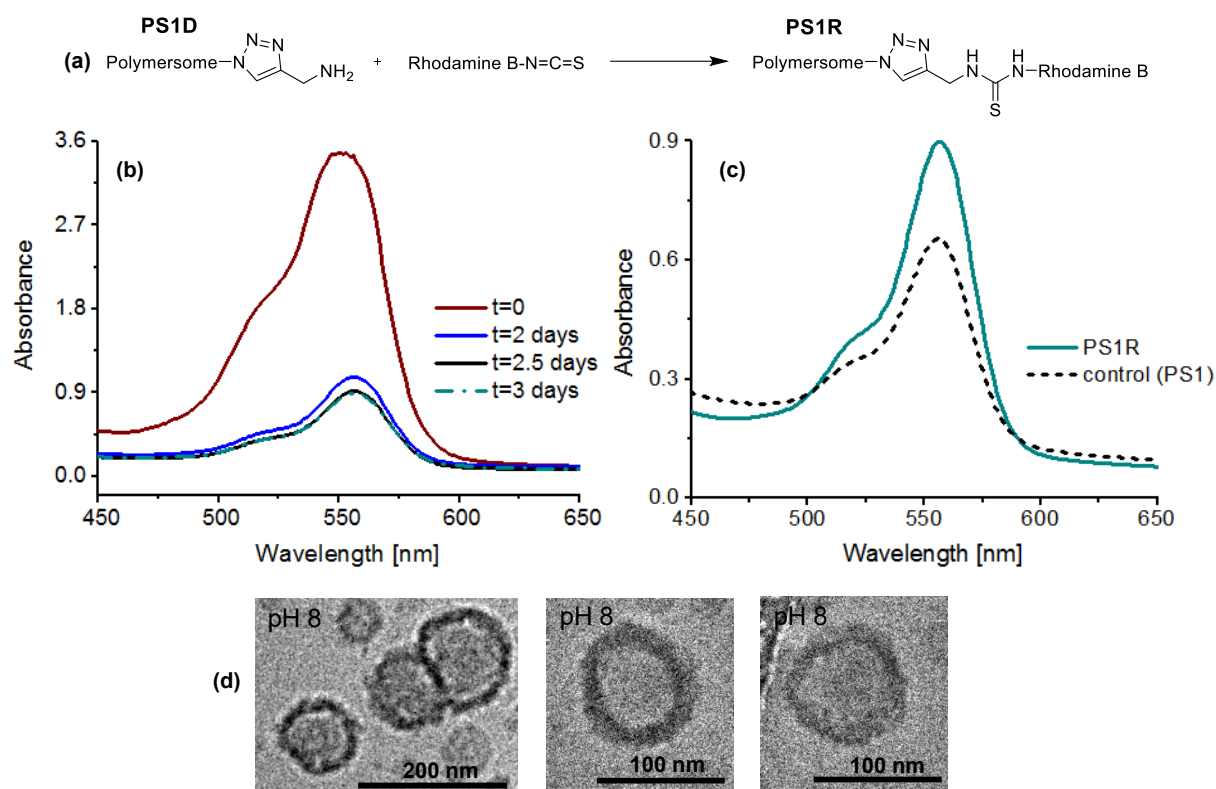


Figure 3.25 (a) Reaction Scheme of RhB-NCS conjugation on PS1D polymersomes. (b) Monitoring RhB-NCS coupling to polymersomes through amino groups (PS1R) with UV-vis analysis during dialysis procedure. (c) UV-vis spectra of RhB-NCS containing polymersomes with (PS1R) and without (PS1) NH₂ groups to show the covalent conjugation of the dye. (d) cryo-TEM micrographs of PS1R polymersomes at pH 8.

As indicated above, functional groups on polymersome surface were placed as antennae with a longer PEG segment to prohibit the concealment and steric effects of the hydrophilic corona.^{8, 41} The relatively high conjugation efficiency of RhB-NCS supports the argument of freely accessible and very reactive amine surface groups (Table 3.3). It is also noteworthy to point out that the amount of freely accessible amine groups on the surface can be tuned by UV exposure which can lead to a controllable surface functionalization. In this regard, the resulting multifunctional polymersome gain the ability of light-tuned responsivity in addition to the tuned-permeability of the membrane by pH trigger. Lastly, cryo-TEM micrographs of PS1R polymersomes verify that the vesicles preserve their shape without any disassembly in this conjugation step (Figure 3.25d) as indicated previously for PS1D polymersomes (Figure 3.19). This result confirmed the stable nature of the polymersomes over the whole sequential conjugation steps which is an essential precondition to use these nanocontainers in various applications.

3.4.3 Non-Covalent Conjugation of β -Cyclodextrin by Host-Guest Interactions

In the last conjugation step, the accessibility of the adamantane functionality on PS1R polymersome surface was studied in a non-covalent approach by the formation of host-guest inclusion complexes with β -cyclodextrin (β -CD) molecules. It is widely reported in literature that adamantane groups tightly fit into the cavity of β -CD molecules showing perfect host-guest interaction with a high association constant between 10^4 to 10^5 M⁻¹.⁴²⁻⁴³ For this non-covalent conjugation approach on PS1R surface, β -CD molecules were modified with a water soluble Sulfo-Cyanine7 (Cy7) dye to monitor the host-guest inclusion complexation by UV-vis spectroscopy. From Figure 3.26a, it is apparent that the absorption band in the range of 600-850 nm demonstrates the attachment of Cy7 labeled β -CD molecules (β -CD-Cy7) to adamantane groups in PS1H. To understand this conjugation behavior in detail, the same process was carried out under identical conditions by using PS0 polymersomes without any adamantane groups (Figure 3.26b). This negative control experiment showed that polymersomes PS0 also interact to some extent with β -CD-Cy7 molecules. A possible explanation is that PEG chains in polymersome corona of PS0 might thread into β -cyclodextrin cavities and form inclusion complexes. Various groups reported such behavior between PEG and α -cyclodextrin molecules.⁴⁴⁻⁴⁵ Another reason for that might be related to the negatively charged sulfonate groups in Cy7 dye. Although membrane of the polymersome at pH 8 is mainly unprotonated, zeta potential results (Figure 3.14) outline a slight positive charge (ζ -potential of about +5 mV). This can induce a weak interaction

between sulfonate moieties and the PDEAEM groups of the membrane. Thus, it is assumed that this unexpected slight β -cyclodextrin binding to polymersomes PS0 without adamantane units is caused mostly by threading behavior of PEG molecules in combination with the slight electrostatic interactions.

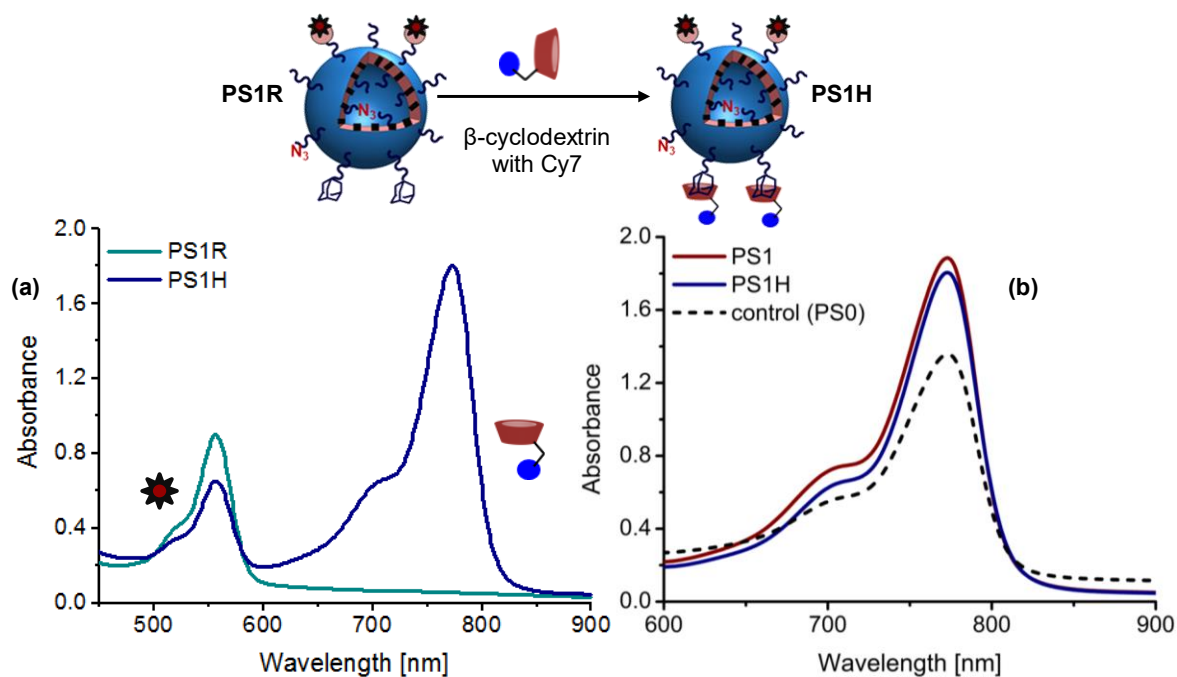


Figure 3.26 (a) UV-vis analysis to show sequential conjugation of cyclodextrin molecule to Rhodamine B NCS modified polymersomes (PS1R) by host-guest interaction. (b) UV-vis spectra of Cy7-CD containing polymersomes with (PS1H, PS1) and without (PS0) adamantane groups on their surface to show the conjugation triggered by host-guest interaction.

However, a comparison of UV-vis spectra of PS1H and PS0 polymersomes (Figure 3.26b) clearly shows that the adamantane groups enhance the binding of CD-Cy7 molecules on polymersome surface in PS1H significantly. Although this nicely proves the successful host-guest inclusion complexation of the β -cyclodextrin-modified dye by the adamantane groups on the polymersome surface (A_{775} of PS1H=1.80, A_{775} of PS0=1.35), an additional investigation was performed on PS1 polymersomes. The concern was to distinguish if there were any other interactions between cyclodextrin molecules and free functional groups on PS1H polymersomes (NVOC: 3.2 mol%, NH_2 : 1.9 mol%). As can be seen in Figure 3.26b, UV-vis spectra of polymersomes having only adamantane groups (A_{775} of PS1=1.87) showed a similar trend as for PS1H. This supports the claim that binding β -cyclodextrin

molecules to the PS1H surface is mainly triggered by the interaction with adamantane groups. To determine the efficiency of this conjugation, the same methodology was used as done for the rhodamine attachment step. The absorbance difference of PS1H and PS0 polymersomes at $\lambda_{\text{max}}=775$ nm was assigned as the value of the non-covalent conjugation which was then used together with the measured molar extinction coefficient of CD-Cy7 molecules (Figure 9.7, experimental part). Finally, this calculation shows that about 58% of adamantane groups on the outer shell of PS1H polymersomes were conjugated to the β -cyclodextrin molecules.

3.5 Reversible pH-switch of Light Responsive Polymersomes

Gathering information about the pH sensitive behavior of the multifunctional polymersomes having NVOC groups as light active molecules is of great significance to ensure the dual-responsivity of the established system. One can assume that the irradiation during photocleavage step would lead to more cross-linking which results in lesser swelling power for PS1D polymersomes. For this purpose, in the final part of this chapter, PS1C (after click reaction) and PS1D (after photocleavage process) polymersomes were assessed in respect to pH responsivity as it was similarly done for PS1 polymersomes.

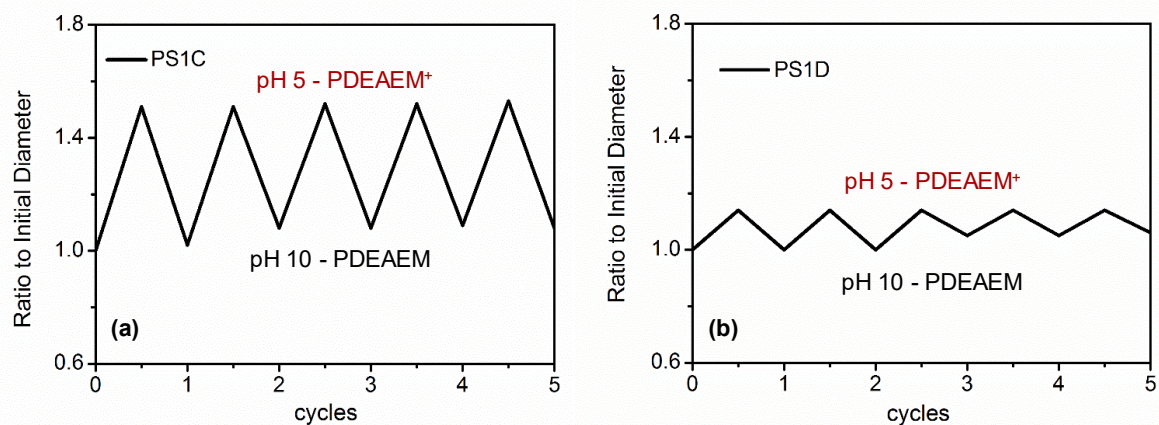


Figure 3.27 Reversible swelling-shrinking of (a) PS1C and (b) PS1D polymersomes upon changes in pH value.

The reversible swelling and shrinking of the polymersomes at acidic and basic states were confirmed by 5 cycles of pH switch experiments as seen in Figure 3.27. This result showed that both polymersomes keep their stable nature and recover the initial size without facing any disassembly problems. Another essential result here is that there is almost no

variation in the overall size increase of PS1C, so called swelling power, in comparison to PS1 polymersomes (Figure 3.15a). However, as it is mentioned before, irradiation during photocleavage process increased the crosslinking degree of the membrane which causes a lower swelling in the acidic state. Although crosslinking degree can be tuned according to the needs of the application,³ it is unknown how this decreased swelling power will contribute to the permeability of the membrane. To investigate this, the doxorubicin release on PS1C and PS1D polymersomes was performed and is given in the next chapter. Thus, the clear outcome of these experiments was that the dual responsivity as well as the stability of the established multifunctional system persisted even in the case of additional UV-irradiation.

3.6 Summary

In this chapter, the formation of multifunctional and dual-responsive polymersomes was discussed. The starting point of the fabrication was to synthesize three block copolymers comprising adamantane, azide and methoxy end groups at their hydrophilic PEG chain whereas pH sensitive DEAEM and a photo-crosslinker BMA groups form together the hydrophobic part. The integrated azide and adamantane groups were utilized to start the sequential post-surface functionalization of the pH sensitive and photo-crosslinked polymersomes with multiple reactive groups through covalent and non-covalent conjugations. To guarantee the accessibility of functional units in these post-modification steps, the hydrophilic length of the azide- and adamantane-terminated block copolymers was designed to be longer than in the methoxy-terminated block copolymer. Moreover, these multi-functionalized polymersomes possessed a reversible swelling (pH 5) and shrinking (pH 10) behavior after photo-crosslinking the membrane. This in turn leads to controlled membrane permeability which is addressed in the next chapter by doxorubicin encapsulation and further release experiments. In line with this, the established polymersomes showed a remarkable pH-stability and preserved their vesicular shape at different pH environments.

One key characteristics of the sequential post-functionalization of polymersome surface was the covalent conjugation of a photolabile NVOC protected amine groups, by azide-alkyne click reaction. This directly induced a light responsiveness to provide selectively free amine functionalities on the surface of polymersomes upon UV exposure. The presence of free amino groups was used for further post-conjugation steps as proven in this study by introducing dye molecules. Besides, the controlled photochemical reaction can be performed

to tune the amount of amino groups by simply varying the irradiation time. This also created an opportunity to tune the surface functionalities and to retain the off-state of NVOC-protected amine groups unless they are triggered externally. Furthermore, the post-conjugation of polymersomes was proceeded with host-guest interaction of adamantane groups with dye-modified β -cyclodextrin molecules. It was thus quantitatively proven that all functional groups were accessible and highly reactive to fabricate multi-functionalized polymersome surfaces with different interaction and reactivity properties. In addition to these findings, the persistence of the pH response as well as the pH stability was demonstrated by performing reversible shrinking/swelling experiments on multifunctional polymersomes having NVOC groups as light active molecules.

Overall, these established polymersomes, possessing various reactive groups as well as pH- and light-responsive nature, exhibit new opportunities for the enhancement of specific targeting and the establishment of multicompartimentalized systems in drug delivery and synthetic biology, but also for future application in “Lab-on-a-Chip” devices.

3.7 References

- [1] Le Meins, J. F.; Sandre, O.; Lecommandoux, S., Recent Trends in the Tuning of Polymersomes' Membrane Properties. *The European Physical Journal E* **2011**, *34*, 1-17.
- [2] Savić, R.; Azzam, T.; Eisenberg, A.; Maysinger, D., Assessment of the Integrity of Poly(Caprolactone)-B-Poly(Ethylene Oxide) Micelles under Biological Conditions: A Fluorogenic-Based Approach. *Langmuir* **2006**, *22*, 3570-3578.
- [3] Yassin, M. A.; Appelhans, D.; Mendes, R. G.; Rummeli, M. H.; Voit, B., Ph-Dependent Release of Doxorubicin from Fast Photo-Cross-Linkable Polymersomes Based on Benzophenone Units. *Chemistry – A European Journal* **2012**, *18*, 12227-12231.
- [4] Iyisan, B.; Kluge, J.; Formanek, P.; Voit, B.; Appelhans, D., Multifunctional and Dual-Responsive Polymersomes as Robust Nanocontainers: Design, Formation by Sequential Post-Conjugations, and pH-Controlled Drug Release. *Chem. Mater.* **2016**, *28*, 1513-1525.
- [5] Discher, D. E.; Eisenberg, A., Polymer Vesicles. *Science* **2002**, *297*, 967-973.
- [6] Du, J.; O'Reilly, R. K., Advances and Challenges in Smart and Functional Polymer Vesicles. *Soft Matter* **2009**, *5*, 3544-3561.
- [7] Blanazs, A.; Armes, S. P.; Ryan, A. J., Self-Assembled Block Copolymer Aggregates: From Micelles to Vesicles and Their Biological Applications. *Macromol. Rapid Commun.* **2009**, *30*, 267-277.
- [8] Yassin, M. A.; Appelhans, D.; Wiedemuth, R.; Formanek, P.; Boye, S.; Lederer, A.; Temme, A.; Voit, B., Overcoming Concealment Effects of Targeting Moieties in the

- PEG Corona: Controlled Permeable Polymersomes Decorated with Folate-Antennae for Selective Targeting of Tumor Cells. *Small* **2015**, *11*, 1580-1591.
- [9] Binder, W. H.; Sachsenhofer, R., 'Click' Chemistry in Polymer and Material Science: An Update. *Macromol. Rapid Commun.* **2008**, *29*, 952-981.
- [10] Du, J.; Tang, Y.; Lewis, A. L.; Armes, S. P., Ph-Sensitive Vesicles Based on a Biocompatible Zwitterionic Diblock Copolymer. *J. Am. Chem. Soc.* **2005**, *127*, 17982-17983.
- [11] Adams, D. J.; Butler, M. F.; Weaver, A. C., Effect of Block Length, Polydispersity, and Salt Concentration on PEO-PDEAMA Block Copolymer Structures in Dilute Solution. *Langmuir* **2006**, *22*, 4534-4540.
- [12] Gaitzsch, J.; Appelhans, D.; Gräfe, D.; Schwille, P.; Voit, B., Photo-Crosslinked and pH Sensitive Polymersomes for Triggering the Loading and Release of Cargo. *Chem. Commun.* **2011**, *47*, 3466-3468.
- [13] Lin, J. J.; Ghoroghchian, P. P.; Zhang, Y.; Hammer, D. A., Adhesion of Antibody Functionalized Polymersomes. *Langmuir* **2006**, *22*, 3975-3979.
- [14] Robbins, G. P.; Saunders, R. L.; Haun, J. B.; Rawson, J.; Therien, M. J.; Hammer, D. A., Tunable Leuko-Polymersomes That Adhere Specifically to Inflammatory Markers. *Langmuir* **2010**, *26*, 14089-14096.
- [15] Brož, P.; Benito, S. M.; Saw, C.; Burger, P.; Heider, H.; Pfisterer, M.; Marsch, S.; Meier, W.; Hunziker, P., Cell Targeting by a Generic Receptor-Targeted Polymer Nanocontainer Platform. *J. Controlled Release* **2005**, *102*, 475-488.
- [16] Egli, S.; Nussbaumer, M. G.; Balasubramanian, V.; Chami, M.; Bruns, N.; Palivan, C.; Meier, W., Biocompatible Functionalization of Polymersome Surfaces: A New Approach to Surface Immobilization and Cell Targeting Using Polymersomes. *J. Am. Chem. Soc.* **2011**, *133*, 4476-4483.
- [17] Pawar, P. V.; Gohil, S. V.; Jain, J. P.; Kumar, N., Functionalized Polymersomes for Biomedical Applications. *Polymer Chemistry* **2013**, *4*, 3160-3176.
- [18] Lee, J. S.; Groothuis, T.; Cusan, C.; Mink, D.; Feijen, J., Lysosomally Cleavable Peptide-Containing Polymersomes Modified with Anti-EGFR Antibody for Systemic Cancer Chemotherapy. *Biomaterials* **2011**, *32*, 9144-9153.
- [19] Georgieva, J. V.; Brinkhuis, R. P.; Stojanov, K.; Weijers, C. A. G. M.; Zuilhof, H.; Rutjes, F. P. J. T.; Hoekstra, D.; van Hest, J. C. M.; Zuhorn, I. S., Peptide-Mediated Blood-Brain Barrier Transport of Polymersomes. *Angew. Chem.* **2012**, *124*, 8464-8467.
- [20] Yang, X.; Grailer, J. J.; Rowland, I. J.; Javadi, A.; Hurley, S. A.; Matson, V. Z.; Steeber, D. A.; Gong, S., Multifunctional Stable and Ph-Responsive Polymer Vesicles Formed by Heterofunctional Triblock Copolymer for Targeted Anticancer Drug Delivery and Ultrasensitive Mr Imaging. *ACS Nano* **2010**, *4*, 6805-6817.
- [21] Bütün, V.; Armes, S. P.; Billingham, N. C., Synthesis and Aqueous Solution Properties of near-Monodisperse Tertiary Amine Methacrylate Homopolymers and Diblock Copolymers. *Polymer* **2001**, *42*, 5993-6008.
- [22] Gräfe, D.; Gaitzsch, J.; Appelhans, D.; Voit, B., Cross-Linked Polymersomes as Nanoreactors for Controlled and Stabilized Single and Cascade Enzymatic Reactions. *Nanoscale* **2014**, *6*, 10752-10761.

- [23] Brinkhuis, R. P.; Rutjes, F. P. J. T.; van Hest, J. C. M., Polymeric Vesicles in Biomedical Applications. *Polymer Chemistry* **2011**, *2*, 1449-1462.
- [24] Ahmed, F.; Pakunlu, R. I.; Brannan, A.; Bates, F.; Minko, T.; Discher, D. E., Biodegradable Polymersomes Loaded with Both Paclitaxel and Doxorubicin Permeate and Shrink Tumors, Inducing Apoptosis in Proportion to Accumulated Drug. *J. Controlled Release* **2006**, *116*, 150-158.
- [25] Egli, S.; Schlaad, H.; Bruns, N.; Meier, W., Functionalization of Block Copolymer Vesicle Surfaces. *Polymers* **2011**, *3*, 252-280.
- [26] Liang, X.; Mao, G.; Ng, K. Y. S., Mechanical Properties and Stability Measurement of Cholesterol-Containing Liposome on Mica by Atomic Force Microscopy. *J. Colloid Interface Sci.* **2004**, *278*, 53-62.
- [27] Liang, X.; Mao, G.; Simon Ng, K. Y., Probing Small Unilamellar Eggpc Vesicles on Mica Surface by Atomic Force Microscopy. *Colloids Surf. B. Biointerfaces* **2004**, *34*, 41-51.
- [28] Park, J.-W., Sulfatide Incorporation Effect on Mechanical Properties of Vesicles. *Colloids Surf. B. Biointerfaces* **2010**, *80*, 59-62.
- [29] del Campo, A.; Boos, D.; Spiess, H. W.; Jonas, U., Surface Modification with Orthogonal Photosensitive Silanes for Sequential Chemical Lithography and Site-Selective Particle Deposition. *Angew. Chem. Int. Ed.* **2005**, *44*, 4707-4712.
- [30] Opsteen, J. A.; Brinkhuis, R. P.; Teeuwen, R. L. M.; Lowik, D. W. P. M.; van Hest, J. C. M., "Clickable" Polymersomes. *Chem. Commun.* **2007**, 3136-3138.
- [31] O'Reilly, R. K.; Joralemon, M. J.; Hawker, C. J.; Wooley, K. L., Facile Syntheses of Surface-Functionalized Micelles and Shell Cross-Linked Nanoparticles. *J. Polym. Sci., Part A: Polym. Chem.* **2006**, *44*, 5203-5217.
- [32] Dispinar, T.; Colard, C. A. L.; Du Prez, F. E., Polyurea Microcapsules with a Photocleavable Shell: Uv-Triggered Release. *Polymer Chemistry* **2013**, *4*, 763-772.
- [33] Ballister, E. R.; Aonbangkhen, C.; Mayo, A. M.; Lampson, M. A.; Chenoweth, D. M., Localized Light-Induced Protein Dimerization in Living Cells Using a Photocaged Dimerizer. *Nat. Commun* **2014**, *5*.
- [34] Yang, J.; Shi, S.; Xu, F.; Nie, J., Synthesis and Photopolymerization Kinetics of Benzophenone Sesamol One-Component Photoinitiator. *Photochemical & Photobiological Sciences* **2013**, *12*, 323-329.
- [35] Hoshino, M.; Arai, S.; Imamura, M.; Ikehara, K.; Hama, Y., Mechanism of Benzophenone Ketyl Radical Formation in Acidic Alcohols Studied by Pulse-Radiolysis and Rigid-Matrix Techniques. *The Journal of Physical Chemistry* **1980**, *84*, 2576-2579.
- [36] Li, B.; Martin, A. L.; Gillies, E. R., Multivalent Polymer Vesicles Via Surface Functionalization. *Chem. Commun.* **2007**, 5217-5219.
- [37] Martin, A. L.; Li, B.; Gillies, E. R., Surface Functionalization of Nanomaterials with Dendritic Groups: Toward Enhanced Binding to Biological Targets. *J. Am. Chem. Soc.* **2008**, *131*, 734-741.
- [38] Mottram, L. F.; Forbes, S.; Ackley, B. D.; Peterson, B. R., Hydrophobic Analogues of Rhodamine B and Rhodamine 101: Potent Fluorescent Probes of Mitochondria in Living *C. Elegans*. *Beilstein Journal of Organic Chemistry* **2012**, *8*, 2156-2165.

- [39] Joseph, V. B.; Satchell, D. P. N.; Satchell, R. S.; Wassef, W. N., Hydrolysis of Aryl and Alkyl Isothiocyanates in Aqueous Perchloric Acid. *Journal of the Chemical Society, Perkin Transactions 2* **1992**, 339-341.
- [40] Kasnavia, T.; Vu, D.; Sabatini, D. A., Fluorescent Dye and Media Properties Affecting Sorption and Tracer Selection. *Ground Water* **1999**, *37*, 376-381.
- [41] Kawano, K.; Maitani, Y., Effects of Polyethylene Glycol Spacer Length and Ligand Density on Folate Receptor Targeting of Liposomal Doxorubicin in Vitro. *Journal of Drug Delivery* **2011**, *2011*.
- [42] Paolino, M.; Ennen, F.; Lamponi, S.; Cernescu, M.; Voit, B.; Cappelli, A.; Appelhans, D.; Komber, H., Cyclodextrin-Adamantane Host–Guest Interactions on the Surface of Biocompatible Adamantyl-Modified Glycodendrimers. *Macromolecules* **2013**, *46*, 3215-3227.
- [43] Böhm, I.; Isenbügel, K.; Ritter, H.; Branscheid, R.; Kolb, U., Cyclodextrin and Adamantane Host–Guest Interactions of Modified Hyperbranched Poly(Ethylene Imine) as Mimetics for Biological Membranes. *Angew. Chem.* **2011**, *123*, 8042-8045.
- [44] Harada, A., Preparation and Structures of Supramolecules between Cyclodextrins and Polymers. *Coord. Chem. Rev.* **1996**, *148*, 115-133.
- [45] Liu, G.; Jin, Q.; Liu, X.; Lv, L.; Chen, C.; Ji, J., Biocompatible Vesicles Based on PEO-b-PMPC/ α -Cyclodextrin Inclusion Complexes for Drug Delivery. *Soft Matter* **2011**, *7*, 662-669.

4 Multifunctional Polymersomes as Nanocontainers

4.1 Introduction

Polymersomes have been widely applied as nanocarriers or nanocontainers in biomedical science for delivery and diagnostic purposes with the aid of their outstanding features like flexible chemical structure, tunable membrane permeability and hosting ability of various hydrophilic and hydrophobic compounds either in their aqueous lumen or in the membrane.¹⁻⁴ As already investigated, this study utilized the first two features to develop multifunctional and responsive polymersomes having various reactive groups at their periphery. In this regard, the hosting capacity of the established polymersomes as well as the limits of the membrane permeability should also be examined by encapsulating drugs or smart nanoparticles like gold NPs. In fact, the latter smart cargo can provide additional functions to the established multi-reactive and responsive polymersomes due to their interesting characteristics.

Gold nanoparticles are known for their unique physical and chemical properties including size and shape dependent optical features like surface plasmon resonance (SPR) and second harmonic generation (SHG).⁵⁻⁶ These optical features enable AuNPs to absorb visible light as well as to convert the light into heat energy which can be used in the field of photothermal therapy, imaging and diagnostic tools.⁷⁻¹⁰ Therefore, incorporation of gold nanoparticles into polymersomes create new insights for selective recognition and targeted delivery purposes by being able to possess both visibility and responsivity. As one example of such combination, doxorubicin/gold nanorod-loaded polymersomes¹¹ were prepared to be used in cancer treatment by utilizing the gold nanorods as heat generator through the trigger of near-infrared light and polymersomes as releasing vehicle for doxorubicin molecules. Furthermore, SHG, a type of nonlinear optical effect, can occur depending on the shape and size of the gold NPs when they are excited by light and lead to frequency doubling. Especially, the noncentrosymmetric gold nanoparticles like nanorods and nanocones are efficient second harmonic emitters¹² and can be used as optical antennae when combined with polymersomes. Apart from these usual application potentials, the combination of gold nanoparticles with polymersomes can be utilized to design sensing or microfluidic devices in which gold NPs have been already used as labels for signal amplifications in biosensing applications.¹³

Another aspect of the applicability of the nanocontainers is to gain information about the permeability of the polymersome membrane. As already mentioned, swelling of the polymersomes induced by the protonation of PDEAEM groups at acidic condition leads to the repelling of the polymer chains which results in a porous membrane structure. These pores are responsible for the permeability and allow passive diffusion of the molecules through the polymersome membrane. Both cross-linking density as well as the size of the encapsulated cargo has played an essential role to understand the limits of this pH controlled diffusion behavior. Therefore, this chapter focuses on firstly encapsulation of doxorubicin molecules as smaller sized anticancer drugs into established azide and adamantane decorated polymersomes by means of pre-loading approach. Afterwards, the photoactive polymersomes were loaded with doxorubicin molecules and further photocleavage reaction was performed in order to induce pH-controlled drug release for clarifying the membrane permeability that has been already published.¹⁴ In addition, two differently-sized gold nanoparticles which have average core diameters of 5 nm and 10 nm, are loaded into the azide and adamantane decorated polymersomes by utilizing both pre-loading and post-loading approaches. Therein, the capability of these two methods as well as the size selective and pH dependent diffusion through the porous membrane at swollen state is discussed in detail.

4.2 Doxorubicin Encapsulation and pH-triggered Release

After successful formation of multifunctional polymersomes, drug release experiments were carried out to demonstrate pH controlled permeability of the established system. As already discussed in the previous chapter, the polymersomes showed sufficient pH responsivity originated by the protonated PDEAEM groups in acidic state. However, there was a reduction in the swelling power of the PS1D polymersomes due to additional UV-irradiation for photocleavage of the attached NVOC groups. To investigate whether this condition led to a change in the membrane permeability, the drug release experiments were performed using PS1C and PS1D polymersomes. Here, doxorubicin hydrochloride (Dox) was selected as a model drug which has a common clinical use in cancer chemotherapy.¹⁵⁻¹⁷

There are two common ways of cargo encapsulation for the pH responsive vesicles in which the cargo can be loaded during self-assembly (pre-loading) or afterwards (post-loading).³ Herein, pre-loading approach was applied to avoid any possible Dox trapped on the outer region of the polymersome membrane which can inhibit an effective drug

encapsulation. In line with this, it was also aimed to investigate the compatibility of the sequential post-conjugation approach with the presence of a carrier. Thus, Dox encapsulation was performed before surface modification of the PS1 polymersomes during its formation as illustrated in Figure 4.1. After the self-assembly and crosslinking of the PS1-Dox polymersomes, an extensive purification using hollow fiber filtration (HFF) system was carried out to remove all non-encapsulated Dox molecules. In this purification method, polymersomes encountered a shear flow with a 130 mbar transmembrane pressure that is close to the normal blood pressure of about 160/106 mbar.¹⁸ Both the shear flow and the Dox incorporation during self-assembly of the block copolymers did not lead to any aggregation behavior as well as a notable size variation in the resulting polymersomes (Figure 4.2). Thus, this outcome fulfilled the expectation of the stable behavior of the established multifunctional polymersomes even in the case of blood capillaries. Afterwards, the outer shell of the PS1-Dox polymersomes were modified with NVOC moieties by click chemistry as done previously for the polymersomes without Dox (PS1), followed by an irradiation for 600 seconds to cleave the NVOC moieties to obtain PS1D-Dox polymersomes (Figure 4.1). In addition, the DLS data of the polymersomes at each step revealed that they showed a monodisperse size distribution having average diameters of 124.2±1.08 nm (PS1-Dox), 115.4±1.01 nm (PS1C-Dox) and 119.4±1.8 nm (PS1D-Dox), respectively, even in the case of drug encapsulation.

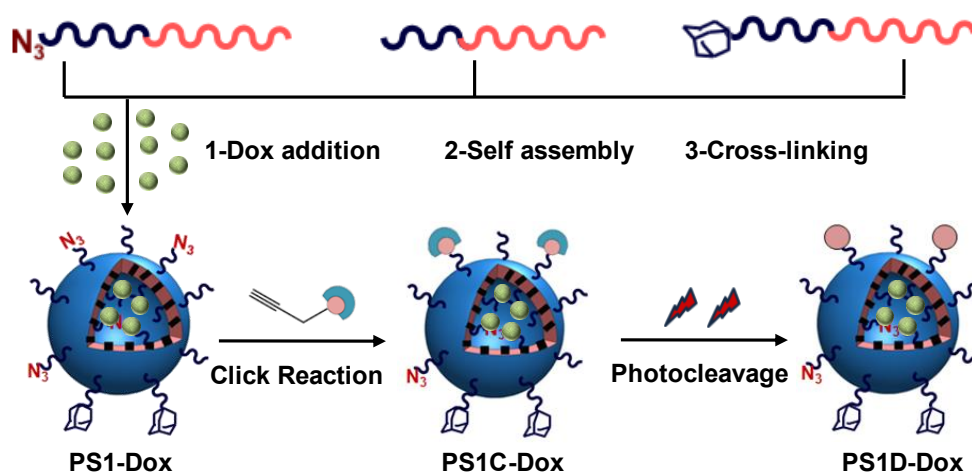


Figure 4.1 Schematic overview of the Dox encapsulated polymersomes formation through pre-loading approach.

Before proceeding release study, any possible Dox leakage was also monitored during purification of NVOC moieties. There was only a slight Dox ($15.5 \pm 2.04\%$) leakage within

two days of intensive dialysis at pH 7.4 condition (Figure 4.3). The UV-vis monitoring of the vesicles before and after the photocleavage process shows that doxorubicin molecules maintain their stability with only a small absorbance drop during the irradiation (Figure 4.3). This was an important issue to be able to analyze and interpret the release data truly.

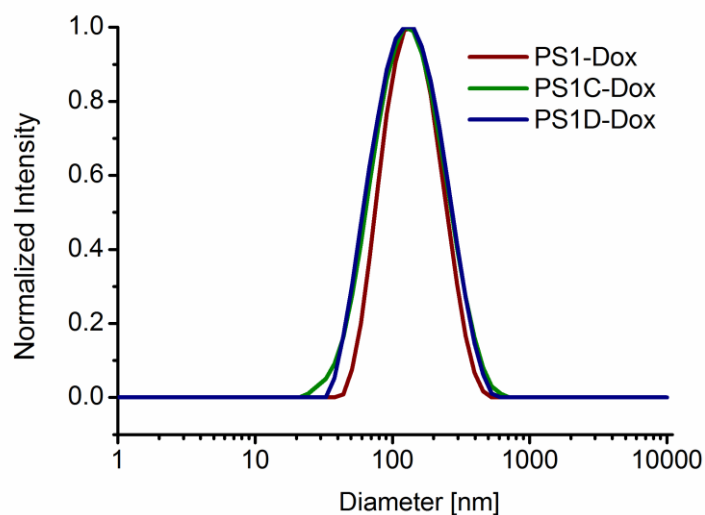


Figure 4.2 Intensity size distribution of Dox encapsulated polymersomes before (PS1-Dox) and after click reaction (PS1C-Dox) and after photocleavage (PS1D-Dox) at pH 7.4.

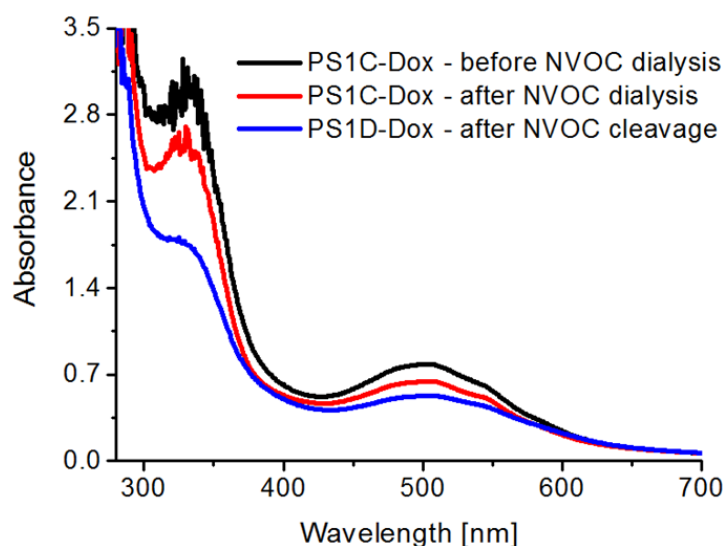


Figure 4.3 UV-vis spectra of Dox encapsulated polymersomes before and after dialysis of NVOC molecules and after subsequent irradiation process

Eventually, *in vitro* doxorubicin release from PS1C-Dox and PS1D-Dox was studied at pH 5 and pH 7.4 under physiological temperature ($T=37\text{ }^{\circ}\text{C}$). As seen in Figure 4.4, both of the polymersome systems exhibit a similar release profile. Dox was released to about 53%

within 140 h at pH 5 from PS1C-Dox polymersomes whereas for PS1D-Dox the release was determined as about 51% under the same condition. Although the membrane of the PS1D-Dox became more compact due to further UV irradiation, the pores induced by repelling of the polymer chains at acidic state were sufficient for an efficient drug release. Moreover, the closed state of the membrane decreased the undesired Dox release in a considerable amount at pH 7.4 to about 20% from PS1C-Dox and 26% from PS1D-Dox within 140 h (Figure 4.4). Both of these results confirm the claim about tunable membrane permeability and reveal the potential of this multifunctional and dual responsive nanocontainer for various biomedical applications.

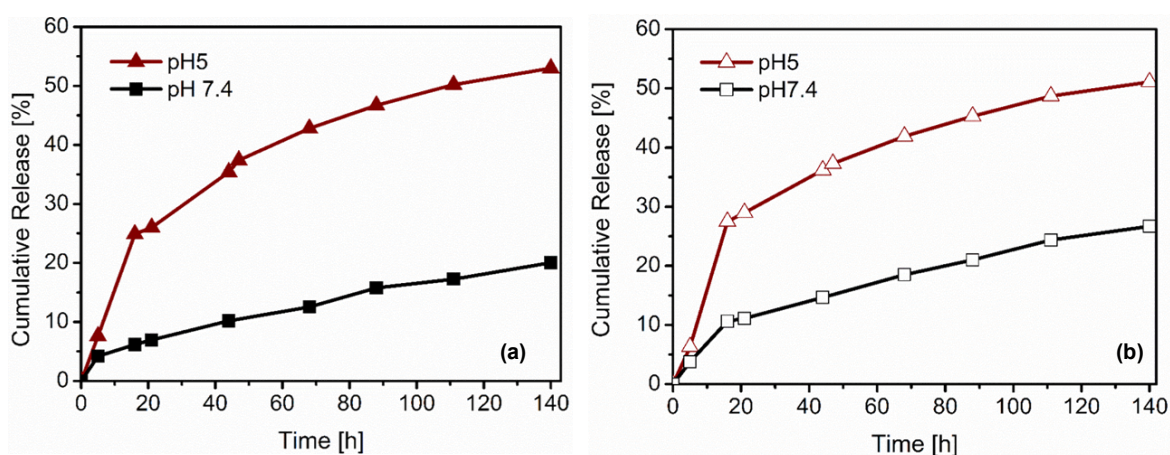


Figure 4.4 In-vitro release of doxorubicin from (a) PS1C-Dox polymersomes and (b) PS1D-Dox polymersomes at 37 °C in different pH medium

4.3 Polymersome/Gold Nanoparticle Assemblies

The doxorubicin encapsulation and further pH-dependent release approved the hosting capacity of the established polymersomes for small drug molecules. However, there is still lack of investigation whether these vesicles can incorporate sufficient amount of larger-sized nanoparticles. In addition, incorporation of a smart particle having remarkable physical and chemical properties like gold nanoparticles (AuNPs) can provide additional functions to the established polymersomes. For this purpose, two different sized-AuNPs (5 and 10 nm) were incorporated to the polymersomes by using pre-loading and post-loading approaches as seen in Figure 4.5. The latter method is performed not only for testing the feasibility of the preparation technique but also to gain information about the pH controlled diffusion behavior as well as possible interactions between gold nanoparticles and the polymersome membrane.

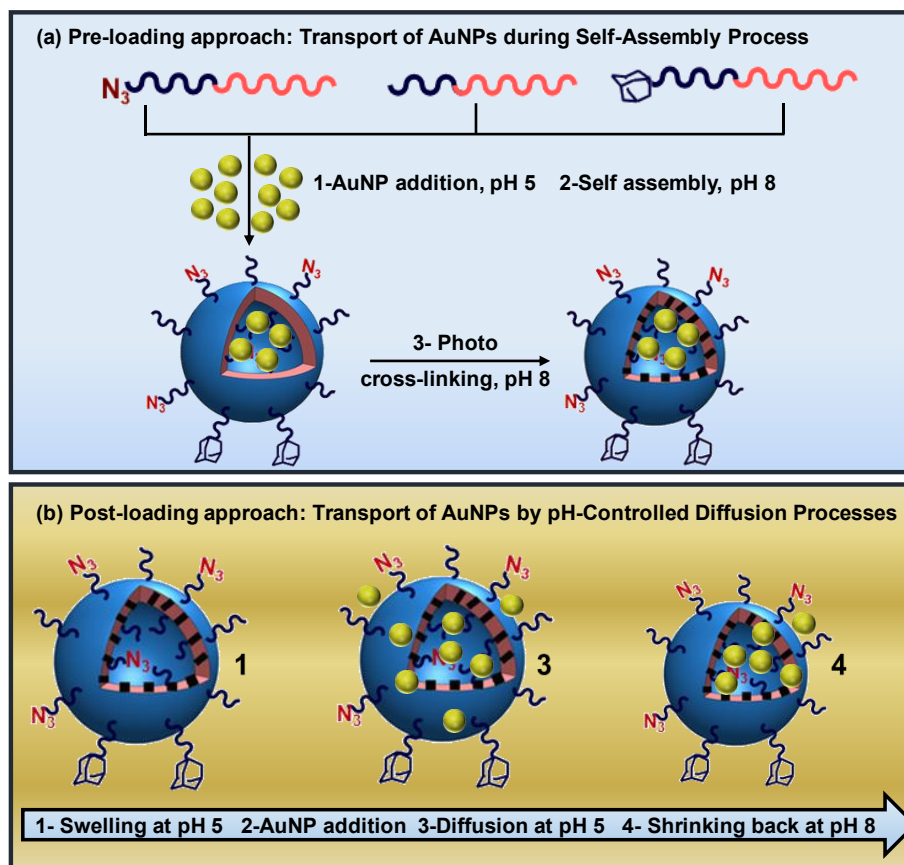


Figure 4.5 Schematic overview of the polymersome/gold nanoparticle preparation through (a) pre-loading approach and (b) post-loading approach.

The pre-loading approach has been performed as similarly done for doxorubicin encapsulation in which gold nanoparticles were loaded during the self-assembly of mixed-block copolymers. This approach functioned well for drug loading which did not disturb the self-assembly process for polymersome formation. However, some challenges have to be taken into account in the case of gold nanoparticle incorporation. Since AuNPs were provided in PBS buffer (0.1 mM), addition of this solution into dissolved block copolymers in acidic water lead to an increase in the salt amount that may cause size increase or even aggregates during the self-assembly process as shown previously on PEO-PDEAMA block copolymers.¹⁹ Therefore, the volume portions of acidic water for block copolymer (BC) dissolution and AuNP solution in PBS buffer has to be balanced to perform a smooth self-assembly process by keeping the BC concentration constant (1 mg/mL) like it was in the previous cases. Thus, two different molar ratios of AuNPs to block copolymers were used for the formation of polymersome/gold nanoparticle assemblies as shown in Table 4.1. Before proceeding to the detailed analysis with UV-Vis and DLS methods, the purification of all samples was performed by using HFF system with a transmembrane pressure of about

150 mbar to remove the non-encapsulated gold nanoparticles. Herein, two HFF membranes were assessed to ensure the sufficient purification of larger-sized gold nanoparticles. Table 4.1 summarizes these results by showing the UV-Vis data before and after the separation steps in which volume of the solutions was conserved. Therein, the control experiment using only gold nanoparticle stock solutions were carried out with two kinds of filtration membrane. In both cases, no traces of gold can be detected by UV-Vis after HFF cleaning which is a sign of successful separation. However, the filtrate collected after separation did also not have reddish color. This may be due to the fact that the removed gold nanoparticles may stick to the waste tubes or filtration membrane after separation and it was not possible to take them into the filtrate solution. Although this led to an unclear outcome for the efficiency of the separation, the UV-Vis monitoring of before and after purification steps for polymersome/gold nanoparticle assemblies approved that the most part of non-integrated gold nanoparticles can be separated with this technique. Since both types of membrane showed similar performance, the one having a 750 kDa MWCO was chosen for the purification of all gold nanoparticle encapsulated polymersomes to avoid any polymersome loss with the 50 nm pore sized-separation module.

Table 4.1 Purification of polymersome/gold nanoparticle assemblies by HFF method

Code	Molar Ratio [AuNP:BC]	Molecular weight cut-off ^a [MWCO]	Before HFF ^b [A at λ_{\max}]	After HFF ^b [A at λ_{\max}]
AuNP-10	only gold NP	750 kDa	0.71	≤ 0.01
		0.05 μm	0.71	≤ 0.01
AuNP-5	only gold NP	750 kDa	0.51	≤ 0.01
		0.05 μm	0.51	≤ 0.01
PS1-Au51	1.1	750 kDa	0.31	0.12
PS1-Au54	3.8	750 kDa	0.28	0.14
PS1-Au101	1.1	750 kDa	0.18	0.09
PS1-Au104	3.8	750 kDa	0.24	0.14

^aHFF mebrane having 750 kDa MWCO and 0.05 μm pore size are made of modified polyethersulfone and polysulfone, respectively. ^bAbsorbance is detected at λ_{\max} =522 nm and λ_{\max} =525 nm for 5 and 10 nm AuNPs, respectively.

Eventually, the UV-Vis spectrum of PS1-Au54 and PS1-A104 after purification showed a clear SPR absorption at $\lambda_{max}=522$ nm and $\lambda_{max}=525$ nm, respectively (Figure 4.6, 4.7). Herein, the sign of polymersomes can be also seen at the spectral range of $\lambda=220-400$ nm. In addition, the DLS data of these polymersomes revealed that the gold nanoparticle encapsulation as well as the slight increase of salt amount due to the PBS buffer did not lead to a noticeable size variation as can be seen in Table 4.2. Although the PDI increased slightly in comparison to the pure polymersomes, the intensity size-distribution of the PS1-Au54 and PS1-Au104 (Figure 4.8) showed a single peak with a monodisperse distribution. Thus, it can be concluded that the higher amount of gold nanoparticle concentration resulted in a satisfactory encapsulation without encountering any self-assembly problems. For this purpose, the further investigations were performed using PS1-Au54 and PS1-Au104 samples.

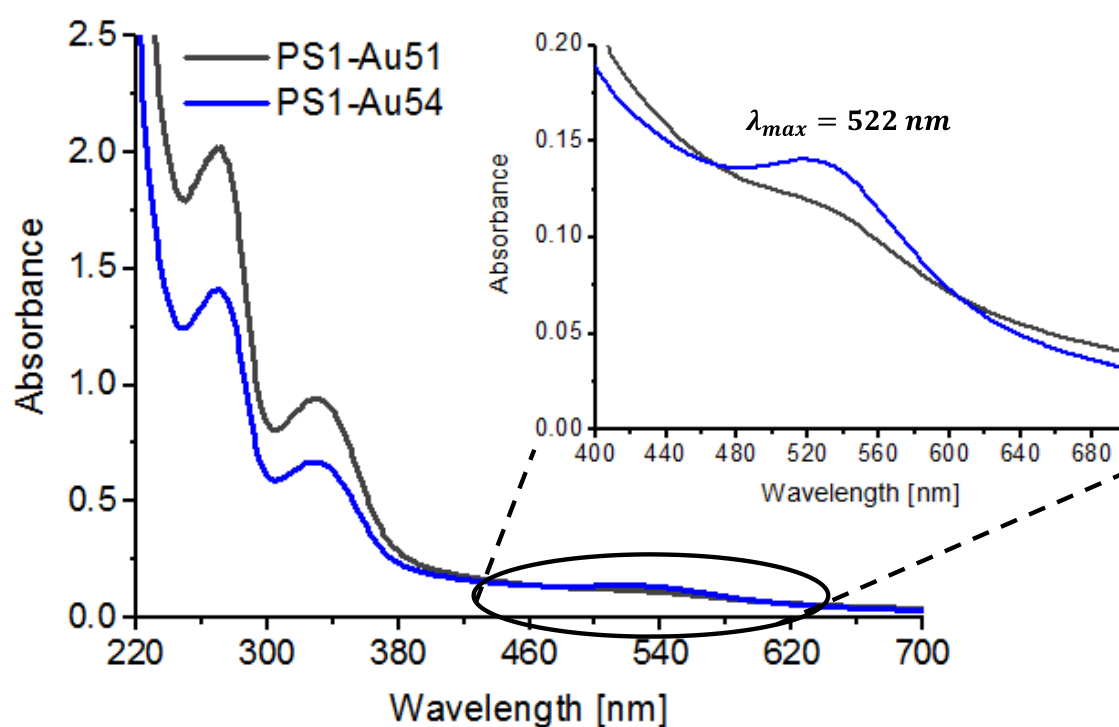


Figure 4.6 UV-vis spectra of 5 nm sized-AuNP encapsulated polymersomes after HFF purification, (a) shows the whole spectra of the PS1-Au51 and PS1-Au54 polymersomes, (b) the enlarged area of the UV-Vis spectra showing the gold nanoparticle absorbance range.

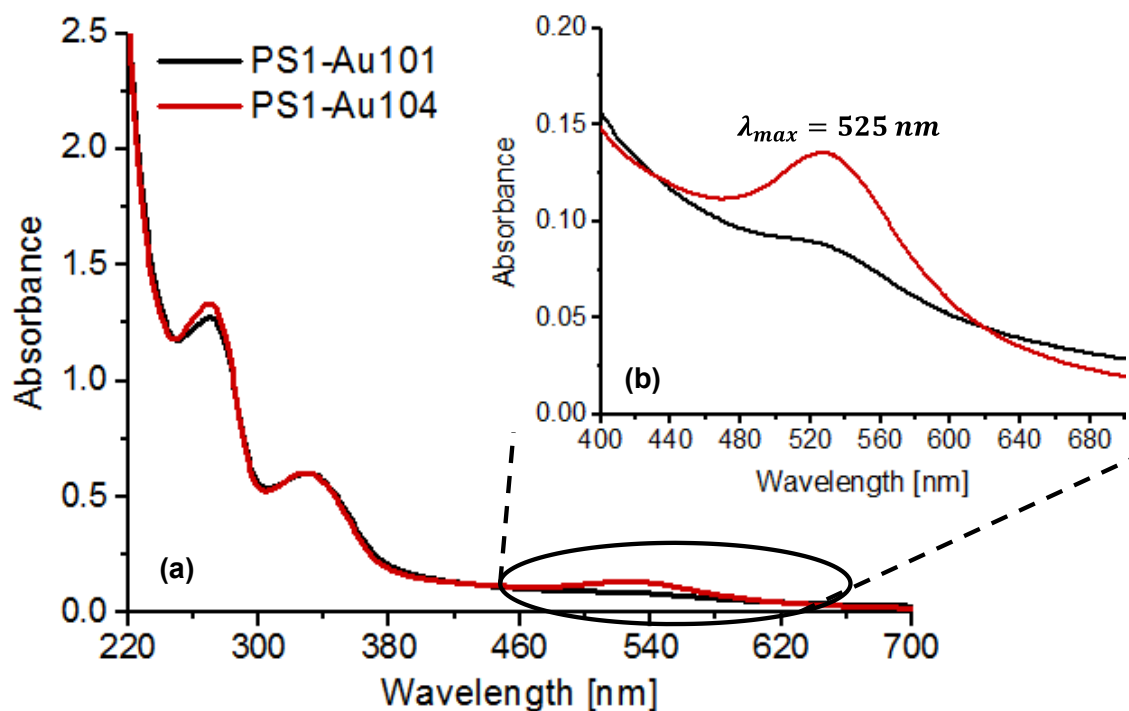


Figure 4.7 UV-vis spectra of 10 nm sized-AuNP encapsulated polymersomes after HFF purification, (a) shows the whole spectra of the PS1-Au101 and PS1-Au104 polymersomes, (b) the enlarged area of the UV-Vis spectra showing the gold nanoparticle absorbance range.

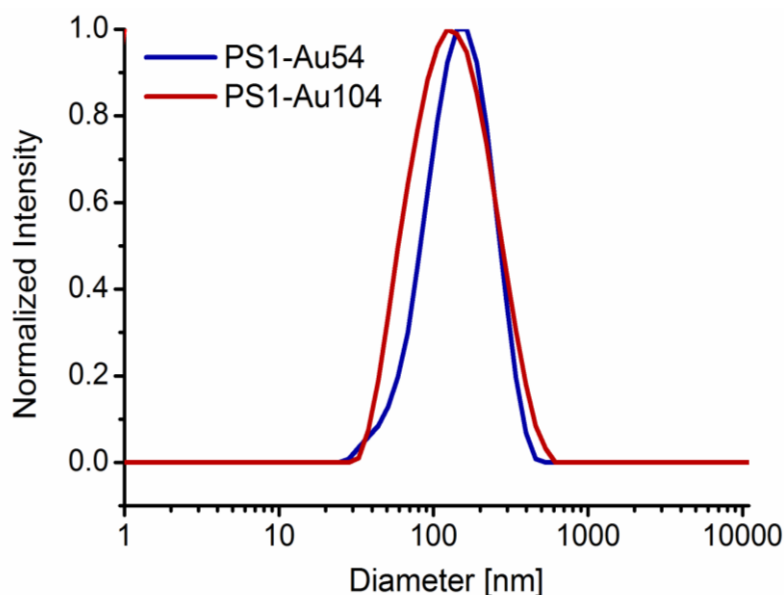


Figure 4.8 Intensity size distribution of gold nanoparticle encapsulated polymersomes through pre-loading method, PS1-A54 and PS1-A104, at pH 8.

As known, one of the characteristic properties of gold nanoparticles are surface plasmon resonance (SPR) which leads to an absorption of visible light and makes them very attractive

for the applications including diagnostic tools and biomarkers.⁸⁻¹⁰ The SPR band is responsible for the red color of the gold nanoparticle solutions which is size-dependent and can be shifted even to the longer wavelengths yielding pale blue or purple solutions for the larger-sized gold nanoparticles. Therefore, it is important to monitor the SPR shift of the polymersome/gold nanoparticle assemblies to gain information about the aggregation phenomena. As can be clearly implied, when AuNPs aggregate, their essential photochemical properties may be lost.

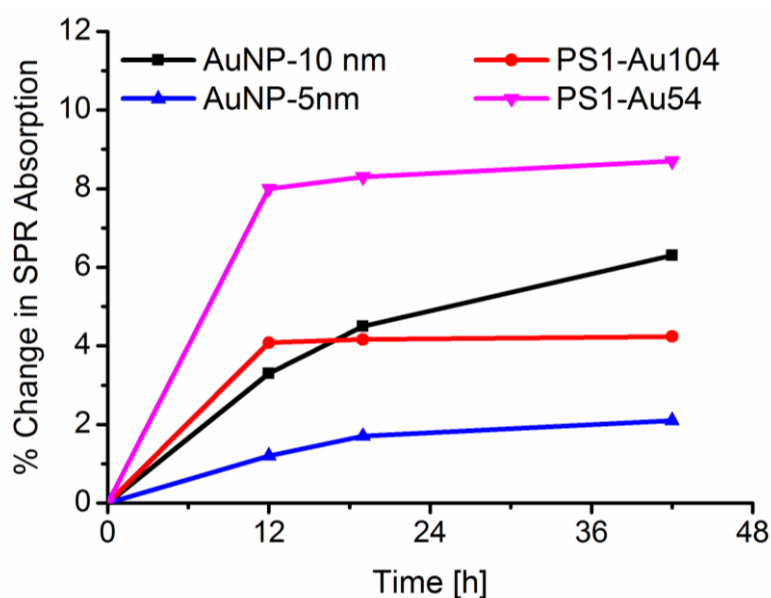


Figure 4.9 The SPR monitoring with respect to time for only gold nanoparticles, AuNP-10nm at $\lambda_{\max}=525$ nm, AuNP-5nm at $\lambda_{\max}=522$ nm, and polymersome/gold nanoparticles assemblies, PS1-Au54 at $\lambda_{\max}=522$ nm, PS1-Au104 at $\lambda_{\max}=525$ nm

For this purpose, the time-dependent UV-Vis monitoring was performed to understand this behavior more in detail (Figure 4.9). The polymersome/gold nanoparticle solutions did not show a shift at the SPR band within 42 hours of storage period which means that there was no aggregation tendency of the encapsulated gold NPs. As a control, the spectrum of only gold nanoparticles was also measured. The SPR absorption loss after 42 hours was almost similar for PS1-Au104 and 10 nm gold nanoparticles which are 4.3% and 6.3%, respectively. In addition, the SPR absorption was decreased of about 8.7 % for PS1-Au54 polymersomes and 2.1% for 5 nm sized gold nanoparticles. Although 5 nm-sized gold nanoparticles showed a slight better performance, these variations are not in a significant amount which demonstrated similar trend for both of the analyzed systems. There are

examples in literature in which gold nanoparticle loading into liposomes enhanced the stability of AuNPs by keeping the SPR absorption constantly up to 12 hours whereas the gold NPs without liposomes lost this unique property within the same storage period.²⁰ Although this is not the case for the analyzed system, polymersomes can be also utilized to avoid the aggregation of unstable gold nanoparticles. Thus, this SPR monitoring revealed that the polymersome/gold nanoparticle assemblies showed a stable phenomenon without facing any aggregation problems which is an important information for further investigations.

Table 4.2 Specifications of polymersomes/gold nanoparticle assemblies

Code	Molar Ratio [AuNP:BC]	Method	Diameter ^a [nm]	PDI ^b	Zeta potential [mV]	
					pH8	pH 5
PS1-Au51	1.1	Pre-loading	124.8±1.0	0.19±0.01	n.d	n.d
PS1-Au54	3.8	Pre-loading	128.2±1.6	0.20±0.01	6.6±1.3	22.9±0.4
PS1-Au101	1.1	Pre-loading	113.9±1.3	0.25±0.01	n.d	n.d.
PS1-Au104	3.8	Pre-loading	116.6±1.2	0.24±0.01	6.8±0.5	24.2±1.0
PS1-Au54P	3.8	Post-loading	133.9±1.4	0.27±0.02	2.5±0.1	17.2±0.3
PS1-104P	3.8	Post-loading	127.4±1.2	0.22±0.02	0.1±0.5	21.3±0.7
PS1	-	-	120.0±1.6	0.20±0.03	5.0±0.9	23.7±0.4

^aHydrodynamic diameter is measured by DLS at pH 8. ^bPDI= polydispersity index of polymersome/gold nanoparticle assemblies that shows the size variation.

As a next step, cryogenic transmission electron microscopy was conducted to visualize polymersome/gold nanoparticle assemblies. Although spectroscopic methods verified the incorporation of the gold nanoparticles into polymersomes, cryo-TEM imaging provides an information about the location of the nanoparticles within the polymeric vesicles (Figure 4.10). As can be inferred, this also enables a direct picture of the shape and morphological

changes if present. The first outcome of PS1-Au54 and PS1-Au104 imaging was that the pre-loading approach did not disturb the final morphologies in a significant manner although a few overlapped and collapsed structures were observed when analyzing many cryo-TEM micrographs. In addition, Figure 4.11 and 4.12 confirm the successful gold nanoparticle encapsulation in which up to 13 AuNPs can be hosted by a single polymersome particle. These micrographs also show that the AuNPs can be placed at different locations within the polymersomes as illustrated in Figure 4.10.

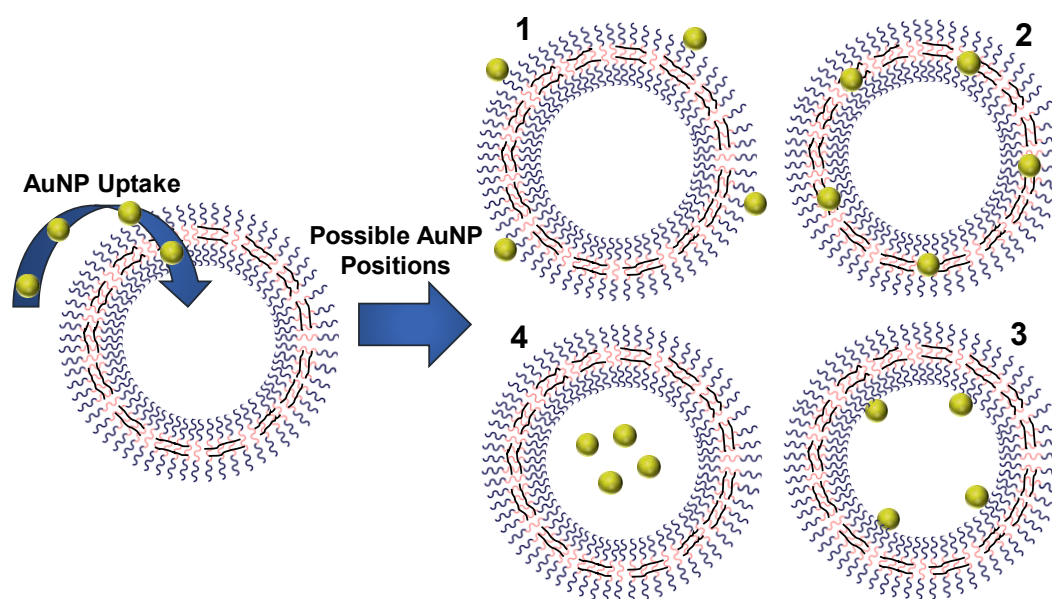


Figure 4.10 Scheme of the possible AuNP positions in polymersomes after the uptake process in which they can be located at the outer (1) or inner (3) hydrophilic part of the bilayer membrane, and are stuck/embedded within the hydrophobic region (2) and finally can be guided into the aqueous lumen (4).

It should be noted that although hydrophilic gold nanoparticles are expected to be in contact with hydrophilic corona or placed at the aqueous lumen, the AuNPs may be stuck at the hydrophobic vesicle wall as well. This phenomenon can relate to molecular interactions, but can relate also to thermodynamic equilibrium of final self-assembled structures as well as the size ratio between AuNPs and the membrane thickness.²¹⁻²² Xu et al. has already shown that the escape of gold nanoparticles from polymeric vesicle walls in spherical micelles is an entropy-driven phenomena.²² By keeping this in mind, the charge of the particles should indeed have a role in this placement since polymersome membrane contains PDEAEM groups. For this purpose, the zeta potential of PS1-Au54 and PS1-Au104 samples

as well as individual gold nanoparticle solutions and polymersomes were measured at pH 8 and pH 5 condition as seen in table 4.2. Gold nanoparticles are highly negatively charged in both acidic and basic states which are having ζ potential of -19.3 ± 2.7 and -25.3 ± 2.4 for 5 nm and 10 nm sized-AuNPs, respectively. Although polymersome/gold nanoparticle assemblies are almost neutral at pH 8, they became highly cationic at acidic condition. In this manner, it is possible that some AuNPs electrostatically interacted with the polymeric chains when added to the solution at pH 5 during self-assembly process which were then freed by increasing the pH to a basic state and form the polymersomes. However, some of them may still be stuck in the hydrophobic membrane and cannot escape due to the interactions and energetic reasons as well as the geometrical considerations as mentioned previously. In order to clarify this claim, post-loading approach was performed which gives more information about the physical interactions of gold nanoparticles and polymersomes since in this approach AuNPs are added after forming the vesicles.

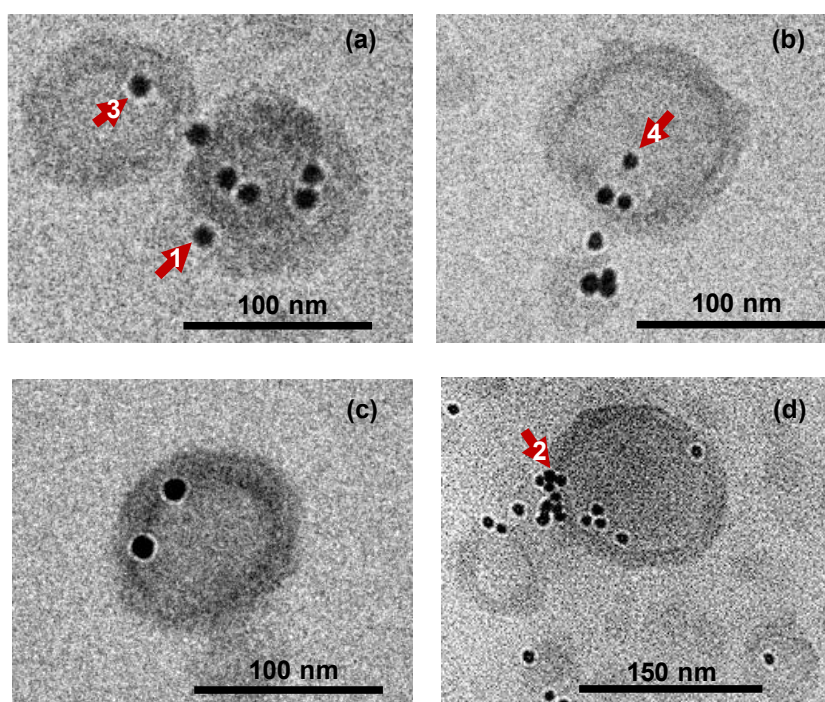


Figure 4.11 cryo-TEM micrographs of PS1-Au104 polymersomes at pH 8. (a,b) AuNPs (~10 nm) were placed at the outer (1) or inner (3) hydrophilic part of the membrane and guided into the aqueous lumen (4). (c) AuNPs were placed at the interphase of shell and the hydrophilic corona. (d) This image shows the maximum number of AuNP incorporation into one single polymersome and exemplifies the embedded AuNPs at the hydrophobic membrane (2).

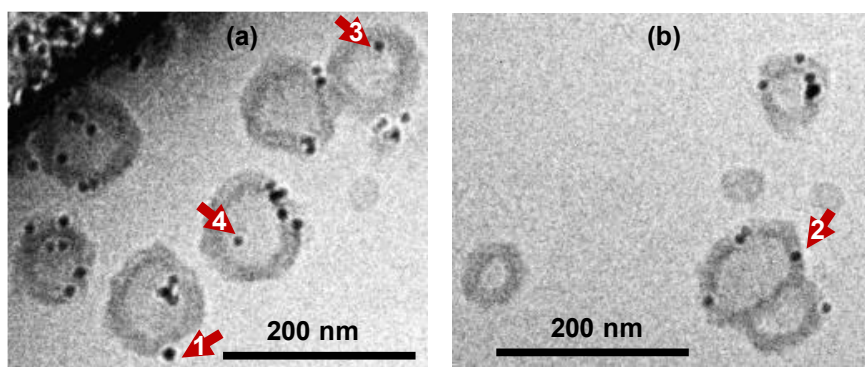


Figure 4.12 cryo-TEM micrographs of PS1-Au54 polymersomes at pH 8. (a,b) AuNPs (~5 nm) were placed at the outer (1) or inner (3) hydrophilic part of the bilayer membrane and are stuck within the hydrophobic region of the membrane (2) as well as guided into the aqueous lumen (4).

In order to form polymersome/gold nanoparticle assemblies by means of post-loading approach, gold nanoparticle solutions were added to the pre-formed polymersomes at acidic condition (pH 5) and the resulting mixture was stirred for an hour to provide sufficient time for the uptake process before increasing the pH to the basic state (pH 8) (Figure 4.5). Herein, no purification was applied since the target was to lighten up the AuNP-polymersome interactions and monitor the diffusion of the larger-sized particles into polymersome lumen. Therefore, the PS1-Au54P and PS1-Au104P samples were directly visualized by cryo-TEM as shown in Figure 4.13. The DLS analysis showed a similar trend like the samples obtained by pre-loading approach and the polymersomes have monodisperse distribution with slight increase in PDI as shown in Table 4.2 and Figure 4.14. Herein, the polymersome morphologies were less disturbed in comparison to the pre-loading approach as monitored by several cryo-TEM micrographs.

The final investigation of this part was the comparison of two approaches by determining the AuNP fraction within the polymersomes. Herein, several polymersomes having gold nanoparticles were analyzed from many cryo-TEM micrographs and the number based ratios are given in Table 4.3. Although pre-loading approach enabled more gold nanoparticle incorporation, the trend of the AuNP internalization was similar for both techniques. Another essential result was that 5 nm sized AuNPs could easily diffuse into the polymersome lumen and only 24.5% of the integrated gold nanoparticles were placed at the outer hydrophilic corona. However, this efficiency was decreased for 10 nm-sized gold nanoparticles. Most of the particles were internalized at the outer region or stuck in the membrane. Only a few of

them diffused into the polymersome lumen. This result showed that the AuNP diffusion into the vesicles is size-dependent as expected but not limited by electrostatic interactions. Since the smaller AuNPs can be easily transported into the polymersome lumen with post-loading approach, it can be concluded that the highly negatively charged gold nanoparticles can be freed when changing the charge of the polymersomes from cationic (pH 5) to neutral (pH 8) and are not embedded at the outer region of the polymersome membrane due to the electrostatic interactions. As proposed previously, the internalization of AuNPs within the polymersomes is triggered randomly and only a few of them were interestingly stuck at the hydrophobic membrane that may be due to geometrical and energetic reasons like size dependence or the entropic effect.

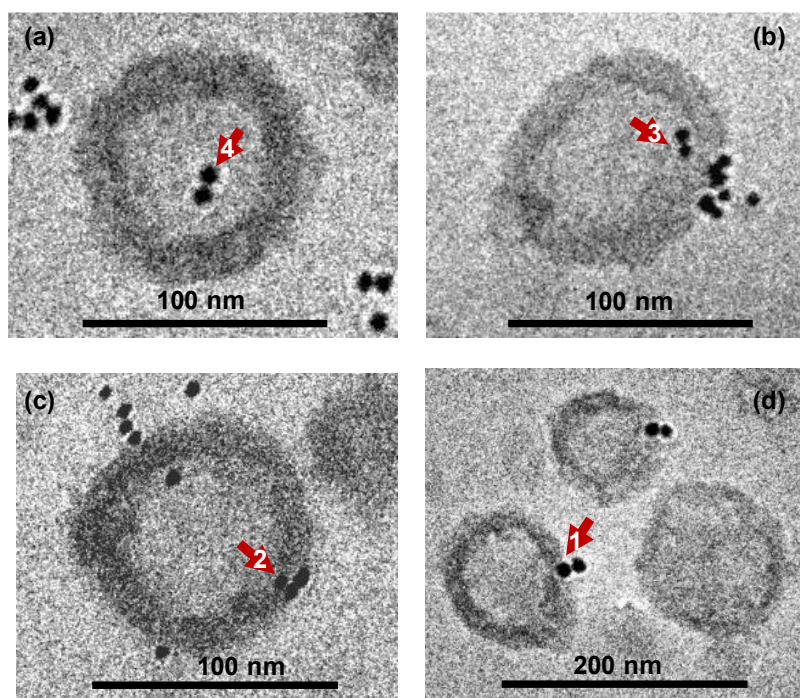


Figure 4.13 cryo-TEM micrographs of PS1-Au54P and PS1-Au104P polymersomes at pH 8. (a,b,c) AuNPs (~5 nm) were placed at the outer (1) or inner (3) hydrophilic part of the membrane and guided into the aqueous lumen (4). (d) AuNPs (~10 nm) were placed at the outer hydrophilic region of the membrane (1).

Table 4.3 AuNP fraction of the polymersome/gold nanoparticle assemblies determined from cryo-TEM micrographs

Code	Method	AuNP Fraction ^a [N _{AuNP} : N _{PS}]	Position Related AuNP Fraction ^b [N _{AuNP} %]		max[N _{AuNP}] in single PS ^c
			1	2 + 3 + 4	
PS1-Au54	Pre-loading	441:148 = 3.0:1	15.6	84.4	9
PS1-Au104	Pre-loading	311:148 = 2.1:1	18.0	82.0	13
PS1-Au54P	Post-loading	184:69 = 2.7:1	24.5	75.5	9
PS1-104P	Post-loading	113:69 = 1.6:1	39.0	61.0	4

^aN_{AuNP} and N_{PS} represent the total number of gold nanoparticles integrated with total number of polymersomes, respectively. ^b1-4 is defined in Figure 4.10 and marked with arrows in the cryo-TEM micrographs of the corresponding samples (Figure 4.11, 4.12 and 4.13) which were calculated with respect to the total number of AuNPs integrated with polymersomes (N_{AuNP}). ^cThis value represents the maximum number of AuNPs hosted by single polymersome particle detected for each sample.

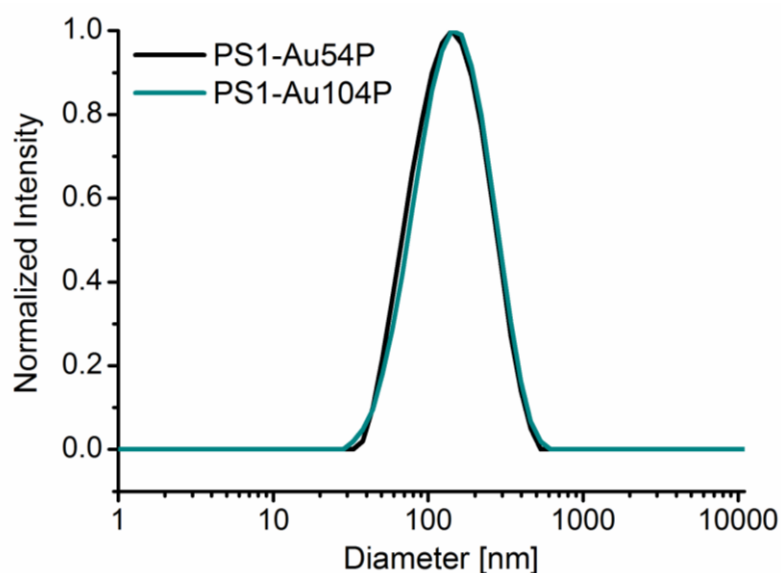


Figure 4.14 Intensity size distribution of gold nanoparticle encapsulated polymersomes prepared with post-loading method, PS1-A54P and PS1-A104P, at pH 8.

4.4 Summary

In conclusion, the hosting capacity of the established polymersomes as nanocontainers was assessed by incorporation of 5 to 10 nm sized gold nanoparticles as well as doxorubicin molecules as an anticancer drug. The first applied method for encapsulation of the cargos was the pre-loading approach in which the doxorubicin or gold nanoparticles were loaded into the azide and adamantane decorated polymersomes during self-assembly of the block copolymers. This method allows increased loading efficiency where many particles can be trapped inside of the polymersomes during formation as demonstrated by combination of different characterization techniques for both doxorubicin molecules and gold nanoparticles.

The drug encapsulation was proceeded by the sequential post-conjugation steps to form the dual responsive polymersomes in the presence of a carrier. As already shown in chapter 3, the photo-cleavage process caused a decreased swelling ratio for the established polymersome system. Since the focus of this chapter is to understand the hosting ability by means of permeability and diffusion limits, pH-dependent drug release was performed for both PS1C-Dox and PS1D-Dox polymersomes. An almost similar amount of drug release at acidic state within 140 hours (53%, PS1C-Dox, and 51%, PS1D-Dox) proved the sufficient permeability for the polymersome membrane from the perspective of drug delivery applications. This result also supports the claim that the diffusion of the molecules through the membrane can be adjusted by combining pH sensitivity and cross-linking.

Furthermore, larger-size gold nanoparticle (5 nm and 10 nm) encapsulation through pre-loading approach was also demonstrated which can provide additional functions to the established polymersomes due to the unique optical characteristics of gold NPs like surface plasmon resonance and second harmonic generation. Although these potential applications were not evaluated in this chapter, the encapsulation of these smart particles into polymersomes gave new insights about the limitations of such colloid formation including the location based-analysis caused by size-dependence and energetic reasons. Although pre-loading approach gave sufficient encapsulation efficiency, it did not provide the information about the membrane permeability for these larger sized particles in comparison to drug molecules. Another issue here was to lighten up the electrostatic interactions of AuNPs within the polymersome membrane. For this purpose, the post-loading approach was applied in which gold NPs were added to the polymersome solutions at swollen state when the porous membrane was formed. Therein, 5 nm sized AuNPs can diffuse through the

polymersome membrane with a high efficiency whereas this performance was considerably decreased for 10 nm sized AuNPs. Among the analyzed particles of 10 nm sized AuNPs, 39% of them have been already located at the outer region of the membrane and only 29% of them can totally diffuse inside and are located at the inner region without sticking to the membrane. This result underlines the permeability as well as the pH-dependent diffusion limits of the established polymersome membrane from both drug delivery perspective and larger-size smart nanoparticle incorporation.

Overall, probing hosting capacity of the polymersomes showed that these vesicles can be utilized to encapsulate several particles to act as smart nanocarriers depending on the application purpose by means of pre-loading or post-loading approaches. Besides, the gold nanoparticle incorporation can be used for signal marking to make the established polymersomes visible to be employed in designing sensing devices for diagnostic tasks.

4.5 References

- [1] Du, J.; O'Reilly, R. K., Advances and Challenges in Smart and Functional Polymer Vesicles. *Soft Matter* **2009**, *5*, 3544-3561.
- [2] Pawar, P. V.; Gohil, S. V.; Jain, J. P.; Kumar, N., Functionalized Polymersomes for Biomedical Applications. *Polymer Chemistry* **2013**, *4*, 3160-3176.
- [3] Balasubramanian, V.; Herranz-Blanco, B.; Almeida, P. V.; Hirvonen, J.; Santos, H. A., Multifaceted Polymersome Platforms: Spanning from Self-Assembly to Drug Delivery and Protocells. *Prog. Polym. Sci.*
- [4] LoPresti, C.; Lomas, H.; Massignani, M.; Smart, T.; Battaglia, G., Polymersomes: Nature Inspired Nanometer Sized Compartments. *J. Mater. Chem.* **2009**, *19*, 3576-3590.
- [5] Daniel, M.-C.; Astruc, D., Gold Nanoparticles: Assembly, Supramolecular Chemistry, Quantum-Size-Related Properties, and Applications toward Biology, Catalysis, and Nanotechnology. *Chem. Rev.* **2004**, *104*, 293-346.
- [6] Clark, H. A.; Campagnola, P. J.; Wuskell, J. P.; Lewis, A.; Loew, L. M., Second Harmonic Generation Properties of Fluorescent Polymer-Encapsulated Gold Nanoparticles. *J. Am. Chem. Soc.* **2000**, *122*, 10234-10235.
- [7] Amstad, E.; Kim, S.-H.; Weitz, D. A., Photo- and Thermoresponsive Polymersomes for Triggered Release. *Angew. Chem. Int. Ed.* **2012**, *51*, 12499-12503.
- [8] Huang, X.; El-Sayed, M. A., Gold Nanoparticles: Optical Properties and Implementations in Cancer Diagnosis and Photothermal Therapy. *Journal of Advanced Research* **2010**, *1*, 13-28.
- [9] Song, J.; Zhou, J.; Duan, H., Self-Assembled Plasmonic Vesicles of Sers-Encoded Amphiphilic Gold Nanoparticles for Cancer Cell Targeting and Traceable Intracellular Drug Delivery. *J. Am. Chem. Soc.* **2012**, *134*, 13458-13469.

- [10] Dykman, L. A.; Khlebtsov, N. G., Uptake of Engineered Gold Nanoparticles into Mammalian Cells. *Chem. Rev.* **2014**, *114*, 1258-1288.
- [11] Liao, J.; Li, W.; Peng, J.; Yang, Q.; Li, H.; Wei, Y.; Zhang, X.; Qian, Z., Combined Cancer Photothermal-Chemotherapy Based on Doxorubicin/Gold Nanorod-Loaded Polymersomes. *Theranostics* **2015**, *5*, 345-356.
- [12] Reichenbach, P.; Eng, L. M.; Georgi, U.; Voit, B. 3d-Steering and Superfocusing of Second-Harmonic Radiation through Plasmonic Nano Antenna Arrays. *J. Laser Appl.*, **2012**; *24*, 042005-1 042005-7.
- [13] Cao, X.; Ye, Y.; Liu, S., Gold Nanoparticle-Based Signal Amplification for Biosensing. *Anal. Biochem.* **2011**, *417*, 1-16.
- [14] Iyisan, B.; Kluge, J.; Formanek, P.; Voit, B.; Appelhans, D., Multifunctional and Dual-Responsive Polymersomes as Robust Nanocontainers: Design, Formation by Sequential Post-Conjugations, and pH-Controlled Drug Release. *Chem. Mater.* **2016**, *28*, 1513-1525.
- [15] Yassin, M. A.; Appelhans, D.; Wiedemuth, R.; Formanek, P.; Boye, S.; Lederer, A.; Temme, A.; Voit, B., Overcoming Concealment Effects of Targeting Moieties in the Peg Corona: Controlled Permeable Polymersomes Decorated with Folate-Antennae for Selective Targeting of Tumor Cells. *Small* **2015**, *11*, 1580-1591.
- [16] Ahmed, F.; Pakunlu, R. I.; Brannan, A.; Bates, F.; Minko, T.; Discher, D. E., Biodegradable Polymersomes Loaded with Both Paclitaxel and Doxorubicin Permeate and Shrink Tumors, Inducing Apoptosis in Proportion to Accumulated Drug. *J. Controlled Release* **2006**, *116*, 150-158.
- [17] Onaca, O.; Enea, R.; Hughes, D. W.; Meier, W., Stimuli-Responsive Polymersomes as Nanocarriers for Drug and Gene Delivery. *Macromol. Biosci.* **2009**, *9*, 129-139.
- [18] Soergel, M.; Kirschstein, M.; Busch, C.; Danne, T.; Gellermann, J.; Holl, R.; Krull, F.; Reichert, H.; Reusz, G. S.; Rascher, W., Oscillometric Twenty-Four-Hour Ambulatory Blood Pressure Values in Healthy Children and Adolescents: A Multicenter Trial Including 1141 Subjects. *The Journal of Pediatrics* **1997**, *130*, 178-184.
- [19] Adams, D. J.; Butler, M. F.; Weaver, A. C., Effect of Block Length, Polydispersity, and Salt Concentration on PEO-PDEAMA Block Copolymer Structures in Dilute Solution. *Langmuir* **2006**, *22*, 4534-4540.
- [20] Kojima, C.; Hirano, Y.; Kono, K., In *Methods Enzymol.*, Nejat, D., Ed. Academic Press: **2009**, pp 131-145.
- [21] Le Meins, J. F.; Sandre, O.; Lecommandoux, S., Recent Trends in the Tuning of Polymersomes' Membrane Properties. *The European Physical Journal E* **2011**, *34*, 1-17.
- [22] Xu, J.; Han, Y.; Cui, J.; Jiang, W., Size Selective Incorporation of Gold Nanoparticles in Diblock Copolymer Vesicle Wall. *Langmuir* **2013**, *29*, 10383-10392.

5 Immobilized-Multifunctional Polymersomes on Solid Surfaces

5.1 Introduction

Fixing polymersomes onto surfaces is in high demand not only for the characterization with advanced microscopy techniques but also for designing specific compartments in microsystem devices in the scope of nanobiotechnology. Unlike liposomes, the use of polymersomes for such purposes is not widely investigated so far. However, the sufficient accessibility and reactivity of the established multifunctional polymersomes can be favored to conjugate bio/chemo recognition elements for sensing purposes to design microsystem devices. Relying on the light responsive nature of the fabricated polymersomes, such recognition processes can be mimicked through photochemical reactions on solid surfaces. In addition, the hosting ability of the polymersomes as nanocontainers can be utilized to encapsulate the signal markers like enzymes or gold nanoparticles as investigated, to function as signal amplifiers for designing sensing devices. Similar approaches have been already used in liposome based biosensors for detection of nucleic acids,¹ antibodies² or large biomacromolecules.³ However, as known, polymersomes show an enhanced stability as well as reduced permeability in comparison to the liposomes which encounter problems like higher diffusion through the membrane, lack of rigidity and lipid oxidation.⁴⁻⁵ In this regard, it is really worthwhile to investigate the potential of polymersomes to design robust, responsive and reactive surfaces for the fabrication of microfluidic devices. This can also give the opportunity to use polymersomes as cell membrane model to provide more insight about complex natural biomacromolecule interactions.

In order to reach the mentioned goals, immobilization of polymersomes onto suitable surfaces is necessary. Most reported vesicle immobilization methods are based on direct adsorption onto silicon or mica substrates via unspecific and/or electrostatic interactions.⁶⁻⁹ Only a few of the reported strategies focused on more controlled ways of immobilization strategies such as biotin-streptavidin conjugations¹⁰⁻¹¹ and covalent attachment through vesicles having aldehyde end groups onto aminated glass surfaces.¹² Due to the proven affinity of adamantane groups on polymersome surface to the β -cyclodextrin molecules, the same chemistry is adapted into this chapter for polymersome immobilization. In addition, the high association constant (10^4 to 10^5 M^{-1})¹³⁻¹⁴ of such host-guest interactions is believed to provide stable binding of the polymersomes on solid substrates. Once surface immobilized polymersomes have been achieved, further insights can be obtained such as understanding

the responsive behavior of the polymer membrane not only in the freely diffusing case but also under several physical constraints and simulating specific interactions. As can be inferred, interactions between the vesicle membrane and its surrounding play an essential role for the application of these nanovesicles in various fields.

Hence, this chapter is already published¹⁵ and firstly deals with the surface immobilization of multifunctional and photo-crosslinked polymersomes as shown in Figure 5.1. The second investigation is tuning the adhesion properties of the polymersomes by varying the attractive forces on β -CD coated substrates. This study is aimed for gaining information about the shape deformation of the vesicles when adhering to the surfaces. This is obviously significant not only for mimicking cellular adhesion but also for the conjugation of these vesicles to other systems like gel particles or polymeric microchannels. The further steps focus on the pH and light sensitive nature of these surface-bound smart vesicles in which the latter one also provides photo-patterning by NIR induced photoreactions through two photon absorption mechanism. This nonlinear optical phenomenon enables to reach the final excited state of the molecules using photons of half the energy leading to a very localized reaction area. Furthermore, the attachment of model fluorescent compounds mimicking biorecognition molecules into locally released amine groups on polymersome surface by IR trigger is also discussed to fulfil the aimed concept for designing microsystem devices in the scope of biomedical applications.

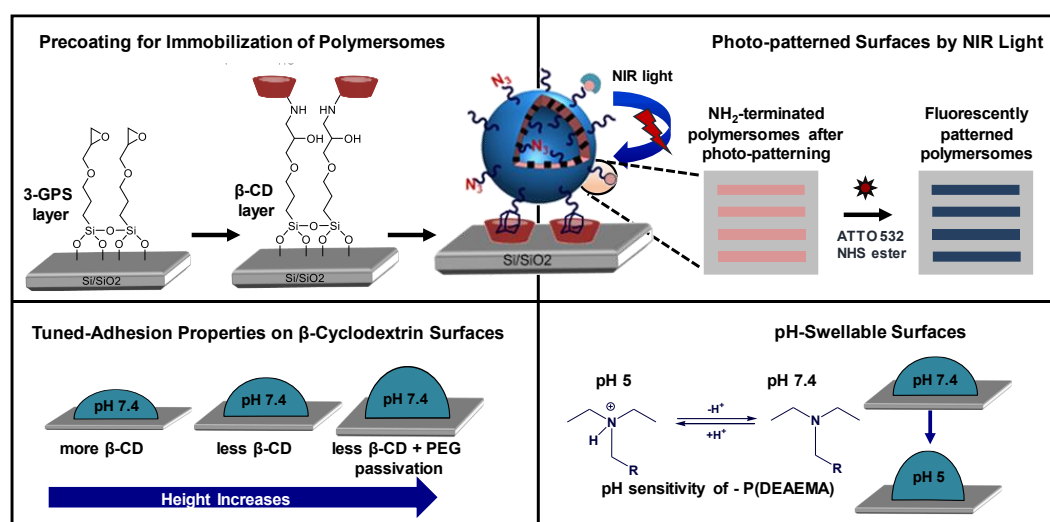


Figure 5.1 Schematic overview of polymersome immobilization by adamantane- β -cyclodextrin host-guest complexation leading to spherical cap like shapes on the surface and further steps including tuned-adhesion properties, pH swellable surfaces and NIR induced photochemical reactions

5.2 Preparation of β -cyclodextrin Coated Substrates

The preparation of β -cyclodextrin coated substrates (S2, S3) was performed by applying a two-step route as shown in Figure 5.2. The process started with the formation of 3-glycidyloxypropyltrimethoxysilane (3-GPS) self-assembled monolayers (SAMs) on the substrate. To realize this modification step, the Si wafers or glass slides were firstly activated with plasma cleaning followed by the treatment with 1 vol% epoxy silane solution in toluene. The chosen concentration as well as the deposition time and temperature play an important role to have a smooth monolayer formation.¹⁶⁻¹⁷ A previous report by Luzinov et al. investigated the effect of several parameters on 3-GPS SAMs fabrication. By analyzing SPM images, contact angles and thickness values of the epoxysilane films, it was observed that the decrease of the solution concentration below 1 vol% resulted in a globular aggregate formation.¹⁷ Therefore, this work was taken as the base for SAMs preparation to have a homogeneous layer formation.

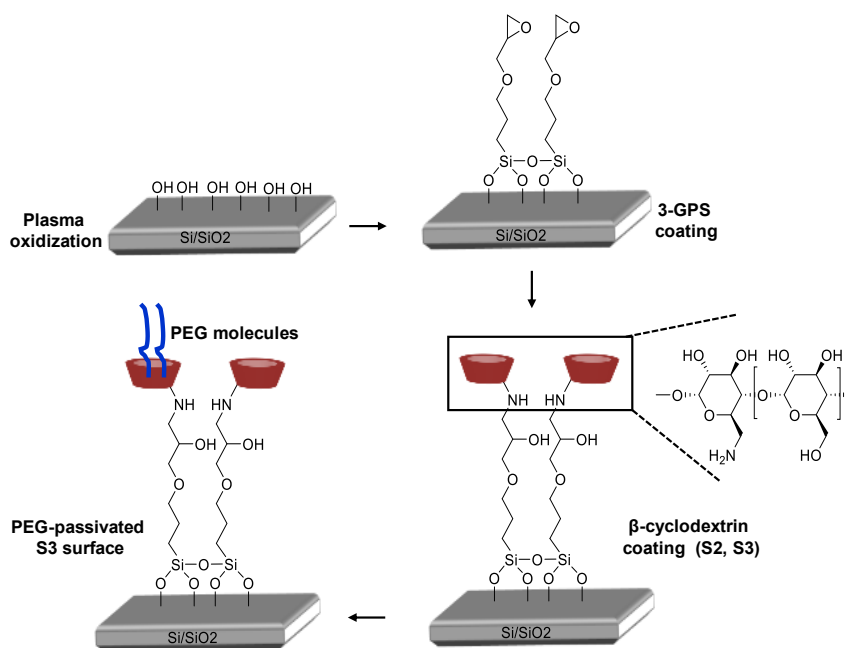


Figure 5.2 Precoating steps to prepare β -cyclodextrin modified substrates (S2, S3) and further PEG passivation on S3 surface by postulated PEG threading into the cavity of cyclodextrin.

As seen in Table 5.1, the values for advancing contact angles of the epoxy silane films show as expected the hydrophilic character of the layers and are consistent with the previously reported studies.^{16, 18} The low deviation in the 15 repeated (5 samples at 3

different regions) measurements supports both homogeneity and the reproducibility for the SAMs layer. In addition, AFM analysis was conducted to gain more information about the surface morphology of the monolayers. The topography images of the 3-GPS coated Si wafer showed a smooth layer without any aggregates having a roughness of about 0.4 nm (Figure 5.3, Table 5.1). This result is also consistent with the thickness values obtained by ellipsometry measurements. As seen in Table 5.1, the thickness of the 3-GPS layer was 1.25 nm which is close to the extended length of the epoxysilane molecules (0.95 nm) estimated from computer models applied by Luzinov et al.¹⁷

Table 5.1 Characterization of the self-assembled monolayers

Code	Coating	Θ_A^a [H ₂ O, deg]		Θ_R^a [H ₂ O, deg]		Thickness ^b [nm]	Roughness ^c [nm]
		Si wafer	Glass	Si wafer	Glass		
S1	3-GPS	61.0±1.1	61.6±1.1	40.3±1.4	33.4±1.3	1.25±0.05	0.41±0.02
S2	β -CD [1 mM]	51.2±1.9	50.7±1.9	30.1±2.2	33.8±1.8	1.05±0.28	0.40±0.11
S3	β -CD [0.1 mM]	52.0±2.1	50.4±2.2	34.1±3.3	32.3±2.5	1.03±0.27	0.50±0.14
S4	PEG passivated S3 surface	48.1±7.3	n.d.	22.6±3.1	n.d.	n.d.	n.d.

^aAdvancing (Θ_A) and receding (Θ_R) water contact angles. ^bThickness determined by ellipsometry measurements. ^cAverage roughness (Ra) determined by AFM

As a next step, the β -cyclodextrin molecules with amino end groups reacted with the available epoxy functionalities on the surface (Figure 5.2) to obtain the aimed substrates for the immobilization of adamantane-decorated polymersomes. It is very common to utilize epoxide-amine ring opening reactions in material science due to the ease of chemistry as well as high conjugation yields at mild reaction conditions.¹⁹ For instance, a similar conjugation was realized in a previous study by simply rinsing NH₂- β -CD aqueous solution on top of a 3-GPS coated Mach-Zehnder interferometer at room temperature.²⁰ To avoid an uncontrolled reaction and thus multilayer or aggregate formation on the surface, it was chosen to perform this coating at room temperature using the mono-amino-terminated CD molecules at two different concentrations (0.1 mM and 1 mM in phosphate buffer at pH 8). The decrease in the advancing contact angles revealed the clear change of the surface hydrophilicity as expected after β -CD coating (Table 5.1). The angle of about 51° together

with the determined 1 nm ellipsometric thickness corresponds to a successful monolayer fabrication which is in agreement with the previous reported studies.²¹⁻²² It is also important to mention that the β -CD cavity has a height of 0.78 nm²⁰ which is very close to the measured ellipsometric thickness. During the optimization of this coating step, it was observed even 4 to 7 nm thickness values at other modification parameters like the use of higher concentration of β -CD molecules. Therefore, 1 nm is a reasonable result to assume that the cavity of the β -CD molecules is positioned on the upper side of the surface (Figure 5.2) which is necessary for the host-guest inclusion formation during polymersome immobilization as previously reported by many groups.^{20, 22} The AFM topographical imaging shows that the surface roughness increases when β -CD content is decreased (Figure 5.3, Table 5.1). However, both S2 ($R_a=0.4$ nm) and S3 ($R_a=0.5$ nm) substrates show satisfactory smoothness to perform polymersome immobilization as the next step.

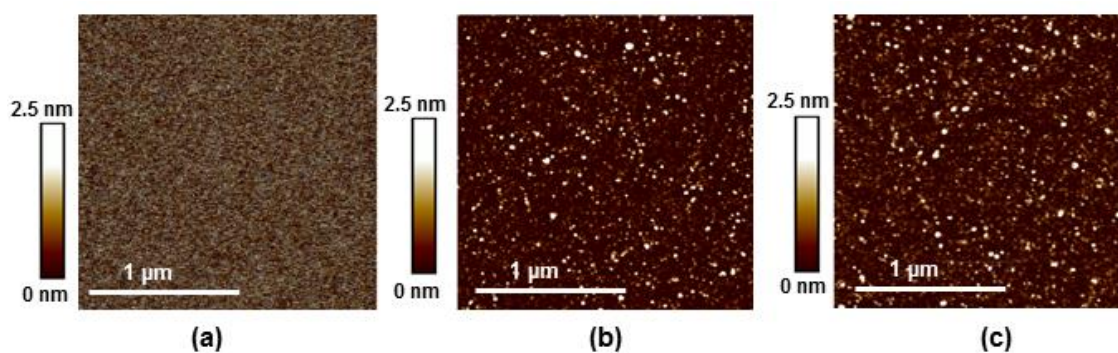


Figure 5.3 Tapping-mode AFM height image of (a) the plasma activated silicon wafer, (b) 3-GPS SAMs layer, S1, (c) β -CD coated layer, S2.

The final surface for polymersome immobilization was prepared by passivation of the β -CD coated surfaces (Table 5.1, S3) with poly(ethylene glycol) (PEG) molecules. Poly(ethylene glycol) has been widely used to obtain protein-resistant surfaces by utilizing them as passivation agent in various fields.²³⁻²⁴ Therefore different concentrations of PEG molecules (MeO-PEG-NH₂, Mn:750 g/mol) were prepared to decide the optimum condition by simply inspecting the surface hydrophilicity. Herein, the substrates were analyzed by contact angle measurements from different regions to see the deviation. The successful surface passivation was found for the highest concentration (0.25 mM, S4, Table 5.1) where the average contact angle of the surface was found as $48.1 \pm 7.3^\circ$. However, the other two passivation concentrations (0.11 mM, 0.05 Mm) did make any considerable change in the surface hydrophilicity. As can be implied that the surface heterogeneity increased since the

receding contact angle was reduced from $34.1 \pm 3.3^\circ$ to $22.6 \pm 3.1^\circ$ (Table 5.1). Since blocking all cyclodextrin molecules on the substrate was not desired, the PEG concentration was not increased anymore and this surface (S4) was used in polymersome immobilization together with other β -cyclodextrin coated surfaces (S2, S3).

5.3 Polymersome Immobilization

The chosen conjugation chemistry to attach polymersomes onto solid surfaces was the well-known adamantane- β -cyclodextrin host-guest interaction mechanism¹³⁻¹⁴ as previously applied using PS1 polymersomes and β -CD molecules (chapter 3). To trigger this non-covalent attachment, the adamantane functionalized polymersome (PS1) was prepared again by simply mixing the suitably end modified block copolymers (Figure 5.4, BC1-BC3) and let them self-assemble via pH switching method.²⁵ As a reminder for this chapter, the previously described block copolymer structures for self-assembly can be seen in Figure 5.4. In addition, the light responsive polymersomes having NVOC moieties were also favored in immobilization study to try out IR-induced photochemical reactions on surfaces. Thus, the polymersomes used in this chapter are summarized in Table 5.2. Therein, the size distributions of the resulting polymersomes measured by DLS and the ratios of the functional groups of all polymersomes are stated.

Table 5.2 Specifications of polymersomes used for immobilization studies

Polymersome	Functional groups [mol%]			Diameter[nm]	PDI ^b
	N ₃	NVOC ^a	Ada		
PS0	-	-	-	117±1.1	0.19±0.03
PS1	29.0	-	9.2	120±1.6	0.20±0.03
PS1C	21.3	7.7	9.2	117±0.2	0.20±0.01
PS3	90.8	-	9.2	116±0.4	0.20±0.01
PS3C	66.7	24.1	9.2	119±0.1	0.19±0.02

^aThese values represent the functionalities only at the outer surface of the membrane and determined according to the estimated conjugation efficiency of NVOC groups (chapter 3).

^bPDI = polydispersity index of polymersomes that shows the size variation.

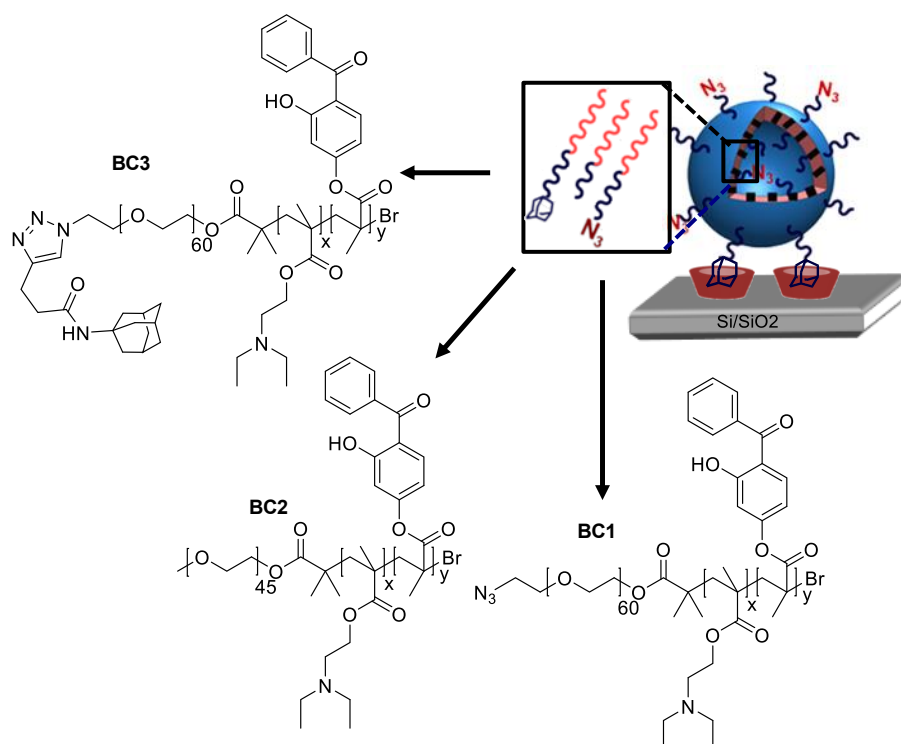


Figure 5.4 The illustrative scheme of the surface-immobilized polymersomes showing the chemical structure the used block copolymers in polymersome formation

Afterwards, incubation of the prepared polymersomes (PS1) with the cyclodextrin coated surfaces by constant stirring led to the surface-bounded polymersomes (Table 5.3) which were then rinsed 3 times with PBS buffer (pH 7.4) to remove any unbounded vesicles from the surface. This way of immobilization (constant stirring) was selected to avoid any aggregated structures on the substrate due to immobilization procedure. Before proceeding to further investigations, the first step was to ensure the successful immobilization with a suitable technique. A typical way to analyze such surface-immobilized vesicles is to use in-situ AFM under a liquid droplet (liquid-AFM) which enables the visualization of assembled supramolecular structures in the wet state. Although liquid-AFM is very advantageous to image the polymersomes in their native environment, the possible deformation of the relatively soft particles during the measurement has to be kept to a minimum. For this purpose, AFM studies were conducted at peak force tapping mode which allows precise control over the probe sample interaction with the lowest available forces and highest resolution imaging in comparison to conventional tapping mode measurements.²⁶⁻²⁷ This clearly helps to maintain the polymersome integrity and avoids the dislocation of the sample due to high shear forces during liquid-AFM measurements. In this regard, the presence of polymersomes, captured on pre-coated silicon wafers in a fluid cantilever holder at pH 7.4

PBS buffer, is confirmed by the corresponding AFM images (Figure 5.5) The selection of this pH value was to mimic the physiological conditions as well as to work under conditions where the membrane of the vesicles is not permeable. The AFM analysis of β -CD coated Si wafer at identical conditions in wet state was also performed to compare it with polymersome-incubated surfaces (Figure 5.5a). As clearly observed in the topography images (Figure 5.5b-d), the particles present are the deposited polymersomes on β -CD surfaces and these are now ready for further analysis.

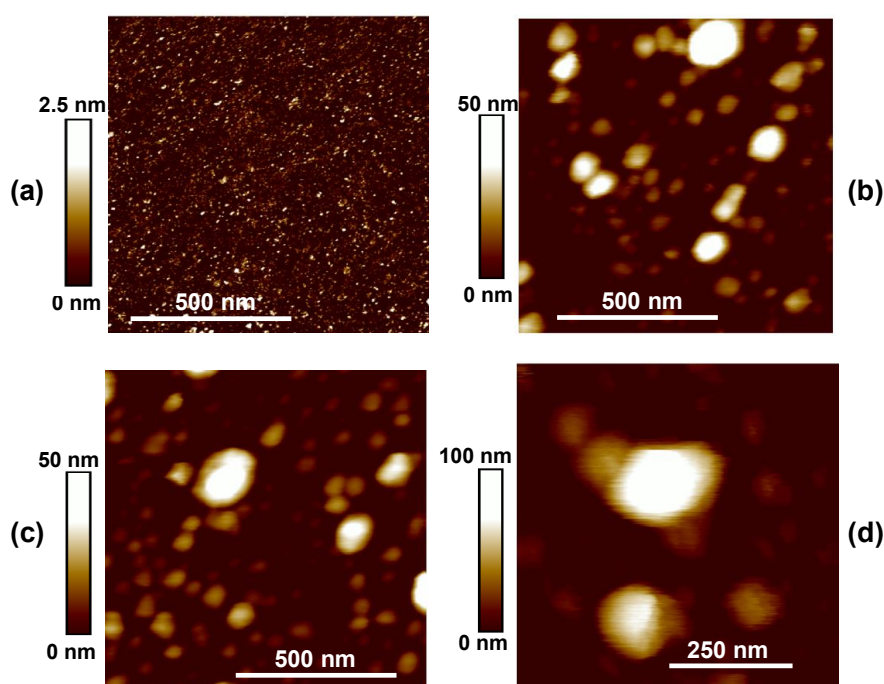


Figure 5.5 (a) Peak force tapping mode liquid-AFM height image of β -CD coated layer (S3) at pH 7.4. (b) small area of PS1-S2 polymersomes (PS1 on S2 surface) at pH 7.4, and (c) at pH 5 in swollen state. (d) small area of PS1-S3 polymersomes (PS1 on S3 surface) at pH 7.4

5.4 Tuning Adhesion Properties of the Immobilized Polymersomes

After achieving the polymersome fixation onto solid substrates, the question how these particles behave upon different adhering surfaces was raised. Because it is a common phenomenon to encounter a deformation or even rupture of such vesicles including liposomes and polymersomes during an immobilization process. Several investigations show that binding a spherical vesicle to a solid substrate often ends up with either spherical caps or bilayer structures depending on the degree of interaction between the adsorbed vesicle and the surface.^{7-10, 12} For this purpose, the immobilization of adamantane functionalized

polymersome (PS1) was carried out using cyclodextrin coated substrates having different level of surface coverage as can be seen in Figure 5.6 and Table 5.3.

Table 5.3 Adsorption behavior of PS1 polymersomes on β -CD coated surfaces

Code ^a	Height ^b [nm]		D/H ^c	
	pH 7.4	pH 5	pH 7.4	pH 5
PS1-S2	42	64	2.30±0.56	1.73±0.46
PS1-S3	52	85	1.89±0.13	1.41±0.18
PS1-S4	70	n.d	1.36±0.15	n.d.

^aRepresents the immobilized polymersomes on S2 to S4 surfaces having different β -CD coverage (see Table 4.1). ^{b,c}Represents the average height and the average ratio of diameter to height values obtained several particle analyses from AFM micrographs.

In this regard, the first assessment was to define the shape geometry of the immobilized polymersomes for each surface. Several well-isolated particles visualized by liquid-AFM were analyzed to obtain the height and diameter values of the vesicles at pH 7.4 condition. From Figure 5.6d and e, one can conclude that the height of the polymersomes has a linear relationship with the diameter for both of the samples (PS1-S2, PS1-S3). This is a logic finding which is in agreement with a previous study where biotinylated-polymersome immobilization onto streptavidin coated substrates was investigated by Battaglia et al.¹⁰ The analysis also gave the opportunity to calculate the average diameter to height ratio of the PS1-S2 and PS1-S3 samples (statistics for about 150 well isolated particles) which are 2.30±0.56, and 1.89±0.13 respectively (Table 5.3, Figure 5.6d and e). This was the first indication to imply that the polymersomes were laying on the surface as spherical caps. However, in the analysis of PS1-S2 surfaces, some flat-like structures having heights of 21 to 23 nm and diameters of 66 to 73 nm have been observed. Since the thickness of the polymersome membrane was found as 18.6 nm from cryo-TEM studies (chapter 3), it is assumed that these structures may have rearranged to a bilayer structure rather than being spherical caps. Thus, polymersomes tend to spread more strongly on the substrate which has more cyclodextrin on it (S2). In addition, the average height of the polymersomes increased from 42 nm (PS1-S2) to 52 nm (PS1-S3) when immobilized to less-concentrated cyclodextrin-coated substrate (S3) (Figure 5.6 d and e). This was another evidence to

indicate that a more active surface led to more spreading as well as flattening of the immobilized polymersomes. A possible explanation to this fact is that the higher amount of attractions between adamantane and cyclodextrin molecules from different sections of the polymersome membrane caused a higher deformation in the shape. This is in agreement with a previous report where the flattening effect of surface activeness on (PDMS-b-PMOXA) vesicles adsorbed on oxidized Si wafers and mica substrates was explored.⁷ This behavior was also supported by another study which showed that the increasing molecular recognition between streptavidin layers and biotinylated-liposomes induced a height decrease in the vesicle structures.²⁸

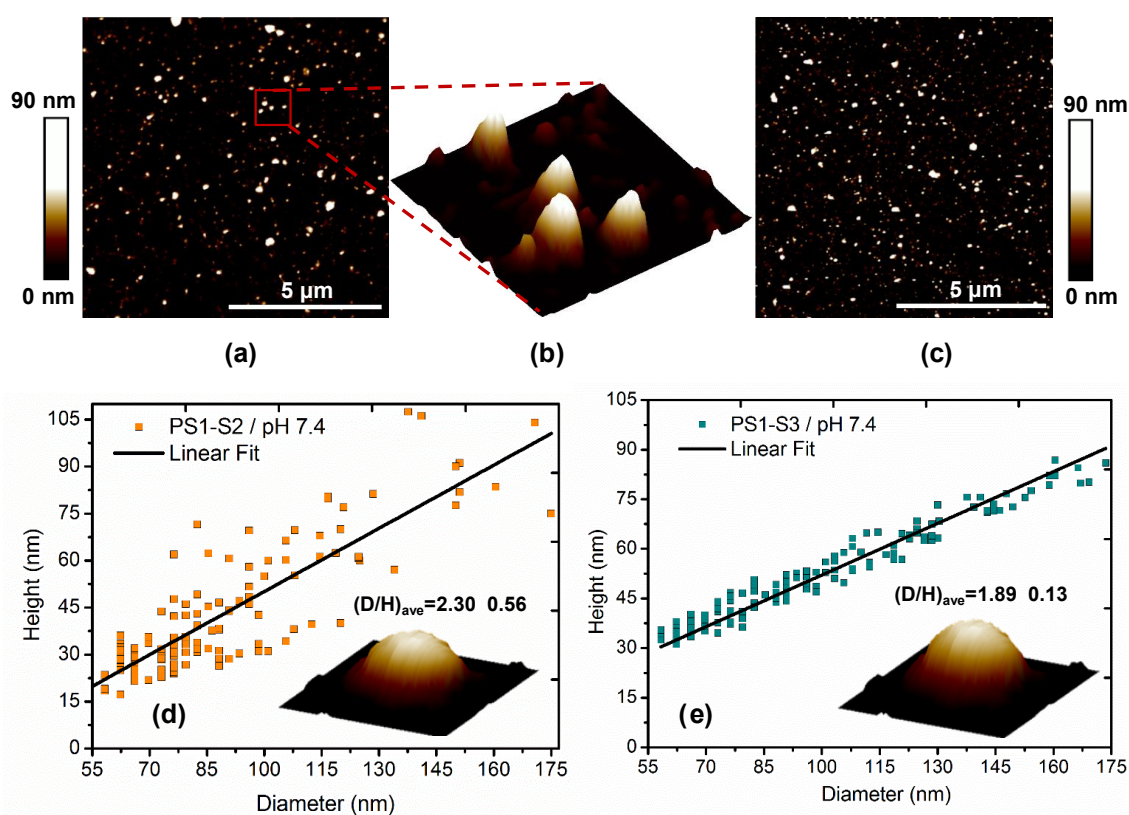


Figure 5.6 Peak force tapping mode liquid AFM height image of PS1-S3 (a) and PS1-S2 (c) polymersomes at pH 7.4 condition, (b) 3D-image of the marked region of the PS1-S3 polymersomes. Height vs diameter relationship for (d) PS1-S2 and (e) PS1-S3 polymersomes (inset schemes: 3D image of a single polymersome illustrating the shape variation due to the different adhering forces on S2 and S3 surfaces)

Furthermore, particle size distributions of the surface-immobilized polymersomes were compared with the data obtained from cryo-TEM analysis (Figure 5.7). Since polymersomes have adopted a shape of spherical caps once attached to the surface, the diameter value

acquired from AFM was not representing the diameter of the corresponding sphere. Although PS1-S3 polymersomes showed a trend to be adsorbed almost as hemisphere, the condition was not the same for PS1-S2 polymersomes. Therefore, the diameter of the undisturbed polymersome was derived via simple geometrical calculations from the following equation to represent the equivalent spherical dimension for a more precise comparison with cryo TEM as well as DLS results of the PS1 vesicles.

$$R_{sphere} = \frac{0.25W^2 + H^2}{2H}; W=\text{width}, H=\text{height}, R=\text{radius} \quad (5.1)$$

Figure 5.7 represents this particle size distribution in comparison with the dimension obtained from cryo-TEM micrographs. Both techniques show a quite good agreement by having a similar trend in the size histograms as well as exhibiting almost identical average sphere diameters obtained from AFM (100 nm) and cryo-TEM (103 nm) analysis. Although there is a small difference between the mentioned methods and the DLS results (120 nm, Table 5.2), the similarity of all analysis revealed that the possible leakage of the liquid from the interior region of the polymersome during immobilization process was not of a significant level. A similar behavior was reported previously in which (PDMS-*b*-PMOXA) vesicles had an average radius of 135 nm from AFM and 153 nm from DLS analysis.⁷

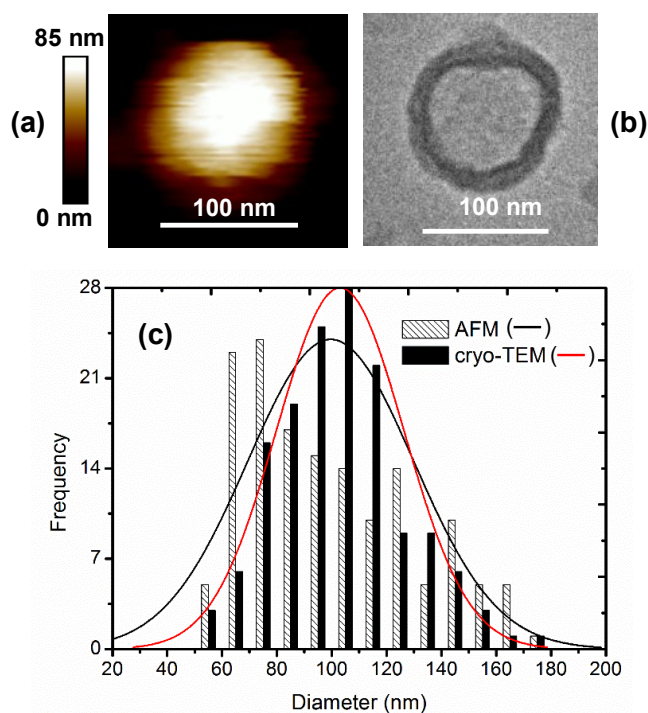


Figure 5.7 (a) Peak force tapping mode liquid-AFM height image and (b) cryo TEM image of a single polymersome, (c) AFM and cryo-TEM measured particle analysis.

The final investigation of this part was to analyze the shape of PS1 polymersomes on PEG-passivated β -CD surfaces (S4, Table 5.1, Figure 5.2). The idea behind this step was to block some of the β -cyclodextrin groups by threading of PEG chains as well as to avoid any other possible non-specific interactions on the surface. The analysis of several particles for PS1-S4 polymersomes (Table 5.3, Figure 5.8) showed that the average height increases significantly to 70 nm with an average sphere diameter of about 103 nm. This matched perfectly well with the PS1-S3 samples as well as the cryo-TEM results of PS1 polymersomes. Furthermore, the diameter to height ratio was decreased to a value of 1.36 ± 0.15 as seen in Table 5.3. Herein, it was possible to analyze more particles (about 211) since polymersomes could interact with the surface more specifically which allowed the attachment of well isolated polymersomes. It is believed that this passivation also helps to decrease the vesicle-vesicle interaction²⁹⁻³⁰ and thus, reduces polymersome aggregates on surface.

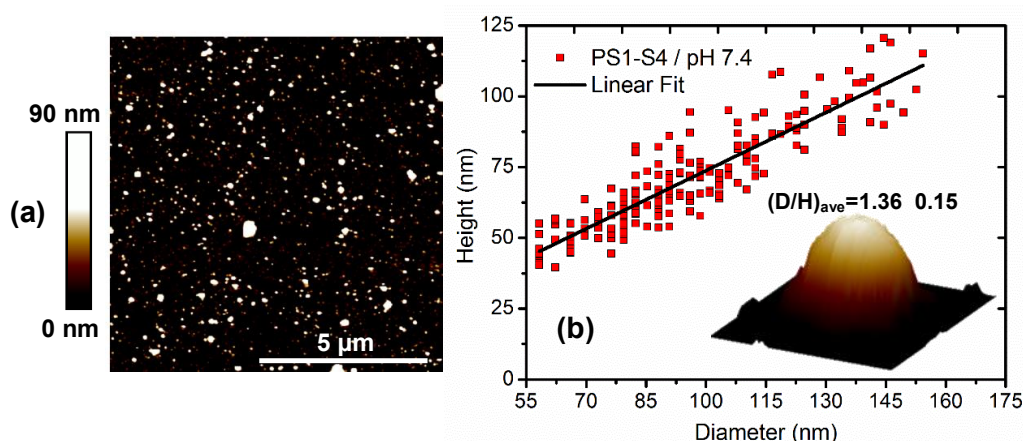


Figure 5.8 (a) Peak force tapping mode liquid AFM height image of PS1-S4 polymersomes at pH 7.4 condition (b) Height vs diameter relationship for PS1-S4 polymersomes (inset scheme: 3D image of a single polymersome illustrating the shape variation due to the different adhering forces on S4 surface).

As a control experiment, polymersomes without any adamantane groups were immobilized onto β -CD (S3) coated surfaces to clarify the nonspecific interactions. Herein, few polymersomes devoid of adamantane groups adsorb on the cyclodextrin layer (S3) which resulted in even large aggregates as visible in the image (Figure 5.9). This is in line with the previously described study for non-confined polymersomes (chapter 3) indicating that PEG chains in the polymersome corona may interact to some extent with the cavity of

β -cyclodextrin compounds. Such behavior between PEG and α -cyclodextrin molecules was also reported by various groups.³¹⁻³² To have an opinion about the level of shape change in this kind of nonspecific interactions, the particles excluding the aggregates were analyzed as done similarly for the previous samples. The average diameter to height ratio was found as 2.78 ± 0.82 with an average height of about 36 nm (Figure 5.9) which results in more flattening due to random and uncontrolled adsorption of polymersomes on the surface

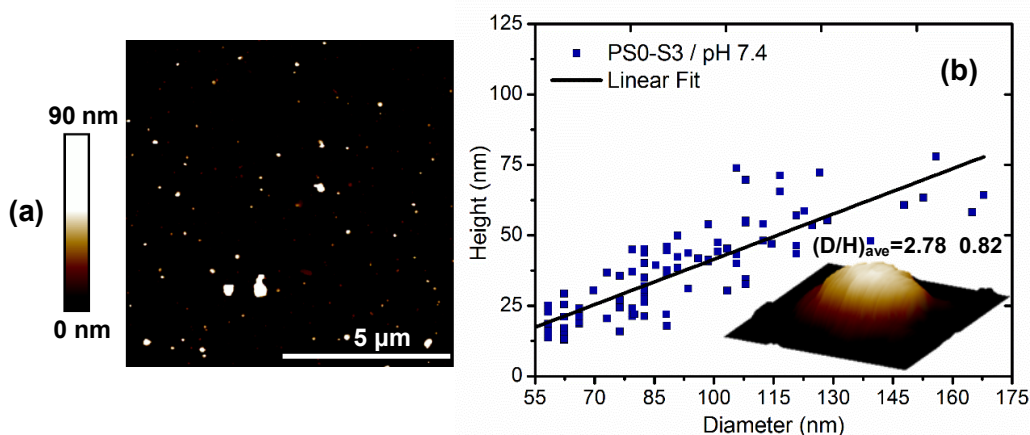


Figure 5.9 (a) Peak force tapping mode liquid AFM height image of PS0-S3 polymersomes (PS0 on S3 surface) without adamantane groups at pH 7.4 condition (b) Height vs diameter relationship for PS0-S3 polymersomes.

Thus, it can be concluded that firstly, although polymersome immobilization is induced by host-guest complexation mechanism, a small contribution of nonspecific interactions is also involved in the process like it has been shown also for biotinylated liposomes on streptavidin monolayers.²⁸ Secondly, the vesicles are pulled more strongly by the more active surface which in turn leads to a more significant change in the shape of the polymersomes during the immobilization. Using a surface passivation with PEG and having a low amount of cyclodextrin moieties significantly helps to obtain intact and isolated polymersomes in a half-spherical shape on a surface.

5.5 pH-Responsive Surface-Immobilized Polymersomes

As already explored, combination of pH sensitivity and cross-linking provides tunable membrane permeability to this multifunctional polymersome system with a swelling ability at acidic pH due to protonation of the poly(2-(diethylamino)ethyl methacrylate) block of the crosslinked membrane (Figure 5.1). This behavior should be noticeable in surface-

immobilized polymersomes as well and is favored to use these smart particles in microfluidic devices. For this purpose, PS1-S2 and PS1-S3 samples (Table 5.3) were visualized in acidic condition (pH 5) to see the response of the surface-immobilized vesicles towards pH stimulus. Figure 5.10 shows the AFM images as well as the particle size distribution for both samples at pH 5. From several particle analyses, it is seen that the average height of PS1-S2 and PS1-S3 vesicles increased to 64 nm and 85 nm, respectively. This indicates a swelling ratio of about 53% and 63 % in z-direction whereas the diameter of the particles rose 3 times less than the height. It clearly implies that polymer chains can repel more freely in z direction than in the lateral direction. Such behavior can be attributed to the competition of forces acting on vesicles within the different directions. It is believed that the adhesion forces, which act in the lateral direction, cause a higher tension within the membrane. This was also mentioned in theoretical studies of Lipowsky and Seifert.^{30, 33} The adhesive forces hamper the repelling of polymer chains which leads to a reduced swelling ratio in lateral direction of about 17% for PS1-S2 and 21% for PS1-S3, as illustrated in Figure 5.10d and e. Besides, the higher height value as well as the higher swelling ratio of PS1-S3 compared to PS1-S2 supports the previous assumption that the decreased cyclodextrin coverage on the surface leads to lower adhesion forces and therefore enables a better swelling of the polymersomes at acidic condition. It has to be emphasized that the retained pH responsivity of the surface-bound polymersomes combined with a high stability at acidic state is well matching with the undisturbed and non-confined polymersomes shown in the previous sections (chapter 3). Therein, the DLS analysis showed that the average hydrodynamic radius of the freely diffusing polymersomes in solution rose about 44% at pH 5 condition. The small difference in average swelling ratios from DLS and AFM is simply due to the confined state of polymersomes in the latter method. Besides, although numerous polymersomes (149 for PS1-S2, 148 for PS1-S3) were analyzed in AFM studies, DLS investigation enables a large scattering area in which a much higher number of particles is analyzed. However, no matter what, one can state that wet-state AFM is a very suitable tool to analyze swelling in surface-immobilized polymersomes and gives comparable results to DLS studies for non-immobilized counterparts. Thus, the clear outcome of this investigation was that the swelling power of the membrane of an immobilized polymersome is basically fully retained even though an asymmetric swelling is observed due to the surface confinement in lateral direction.

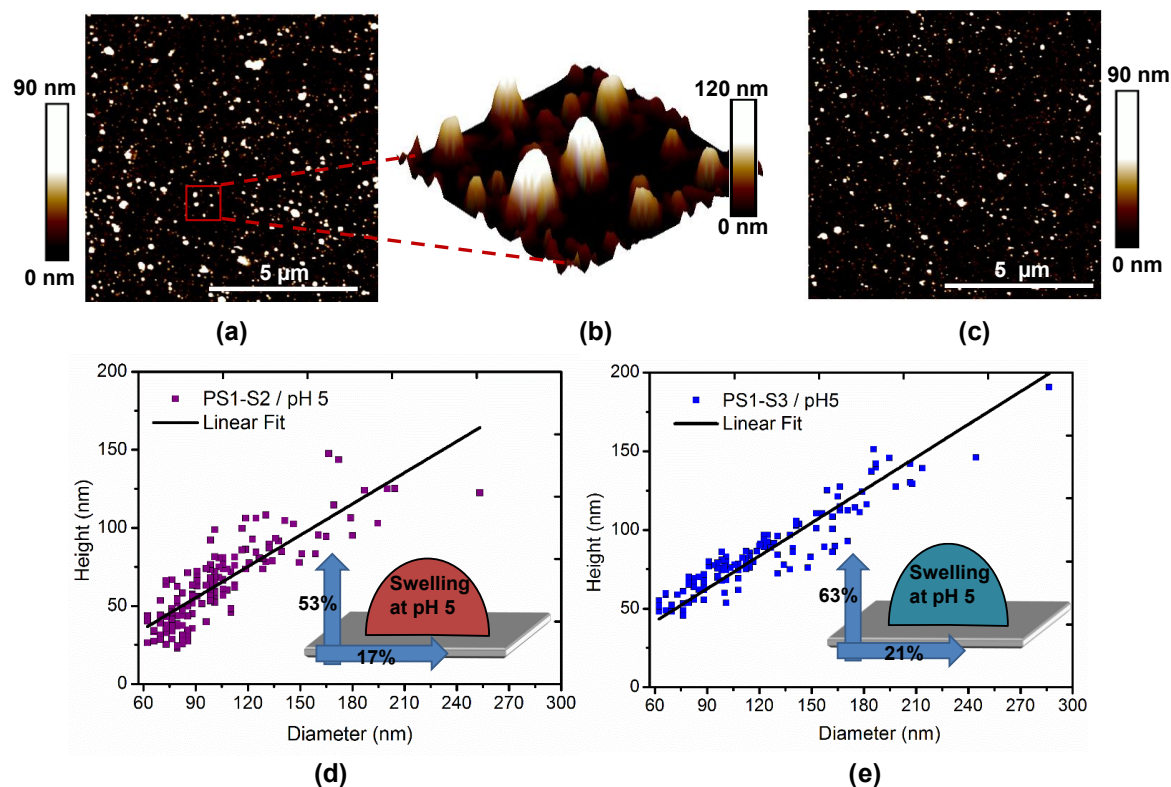
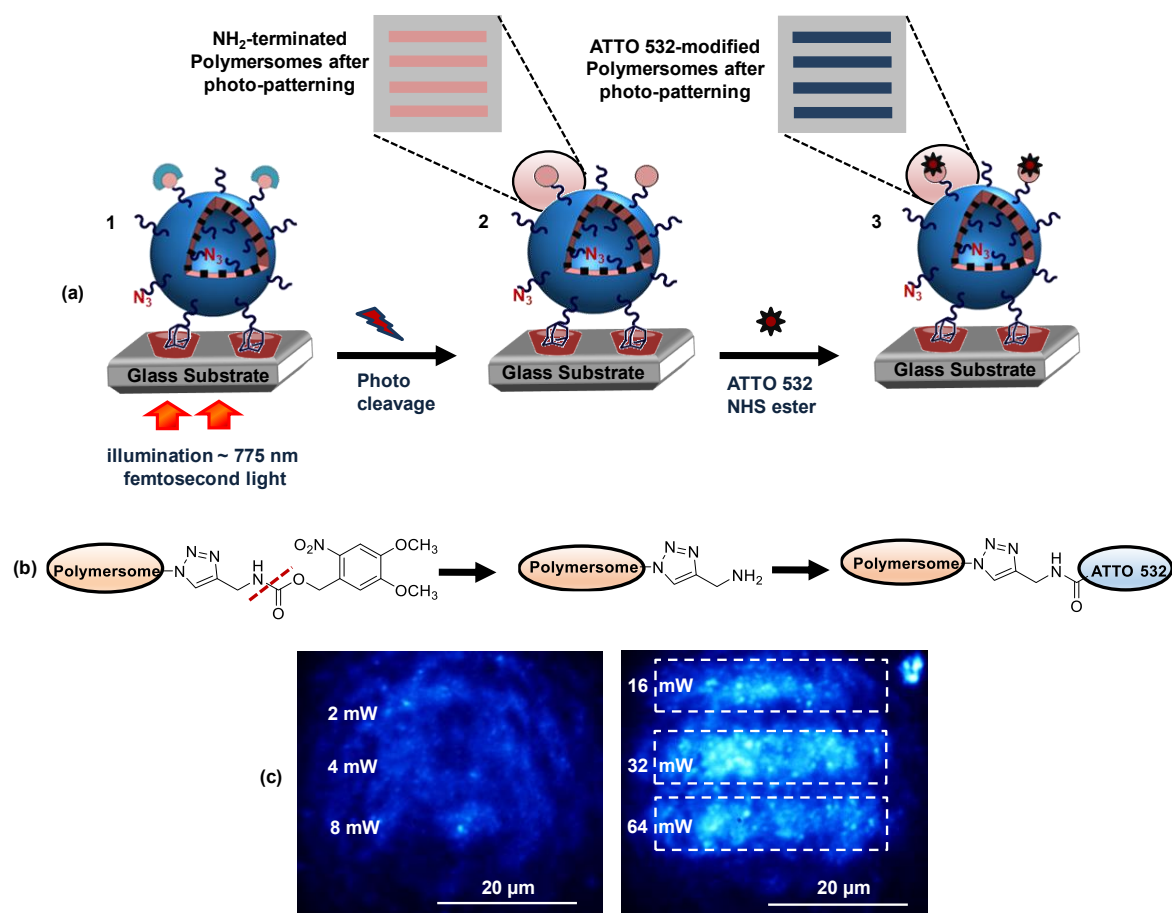


Figure 5.10 Peak force tapping mode liquid AFM height image of (a) PS1-S3 and (c) PS1-S2 polymersomes at pH 5 condition. (b) 3D-image of the marked region of the PS1-S3 polymersomes. Height vs diameter relationship for (d) PS1-S2 and (e) PS1-S3 polymersomes at pH 5 (inset schemes: representative shapes of polymersomes showing the distinct swelling ratios due to the different adhering forces on S2 and S3 surfaces as well as in different directions)

5.6 Infrared Light Induced Photochemical Reactions

To realize light responsivity of the surface-immobilized polymersomes, the previously described light responsive polymersomes were utilized in the current study in collaboration with Dr. Philipp Reichenbach (TU Dresden, IAPP) in the scope of an interdisciplinary project (SPP1327, DFG). For this purpose, NVOC-modified polymersomes with two different concentrations of 7.7 mol% (PS1C) and 24.1 mol% (PS3C) NVOC moieties were prepared (Table 5.2). As already investigated, NVOC protected amino groups on PS1C polymersomes can be cleaved selectively to obtain free amino groups on the surface by the trigger of UV light through one photon absorption mechanism (OPA). However, UV light has some drawbacks like less penetration ability and being possibly harmful to biological systems.³⁴ Therefore, here the investigation was to see whether this photocleavage was

possible by the trigger of IR light via two photon absorption mechanism (TPA). In comparison to OPA, TPA holds great advantages which can broaden the applicability of the established multifunctional system in various fields including biomedical usage. The first benefit is that TPA induced reactions are more localized than linear absorbing systems because the excitation of photons is confined to a very small volume (smaller than a femtoliter) which can enable selective reactions in a very confined region. In addition, IR light exhibits improved penetration into organic materials and can be used more safely in biological environments.³⁵



Due to these outstanding advantages, PS1C and PS3C polymersomes (Table 5.2) were immobilized onto β -cyclodextrin coated glass slides (S3) followed by an irradiation by a femtosecond laser at 775 nm wavelength with pulse duration of 100 fs (Figure 5.11). The laser irradiation was performed by writing lines of 30 μm length at different power densities. These photo-patterned lines are separated by a distance of 10 μm . All this operation was performed in pH 8 buffer solution to avoid any collapsed structures of the polymersomes in dry state as well as to keep them in their native environment and shape. As a next step, the laser-irradiated samples were immersed into a solution of fluorescent dye (ATTO 532 NHS ester) which reacts with free amino groups, to monitor the success of the photocleavage of NVOC groups on polymersome surface. After 1 day of this labelling reaction, intensive purification from unbound dye was performed by immersing the samples into a buffer solution for 2 additional days. Subsequently, the samples were visualized by fluorescence microscopy and as can be seen in Figure 5.11, fluorescent lines of the imaged parts become clearly visible with increasing power densities starting from 16 mW for the higher NVOC concentrated polymersome (PS3C) on glass slides. Here, the attachment of dye molecule does not prove only the liberated amine groups on the surface but also it mimics the conjugation of biological molecules like enzymes and proteins which requires the same conjugation chemistry. Thus, this shows a potential application of the established NVOC conjugated polymersomes to build up sensing devices for a possible selective attachment of bioreceptors.

However, although an efficient photocleavage reaction of the amino protecting group by direct UV exposure was obtained previously with freely diffusing, not surface-constrained PS1C polymersomes, a clear photo-patterned structure with surface bound PS1C by IR light (Figure 5.12) could not be reached as found in case of PS3C (Figure 5.11). But from the experiment with PS3C we can conclude that the higher the light power as well as the polymersome concentration, the more effective is the photoreaction, similar as observed previously for the photoreaction on P(MMA-co-NVOC-AEMA) copolymers via TPA mechanism.³⁶ As known, extremely high momentary intensity as provided by pulsed laser light is necessary for all nonlinear optical phenomena including TPA which cannot be obtained by continuous wave (CW) illumination with the same average power.³⁷⁻³⁸ For this purpose, as a control experiment, the same reaction was performed also with CW irradiation and, as expected, no photoreaction was observed in this condition. This supports our claim

that the immobilized NVOC conjugated polymersomes showed TPA induced photoreactions triggered by harmless IR light.

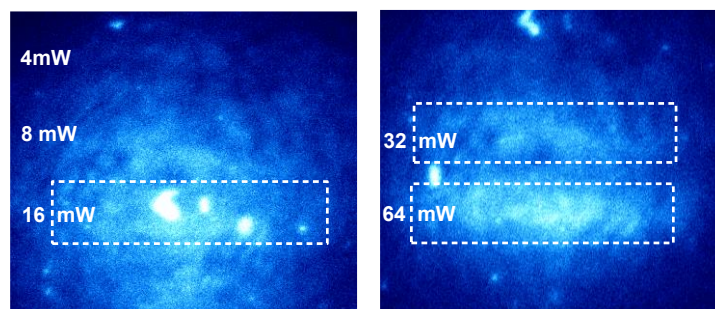


Figure 5.12 Fluorescence microscopy images of lines photochemically written on substrates with immobilized PS1C polymersomes (PS1C on S3) at pH 8 condition after labeling with fluorescent dye

5.7 Summary

In the present work, the successful immobilization of multifunctional, responsive and photo-crosslinked polymersomes having adamantane groups in the membrane onto β -cyclodextrin coated substrates was demonstrated. This approach allowed to creating spherical cap-shaped polymersome compartments at the substrate, as shown by investigation through AFM imaging in the wet state and under different environmental conditions.

The polymersomes were assessed for their adhering potential on substrates not only by specific binding through host-guest interactions but also by nonspecific interactions. This showed that shape change can be controlled and possible rupture of the vesicles can be avoided by tuning the binding forces such as decreasing β -cyclodextrin coverage on the surface as well as passivating the substrate with PEG molecules for reducing the level of nonspecific adsorption. In addition, the swelling ability of these photo-crosslinked and multifunctional polymersomes at acidic condition was preserved also in the surface-immobilized state. As expected, the swelling amount was considerably higher when the polymersomes were bound to the surface with less host-guest interactions. Thus, this study gives insight about the effect of the adhering forces between a specific surface and the vesicles on compartment shape and responsiveness at different physiological conditions (pH 5 and pH 7.4) which can be useful for future studies to mimic specific cell environments.

Another key feature of this polymersome system is light responsivity provided by conjugating photo-sensitive compounds, NVOC-protected amino groups, to the azido

moieties of the vesicle before immobilization. This previously established system (chapter 3) was used in this chapter to assess the light sensitivity of surface immobilized polymersomes towards IR irradiation via two photon absorption mechanism. It could be shown that femtosecond pulsed laser exposure ($\lambda=775$ nm) causes the cleavage of the NVOC groups. This in turn leads to controlled photopatterned structures and to free amino groups on the surface of the immobilized-vesicles which had been subsequently conjugated with a fluorescent dye and the successful binding was imaged by fluorescence microscopy imaging. Here, this simple dye molecule is a model compound to mimic biological molecules like enzymes and proteins which require the same chemistry for conjugation. IR light provides a deeper penetration depth into organic matter compared to UV light and it is not harmful for biomolecules, therefore, it is believed that this surface-immobilized polymersomes with IR light sensitive NVOC protected amines can be a promising tool for integrating targeted and selective recognition processes e.g. into microfluidic devices and in system biology.

Overall, the described findings in this chapter are highly versatile and thus exhibit new possibilities for the design of multifunctional, smart and stable compartments at surfaces which is highly interesting for many applications including development of microsystem devices, design of chemo/biosensors, and also for mimicking cell membrane functions to understand complex biological interactions.

5.8 References

- [1] Goral, V. N.; Zaytseva, N. V.; Baeumner, A. J., Electrochemical Microfluidic Biosensor for the Detection of Nucleic Acid Sequences. *Lab on a Chip* **2006**, *6*, 414-421.
- [2] Katoh, S.; Sohma, Y.; Mori, Y.; Fujita, R.; Sada, E.; Kishimura, M.; Fukuda, H., Homogeneous Immunoassay of Polyclonal Antibodies by Use of Antigen-Coupled Liposomes. *Biotechnol. Bioeng.* **1993**, *41*, 862-867.
- [3] Ho, J.-a. A.; Zeng, S.-C.; Huang, M.-R.; Kuo, H.-Y., Development of Liposomal Immunosensor for the Measurement of Insulin with Femtomole Detection. *Anal. Chim. Acta* **2006**, *556*, 127-132.
- [4] Liu, Q.; Boyd, B. J., Liposomes in Biosensors. *Analyst* **2013**, *138*, 391-409.
- [5] Antonietti, M.; Förster, S., Vesicles and Liposomes: A Self-Assembly Principle Beyond Lipids. *Adv. Mater.* **2003**, *15*, 1323-1333.
- [6] Li, F.; Ketelaar, T.; Cohen Stuart, M. A.; Sudhölter, E. J. R.; Leermakers, F. A. M.; Marcelis, A. T. M., Gentle Immobilization of Nonionic Polymersomes on Solid Substrates. *Langmuir* **2007**, *24*, 76-82.

- [7] Jaskiewicz, K.; Makowski, M.; Kappl, M.; Landfester, K.; Kroeger, A., Mechanical Properties of Poly(Dimethylsiloxane)-b-Poly(2-Methyloxazoline) Polymersomes Probed by Atomic Force Microscopy. *Langmuir* **2012**, *28*, 12629-12636.
- [8] Chen, Q.; Schonherr, H.; Vancso, G. J., Mechanical Properties of Block Copolymer Vesicle Membranes by Atomic Force Microscopy. *Soft Matter* **2009**, *5*, 4944-4950.
- [9] Gaitzsch, J.; Appelhans, D.; Janke, A.; Stempel, M.; Schwille, P.; Voit, B., Cross-Linked and Ph Sensitive Supported Polymer Bilayers from Polymersomes - Studies Concerning Thickness, Rigidity and Fluidity. *Soft Matter* **2014**, *10*, 75-82.
- [10] Battaglia, G.; LoPresti, C.; Massignani, M.; Warren, N. J.; Madsen, J.; Forster, S.; Vasilev, C.; Hobbs, J. K.; Armes, S. P.; Chirasatitsin, S.; Engler, A. J., Wet Nanoscale Imaging and Testing of Polymersomes. *Small* **2011**, *7*, 2010-2015.
- [11] Grzelakowski, M.; Onaca, O.; Rigler, P.; Kumar, M.; Meier, W., Immobilized Protein-Polymer Nanoreactors. *Small* **2009**, *5*, 2545-2548.
- [12] Domes, S.; Filiz, V.; Nitsche, J.; Frömsdorf, A.; Förster, S., Covalent Attachment of Polymersomes to Surfaces. *Langmuir* **2010**, *26*, 6927-6931.
- [13] Paolino, M.; Ennen, F.; Lamponi, S.; Cernescu, M.; Voit, B.; Cappelli, A.; Appelhans, D.; Komber, H., Cyclodextrin-Adamantane Host-Guest Interactions on the Surface of Biocompatible Adamantyl-Modified Glycodendrimers. *Macromolecules* **2013**, *46*, 3215-3227.
- [14] Böhm, I.; Isenbügel, K.; Ritter, H.; Branscheid, R.; Kolb, U., Cyclodextrin and Adamantane Host-Guest Interactions of Modified Hyperbranched Poly(Ethylene Imine) as Mimetics for Biological Membranes. *Angew. Chem.* **2011**, *123*, 8042-8045.
- [15] Iyisan, B.; Janke, A.; Reichenbach, P.; Eng, L. M.; Appelhans, D.; Voit, B., Immobilized Multifunctional Polymersomes on Solid Surfaces: Infrared Light-Induced Selective Photochemical Reactions, Ph Responsive Behavior, and Probing Mechanical Properties under Liquid Phase. *ACS Applied Materials & Interfaces* **2016**, *8*, 15788-15801.
- [16] Tsukruk, V. V.; Luzinov, I.; Julthongpiput, D., Sticky Molecular Surfaces: Epoxysilane Self-Assembled Monolayers. *Langmuir* **1999**, *15*, 3029-3032.
- [17] Luzinov, I.; Julthongpiput, D.; Liebmann-Vinson, A.; Cregger, T.; Foster, M. D.; Tsukruk, V. V., Epoxy-Terminated Self-Assembled Monolayers: Molecular Glues for Polymer Layers. *Langmuir* **2000**, *16*, 504-516.
- [18] Elender, G.; Kühner, M.; Sackmann, E., Functionalisation of Si/SiO₂ and Glass Surfaces with Ultrathin Dextran Films and Deposition of Lipid Bilayers. *Biosens. Bioelectron.* **1996**, *11*, 565-577.
- [19] Reddy, L. R.; Bhanumathi, N.; Rao, K. R., Dynamic Kinetic Asymmetric Synthesis of β -Aminoalcohols from Racemic Epoxides in Cyclodextrin Complexes under Solid State Conditions. *Chem. Commun.* **2000**, 2321-2322.
- [20] Busse, S.; DePaoli, M.; Wenz, G.; Mittler, S., An Integrated Optical Mach-Zehnder Interferometer Functionalized by B-Cyclodextrin to Monitor Binding Reactions. *Sensors Actuators B: Chem.* **2001**, *80*, 116-124.
- [21] Onclin, S.; Mulder, A.; Huskens, J.; Ravoo, B. J.; Reinhoudt, D. N., Molecular Printboards: Monolayers of B-Cyclodextrins on Silicon Oxide Surfaces. *Langmuir* **2004**, *20*, 5460-5466.

- [22] Méndez-Ardoy, A.; Steentjes, T.; Kudernac, T.; Huskens, J., Self-Assembled Monolayers on Gold of B-Cyclodextrin Adsorbates with Different Anchoring Groups. *Langmuir* **2014**, *30*, 3467-3476.
- [23] Jain, A.; Liu, R.; Xiang, Y. K.; Ha, T., Single-Molecule Pull-Down for Studying Protein Interactions. *Nat. Protocols* **2012**, *7*, 445-452.
- [24] Kannan, B.; Castelino, K.; Chen, F. F.; Majumdar, A., Lithographic Techniques and Surface Chemistries for the Fabrication of Peg-Passivated Protein Microarrays. *Biosens. Bioelectron.* **2006**, *21*, 1960-1967.
- [25] Du, J.; Tang, Y.; Lewis, A. L.; Armes, S. P., Ph-Sensitive Vesicles Based on a Biocompatible Zwitterionic Diblock Copolymer. *J. Am. Chem. Soc.* **2005**, *127*, 17982-17983.
- [26] Alsteens, D.; Dupres, V.; Yunus, S.; Latgé, J.-P.; Heinisch, J. J.; Dufrêne, Y. F., High-Resolution Imaging of Chemical and Biological Sites on Living Cells Using Peak Force Tapping Atomic Force Microscopy. *Langmuir* **2012**, *28*, 16738-16744.
- [27] Heu, C.; Berquand, A.; Elie-Caille, C.; Nicod, L., Glyphosate-Induced Stiffening of Hacat Keratinocytes, a Peak Force Tapping Study on Living Cells. *J. Struct. Biol.* **2012**, *178*, 1-7.
- [28] Pignataro, B.; Steinem, C.; Galla, H.-J.; Fuchs, H.; Janshoff, A., Specific Adhesion of Vesicles Monitored by Scanning Force Microscopy and Quartz Crystal Microbalance. *Biophys. J.* **2000**, *78*, 487-498.
- [29] Yu, K.; Eisenberg, A., Bilayer Morphologies of Self-Assembled Crew-Cut Aggregates of Amphiphilic Ps-B-Peo Diblock Copolymers in Solution. *Macromolecules* **1998**, *31*, 3509-3518.
- [30] Lipowsky, R.; Seifert, U., Adhesion of Vesicles and Membranes. *Molecular Crystals and Liquid Crystals* **1991**, *202*, 17-25.
- [31] Harada, A., Preparation and Structures of Supramolecules between Cyclodextrins and Polymers. *Coord. Chem. Rev.* **1996**, *148*, 115-133.
- [32] Liu, G.; Jin, Q.; Liu, X.; Lv, L.; Chen, C.; Ji, J., Biocompatible Vesicles Based on PEO-b-PMPC/ α -Cyclodextrin Inclusion Complexes for Drug Delivery. *Soft Matter* **2011**, *7*, 662-669.
- [33] Seifert, U.; Lipowsky, R., Adhesion of Vesicles. *Physical Review A* **1990**, *42*, 4768-4771.
- [34] McCray, J. A., In *Methods Enzymol.*, Academic Press: **1998**, pp 175-202.
- [35] Smith, A. M.; Mancini, M. C.; Nie, S., Bioimaging: Second Window for in Vivo Imaging. *Nat Nano* **2009**, *4*, 710-711.
- [36] P Reichenbach, U. G., U Oertel, T Kämpfe, B Nitzsche, B Voit, and LM Eng., In *Optically Induced Nanostructures: Biomedical and Technical Applications*, König K, O. A., Ed. De Gruyter: Berlin, **2015**; Chapter 6.
- [37] Peng, K.; Tomatsu, I.; van den Broek, B.; Cui, C.; Korobko, A. V.; van Noort, J.; Meijer, A. H.; Spaink, H. P.; Kros, A., Dextran Based Photodegradable Hydrogels Formed Via a Michael Addition. *Soft Matter* **2011**, *7*, 4881-4887.
- [38] Zipfel, W. R.; Williams, R. M.; Webb, W. W., Nonlinear Magic: Multiphoton Microscopy in the Biosciences. *Nat Biotech* **2003**, *21*, 1369-1377.

6 Probing Mechanical Properties of Polymersomes

6.1 Introduction

Gathering information about the mechanical properties of the polymersomes is of great significance in the context of stability issues for the uses of established multifunctional system. Obviously, the polymersomes should have sufficient mechanical strength to be utilized in the prospective application areas. However, stability does not mean having only higher elastic or bending modulus value. It has to be optimized according to the specific tasks of the materials. One apparent example for this is red blood cells which have a membrane with the lowest bending resistance known.¹ But on the other side, they are highly resistant against stretching that allows fulfilling their task in the blood circulation system.

Furthermore, the adhesion properties of polymersomes are linked to their mechanical properties. Although several factors like surface chemistry, size and contact area have an impact on the adhering potential as investigated in the previous chapter, knowing the flexibility and mechanical strength of the membrane is helpful to understand this phenomenon in detail. In fact, this can also clarify whether the established polymersomes can be used as model cell membrane to study complex biological interactions or not. For instance, high rigidity like in glassy polymers is not favorable to mimic the biomembranes since they are naturally robust but also flexible. Apart from these issues, mechanical properties have also a role in transport behavior of the polymersomes through microchannels or in blood vessels when used as drug delivery vehicles. The vesicles should show sufficient resistance against the shear forces encountered within the fluid flow. The attractive forces due to the adhesive surfaces may contribute to the transport properties of the polymersomes as well.² Thus, this chapter focuses on mechanical properties of the fabricated polymersomes to understand their physicochemical behavior more deeply.

A convenient method to probe the mechanical properties of polymersomes is the use of atomic force microscopy through force measurements. Similar approaches have been applied previously for liposomes,³ polyelectrolyte multilayer capsules,² natural membrane nanovesicles⁴ and different polymersome structures.⁵⁻⁶ This technique allows monitoring local deformation under different forces which has been widely utilized to assess the hardness and elastic properties of the soft materials. Nevertheless, the nanometer size of the polymersomes excludes using other common techniques like micropipette aspiration. This method has been successfully applied for micron-sized polymersomes and liposomes so

far.⁷⁻¹⁰ However, it cannot be applied for nano-scaled vesicles due to technical restrictions. One reason is that a micropipette having an inner diameter of about several microns is required for the suction of vesicles when the pressure is applied. Another limitation is sourced by the necessity of optical microscopy to monitor the shape deformation as a function of applied pressure. As can be inferred, due to the diffraction limited resolution of the optical detection, the deformation of the nano-scaled polymersomes cannot be probed by this way.

Thus, in the final part of this thesis, the mechanical properties of the established polymersomes are investigated by using AFM under a liquid phase which has been already published.¹¹ Wet-state environment is crucial to avoid any variation in the mechanical strength due to the collapsing and drying of polymersomes. Here, the discussion is started with the available analytical models to study the stiffness of polymersomes and finishes with the prediction of Young's and Bending modulus values of the polymersome membrane.

6.2 Selection of the Analytical Model

Before analysis of the force curves obtained from AFM measurements in wet state, a suitable approach for modulus prediction has to be chosen. Several issues have to be considered when probing mechanical properties of the colloidal systems like the established multifunctional polymersomes. Therefore, a deep discussion should be done to clarify all assumptions for the most relevant mathematical approach. The potential problems that can be encountered during measurements or afterwards are listed as follows:²

- These vesicles contain water and the volume conservation should be ensured for the quality of the calculations.
- They are relatively soft materials and special attention should be paid to secure the reversible deformations by focusing on the elastic region.
- They may act like a composite due to the height variation of the vesicles on surface. This may lead to a contribution from the substrate in the thinner regions during force measurements.
- The charged membrane may lead to tensions in the shell due to the self-repulsion of the polymer chains.

By taking into account of all these factors, two common analytical models, named as Hertz Model¹² and Reissner's Thin Shell Theory¹³ can be the potential methods to determine the

stiffness of the polymersomes. These approaches are frequently used to compute the elastic modulus of micro- and nanocapsules. However, Fery et al. has already shown that the latter model is more relevant to shell systems by performing analysis on hollow micro capsules² and on nano-sized liposomes.³ This is due to the fact that Shell Theory takes into account the bending rigidity of the membrane together with the size dependency of the vesicle deformation whereas the Hertz model does not consider any of these phenomena.^{2-3, 5-6} This has been demonstrated on DPPC based liposomes in which the stiffness increased when the radius of the liposomes decreased.³ In addition, the deformation analysis of such shell systems from numerical models such as Finite Element Method (FEM) agrees well with the analytical quantifications based on Reissner Shell Theory.¹⁴ Thus, Thin Shell Theory seems to be more applicable for the established multifunctional polymersome system and it was chosen to compute the Young's Modulus (E) by considering small deformations that are in the order of the membrane thickness (h) which is a prerequisite of the model.² However, the relevance of the theory has to be supported by clarifying the above-indicated potential problems. These issues can be pointed out by the response of the established multifunctional polymersomes against force indentation experiments and the detailed discussions of the results will be given in the next part.

6.3 Prediction of the Young's and Bending Modulus

The AFM force measurements were carried out in PBS buffer (pH 7.4) to determine the elastic modulus of the multifunctional polymersomes (PS1) immobilized on S3 surface (PS1-S3). The selection of this pH was to ensure the impermeable state of the vesicles to avoid any loss of water during the force measurements. This was also supposed to avoid the potential membrane tension due to charged polymer chains by keeping the PDEAEM groups at their unprotonated state. Figure 6.1a shows the principle of this experiment where the piezo scanner movement in z direction leads to cantilever deflection as well as sample indentation after the tip contacts to the vesicles. These measured data as cantilever deflection versus piezo extension were converted into the required force-separation curves for the indentation analysis (Figure 6.1b).

Firstly, as seen in Figure 6.1b, the force-separation curve exhibits an initial linear regime up to a certain point, followed by a second regime at higher indentations where the curve reveals exponential relation. This behavior was similarly observed in other shell systems including natural membrane nanovesicles⁴ and self-assembled protein nanotubes¹⁵ in which

higher deformation may lead to buckling instabilities or irreversible shape variation indicating the plastic response. Note that the incompressible fluid inside the vesicles plays a role in large deflection points. The pressure and resistance of the water lead to a substantial increase in the force. This is shown by the force-deformation analysis of a water-filled racquetball where the analytical predictions from Shell Theory matches well for water-filled and empty spheres up to deformations belonging to 20% of the radius.¹⁶ Secondly, another essential issue here is that the analyzed shell systems were rather thick shells ($h/R > 0.1$) as also observed in the study of Chen et al. ($0.18 \geq h/R \geq 0.32$).⁶ This confirms the applicability of the shell theory even in the case of thicker membrane when small deformation regime has been taken into account. Additionally, the substrate may have an influence at higher indentations¹⁷ when the tip moves over the edge of the particles which may lead to the measurement of thinner regions. This can also contribute to linearity variation after a certain point in the force curve which may lead to higher, deceivable elastic modulus values. To avoid this situation, it is reasonable to focus on the small deformation region that certainly represents the polymersome structure. Thus, on the basis of all these factors, the Young's modulus of individual polymersomes was determined by taking into account the initial linear region of the force curves. It should be also noted that this confined regime corresponds to indentations up to 20% of the polymersome radius which agrees well with the previous findings in literature.^{2, 6} Thus, the zero distance between tip and the sample (contact point) was determined by following the start of the force increase with a stable trend to convert the data into indentation-force relation (Figure 6.2).

As a next step, from the slope of the linear indentation-force curve (Figure 6.2), the membrane stiffness (k) was determined and used in the following equation (6.1)^{3, 5-6, 13} relating with the Young's Modulus (E) where ν is the Poisson ratio as 0.5,⁵⁻⁶ h denotes the membrane thickness as 18.6 ± 1.7 nm from cryo-TEM analysis (determined in chapter 3) and R is the radius of the curvature of a vesicle which forms a spherical cap and it was determined by simple geometrical calculations from width and height of the polymersomes (equation 5.1, chapter 5). In addition, the bending modulus (k_{bend}) of the vesicles can be derived from the following equation (6.2) in which the calculated Young's Modulus (E) was utilized as applied previously for different polymersome systems⁵⁻⁶ and lipid vesicles.³

$$k = \frac{4Eh^2}{R\sqrt{3(1-\nu^2)}} \Rightarrow E = \frac{kR\sqrt{3(1-\nu^2)}}{4h^2} \quad (6.1) \quad k_{bend} = \frac{Eh^3}{12(1-\nu^2)} \quad (6.2)$$

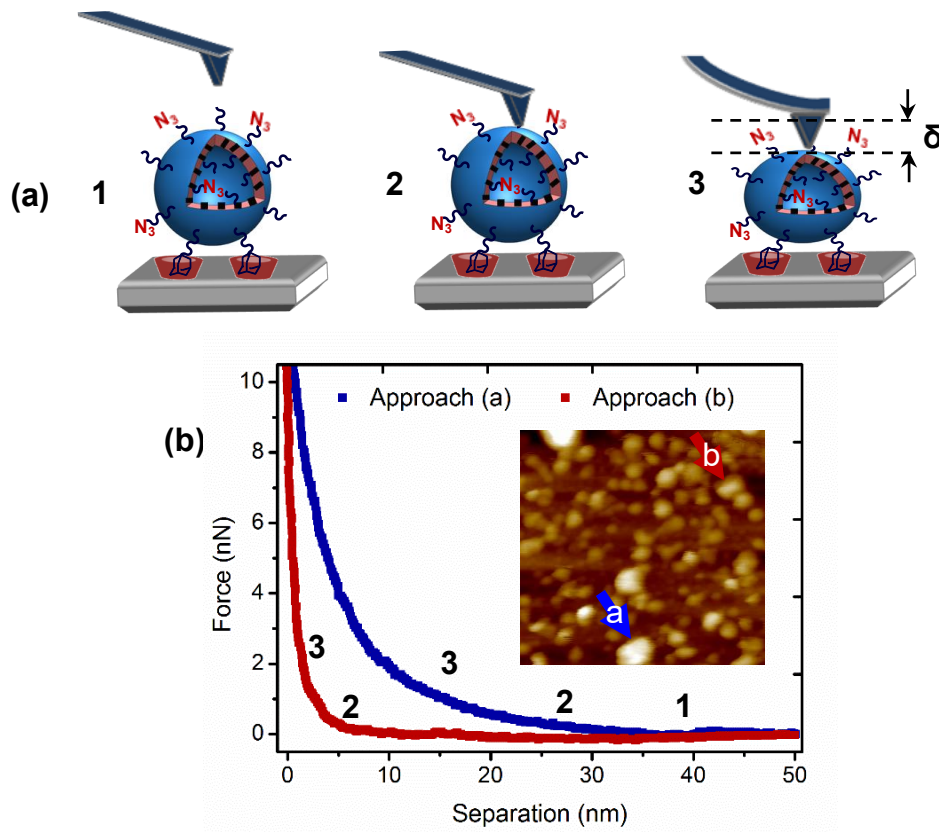


Figure 6.1 (a) Schematic illustration of the AFM indentation experiment: tip and vesicles are not in contact (1), first contact (2), indented (3). (b) Force vs separation curve of two different sized-polymersomes marked by blue and red arrow in the AFM height image at inset of the graph.

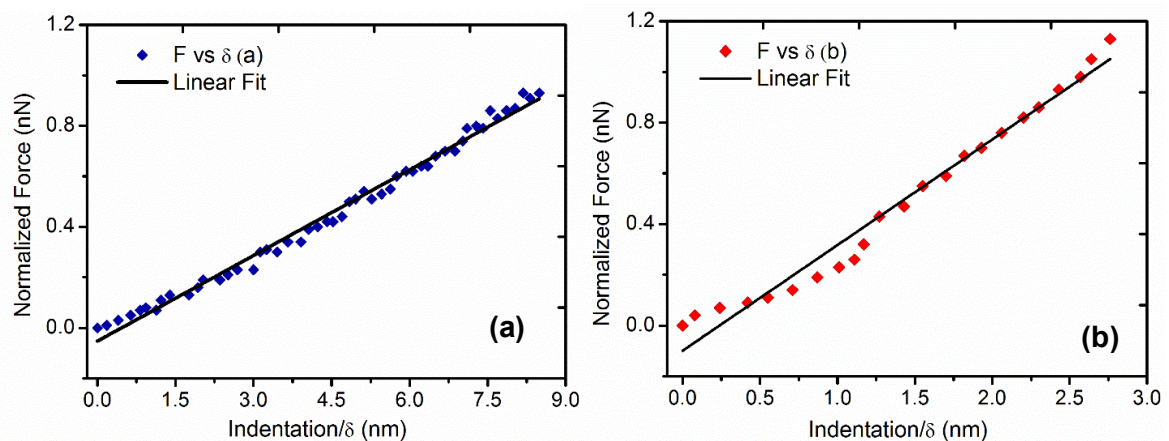


Figure 6.2 (a,b) Force vs indentation curves of corresponding polymersomes shown in the inset of force-separation graph (Figure 6.1b) to find membrane stiffness, k by linear fitting.

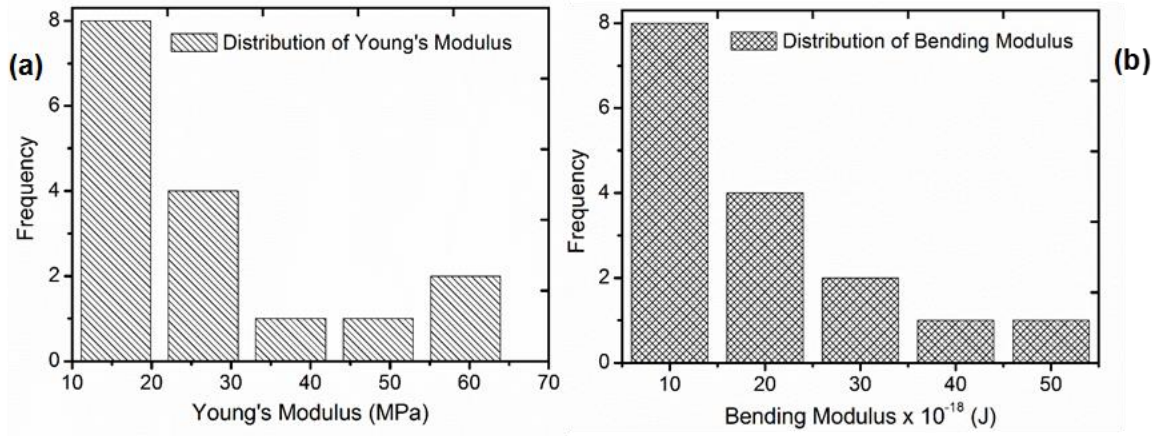


Figure 6.3 (a) Histogram of the Young's modulus and (b) bending modulus of the polymersomes.

By analyzing force-indentation curves of 16 different polymersomes, the average value of Young's and bending modulus was found as 27 ± 16 MPa and $19 \pm 11.4 \times 10^{-18}$ J, respectively, as seen in the histograms of the corresponding data (Figure 6.3a,b). Note that these values do not consider the distribution of the membrane thickness (18.6 ± 1.7). In this manner, to define the range of modulus values more precisely, uncertainty analysis presented by Kline and McClintock¹⁸ was applied through the following equations where w_E and w_{kbend} denote the deviation values including the thickness distribution.

$$w_E = \pm \left[\left(\frac{\partial E}{\partial k} w_k \right)^2 + \left(\frac{\partial E}{\partial R} w_R \right)^2 + \left(\frac{\partial E}{\partial h} w_h \right)^2 \right]^{1/2} \quad (6.3)$$

$$w_{kbend} = \pm \left[\left(\frac{\partial kbend}{\partial E} w_E \right)^2 + \left(\frac{\partial kbend}{\partial h} w_h \right)^2 \right]^{1/2} \quad (6.4)$$

This leads to values in the range of 27 ± 17.5 MPa and $19 \pm 12.5 \times 10^{-18}$ J for Young's and bending modulus, respectively, of the multi-functionalized polymersomes. These values reveal a less stiff nature of the established polymersomes than polymersomes based on polystyrene-block-poly(acrylic acid) (PS-b-PAA)⁶ ($h=22 \pm 1$ nm, $E=61 \pm 6$ MPa, $k_{bend}=71.6 \pm 10.3 \times 10^{-18}$ J) while they are more rigid in comparison to poly(dimethylsiloxane)-block-poly(2-methyloxazoline) (PDMS-b-PMXO) polymersomes⁵ ($h=16 \pm 2$ nm, $E=17 \pm 11$ MPa, $k_{bend}=7 \pm 5 \times 10^{-18}$ J). Firstly, the membrane thickness has an effect on the elasticity of

the vesicles⁸ which also explains the better mechanical stability of the analyzed polymersomes compared to the liposomes based e.g. on egg yolk phosphatidylcholin (EggPC, $h=6\pm 0.6$, $E=2\pm 0.8$, $k_{\text{bend}}=0.03\times 10^{-18}$ J).¹⁹ In addition, the mechanical behavior of the vesicles also depends on the intrinsic properties of the block copolymer used in the self-assembly process. For this purpose, thermal behavior of the BC2 polymer was investigated by differential scanning calorimetry to determine T_g value. Although the established polymersomes consisted of the mixture of three polymers (BC1, BC2, BC3, chapter 3), the adamantane and azide groups would not have much impact on the thermal behaviors. Therefore, to have more understanding and to make comparisons with the mechanical properties of the previously published polymersomes with a clearer way, the nonfunctional PEG-DEAEM-BMA (BC2) was chosen for this analysis. Thus, the glass transition temperature was found as about -4 °C from the second heating run of the DSC curves to avoid the influence of the thermal history although similar values were deducted from first heating or cooling steps as well. Apart from gaining the idea of stiffness, the additional important point here is that the single T_g value for a block copolymer supports the consistence of the monomers in the polymer structure and they did not behave like a blend to show the glass transition of each polymer.

In this manner, PS-*b*-PAA have a higher glass transition temperature than our system (T_g-BC2 = -4 °C,) since both polystyrene (T_g-PS = 100 °C) and polyacrylic acid (T_g-PAA = 106 °C) are in the glassy state at room temperature which makes the PS-*b*-PAA vesicles much stiffer. It should be also noted that the established multifunctional polymersomes have a cross-linked membrane which enhances the stiffness as proven previously by comparing Young's modulus of cross-linked and non-cross-linked bilayers based on poly(ethylene glycol)-block-poly[2-(diethylamino)ethyl methacrylate-*stat*-3,4-dimethyl maleic imidobutyl methacrylate] (PEG45-*b*-PDEAEM-*s*PDMIBM).¹⁷ Thus, this moderate stiffness values for the established system among other published polymersomes showed that a good balance in elasticity and rigidity can be achieved to use these nanovesicles for various biomedical applications.

6.4 Summary

In this chapter, the mechanical stability of the established polymersomes was investigated by computing Young's and bending modulus through force curves obtained by AFM measurements. Among the available analytical models for modulus prediction, Reisner's

Thin Shell Theory was found more applicable to the investigated system since it considers both bending rigidity of the membrane and size dependency of the vesicle deformation. Furthermore, the thermal behavior of the polymersome forming block copolymer was examined by differential scanning calorimetry which led to the glass transition temperature of -4 °C. This value supported the modulus results when compared with other polymersome systems in literature. Table 6.1 summarizes the mechanical properties of the different vesicular systems determined by AFM using similar mathematical approach. Therein, it is clear that the established polymersomes found a place in between PS-b-PAA and PDMS-b-PMXO polymersomes from the perspective of rigidness and flexibility.

Overall, the findings in this chapter demonstrate the robust but still flexible nature of the polymersomes which have a “breathable” membrane of a moderate stiffness. This result also supports the prospective aim of the established system which is robust enough to design stable compartments but also flexible enough to mimic the cell membrane functions. Finally, this mechanical probing part showed the limits of the created system and fulfills the missing information to understand the essential key characteristics of the fabricated polymersomes like responsive nature and adsorption behavior as described previously.

Table 6.1 Summary of mechanical and thermal properties of different vesicle systems

Vesicle	h ^a [nm]	E ^b [MPa]	k ^b [10 ⁻¹⁸ J]	Tg ^c [°C]
This study	18.6 ± 1.7	27±17.5	19±12.5	-4
PDMS-b-PMXO polymersomes ⁵	16 ± 2	17 ± 11	7 ± 5	-124
PS-b-PAA polymersomes ⁶	22 ± 1	61 ± 6	71.6 ± 10.3	~100
EggPC liposomes ¹⁹	6 ± 0.6	2 ± 0.8	0.03	n.d.

^aRepresents the average thickness of the vesicle membrane. ^bRepresent Young’s (E) and bending modulus (k) values, respectively. ^cShows the glass transition temperature of the used block copolymers for polymersome formation.

6.5 References

- [1] Lipowsky, R.; Sackmann, E., *Structure and Dynamics of Membranes: I. From Cells to Vesicles/II. Generic and Specific Interactions*. Elsevier: **1995**; Vol. 1.
- [2] Fery, A.; Weinkamer, R., Mechanical Properties of Micro- and Nanocapsules: Single-Capsule Measurements. *Polymer* **2007**, *48*, 7221-7235.

- [3] Delorme, N.; Fery, A., Direct Method to Study Membrane Rigidity of Small Vesicles Based on Atomic Force Microscope Force Spectroscopy. *Physical Review E* **2006**, *74*, 030901.
- [4] Calo, A.; Reguera, D.; Oncins, G.; Persuy, M.-A.; Sanz, G.; Lobasso, S.; Corcelli, A.; Pajot-Augy, E.; Gomila, G., Force Measurements on Natural Membrane Nanovesicles Reveal a Composition-Independent, High Young's Modulus. *Nanoscale* **2014**, *6*, 2275-2285.
- [5] Jaskiewicz, K.; Makowski, M.; Kappl, M.; Landfester, K.; Kroeger, A., Mechanical Properties of Poly(Dimethylsiloxane)-Block-Poly(2-Methyloxazoline) Polymersomes Probed by Atomic Force Microscopy. *Langmuir* **2012**, *28*, 12629-12636.
- [6] Chen, Q.; Schonherr, H.; Vancso, G. J., Mechanical Properties of Block Copolymer Vesicle Membranes by Atomic Force Microscopy. *Soft Matter* **2009**, *5*, 4944-4950.
- [7] Discher, B. M.; Won, Y.-Y.; Ege, D. S.; Lee, J. C.-M.; Bates, F. S.; Discher, D. E.; Hammer, D. A., Polymersomes: Tough Vesicles Made from Diblock Copolymers. *Science* **1999**, *284*, 1143-1146.
- [8] Bermudez, H.; Hammer, D.; Discher, D., Effect of Bilayer Thickness on Membrane Bending Rigidity. *Langmuir* **2004**, *20*, 540-543.
- [9] Bermudez, H.; Brannan, A. K.; Hammer, D. A.; Bates, F. S.; Discher, D. E., Molecular Weight Dependence of Polymersome Membrane Structure, Elasticity, and Stability. *Macromolecules* **2002**, *35*, 8203-8208.
- [10] Le Meins, J. F.; Sandre, O.; Lecommandoux, S., Recent Trends in the Tuning of Polymersomes' Membrane Properties. *The European Physical Journal E* **2011**, *34*, 1-17.
- [11] Iyisan, B.; Janke, A.; Reichenbach, P.; Eng, L. M.; Appelhans, D.; Voit, B., Immobilized Multifunctional Polymersomes on Solid Surfaces: Infrared Light-Induced Selective Photochemical Reactions, Ph Responsive Behavior, and Probing Mechanical Properties under Liquid Phase. *ACS Applied Materials & Interfaces* **2016**, *8*, 15788-15801.
- [12] Hertz, H., On the Contact of Elastic Solids. *J. reine angew. Math* **1881**, *92*, 156-171.
- [13] Reissner, E., Stresses and Small Displacements of Shallow Spherical Shells. II. *Journal of Mathematics and Physics* **1946**, *25*, 279-300.
- [14] N. Elsner, F. D., R. Weinkamer, M. Wasicek, F.D. Fischer, A. Fery, In *Characterization of Polymer Surfaces and Thin Films*, Grundke, K.; Stamm, M.; Adler, H.-J., Eds. Springer Berlin Heidelberg: **2006**, pp 117-123.
- [15] Graveland-Bikker, J. F.; Schaap, I. A. T.; Schmidt, C. F.; de Kruijff, C. G., Structural and Mechanical Study of a Self-Assembling Protein Nanotube. *Nano Lett.* **2006**, *6*, 616-621.
- [16] Taber, L. A., Large Deflection of a Fluid-Filled Spherical Shell under a Point Load. *Journal of Applied Mechanics* **1982**, *49*, 121-128.
- [17] Gaitzsch, J.; Appelhans, D.; Janke, A.; Stempel, M.; Schwille, P.; Voit, B., Cross-Linked and Ph Sensitive Supported Polymer Bilayers from Polymersomes - Studies Concerning Thickness, Rigidity and Fluidity. *Soft Matter* **2014**, *10*, 75-82.

- [18] Kline, S. J.; McClintock, F., Describing Uncertainties in Single-Sample Experiments. *Mech. Eng.* **1953**, 75, 3-8.
- [19] Liang, X.; Mao, G.; Ng, K. Y. S., Mechanical Properties and Stability Measurement of Cholesterol-Containing Liposome on Mica by Atomic Force Microscopy. *J. Colloid Interface Sci.* **2004**, 278, 53-62.

7 Conclusion and Outlook

The requirement of specific recognition and external stimuli controlled systems in the scope of biomedical applications is the basic driving force of this study. These key functions are especially very useful in the design of targeted drug delivery vehicles as well as conducting selective reactions in nanoreactors or designing sensing devices in the scope of microsystem technology. Therefore, this thesis aimed to develop multifunctional and stimuli-responsive polymersomes possessing various abilities including pH, UV and IR light sensitivity as well as many reactive groups with sufficient accessibility to be used as smart and cognitive nanocontainers. In this manner, the main features of the developed polymersomes are:

- (i) Functional reactive groups for introducing multiple targeting ligands through covalent and non-covalent conjugations.
- (ii) UV and IR light triggered photoreactivity for selective recognition functions.
- (iii) pH-controlled membrane permeability to host and release various cargos.
- (iv) Persistence of the pH and light sensitivity also in confined environments which correspond to capabilities of immobilized polymersomes on solid surfaces.

Each of these findings were shown at different stages of the whole research period as summarized in Figure 7.1. These are fulfilling the sub-objectives of the thesis to reach the overall goal. The first and second part of this work describe the successful polymersome fabrication realized through the synthesis of pH sensitive, photocrosslinkable and functionalized amphiphilic block copolymers and further post-conjugations to the polymersome surface. Besides, the pH-dependent release and diffusion limits of the developed polymersomes were shown by probing the hosting capacity through drug and gold nanoparticle encapsulation. Lastly the surface-immobilized polymersomes were achieved with the aid of host-guest interactions of adamantane- β -cyclodextrin molecules which enabled to trigger near-infrared light induced selective photochemical reactions and mechanical probing under liquid phase. This fixation and immobilization study is indeed a very less investigated area in polymersome field, and opens up new opportunities for using these vesicles in sensing devices as well as characterizing them thoroughly with advanced microscopy techniques.

In this context, the starting point of this work was the synthesis of polymersome forming amphiphilic block copolymers by using ATRP with a controlled manner, which were then self-assembled to prepare the azide and adamantane decorated polymersomes to induce the

post-conjugation processes at the vesicle periphery. The produced polymers consist of polyethylene glycol (PEG) as the hydrophilic segment having azido, adamantyl or methoxy end-groups, whereas pH sensitive 2-(diethylamino)ethyl methacrylate (DEAEM) and a photo cross-linker benzophenone (BMA) groups form together the hydrophobic part. The characterization of the resulting polymers by ^1H NMR and SEC techniques revealed relatively low molar mass dispersities as well as desired hydrophilic mass fraction of about 0.1 to 0.13 for vesicle formation. In addition, the homogeneity of the multi-functionalized polymersomes was ensured by keeping the hydrophobic block length of the polymers almost equal. However, hydrophilic length of the azide- and adamantane-functionalized block copolymers was designed to be longer than the non-functional methoxy terminated block copolymer to increase the accessibility of the reactive groups on the polymersome surface.

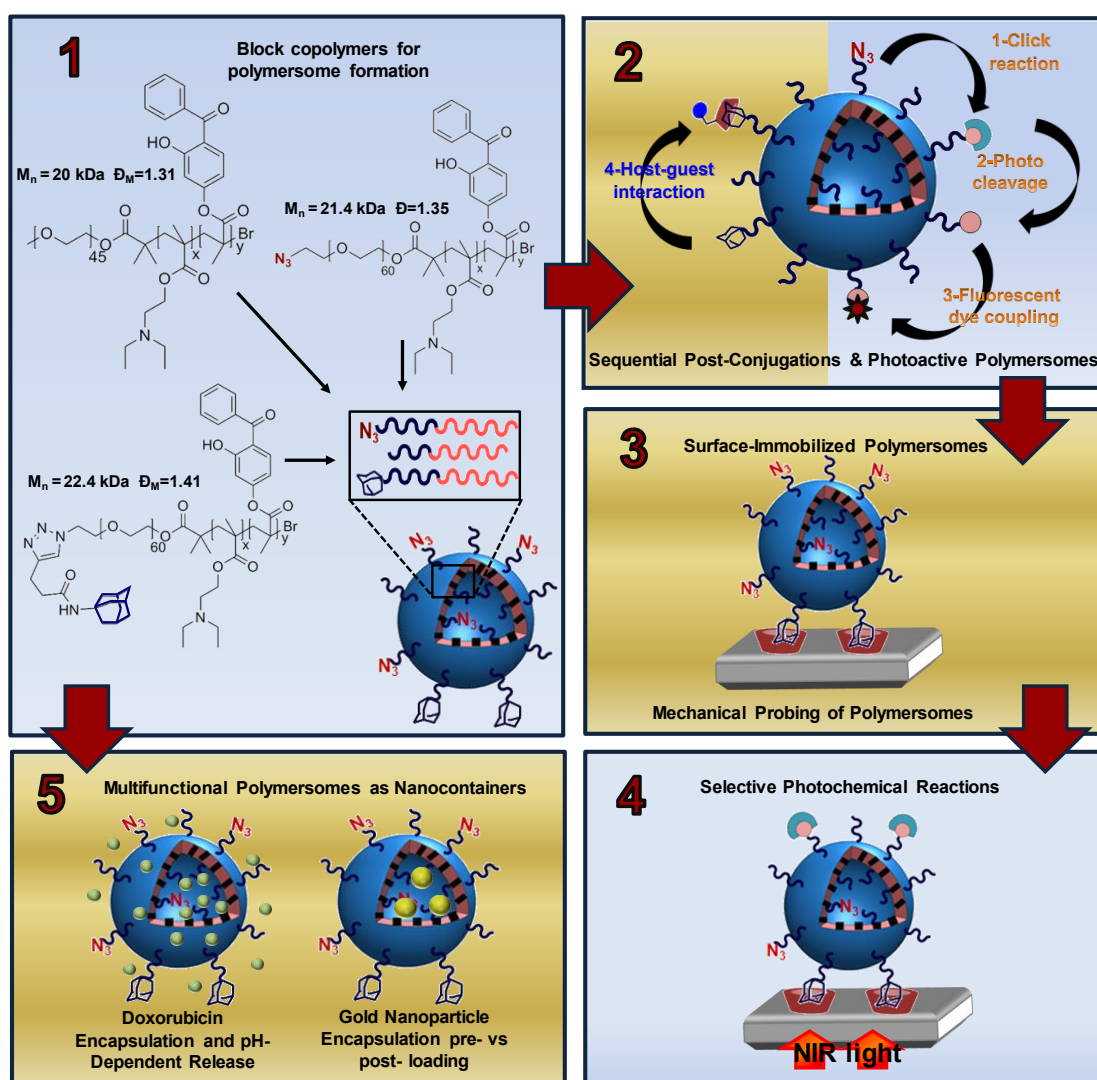


Figure 7.1 General overview of the main research developments within this work indicating the sub-divisions (1&2: chapter 3, 5: chapter 4, 3&4: chapter 5 and 6).

After the successful polymersome formation possessing adamantane and azide functionalities at inner and outer hydrophilic corona of the vesicles, the photo-crosslinking of the membrane with the aid of BMA units was realized. The tunable pH-responsive nature to the multifunctional polymersomes was provided in terms of reversible swelling and shrinking abilities up to 5 cycles in which the hydrodynamic diameter of the polymersomes was increased about 42% at acidic condition and shrank back to the original size without facing any disassembly problems. In addition, the established polymersomes also demonstrated a remarkable pH-stability at different pH environments as seen in Figure 7.2.

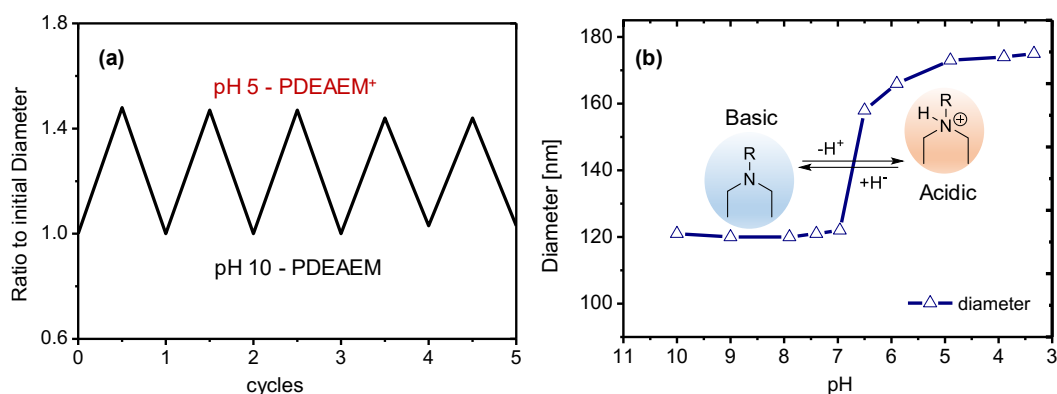


Figure 7.2 (a) Reversible swelling-shrinking of surface functionalized-polymersomes (PS1) upon changes in pH value. (b) pH-dependent diameter variation of the corresponding polymersomes (PS1).

Accessible and sufficiently reactive groups were found when photoactive moieties as well as β -cyclodextrin molecules were conjugated to the pre-formed polymersomes by means of click chemistry and strong host-guest complexations. The photoactive groups, as UV and IR cleavable NVOC molecules, provided light responsivity to the established multifunctional polymersomes. This was demonstrated firstly by UV-triggered photochemical reactions which resulted in free amino groups on the polymersome surface as an additional functionality. The liberated amino groups were further conjugated with a fluorescent compound to evaluate the reactivity as well as simulate the concept of selective binding approaches. The subsequent attachment of fluorescently labeled- β -cyclodextrin molecules was also carried out and the success of all conjugation steps was monitored by UV-Vis spectroscopy. Another important outcome from this fabrication process was that the polymersomes preserved their shape and stability throughout the whole steps as confirmed by cryo-TEM visualization (Figure 7.3).

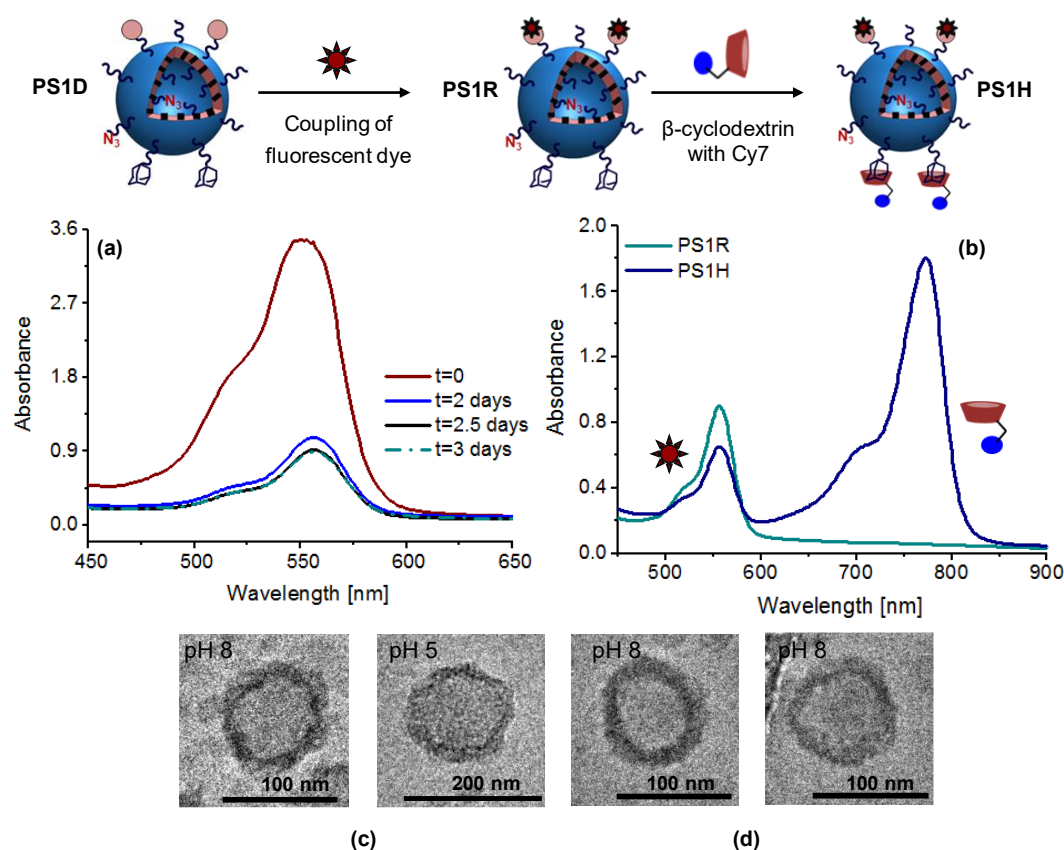


Figure 7.3 (a) Monitoring RhB-NCS coupling to polymersomes through amino groups with UV-vis analysis during dialysis procedure to finally obtain PS1R polymersomes (b) UV-vis analysis to show sequential conjugation of cyclodextrin molecule to Rhodamine B NCS modified polymersomes (PS1R) by host-guest interaction. (c) cryo-TEM micrographs of PS1D polymersomes at pH 8 and pH 5. (d) cryo-TEM micrographs of PS1R polymersomes at pH 8.

In addition, encapsulation of gold nanoparticles and doxorubicin molecules as an anticancer drug proved the hosting ability as well as the sufficient membrane permeability of the established polymersomes which demonstrated the applicability as nanocontainers or nanocarriers. The important finding here was that the polymersomes before and after photocleavage step showed similar performance in pH-dependent drug release although additional UV exposure led to a more compact membrane. Another outcome was that the post-loading of highly negatively charged-gold nanoparticles was not restricted by electrostatic interactions and was realized successfully for 5 nm sized AuNPs. However, the particle uptake was decreased to some extent for 10 nm sized AuNPs that demonstrated the size dependence of pH-controlled diffusion processes.

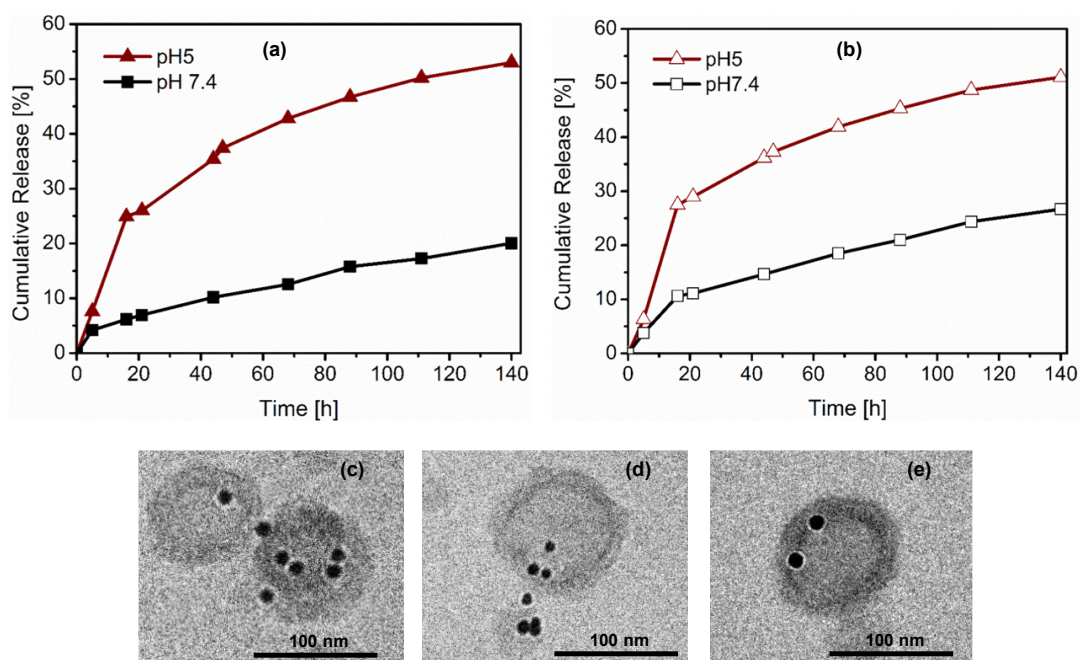


Figure 7.4 In-vitro release of doxorubicin from (a) PS1C-Dox polymersomes (before photocleavage) and (b) PS1D-Dox polymersomes (after photocleavage) at 37 °C in different pH medium. (c-e) cryo-TEM micrographs of PS1-Au104 polymersomes at pH 8 (10 nm sized AuNP loaded).

The multifunctional polymersomes were finally immobilized onto solid substrates via adamantane- β -cyclodextrin conjugations and confirmed by in-situ AFM monitoring under liquid phase at pH 7.4 PBS buffer as well as at acidic condition, pH 5. The approach enabled spherical cap-shaped polymersome compartments at the cyclodextrin coated substrate in which the shape was highly dependent on the level of binding forces. Several investigations including adhesion behavior, pH sensitivity and finally the IR-induced selective photochemical reactions on immobilized polymersomes were reported. Therein, the released amino groups on the polymersome surface were further conjugated with a model fluorescent compound for mimicking the attachment of biorecognition elements. The possibility to use the advantages of IR light like being safe to biological compounds as well as deep penetration ability to organic materials outlines the potential of established multifunctional and stimuli responsive polymersomes for various biomedical applications. In particular, the efficient reactive groups and the presence of light and pH responsivity render these smart nanovesicles especially suitable for the design of targeted and selective recognition systems which can be useful for building microsystem devices with sensing functions.

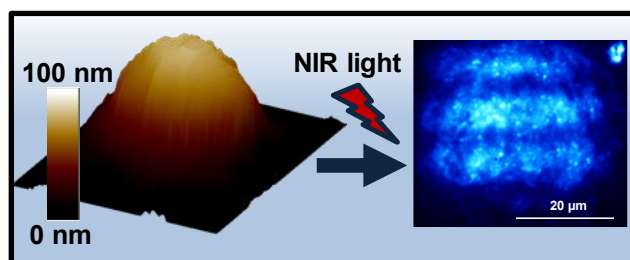


Figure 7.5 Immobilized spherical cap-shaped polymersomes and NIR induced selective photochemical reactions in which the released amino groups were conjugated with ATTO 532-NHS ester molecules for mimicking the biorecognition systems.

In the final part of this work, the mechanical properties of the polymersomes were determined by computing Young's and bending modulus of the membrane ($E=27\pm 17.5$ MPa, $k=19\pm 12.5 \times 10^{-18}$ J) through force curves obtained by atomic force microscopy measurements in the wet state. This was a complementary study to understand the constraints of the established vesicles from the perspective of mechanical strength which is indeed necessary for the applicability in biomedical science.

Based on the achieved goals, this work can go further in diverse directions, demonstrating the potential of the established smart and multifunctional nanocontainers for many biomedical applications. Indeed, the various functions of one single polymersome system widen the application aspect not only as carrier devices but also as smart multicompartments in the design of microsystem devices. It is possible to use the developed concept for building sensing devices in which the selective recognition can be realized either through light-trigger or host-guest interactions.

In addition, the post-surface functionalization can be performed not only at the outer corona as investigated in this study, but the conjugation to the inner bilayer membrane is also possible at acidic conditions when the polymersomes are in swollen state. This approach can be favored to decorate the outer and inner region with different molecules according to the needs. In the light of this possibility, the post-conjugation steps can be also utilized for the attachment of targeting molecules like proteins, enzymes and antibodies to the polymersome surface which enhances the selectivity and provides potential for the established polymersomes to be used in pharmaceutical market as drug delivery vehicles and in synthetic biology as nanoreactors or artificial organelles.

Another potential lies in the gold nanoparticle loaded polymersomes which can be utilized for photothermal therapy since AuNPs can convert the absorbed light into heat

energy when irradiation is applied. Herein, the additional opportunity is to trigger the NIR-selective photochemical reactions through second harmonic generation which is a type of nonlinear optical phenomenon sourced by gold nanoparticles. However, SPR band is highly affected by the particle dimension and red shifted with increased size of the gold nanoparticles. Since the established polymersomes do not allow to encapsulate larger AuNPs, in the range of 50-100 nm, the azide and adamantane groups can be used to attach these relatively bigger particles through covalent and noncovalent conjugations. In this regard, gold nanoparticles can act either as optical antennae or heat generator to be used for diagnostic or therapeutic applications in biomedical science.

Furthermore, the successful immobilization of polymersomes onto solid substrates showed that the shape is highly dependent on the attractive forces of the substrate in which decreased cyclodextrin amount and additional passivation with PEG molecules led to more intact polymersomes. In this manner, further investigations can be done by conducting molecular printing methods in combination with PEG passivation for the pre-coating steps which may be useful in improving the shape of the polymersomes on surfaces.

Hence, the accessible and sufficiently reactive groups of the established polymersomes make these smart nanocontainers a toolbox for several other technologies by conjugating any desired or required molecules to the polymersome surface. For this purpose, the future prospective of these established polymersomes is not limited with only the mentioned opportunities but can be increased in the hands of the next researcher.

III. Experimental Part

8 Materials and Methods

8.1 Materials

All commercial materials were used as received without further purification, unless stated. Anhydrous solvents were stored over molecular sieves. Dialysis membranes were rinsed with distilled water prior to use. The pH of the aqueous dialysis media was adjusted by NaOH or HCL solutions unless otherwise indicated.

Table 8.1 List of chemicals

Chemical/Specification	Supplier
Azide terminated poly(ethylene glycol) (N ₃ PEG-OH); M _n :2700 g/mol, Đ:1.18; azide functionality: 90% by ¹ H NMR	Polymer Source
Poly(ethylene glycol) methyl ether ; M _n :2000 g/mol, Đ:1.05	Sigma-Aldrich
2-Hydroxy-4-(methacryloyloxy) benzophenone (BMA), 99%	Alfa Aesar
6-Monodeoxy-6-monoamino-β-cyclodextrin.HCl, >98%	Cyclodextrin Shop
1-Aminoadamantane, 97% ; Propargylamine, 98%	Sigma-Aldrich
4,5-Dimethoxy-2-nitrobenzyl chloroformate (NVOC-Cl), 97%	Sigma-Aldrich
4-Pentynoic acid (98%)	Across Organics
Sulfo-cyanine7 NHS ester, 95%	LumiProbe GmbH
Sodium ascorbate, ≥98%	Sigma-Aldrich
Copper(I) bromide, 98% ; Copper(I) iodide, ≥98%	Sigma-Aldrich
Copper(II) sulfate pentahydrate, ≥98%	Sigma-Aldrich
2-Bromoisobutyryl bromide, 98%	Sigma-Aldrich
2,2'-Bipyridine (bpy), >99%	Sigma-Aldrich
Aluminum oxide (neutral, activated), Brockmann I grade	Sigma-Aldrich

Table 8.1 continued

2-(Diethylamino)ethyl methacrylate (DEAEMA), 99%	Sigma-Aldrich
Rhodamine B isothiocyanate, mixed isomers	Sigma-Aldrich
Triethylamine, $\geq 99.5\%$; 2-butanone (MEK), anhydrous	Sigma-Aldrich
Doxorubicin hydrochloride (Dox), $\geq 98\%$	Carbosynth Limited
Tris-(benzyltriazolylmethyl) amine (TBTA), 97%	Sigma-Aldrich
N,N-Diisopropylethylamine (DIPEA), 99.5%	Sigma-Aldrich
Dimethyl sulfoxide (DMSO), anhydrous, 99.9%	Sigma-Aldrich
N,N-Dimethylformamide (DMF), anhydrous, 99.8%	Sigma-Aldrich
Sodium bicarbonate, 99.5%	Acros Organics
Tetrahydrofuran (THF), anhydrous, 99.5%	Acros Organics
N,N'-Dicyclohexylcarbodiimide (DCC), 99%	Acros Organics
Dichloromethane (DCM), anhydrous, 99.9%	Acros Organics
Ethyl acetate, 99.5% ; Chloroform, 99.8% ; n-Hexane, 99%	Acros Organics
Silica Gel, high purity grade, mesh: 200-400	Merck
Ethylenediaminetetraacetic acid tetrasodium salt dehydrate, 99%	Sigma-Aldrich
Sodium Phosphate dibasic heptahydrate, N/A	Sigma-Aldrich
Sodium Phosphate monobasic, anhydrous, $\geq 99\%$	Sigma-Aldrich
Acetic Acid (glacial), 100%	Merck
Sodium Acetate, $\geq 99\%$	Fluka

Table 8.1 continued

Sodium Hydroxide, $\geq 97\%$	Sigma-Aldrich
Hydrochloric Acid, fuming 37%	Merck
Phosphate Buffered Saline (PBS), Biotech grade	Sigma-Aldrich
3-(Glycidyloxypropyl) trimethoxysilane, $\geq 98\%$	Sigma-Aldrich
Toluene, anhydrous, 99.8%	Sigma-Aldrich
Ethanol, absolute, ACS reagent, 99.5%	Acros Organics
ATTO 532 NHS ester, Bioreagent, Mw:1081 g/mol	ATTO-TEC GmbH
Amino-terminated poly(ethylene glycol) (MeO-PEG-NH ₂), M _n :750 g/mol)	IRIS Biotech

Table 8.2 List of separation tools and materials

Material/Specification	Supplier
Dialysis Membrane, made of regenerated cellulose, MWCO 5000	Carl Roth
Dialysis Membrane, made of regenerated cellulose, MWCO 50000	Carl Roth
Hollow fiber filtration modules, modified polyethersulfone (mPES), MWCO: 100 kDa, 750 kDa, 0.05 μm	Spectrum Labs
Gold Nanoparticles, 5 nm, suspension in 0.1 mM PBS, reactant free	Sigma-Aldrich
Gold Nanoparticles, 10 nm, suspension in 0.1 mM PBS, reactant free	Sigma-Aldrich
Silicon Wafers (~ 30 nm of SiO ₂ layer thickness)	Silicon Materials
Glass slides, 15x15 mm	VWR Foundation

Table 8.3 List of buffer solutions

Buffer solution	Ingredients
Phosphate buffer, pH 7.4, 10 mM	NaH ₂ PO ₄ (0.27 g), NaHPO ₄ ·7H ₂ O (2.08g), Millipore water (1 L)
Phosphate buffer, pH 8, 10 mM	NaH ₂ PO ₄ (0.082g), NaHPO ₄ ·7H ₂ O (2.5 g), Millipore water (1 L)
Acetate buffer, pH 5, 10 mM	Acetic acid (0.165 mL), Sodium acetate (0.692), Millipore water (1 L)

8.2 Analytical Methods

8.2.1 Nuclear Magnetic Resonance Spectroscopy

¹H NMR (500.13 MHz) and ¹³C NMR (125.76 MHz) spectra were recorded using BrukerAvance III 500 spectrometer (BrukerBiospin, Germany) with CDCl₃ or DMSO-*d*₆ as a solvent at room temperature. Chemical shifts are expressed in ppm and referenced to the corresponding solvent signals (CDCl₃: δ=7.26, 77.0 ppm; DMSO-*d*₆: δ= 2.50 ppm).

8.2.2 Size Exclusion Chromatography

The molar mass distributions (\bar{M}) of the block copolymers were determined using Size Exclusion Chromatography (SEC) equipped with a multi-angle laser light scattering (MALLS) detector (MiniDAWN-LS detector, Wyatt Technology, USA) and a refractive index (RI) detector (K2301, Fa. KANUER, Germany). The pump (HPLC pump, Agilent 1200 series) and the column (PolarGel-M, 300x7.5 mm) of the system were from Agilent Technologies (USA). The eluent was DMAc with 3 g/L LiCl and the flow rate is 1mL/min.

The molar mass distributions (\bar{M}) of the poly(ethylene glycol) macroinitiators were measured using an analogous SEC-system equipped with a MALLS detector (MiniDAWN-LS detector, Wyatt Technology, USA) and a viscosity/refractive index (RI) detector (ETA-2020, WGE Dr. Bures, Germany). The pump (HPLC pump, Agilent 1200 series) and the column (PL MIXED-C with a pore size of 5 μm, 300x7.5 mm) of this Size Exclusion Chromatography were again from Agilent Technologies (USA). The eluent was THF with a flow rate of 1 mL/min. The calibration was based on polystyrene standards ranging from 580 to 210500 g/mol.

8.2.3 Infrared Spectroscopy

The spectra were recorded on Vertex 80V (Bruker) FT-IR spectrometer. The samples were prepared with KBr-Pellet method.

8.2.4 Dynamic Light Scattering

Dynamic Light Scattering (DLS) measurements were performed at 25 °C using Zetasizer Nano-series instrument (Malvern Instruments, UK) equipped with a multi-purpose autotitrator and a 633 nm He-Ne laser at fixed scattering angle of 173°. The hydrodynamic size of polymersomes (1 mg/mL) is given as intensity-average diameter (Z_{average}) values assuming refractive index of the polymer as 1.50. The data evaluation was carried out by using Malvern Software 7.11.

8.2.5 Zeta-Potential Measurements

Zeta potential (ζ potential) of the polymersomes (1 mg/mL) as well as gold nanoparticles was determined by Zetasizer Nano-series instrument (Malvern Instruments, UK) through electrophoretic light scattering. The autotitration of polymersomes against HCl (0.1 mol/L) and KOH (0.1 mol/L) solution allowed to measure the zeta potential at different pH values so as to determine the isoelectronic point. During this titration, size of polymersomes was also recorded in order to observe the stability and swelling behavior of the vesicles. The data evaluation was carried out by using Malvern Software 7.11.

8.2.6 UV-Vis Spectroscopy

UV-vis measurements were carried out using Specord 210 Plus double beam UV-vis spectrophotometer (analytikjena, Germany). Samples were analyzed at desired wavelength range in quartz cuvettes. To monitor in vitro drug release experiments as well as the SPR of gold nanoparticle encapsulated polymersomes; disposable micro cuvettes were used for the measurements.

8.2.7 Contact Angle Measurements

The water contact angles of the substrates were measured on an OCA35L (DataPhysics, Germany) automatic contact angle instrument using the sessile drop technique at room temperature. Both advancing and receding angle was given with an average value of the measurements from 5 different samples at 3 (Si wafer) or 2 (Glass slide) different regions of each coated surface.

8.2.8 Differential Scanning Calorimetry

Differential Scanning Calorimetry (DSC) measurements of PEG₄₅-b-P(DEAEMA₈₁-stat-BMA₁₀) was performed at 10 K/min heating rate (-80 °C to 100 °C) under nitrogen using DSC Q2000 device (TA Instruments, USA).

8.2.9 Spectroscopic Ellipsometry

The monolayer thickness of the epoxysilane and cyclodextrin coated wafers was determined by using the multiwavelength ellipsometer in the spectral range of 380-900 nm with an incidence angle of 70 °C (alpha-SE ellipsometer, J.A. Woollam Company, USA). The thickness measurement was performed by using the same Si wafer with the same optical model after each coating step. The model used for the measurement is available in Complete Ease Software which consists of a Si substrate and an interface layer with thermal SiO₂. This means that the monolayer thickness measurements were also carried out with the same refractive index (1.46) as the SiO₂ layer.¹⁻² All reported thickness values were averaged from 5 different samples from the following equation.

$$\begin{aligned} \text{Monolayer Thickness (nm)} \\ = \text{Total thickness after coating} - \text{Total thickness before coating} \end{aligned} \quad (8.1)$$

8.3 Imaging Techniques and Analysis

8.3.1 Cryo-Transmission Electron Microscopy

Cryo-Transmission Electron Microscopy (cryo-TEM) images were obtained using Libra 120 microscope (Carl Zeiss Microscopy GmbH, Oberkochen, Germany) at an acceleration voltage of 120 kV. Samples were prepared by dropping 1 µl of polymersome solution (1 mg/mL) on each side of a copper grid coated with holey carbon foil (so-called Lacey type). A piece of filter paper was used to remove the excess water; the sample was then rapidly frozen in liquid ethane at -178 °C. The blotting with the filter paper and plunging into liquid ethane was done in a Leica GP device (Leica Microsystems GmbH, Wetzlar, Germany). All images were recorded in bright field at -172 °C. The image analysis to determine the thickness of the polymersome membrane as well as the diameter was performed using Olympus Scandium Software 5.2.

8.3.2 Atomic Force Microscopy

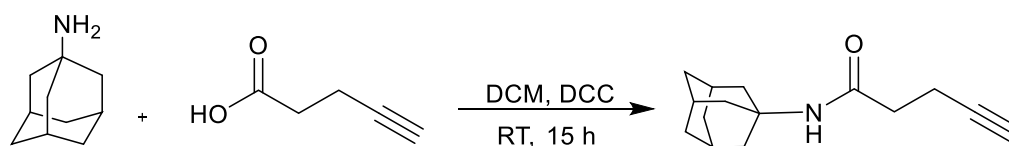
Atomic Force Microscopy (AFM) measurements of the polymersome-coated surfaces were performed under aqueous solution (PBS, pH 7.4 or pH 5) using a Dimension Icon AFM with NanoScope V Controller (Bruker-Nano, Santa Barbara, CA). The peak force tapping mode was applied using ScanAsyst-Fluid+ silicon nitride probes for imaging and ScanAsyst-Fluid silicon nitride probes (Bruker-Nano) for force measurements with a nominal spring constant of about $k=0.7$ N/m. The shape of the cantilever was triangular and tip radius of the probes used in topography and force measurements was 5 nm and 20 nm respectively. For a quantitative modulus analysis in force measurements, the deflection sensitivity (29.4 nm/V) was determined by recording cantilever deflection vs piezo position curves on a hard surface followed by the calibration of spring constant ($k=1.22$ N/m) using thermal tune method. The image analyses were carried out by NanoScope Analysis 1.5 Software by determining height and diameter values of several well-isolated particles from the corresponding images. Monolayer images (β -CD and epoxy silane) were captured by using Dimension 3100 AFM (Bruker-Nano, Santa Barbara, CA) under ambient conditions with tapping mode using etched silicon probes TAP 300 (Budget Sensors, Bulgaria) with a nominal spring constant of about $k=40$ N/m.

8.3.3 Fluorescence Microscopy

Fluorescence images of surface-immobilized polymersomes with photocleavable moieties were acquired by illumination of 1 mW laser beam at 532 nm. A bandpass filter transmitting between 570 and 620 nm (593/40 nm BrightLine bandpass filter from Semrock) transmits only the fluorescent light and it is detected by an AndoriXon+ camera. Image processing was performed using the Andor Solis (i) software.

8.4 Synthetic Methods and Characterization

8.4.1 Synthesis of Alkyne Functionalized Adamantane Molecule



The previously reported method was slightly modified as follows:³ 1-Aminoadamantane (0.6 g, 4 mmol) was charged into a round-bottom flask followed by adding anhydrous DCM (20

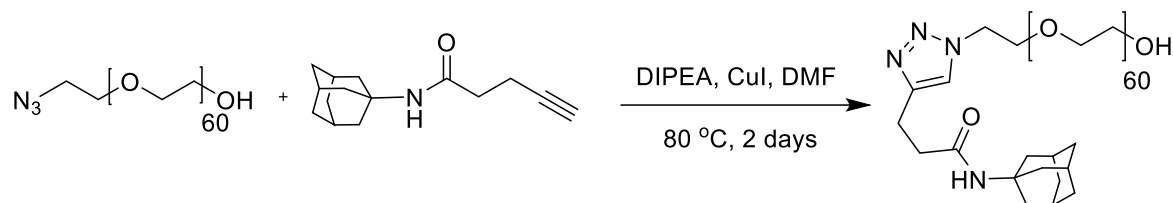
mL). In another flask, 4-pentynoic acid (0.4 g, 4 mmol) and N,N'-dicyclohexylcarbodiimide (DCC, 1.65 g, 8 mmol) were dissolved in anhydrous DCM (80 mL) under nitrogen atmosphere. The prepared 1-aminoadamantane solution was added dropwise to 4-Pentynoic acid-DCC solution, then the reaction mixture was stirred for 15 h at room temperature. After 15 h, the mixture was filtered and the solvent was removed under reduced pressure. Finally, the product was obtained by purification with column chromatography on silica gel using hexane/ethyl acetate=2:1(Yield: 70%).

Analytical Data:

^1H NMR (500.13 MHz, DMSO- d_6 , δ): 1.61 (s, 6H), 1.91 (d, $J=2.5$ Hz, 6H), 1.99 (s, 3H), 2.21 (t, $J=6.9$ Hz, 2 H), 2.30 (td, $J=6.9, 2.5$ Hz, 2H), 2.72 (t, $J=2.5$ Hz, 1H), 7.29 (s, NH).

IR (cm^{-1}): 3305 (NH), 2908 (CH), 1636 (Amide I), 1548 (Amide II), 680 (NH).

8.4.2 Synthesis of Adamantane Functionalized Poly(ethylene glycol)



Synthesis procedure was performed by modifying a previous method.³⁻⁴ N₃-PEG₆₀-OH (0.35 g, 0.13 mmol), alkyne functionalized adamantane (0.065 g, 0.28 mmol) and copper (I) iodide (0.013 g, 0.007 mmol) was loaded into a flask. This mixture was degassed for 30 min under vacuum. In a separate flask, DMF (10 mL) was deoxygenated by freeze pump thaw cycles and added to reaction flask under nitrogen atmosphere. After addition of DIPEA (0.091 mL, 0.52 mmol), the reaction mixture was stirred for 2 days at 80 °C. Solvent of the resulting reaction mixture was evaporated under reduced pressure, followed by dissolving the solid product in THF. Finally, Ada-PEG₆₀-OH was obtained as a white solid by precipitation in *n*-hexane. For further purification, Ada-PEG₆₀-OH was dissolved in millipore H₂O and dialyzed for 24 h against EDTA solution to remove the copper species. After freeze drying, the pure product (0.2 g) was obtained with a yield of 53%.

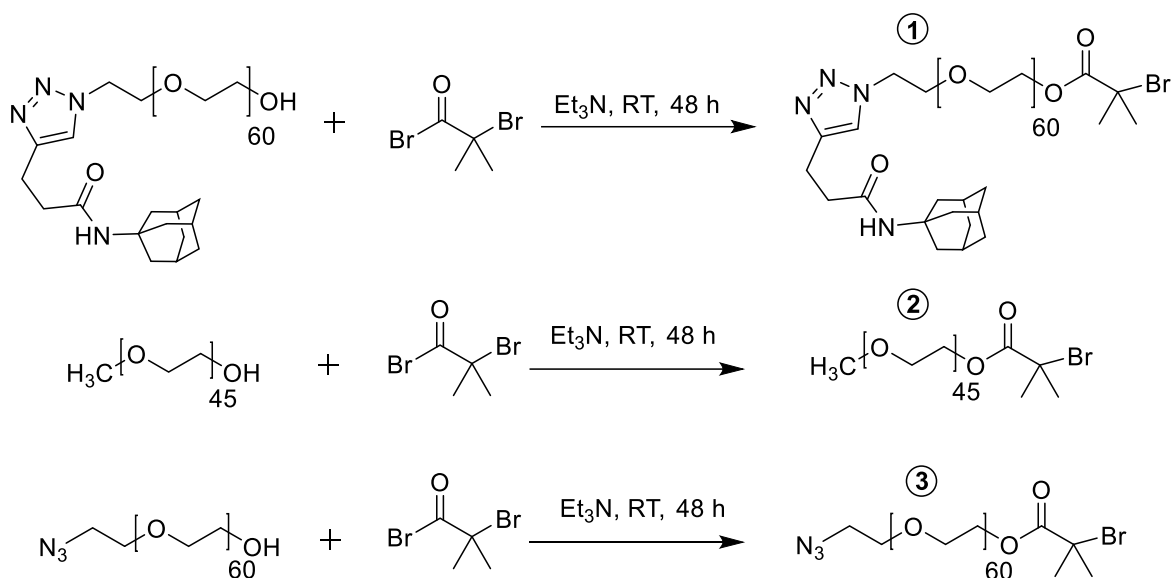
Analytical Data:

IR (cm^{-1}): 3438 (OH), 2889 (CH), 1644 (Amide I), 1541(Amide II), 1467 (CH₂), 1344 (C-O-C), 1114 (C-O).

$^1\text{H NMR}$ (500.13 MHz, CDCl_3 , δ): 1.66 (s, 6H), 1.94 (6H), 2.05 (s, 3H), 2.51 (t, $J=7.6$ Hz, 2H), 2.58 (OH), 3.01 (t, $J=7.6$ Hz, 2H), 3.65 (s, 248H), 3.86 (t, $J=5.6$ Hz, 2H), 4.50 (t, $J=5.0$ Hz, 2H), 5.39 (s, NH), 7.52 (s, 1 H)

$^1\text{H NMR}$ (500.13 MHz, $\text{DMSO-}d_6$, δ): 1.61 (s, 6H), 1.91 (s, 6H), δ 1.99 (s, 3H), 2.34 (t, $J=7.6$ Hz, 2 H), δ 2.78 (t, $J=7.6$ Hz, 2H), 3.51 (s, 248H), 3.77 (t, $J=5.7$ Hz, 2H), 4.45 (t, $J=5.7$ Hz, 2H), 4.52 (OH), 7.25 (s, NH), 7.74 (s, 1H).

8.4.3 Synthesis of Poly(ethylene glycol) Macroinitiators with Different End-Groups



The previously reported method was used as follows.⁵ Polyethylene glycol with corresponding end groups (methoxy, azide or adamantane, 1 eq.) was charged into a flask and dried under vacuum for 30 min. Subsequently, anhydrous THF was added and the flask was flushed with nitrogen followed by addition of triethylamine (2 eq.). Then 2-bromoisobutyryl bromide (2 eq.) was diluted in anhydrous THF and added dropwise to reaction mixture. The reaction was carried out for 48 h at room temperature. After that, the mixture was filtered to remove the salt and the resulting solution was concentrated under reduced pressure. Finally, PEG macroinitiator was precipitated in cold *n*-hexane and isolated by decantation. Yield of the reaction was 82% for azide terminated PEG, 80% for methoxy terminated PEG and 72% for adamantane terminated PEG macroinitiators.

Analytical Data:

PEG Macroinitiator with azide end groups: $^1\text{H NMR}$ (500.13 MHz, CDCl_3 , δ): 1.95 (s, 6H), 3.40 (t, 2H), 3.65 (s, 248H), 4.33 (t, $J=5.0$ Hz, 2H)

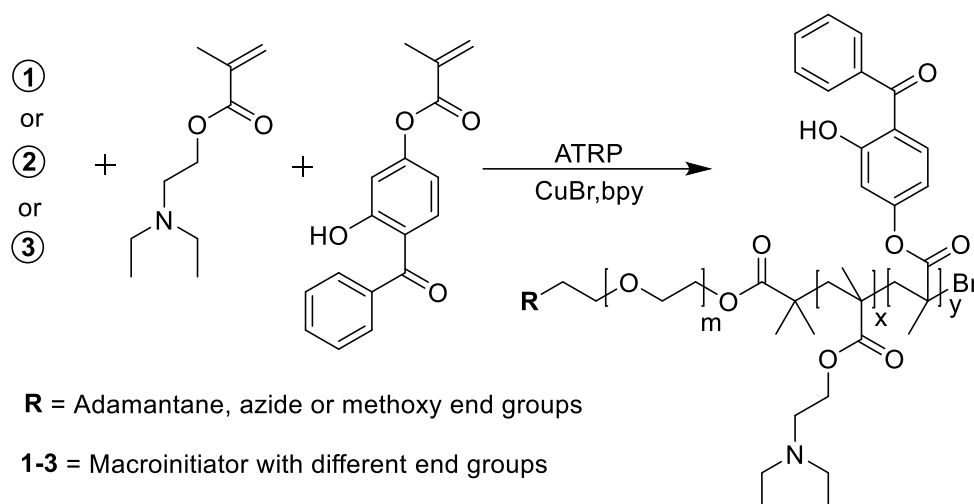
PEG Macroinitiator with methoxy end groups: ^1H NMR (500.13 MHz, CDCl_3 , δ): 1.95 (s, 6H), 3.38 (s, 3H), 3.65 (s, 180H), 4.33 (t, $J=5.0$ Hz, 2H)

PEG Macroinitiator with adamantane end groups: ^1H NMR (500.13 MHz, CDCl_3 , δ): 1.66 (s, 6H), 1.94 (6H), 1.95 (s, 6H), 2.05 (s, 3H), 2.51 (t, $J=7.6$ Hz, 2H), 3.01 (t, $J=7.6$ Hz, 2H), 3.65 (s, 248H), 3.86 (t, $J=5.6$ Hz, 2H), 4.33 (t, $J=5.1$ Hz, 2H), 4.50 (t, $J=5.1$ Hz, 2H), 5.39(s, NH),7.52 (s,1 H)

8.4.4 Synthesis of Block Copolymers

Block copolymers were synthesized by using standard atom transfer radical polymerization (ATRP) procedure with slight modifications as reported previously.⁵

8.4.4.1 Synthesis of Block Copolymers with Crosslinker



A round bottom flask was loaded with the desired poly(ethylene glycol) macroinitiator possessing different end groups (1 eq.), 2,2'-bipyridine (2 eq.), Cu(I)Br (1 eq.) and BMA (10 eq., 10 mol%) respectively where the exact feed amounts of each polymer synthesis is given in Table 8.1. This mixture was degassed for 30 minutes under vacuum. In two other flasks, DEAEMA (90 eq.) and 2-butanone were separately deoxygenated by freeze pump thaw cycles, and then were added to the reaction mixture. The reaction of BC1-BC3 was carried out for 19 h at 50 °C under nitrogen atmosphere. The polymerization was terminated by exposure of the mixture to air by adding THF. The oxidized copper catalyst was removed by passing through the mixture over an activated neutral aluminum oxide with THF as an eluent. Final solution was concentrated by evaporating most of the solvent, followed precipitation in cold n-hexane. The block copolymers were then washed with water to

remove the unreacted macroinitiator and dried under vacuum. The yields of the obtained polymers were 75% for BC2, 65% for BC1, 60% for BC3. It should be noted that the larger scaled polymerizations ended with higher yields.

Table 8.4 Feed amounts of the reagents for block copolymer synthesis

Code	Feed amounts (mmol)				
	^a R-PEG-Br	2,2'-bipyridine	Cu(I)Br	DEAEMA	BMA
BC1	0.08	0.16	0.08	7.2	0.8
BC2	0.23	0.46	0.23	20.7	2.3
BC3	0.04	0.08	0.04	3.6	0.4

^aR: Azide, methoxy or adamantane for BC1, BC2 and BC3 polymers, respectively.

Analytical Data:

N₃PEG₆₀-b-P(DEAEMA₈₂-stat-BMA₁₂), BC1:

¹H NMR (500.13 MHz, CDCl₃, δ): 0.80-0.96 (m, 3 H), 0.97-1.25 (m, 6 H), 1.71–2.20 (m, 2 H), 2.48-2.63 (m, 4 H), 2.65-2.80 (m, 2 H), 3.49-3.75 (m, 4H), 3.90–4.18 (m, 2 H), 6.59-7.72 (m, 8H).

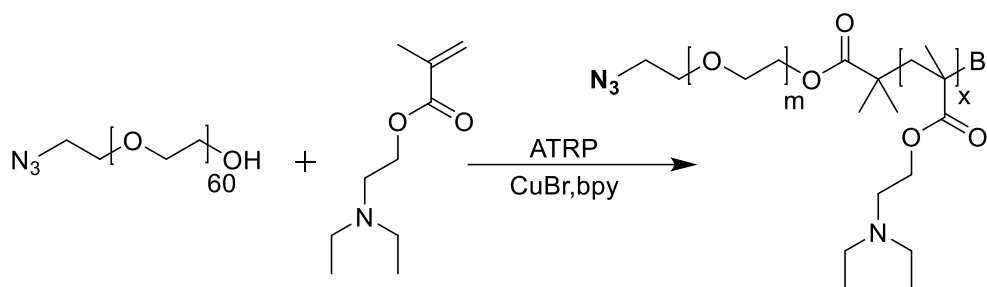
PEG₄₅-b-P(DEAEMA₈₁-stat-BMA₁₀), BC2:

¹H NMR (500.13 MHz, CDCl₃, δ): 0.80-0.96 (m, 3 H), 0.97-1.25 (m, 6 H), 1.71–2.20 (m, 2 H), 2.48-2.63 (m, 4 H), 2.65-2.80 (m, 2 H), 3.39 (s, 3 H), 3.49-3.75 (m, 4 H), 3.90–4.18 (m, 2 H), 6.60-7.72 (m, 8H).

AdaPEG₆₀-b-P(DEAEMA₈₂-stat-BMA₁₅), BC3:

¹H NMR (500.13 MHz, CDCl₃, δ): 0.80- 0.96 (m, 3 H), 0.97 - 1.25 (m, 6 H), 1.65-1.70 (m,6 H), 1.71 – 2.20 (m, 6 H, m, 6H, m, 3H), 2.46 - 2.61 (m, 4 H), 2.64 - 2.79 (m, 2 H), 3.01 (t, J=7.6 Hz, 2H), 3.49-3.75 (m, 4H), 3.90 – 4.18 (m, 2 H), 4.50 (t, J=5.0 Hz, 2H), 5.39 (s, NH), 6.60-7.72 (m, 8H).

8.4.4.2 Synthesis of azide-terminated Block Copolymer without Crosslinker



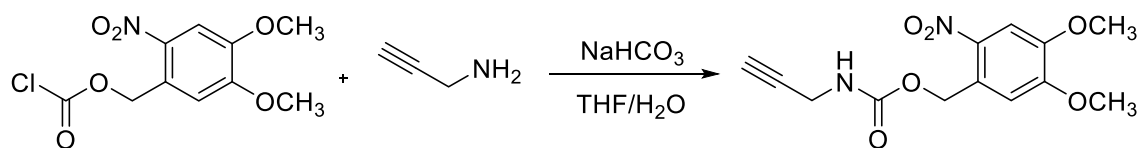
A round bottom flask was loaded with the azide terminated poly(ethylene glycol) macroinitiator (0.04 mmol), 2,2'-bipyridine (0.08 mmol) and Cu(I)Br (0.04 mmol) respectively. This mixture was degassed for 30 minutes under vacuum. In two other flasks, DEAEMA (4.8 mmol) and 2-butanone were separately deoxygenated by freeze pump thaw cycles, and then were added to the reaction mixture. The reaction of BC4 was carried out for 15 h at 50 °C under nitrogen atmosphere. The further steps were performed identically as described above to obtain the block copolymer without crosslinker.

N₃PEG₆₀-b-P(DEAEMA₁₅₀), BC4:

¹H NMR (500.13 MHz, CDCl₃, δ): 0.80-0.96 (m, 3 H), 0.98-1.25 (m, 6 H), 1.70–2.20 (m, 2 H), 2.52-2.64 (m, 4 H), 2.67-2.81 (m, 2 H), 3.49-3.75 (m, 4 H), 3.92-4.13 (m, 2 H).

8.4.5 Synthesis of Photoactive Compounds

8.4.5.1 Synthesis of Nitroveratryloxycarbonyl (NVOC) Protected Amine Groups



To an aqueous mixture of propargylamine (0.11 mL, 1.7 mmol) and sodium bicarbonate (0.3 g, 3.6 mmol), a solution of nitroveratryloxycarbonylchloride (0.5 g, 1.8 mmol) in THF was added dropwise. After 15 hours of stirring at room temperature, the precipitation was filtered and THF was evaporated under reduced pressure. The obtained suspension was diluted with water and extracted with ethyl acetate followed by drying with sodium sulfate. Then ethyl acetate was evaporated to obtain the solid product (yield 88%). Since the product was not

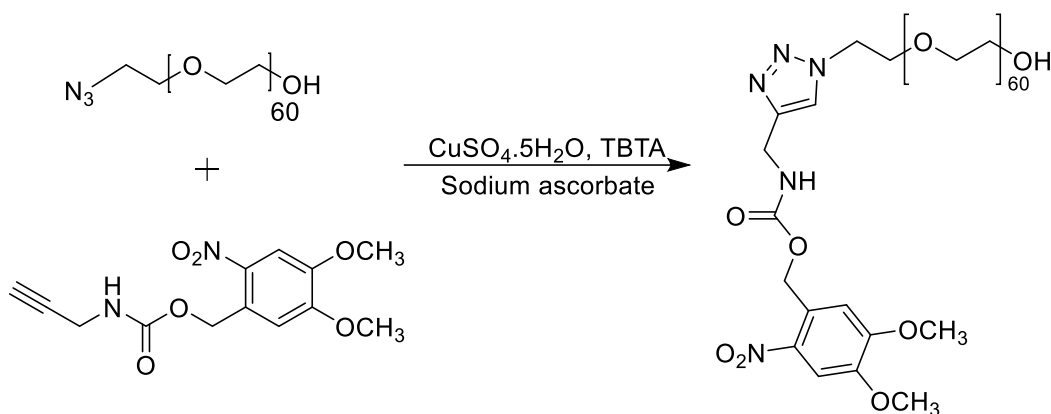
pure enough determined by NMR spectra, it was further purified with column chromatography on silica gel using *n*-hexane/ethyl acetate=1:2 (Yield: 50%).

Analytical Data:

¹H NMR (500.13 MHz, CDCl₃, δ): 2.26 (t, J=2.5 Hz, 1 H), 3.96 (s, 3 H), 3.99 (s, 3 H), 4.03 (dd, J=5.7, 2.5 Hz, 2H), 5.07 (br, NH), 5.55 (s, 2H), 7.0 (s, 1 H), 7.72 (s, 1 H).

¹³C NMR (125.76 MHz, CDCl₃, δ): 31.00 (C-d), 56.41 (C-b, C-c), 63.85 (C-f), 71.77 (C-a), 79.43 (C), 108.23 (C-g), 110.31 (C-h), 127.67 (C-i), 139.92 (C-m), 148.22 (C-l), 153.56 (C-k), 155.37 (C-j).

8.4.5.2 Synthesis of Model Compound (NVOC-PEG₆₀OH), M1C



A round bottom flask was charged with aqueous solution of N₃-PEG₆₀-OH (1 mol eq.) and purged with nitrogen for 30 min. Subsequently, aqueous solutions of CuSO₄·5H₂O (0.25 mol eq.), TBTA (0.25 mol eq. in DMSO), sodium ascorbate (0.5 mol eq.) and alkyne modified NVOC groups (1.5 mol eq. in DMSO) were added to reaction flask as the same way mentioned above. After 2 days of stirring at room temperature, the reaction mixture was extensively dialyzed against water for 2 days and then freeze dried for characterization.

Analytical Data:

¹H NMR (500.13 MHz, CDCl₃), δ (ppm): 2.52 (OH), 3.65 (s, 248 H), 3.95-3.96 (each 3 H at 50 C°), 4.49 (d, J=5.6 Hz, 2H), 4.52 (t, J=5.1 Hz, 2 H), 5.53 (s, 2H), 5.67 (br, NH), 7.01 (s, 1 H), 7.72 (s, 1 H), 7.74 (s, H)

8.4.5.3 Disassembly of the Photoactive Polymersomes (PS2C) by Freeze-Drying

In order to monitor the NVOC conjugation to the non-crosslinked polymersomes by chemical structure characterization with ¹H NMR spectroscopy, the PS2C vesicles (1

mg/mL) were disassembled to obtain the corresponding polymers using freeze dryer ALPHA1-2 LD_{Plus} (Fisher Bioblock Scientific, France). After overnight, the freeze dried PS2C polymersomes were analyzed by ¹H NMR spectroscopy.

Analytical Data:

¹H NMR (500.13 MHz, CDCl₃, δ): 0.80-0.96 (m, 3 H), 0.98-1.20 (m, 6 H), 1.74–2.20 (m, 2 H), 2.52-2.65 (m, 4 H), 2.67-2.81 (m, 2 H), 3.49-3.75 (m, 4 H), 3.92-4.13 (m, 2 H), 4.49 (d, J=5.6 Hz, 2H), 4.52 (t, J=5.0 Hz, 2 H), 5.39 (s, NH), 5.54 (s, 2H), 7.71 (s, 1 H), 7.75 (s, 1 H).

8.5 References

- [1] Luzinov, I.; Julthongpiput, D.; Liebmann-Vinson, A.; Cregger, T.; Foster, M. D.; Tsukruk, V. V., Epoxy-Terminated Self-Assembled Monolayers: Molecular Glues for Polymer Layers. *Langmuir* **2000**, *16*, 504-516.
- [2] Herzinger, C. M.; Johs, B.; McGahan, W. A.; Woollam, J. A.; Paulson, W., Ellipsometric Determination of Optical Constants for Silicon and Thermally Grown Silicon Dioxide Via a Multi-Sample, Multi-Wavelength, Multi-Angle Investigation. *J. Appl. Phys.* **1998**, *83*, 3323-3336.
- [3] Kluge, J. Oberflächenfunktionalisierung von Polymersomen Mittels Chemischer Konjugation. Masterarbeit, Technischen Universität Dresden, **2012**.
- [4] Stadermann, J.; Komber, H.; Erber, M.; Däbritz, F.; Ritter, H.; Voit, B., Diblock Copolymer Formation Via Self-Assembly of Cyclodextrin and Adamantyl End-Functionalized Polymers. *Macromolecules* *44*, 3250-3259.
- [5] Yassin, M. A.; Appelhans, D.; Mendes, R. G.; Rummeli, M. H.; Voit, B., Ph-Dependent Release of Doxorubicin from Fast Photo-Cross-Linkable Polymersomes Based on Benzophenone Units. *Chemistry – A European Journal* *18*, 12227-12231.

9 Polymersome Formation and Encapsulation Procedures

9.1 Preparation of Multi-functionalized Polymersomes

A mixture of block copolymers was dissolved in aqueous HCl solution (pH 2), then passed through 0.2 μm nylon filter to remove any impurities. The degree of functionalization was controlled by varying the weight percentages of the desired block copolymers in solution. To initiate the self-assembly process, pH was slowly increased to pH 9 by adding 1 M NaOH. The total block copolymer concentration was 1 mg/mL and the polymersomes (PS1, PS3) were formed after four days of stirring in dark condition.

9.2 Preparation of Polymersomes from Single Block-Copolymer

The same procedure was applied as described in the previous section. The desired block copolymer (BC1 or BC4) was dissolved in aqueous HCl solution (pH 2), then passed through 0.2 μm nylon filter to remove any impurities. Then self-assembly of the block copolymers was triggered by increasing the pH value gradually to pH 9 through the addition of 1 M NaOH. The block copolymer concentration was 1 mg/mL and after 4 days of stirring in dark state, the polymersomes (PS0 or PS2) were formed.

9.3 Cross-linking of Polymersomes

After the formation of polymersomes, the solutions were further passed through the 0.8 μm nylon filter to remove any impurities. Then they were placed in the UV chamber equipped with an iron lamp (UVACUBE 100, honle UV Technologies, Germany) and irradiated for 30 min. The photo-crosslinking was performed in round shaped-glass vials in which the path length of light is adjusted as 1.5 cm. The intensity of the light at this condition was measured with a power meter (Coherent Fieldmax II TO, USA) and found as 80 mW/cm².

9.4 Reversible Swelling and Shrinking of Crosslinked Polymersomes

To monitor the swelling power of the cross-linked polymersomes, they were titrated by addition of 1 M HCL or 1 M NaOH to reach the pH 5 or pH 10 values respectively. The diameter of the vesicles was determined by DLS at each pH condition and this process was repeated for 5 cycles.

9.5 Polymersome Surface Functionalization

9.5.1 NVOC Modification of Polymersomes

Previously published methods were modified as follows:¹⁻² The aqueous solutions of $\text{CuSO}_4 \cdot 5\text{H}_2\text{O}$ (0.25 mol eq.), sodium ascorbate (0.5 mol eq.), TBTA (0.25 mol eq. in DMSO), and alkyne modified NVOC groups (1.5 mol eq. in DMSO) were added to the 1 mg/mL polymersome solution at pH 8 (PS1, PS2 or PS3, azide groups, 1 mol eq.). The reaction mixture was stirred for 2 days at room temperature. Subsequently, the polymersome solution was transferred to a dialysis membrane (5 kDa MWCO) and extensively dialyzed against EDTA solution in millipore water (5 liters, 0.055 mM, pH 8) for 2 days by changing the media 3 times a day. To ensure the purification efficiency, dialysis of same amount of NVOC molecules without polymersomes was also performed as done identically for purification after click reaction on PS1 surface (Figure 9.1).

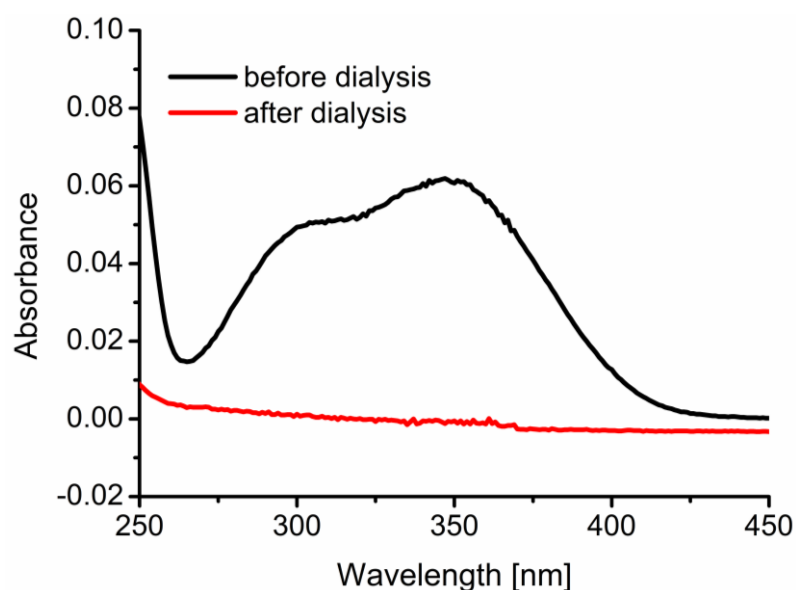


Figure 9.1 Dialysis of same amount of NVOC molecules without polymersomes for purification assesment (Diaysis duration=2 days with the 5 kDa MWCO membrane)

9.5.2 Photocleavage of NVOC groups via UV-irradiation

The polymersome solutions were placed in round-shaped glass vials by keeping the path length of the light as 1.5 cm. Then the irradiation was carried out at a distance of 1 cm from the UV lamp in the range of 0-600 seconds (Omnicure S2000, Lumen Dynamics Group Inc., Canada). The UV chamber was equipped with a high pressure mercury lamp and the light intensity at described condition was measured as 0.35 W/cm^2 using a power meter (Coherent

Fieldmax II TO, USA). The decrease in absorbance at 345 nm was monitored by UV-vis spectroscopy. Then, the final polymersome solution was dialyzed against water (pH 8) for 4 hours to remove byproducts of the deprotection reaction.

9.5.3 Rhodamine B NCS Modification of Polymersomes

To a 1 mg/mL polymersome solution at pH 8 (PS1D) was added 19 μ L of Rhodamine B NCS solution in DMSO (RhB-NCS, 0.03 mM). The reaction mixture was stirred for 12 hours at room temperature, then the polymersome solution was extensively dialyzed against water (5 liters, pH 8) for 3 days using a 50 kDa MWCO membrane by changing the media 3 times a day. The same process was applied also to PS1 polymersomes as a negative control.

9.5.4 β -Cyclodextrin Modification of Polymersomes

Aqueous solution of sulfo-cyanine7 labeled cyclodextrin (β -CD-Cy7, 6 mol eq.) was added to polymersomes which were already reacted with Rhodamine B NCS fluorescent dye (PS1R, Ada groups 1 mol eq.). After 20 hours of stirring at room temperature, the polymersome solution was transferred to a dialysis membrane (MWCO: 50kDa) and dialyzed extensively against water (5 liters, pH 8) for 3 days by changing the media 3 times a day. As a control experiment, the same procedure was also applied to polymersomes without any adamantane groups (PS0) and also PS1 polymersomes with adamantane groups.

9.5.5 Predicting the Accessibility of the Functional Groups

9.5.5.1 Functionalization Degree of NVOC groups

A similar method as described previously was applied as follows:¹ PS2C polymersome was freeze dried and dissolved in CHCl_3 at different concentrations. Then, absorbance of the prepared solutions was measured at 345 nm using UV-vis spectroscopy and fitted to a linear line ($A=6289.52c$, $R^2=0.997$, Figure 9.2). To obtain the comparative relationship, the same approach was also applied to a model compound (NVOC-PEG₆₀OH, M1C) which had 50% NVOC functionalization (X_{M1C}) determined from ¹H NMR spectrum ($A=3330.33c$, $R^2=0.998$, Figure 9.3). Subsequently, the ratio of the slopes of the regression lines was related with the functionalization degree of the two compounds ($1.88X_{\text{PS2C}}= X_{\text{M1C}}$) to estimate the relative amount of NVOC modification on polymersome surfaces.

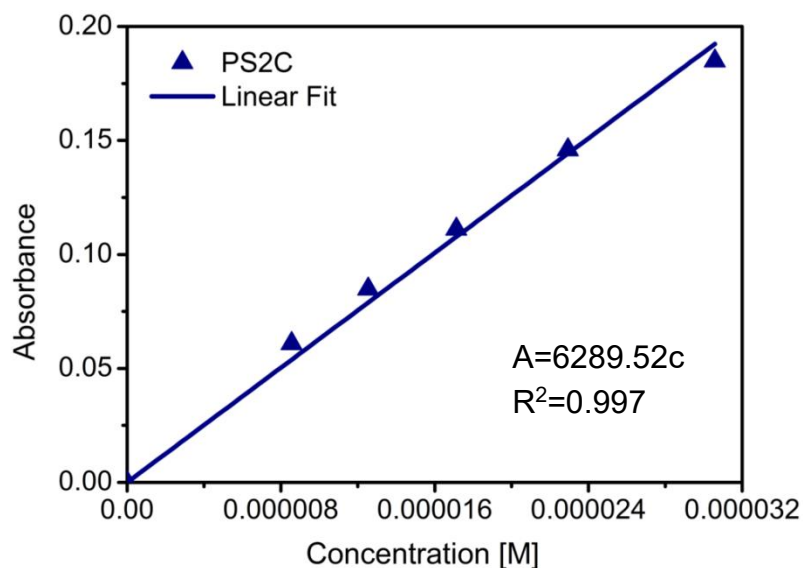


Figure 9.2 Calibration curve of PS2C determined from absorbance values at $\lambda=345$ nm, measured in CHCl_3 , to calculate the relative NVOC functionalization degree of polymersomes (path length of the quartz cuvette =1 cm)

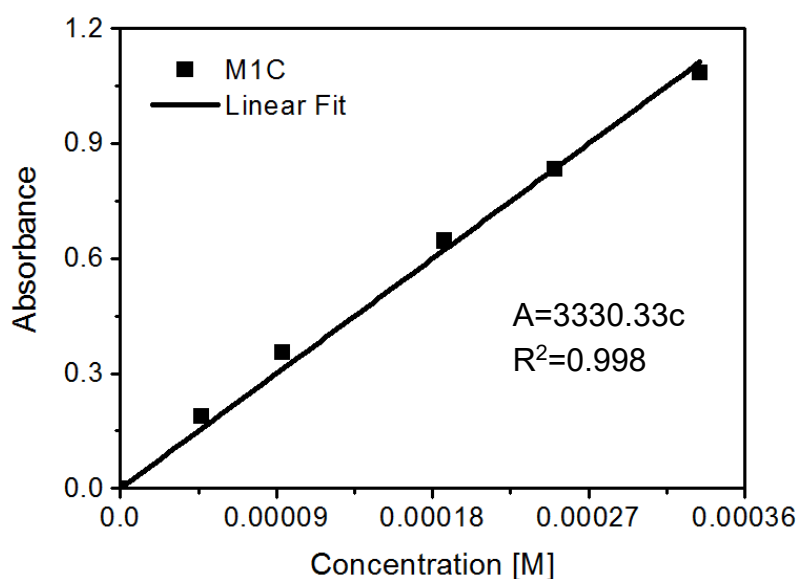


Figure 9.3 Calibration curve of M1C determined from absorbance values at $\lambda=345$ nm, measured in CHCl_3 , to calculate the relative NVOC functionalization degree of polymersomes (path length of the quartz cuvette =1 cm)

9.5.5.2 Photocleavage Efficiency of NVOC Groups

PS2C polymersomes were irradiated for 600 seconds as described in the previous section and then dialyzed against water (pH 8) for 4 hours. The polymersome solutions before and after irradiation were freeze dried and dissolved in acidic water (1 mg/mL) for UV-vis

characterization as shown in Figure 9.4. Then, the absorbance values at 345 nm were determined and the photocleavage efficiency was predicted by calculating the amount of NVOC chromophore cleavage from three different batches of PS2C polymersomes (Figure 9.5) by means of equation 9.1.

$$\text{NVOC Chromophore Cleavage (\%)} = \frac{\text{Absorbance before irradiation} - \text{Absorbance after irradiation}}{\text{Absorbance before irradiation}} \times 100 \quad (9.1)$$

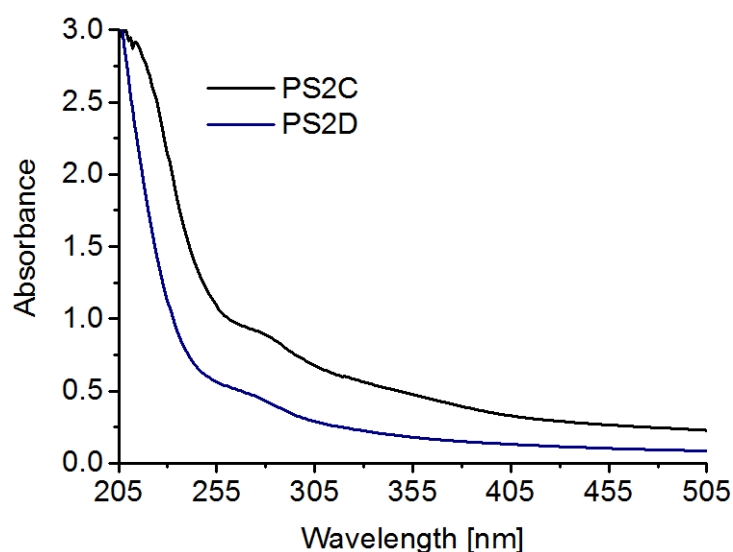


Figure 9.4 UV-vis spectra of freeze dried PS2C and PS2D in acidic water

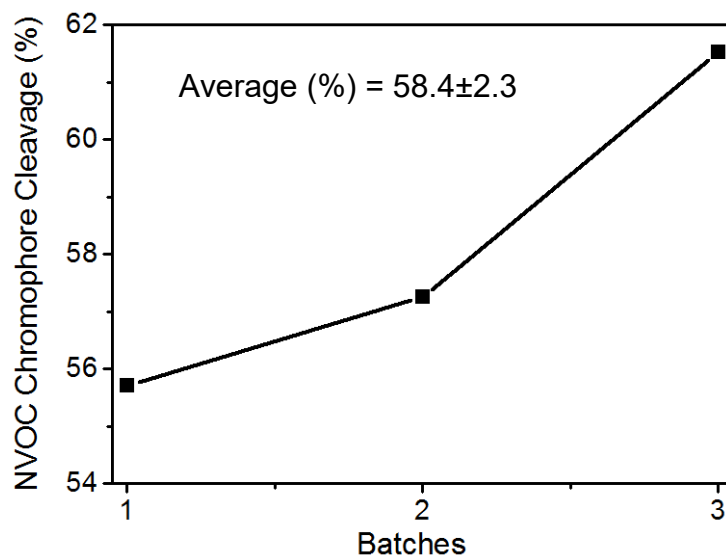


Figure 9.5 Monitoring the cleavage of NVOC chromophore from 3 different batches of PS2C polymersomes to calculate the photocleavage efficiency

9.5.5.3 Efficiency of the Rhodamine B NCS Modification

To predict the accessibility of released NH_2 groups after photocleavage step, both PS1R and PS1 polymersomes was analyzed by UV-Vis spectroscopy. The concentration of NH_2 groups reacted with RhB-NCS dye was determined by using the subtracted absorbance value of PS1R and PS1 polymersomes at 555 nm and the measured molar absorption coefficient ($\epsilon_{\text{RhNCS}}=136811$ at 555 nm) of RhB-NCS in polymersome solutions (Figure 9.6). Afterwards, the reactivity of NH_2 groups on the polymersome surface was determined by equation 9.2.

$$\text{Accessible } \text{NH}_2 \text{ groups on surface (\%)} = \frac{(\text{Concentration of attached RhBNCS})_{\text{PS1R-PS1}}}{\text{Concentration of total free } \text{NH}_2 \text{ groups}} \times 100 \quad (9.2)$$

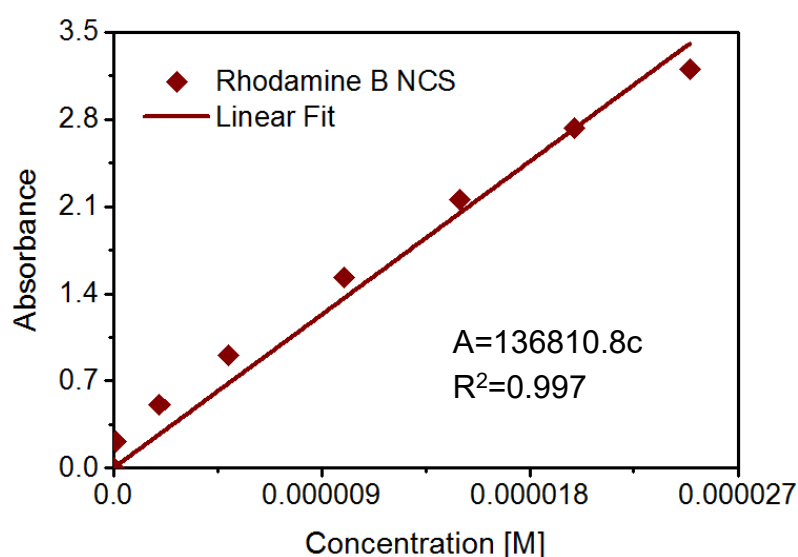


Figure 9.6 Calibration Curve of Rhodamine B NCS determined from absorbance values at $\lambda = 555$ nm, measured in polymersome solutions, to calculate the molar extinction coefficient (ϵ) of the corresponding dye (path length of the quartz cuvette = 1 cm)

9.5.5.4 Efficiency of the β -Cyclodextrin Modification

The conjugation efficiency of β -CDCy7 molecules was determined with a similar strategy as done for the evaluation of amino groups. The molar absorption coefficient of β -CDCy7 was measured as $\epsilon_{\text{CDCy7}}=113964.8$ at 775 nm in polymersome solutions (Figure 9.7) and used to calculate the accessible adamantane groups on PS1H surface from equation 9.3.

Accessible Ada groups on surface (%)

$$= \frac{(\text{Concentration of attached } CD_{Cy7})_{PS1H-PS0}}{\text{Concentration of Ada groups on outer shell}} \times 100 \quad (9.3)$$

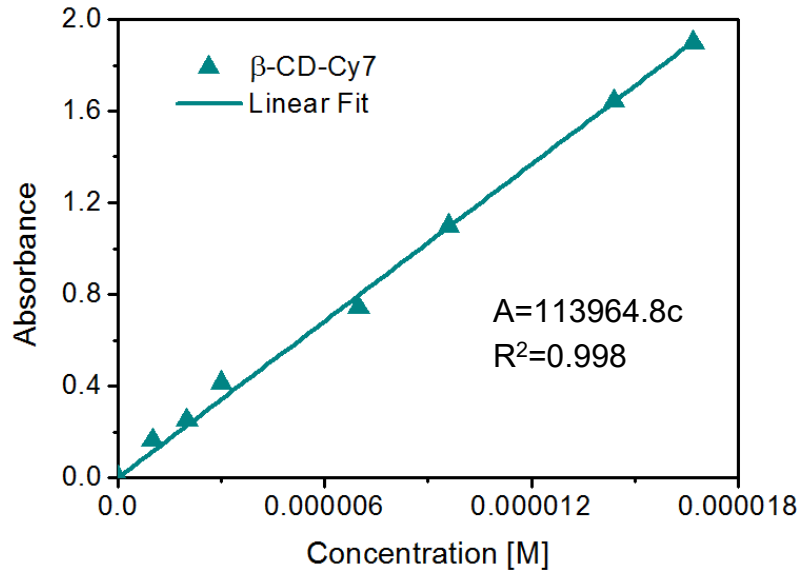


Figure 9.7 Calibration Curve of Cy7-labelled β -cyclodextrin determined from absorbance values at $\lambda = 775$ nm, measured in polymersome solutions, to calculate the molar extinction coefficient (ϵ) of the corresponding dye (path length of the quartz cuvette = 1 cm)

9.6 Doxorubicin-Encapsulated Polymersomes

Doxorubicin encapsulation was performed during the polymersome formation process with pre-loading approach. A mixture of block copolymers (29 mol% BC1, 61.8 mol% BC2, 9.2 mol% BC3) was dissolved in aqueous HCl solution (pH 2) then passed through 0.2 μ m nylon filter. Afterwards, pH was increased to a value of pH 5 by utilizing 1 M NaOH solution. Doxorubicin (3 mg, 0.5 mL in millipore H₂O) was added to the block copolymer solution in this step followed by increasing the pH to pH 7.4 to initiate the self-assembly process. The final concentration of the block copolymer was adjusted as 1 mg/mL whereas Dox concentration was 0.13 mg/mL. After stirring the mixture four days in dark condition, polymersomes were photo-crosslinked for 30 minutes as identically done for polymersomes without dox incorporation. By following this, the non-encapsulated Dox molecules were separated from the polymersome solutions by using hollow fiber filtration system. The separation was performed using modified polyethersulfone (mPES) based filter modules (MWCO: 100 kDa,) with transmembrane pressure (TMP) of 130 mbar by washing the samples with phosphate buffer at pH 7.4 for several cycles. To calculate the encapsulation

efficiency, all wash solutions during filtration were collected and absorbance at $\lambda=480$ nm was measured with UV-vis spectroscopy. From the calibration curve at pH 7.4 (Figure 9.8a), the amount of free Dox was defined and the encapsulation efficiency ($71.9\pm 0.4\%$) of the PS1-Dox polymersomes was determined by means of equation 9.4.

$$\text{Encapsulation Efficiency (\%)} = \frac{(\text{Initial Dox amount} - \text{Free Dox amount})}{\text{Initial Dox amount}} \times 100 \quad (9.4)$$

As a next step, to obtain NVOC modified Dox-loaded polymersomes (PS1C-Dox), the same procedure was applied to PS1-Dox polymersomes like it was done for PS1 vesicles previously. Here, only the reaction medium retained at pH 7.4 rather than pH 8 to avoid any Dox instability. As the final step, some portion of PS1C-Dox polymersomes were used in photocleavage process to obtain PS1D-Dox vesicles for further release studies.

9.7 In Vitro Release of Doxorubicin

Before proceeding to in-vitro release study, the calibration curves of doxorubicin at pH 7.4 and pH 5 were prepared in the range of 0-50 $\mu\text{g/mL}$ using phosphate buffer (PBS, pH 7.4) and acetate buffer (pH 5) from the stock solution of Dox in milipore water (0.1 mg/mL). Then the corresponding DOX solution in PBS or acetate buffer was measured with UV-Vis spectroscopy to define the absorbance values. Finally, the linearization of the Dox concentration versus absorbance data gives the required relationship (Figure 9.8, embedded equations in graphs) to calculate the unknown drug amount during release period.

For in vitro release study, Dox encapsulated polymersomes at pH 5 and pH 7.4 (4 mL, PS1C-Dox and PS1D-Dox) were poured into dialysis tubes (MWCO 5000) which were then placed into a 2-liter buffer containing beaker at constant temperature (37°C) and stirring (200 rpm) condition. Two different release media were prepared as acetate buffer (0.01 M) for pH 5 profile and phosphate buffer (0.01 M) for pH 7.4 profile. To determine the drug release, 0.8 mL samples were taken at selected time intervals for UV-Vis analysis ($\lambda=480$ nm) and returned back into the dialysis membrane after the measurement. The amount of remaining Dox at each sampling point was then calculated from the calibration curves at pH 5 and pH 7.4 (Figure 9.8). Finally, the cumulative Dox release at each time interval was obtained from equation 9.5.

Cumulative Dox Release(%) =

$$\frac{(\text{Initial Dox} - \text{Residual Dox, each sampling point})}{\text{Initial Dox}} \times 100 \quad (9.5)$$

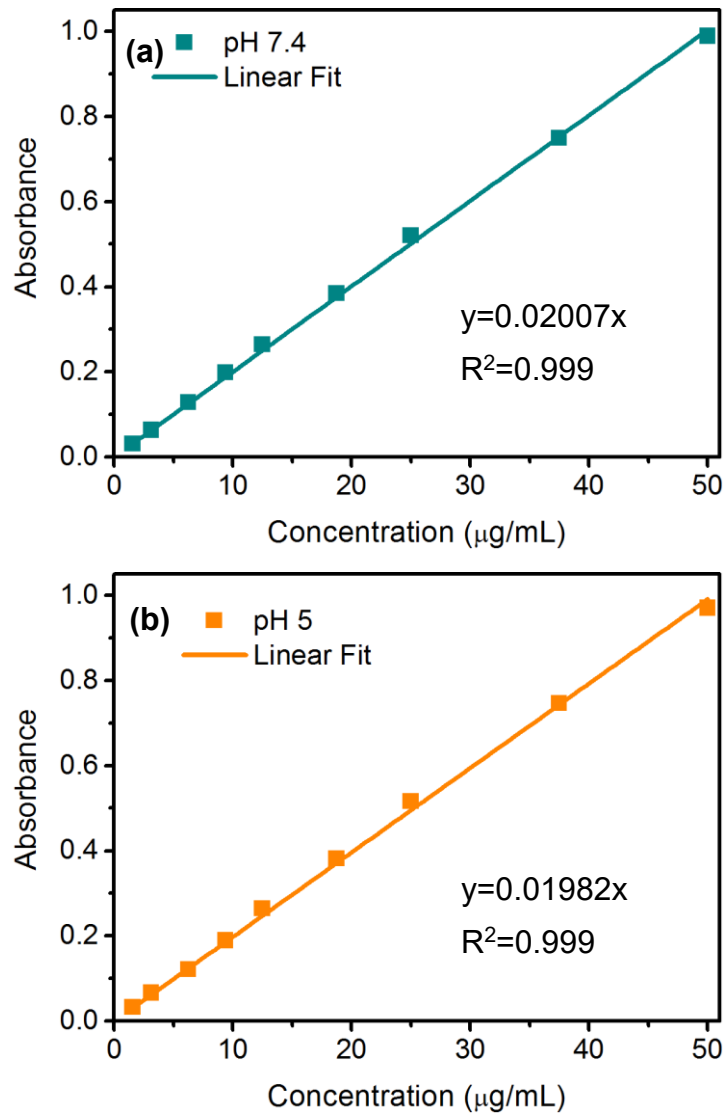


Figure 9.8 Calibration curve of Doxorubicin at (a) pH 7.4 and (b) pH 5 determined from absorbance values at $\lambda = 480 \text{ nm}$ to calculate the cumulative release

9.8 Preparation of Polymersome/Gold Nanoparticle Assemblies

9.8.1 Pre-loading Approach

In pre-loading approach, gold nanoparticle encapsulated polymersomes were prepared during self-assembly of block copolymers. As similarly done for doxorubicin encapsulation, a mixture of block copolymers (29 mol% BC1, 61.8 mol% BC2, 9.2 mol% BC3) was dissolved in aqueous HCl solution (pH 2) then passed through 0.2 μm nylon filter.

Afterwards, pH was increased to a value of pH 5 by utilizing 1 M NaOH solution. The addition of gold nanoparticles (in 0.01 mM phosphate buffer, 5 or 10 nm) was performed dropwise along with constant stirring. Afterwards, the pH was increased to pH 8 to obtain the polymersome/gold nanoparticle assemblies followed by stirring four days in dark condition. Finally, the photo cross-linking of polymersome membrane was carried out for 30 minutes as described previously. The total block copolymer concentration was kept as 1 mg/mL and the molar ratio of gold NPs to block copolymers was adjusted as 1.1 or 3.8. For purification of non-encapsulated gold nanoparticles; hollow fiber filtration system with modified polyethersulfone (mPES) based filter modules (MWCO: 750 kDa) was used. The transmembrane pressure (TMP) was maintained as 150 mbar during the filtration and phosphate buffer at pH 8 was used to wash the polymersome/gold nanoparticle solutions for several cycles of filtration process.

9.8.2 Post-loading Approach

In post-loading approach, gold nanoparticle encapsulated polymersomes was prepared after self-assembly of the block copolymers. The polymersomes solutions (PS1, 1 mg/mL) were prepared as identically described in chapter 8. Afterwards, the pH of the polymersomes was gradually decreased to pH 5 by addition of HCL (0.1 mM) solution which led to the swollen state of the polymersomes. By following this, the addition of gold nanoparticles (in 0.01 mM phosphate buffer, 5 or 10 nm) to the acidic polymersomes was carried out dropwise along with constant stirring. In order to provide sufficient time for gold nanoparticles to diffuse into the polymersome lumen, the polymersome/gold NPs mixture was stirred for an hour before pH was increased to the basic state (pH 8). The adjustment of the pH was performed by slow addition of NaOH solution (1 M). Herein, the molar ratio of gold NPs to block copolymers was kept as 3.8 which is the same like the pre-loading approach. The final block copolymer concentration after gold nanoparticle incorporation was 0.64 mg/mL and 0.66 mg/mL for PS1-Au10P and PS1-Au5P, respectively.

9.9 References

- [1] Opsteen, J. A.; Brinkhuis, R. P.; Teeuwen, R. L. M.; Lowik, D. W. P. M.; van Hest, J. C. M., "Clickable" Polymersomes. *Chem. Commun.* **2007**, 3136-3138.
- [2] O'Reilly, R. K.; Joralemon, M. J.; Hawker, C. J.; Wooley, K. L., Facile Syntheses of Surface-Functionalized Micelles and Shell Cross-Linked Nanoparticles. *J. Polym. Sci., Part A: Polym. Chem.* **2006**, *44*, 5203-5217.

10 Polymersome Immobilization onto Solid Substrates

10.1 Epoxy silane Coating of Substrates

The procedure of Luzinov et al. was modified as follows.¹ Silicon wafers and glass slides were firstly cleaned in ethanol via sonication for 30 minutes followed by rinsing several times with Millipore water. Then the substrates were dried under a stream of nitrogen before they were treated with plasma for 140 seconds at middle setting of the Harric Plasma Cleaner (PDC002, USA). As a next step, substrates were gently placed into teflon Si wafer holders (which enable the stirring of the solution for a more homogeneous layer formation) and immersed immediately into epoxysilane solutions (1 vol% in toluene) under inert atmosphere. After 23 hours of deposition time at 25 °C, the Si wafers and glass slides were rinsed 3 times with toluene and additionally placed in ethanol at ultrasonic bath for 15 minutes to remove unbound silane compounds. Finally, the SAMs were blow-dried with nitrogen stream and kept overnight under vacuum before the next coating step.

10.2 β -cyclodextrin Coating of Substrates

The previously published method was adopted as follows.² Solutions of NH_2 - β -CD as 0.1 mM and 1 mM were prepared in phosphate buffer at pH 8 (10 mM) and stirred for 2 hours for deprotection of the amino groups before using in the coating process. Afterwards, the epoxysilane covered substrates were gently placed into teflon Si wafer holders as done similarly for the previous step and immersed in this solution. The duration of the coating was 24 hours at 25 °C. After the deposition time, the substrates were rinsed 3 times with phosphate buffer and placed in Millipore water at ultrasonic bath for 15 minutes to remove unbound cyclodextrin molecules. Finally, β -cyclodextrin covered surfaces were obtained by drying the substrates with nitrogen stream and kept under vacuum.

10.3 Passivation of β -Cyclodextrin Coated Substrates with PEG molecules

The less-active β -cyclodextrin covered Si wafers (0.1 mM) were placed into special teflon Si wafer holders and immersed in polyethylene glycol solutions (in phosphate buffer, pH 8). The Si wafers were kept overnight in this solution after NH_2 - β -CD coating. Three different concentrations were used for the PEG solution (0.25 mM, 0.11 mM and 0.05 mM) to optimize the passivation level of the surface.

10.4 Polymersome Immobilization

β -Cyclodextrin-coated Si wafers or glass slides were placed into teflon Si wafer holders and immersed into 1 mg/mL polymersome solution at pH 7.4. After 20 hours of deposition time, the substrates were rinsed with PBS buffer at pH 7.4 for 3 times then imaged with AFM under the same aqueous solution. For the samples of photoreaction experiments, the pH value was kept at pH 8 (in phosphate buffer) to obtain a high conjugation yield of the amine reactive fluorescent marker.

10.5 Two Photon Absorption (TPA) Induced Photochemical Reactions

This work was performed in collaboration with Dr. Philipp Reichenbach in the group of Prof. Lukas M. Eng from Applied Photophysics Institute (IAPP) of Dresden Technical University in the scope of SPP 1327 Project of German Research Foundation. The samples were irradiated by a femtosecond laser beam at 775 nm central wavelength with pulse duration of 100 fs at a repetition of 75 MHz. The sample illumination was realized through an air objective (40x Zeiss Achrostat with N.A=0.65) and the laser beam is defocused on the surface (by approximately 8 μ m) to illuminate a larger number of polymersomes. By utilizing the piezo stage, the samples were moved against the laser beam to write the lines of 30 μ m length at different powers from 1 mW to 64 mW. The laser-written lines were separated by a distance of 10 μ m and all irradiation experiments were performed in wet state (in pH 8 buffer solution). After the irradiation step, the samples were immersed into the ATTO 532-NHS ester dye solution (0.3 mM, pH 8) for one day. To remove the unbound dye, the samples were rinsed with buffer solution (pH 8) for 3 times which is then placed into the buffer for two additional days not to have any unspecific dye attachment. After this intensive purification of dye molecules, the samples were placed into fresh pH 8 buffer solutions and visualized by fluorescence microscopy. To mark the positions of the polymersomes during fluorescence imaging, Au stripes were deposited onto glass slides by using a mask through the middle of the sample by evaporating 1.5 nm Cr and 15 nm Au in a vacuum evaporator. Before carrying out the 3-GPS coating step, scratches were drawn into these stripes to mark certain position in the neighborhood of the gold stripe. All further coating steps including polymersome deposition are identical as explained above.

10.6 References

- [1] Tsukruk, V. V.; Luzinov, I.; Julthongpiput, D., Sticky Molecular Surfaces: Epoxysilane Self-Assembled Monolayers. *Langmuir* **1999**, *15*, 3029-3032.
- [2] Busse, S.; DePaoli, M.; Wenz, G.; Mittler, S., An Integrated Optical Mach–Zehnder Interferometer Functionalized by B-Cyclodextrin to Monitor Binding Reactions. *Sensors Actuators B: Chem.* **2001**, *80*, 116-124.

Abbreviations and Symbols

Ada	Adamantane
AFM	Atomic force microscopy
ATRP	Atom transfer radical polymerization
AuNP	Gold nanoparticles
BMA	4-(methacryloyloxy) benzophenone
BC	Block copolymer
β-CD	β -cyclodextrin
bpy	Bipyridine
CRP	Controlled radical polymerization
Cryo-TEM	Cryogenic transmission electron microscopy
Cy7	Sulfo-Cyanine 7
CW	Continuous wave
DLS	Dynamic light scattering
DEAEM	2-(diethylamino) ethyl methacrylate
DPA	2-(Diisopropylamino) ethyl methacrylate
Dox	Doxorubicin
DMSO	Dimethyl sulfoxide
DMAC	Dimethylacetamide
DMF	Dimethylformamide
DIPEA	Diisopropylethylamine
DPPC	Dipalmitoylphosphatidylcholine
EDTA	Ethylenediaminetetraacetic acid
EggPC	Egg yolk phosphatidylcholin
FEM	Finite element method

3-GPS	3-Glycidyloxypropyltrimethoxysilane
HFF	Hollow fiber filtration
MWCO	Molecular weight cut-off
NHS	N-hydroxysuccinimide
NIR	Near-infrared
NMR	Nuclear magnetic resonance
NVOC	Nitroveratryloxycarbonyl
ONB	o-Nitrobenzyl
OPA	One photon absorption
PAA	Poly(acrylic acid)
PBS	Phosphate buffered saline
PEG	Poly(ethylene glycol)
PDI	Polydispersity index
PDMS	Poly(dimethylsiloxane)
PDMIBM	Poly(dimethylmaleic imide butyl methacrylate)
PMCL	Poly(methyl caprolactone)
PMOXA	Poly(2-methyloxazoline)
RhB-NCS	Rhodamine B isothiocyanate
SAMs	Self-assembled monolayers
SEC	Size exclusion chromatography
SHG	Second harmonic generation
SPR	Surface plasmon resonance
TBTA	Tris-(benzyltriazolymethyl) amine
THF	Tetrahydrofuran
TMP	Transmembrane pressure
TPA	Two photon absorption

UV-vis	Ultraviolet-visible
A	Absorbance
E	Young's Modulus
ζ	zeta potential
R_H	z-average hydrodynamic radius
D	Dispersity of polymers
M_n	Number average molecular weight
M_w	Mass average molecular weight
k_B	Boltzmann constant
η	Viscosity
pKa	Acid dissociation constant
kbend	Bending modulus
Θ_A	Advancing contact angle
Θ_R	Receding contact angle
Ra	Surface roughness
GM	Göppert-Mayer unit
ϵ	Molar absorption coefficient
ρ	Molecular packing parameter
λ	Wavelength
N_{AuNP}	Total number of AuNPs interacted with polymersomes
N_{PS}	Total number of polymersomes interacted with AuNPs
Tg	Glass transition temperature
h	Polymersome membrane thickness

List of Tables

Table 1.1 Polymersome forming block copolymers produced by ATRP	6
Table 1.2 Packing parameter and hydrophilic fraction of different self-assemblies ^{8, 24-26} ...	9
Table 3.1 Molecular parameters of polymers synthesized by ATRP	61
Table 3.2 Specifications of unfunctional and multifunctional polymersomes	62
Table 3.3 Specification of the polymersomes with different functional groups.....	70
Table 4.1 Purification of polymersome/gold nanoparticle assemblies by HFF method.....	91
Table 4.2 Specifications of polymersomes/gold nanoparticle assemblies.....	95
Table 4.3 AuNP fraction of the polymersome/gold nanoparticle assemblies determined from cryo-TEM micrographs	100
Table 5.1 Characterization of the self-assembled monolayers	108
Table 5.2 Specifications of polymersomes used for immobilization studies.....	110
Table 5.3 Adsorption behavior of PS1 polymersomes on β -CD coated surfaces.....	113
Table 6.1 Summary of mechanical and thermal properties of different vesicle systems .	134
Table 8.1 List of chemicals.....	147
Table 8.2 List of separation tools and materials	149
Table 8.3 List of buffer solutions.....	150
Table 8.4 Feed amounts of the reagents for block copolymer synthesis	157

List of Figures

Figure 1.1 Illustration of liposome and polymersome structures. The graph represents the molecular weight dependent membrane properties of the corresponding self-assembled structures which show enhanced stability of polymersomes compared with liposomes. ⁸	4
Figure 1.2 Illustration of different initiation mechanisms for anionic polymerization.	5
Figure 1.3 Synthetic mechanism for anionic polymerization of PEG-PEE block copolymer ¹¹	6
Figure 1.4 General mechanism of the transition-metal catalyzed ATRP having the following reaction rate constants: k_{act} (activation), k_{deact} (deactivation), k_p (propagation), k_t (termination) ¹⁴	7
Figure 1.5 Description of amphiphile shape in terms of molecular packing parameter (p) and its relation to the to the interfacial mean curvature (H) and Gaussian curvature (K). ²²	8
Figure 1.6 Schematic representation and corresponding TEM micrographs of pH-induced inversion of vesicles based on poly(acrylic acid)- <i>b</i> -polystyrene- <i>b</i> -poly(4-vinylpyridine) (PAA- <i>b</i> -PS-P4VP) vesicles. Adapted from Eisenberg et al. ⁵⁹ ..	12
Figure 1.7 (a) Formation of pH-responsive polymersomes from PEO- <i>b</i> -P[DEA- <i>stat</i> -TMSPMA]) block copolymers. Adapted from Armes et al. ¹⁵ (b) Formation of pH-responsive polymersomes from PMPC- <i>b</i> -PDPA block copolymers. Adapted from Armes et al. ¹⁶	14
Figure 1.8 Schematic view and chemical structure of the poly(methyl caprolactone)-ONB-poly(acrylic acid) diblock copolymer and its degradation products after UV exposure. ⁵¹	15
Figure 1.9 Scheme showing the polymersomes, and the conformation of the assembled polymer chains forming the membrane (A). The corona containing the PAA chains cleaved upon UV-trigger and separated from the PMCL chains (B). Finally, polymersome membrane was destroyed and the cargo released (C). ⁵¹	16
Figure 1.10 Reversible polymersome formation through UV/visible light irradiation. ⁵⁸	17

Figure 1.11 Principle of (a) one photon absorption (OPA) and (b) two photon absorption (TPA) optical processes.....	18
Figure 1.12 Scheme showing (a) the polymersomes with gold nanoparticles loaded with a green dye and (b) the polymersomes without gold nanoparticles loaded with a red dye. (c) A series of confocal microscope images of the mixture of corresponding polymersomes irradiated with lasers at room temperature. Adapted from Weitz et al. ⁸⁵	19
Figure 1.13 Scheme showing the principle of pre/post-functionalization routes.....	20
Figure 1.14 Clickable polymersomes self-assembled from azido-terminated PS-b-PAA block copolymers (pre-functionalization) and further post-functionalization with different molecules. ¹⁷	21
Figure 1.15 Scheme illustrating the immobilization of biotin-functionalized PMOXA-b-PDMS-b-PMOXA based polymersomes onto a glass substrate through streptavidin binding for realizing a nanoreactor platform. ⁸⁷	21
Figure 1.16 Surface modification of polymersomes with β -cyclodextrin molecules by pre-functionalization and further post-conjugation of adamantane-modified PEG having different molecular weights. ¹⁰⁴	22
Figure 1.17 Electronic transitions and corresponding energy levels for bonding (σ , π) and nonbonding (n) orbitals.....	25
Figure 1.18 Scheme of the Atomic Force Microscopy setup. Adapted from Averett et al. ¹²²	26
Figure 1.19 Scheme of ideal force-distance curves of AFM, eg. on a hard surface, where tip is approaching (1), contacting (2) and deflecting (3) respectively whereas the set point leads to the retraction of the tip from the sample surface (4) and further jump out occurs showing the complete retraction of the tip. Adapted from Leggett et al. ¹²¹	27
Figure 3.1 Overview of the multifunctional polymersome formation by sequential post-conjugations starting from the self-assembly of block copolymers having azide (BC1), methoxy (BC2) and adamantane (BC3) functionalities.....	52
Figure 3.2 Overall synthetic pathway of block copolymers (BC1, BC2, BC3, BC4).....	54

Figure 3.3	$^1\text{H-NMR}$ spectrum of alkyne functionalized adamantane in DMSO-d ₆	55
Figure 3.4	$^1\text{H NMR}$ spectrum of adamantane functionalized PEG in DMSO-d ₆	55
Figure 3.5	IR spectrum of azide/adamantane functionalized poly(ethylene glycol)	56
Figure 3.6	$^1\text{H-NMR}$ spectrum of poly(ethylene glycol) with azide end groups in CDCl_3	56
Figure 3.7	$^1\text{H-NMR}$ spectrum of poly(ethylene glycol) with methoxy end groups in CDCl_3	57
Figure 3.8	$^1\text{H-NMR}$ spectrum of poly(ethylene glycol) with adamantane end groups in CDCl_3	57
Figure 3.9	$^1\text{H-NMR}$ spectrum of $\text{N}_3\text{PEG}_{60}\text{-b-P}(\text{DEAEMA}_{82}\text{-stat-BMA}_{10})$ (BC1) block copolymer in CDCl_3	59
Figure 3.10	$^1\text{H-NMR}$ spectrum of $\text{PEG}_{45}\text{-b-P}(\text{DEAEMA}_{81}\text{-stat-BMA}_{10})$ (BC2) block copolymer in CDCl_3	59
Figure 3.11	$^1\text{H-NMR}$ spectrum of $\text{AdaPEG}_{60}\text{-b-P}(\text{DEAEMA}_{82}\text{-stat-BMA}_{15})$ (BC3) block copolymer in CDCl_3	60
Figure 3.12	$^1\text{H-NMR}$ spectrum of $\text{N}_3\text{PEG}_{60}\text{-b-P}(\text{DEAEMA}_{150})$ (BC4) block copolymer in CDCl_3	60
Figure 3.13	pH-dependent diameter variation of multifunctional polymersomes (PS1)....	64
Figure 3.14	Zeta potential variation of multifunctional (PS1) and unfunctional (PS0) polymersomes at different pH values	64
Figure 3.15	(a) Reversible swelling-shrinking of polymersomes (PS1) upon changes in pH value. (b) Intensity size distribution of PS1 polymersomes at pH 5 and pH 10 with average hydrodynamic diameter of 173 nm and 120 nm, respectively. (c) Schematic illustration of reversible size switch at basic and acidic condition.	65
Figure 3.16	cryo-TEM micrographs of polymersomes (PS1) at pH 9 (a) and pH 5 (c). (b) Membrane thickness distribution of polymersomes (PS1) determined from corresponding cryo-TEM micrographs by analyzing 57 particles at pH 9 and 42 particles pH 5.....	66
Figure 3.17	The synthetic scheme and $^1\text{H-NMR}$ spectrum of NVOC protected amine groups in CDCl_3	67

Figure 3.18 (a) Reaction scheme of NVOC conjugation and cleavage process on PS1 polymersomes. (b) UV-vis spectra of PS1C polymersomes upon UV exposure up to 600s showing the decrease of absorption bands due to NVOC cleavage. (c) The absorbance change (%) of PS1 and PS1C at $\lambda=345$ nm versus irradiation time under identical UV exposure.....	68
Figure 3.19 (a) Intensity size distribution of crosslinked polymersomes PS1, PS1C and PS1D (b,c) cryo-TEM micrographs of PS1D polymersomes at pH 8 and pH 5.....	71
Figure 3.20 (a) Reaction Scheme of NVOC conjugation on PS2 polymersomes via identical click modification as done for PS1 polymersomes (b) UV-vis spectra of freeze dried PS2 and PS2C in CHCl_3	72
Figure 3.21 $^1\text{H-NMR}$ spectrum of freeze dried PS2C polymersome in CDCl_3	72
Figure 3.22 (a) Reaction Scheme of NVOC conjugation on short PEG molecule via identical aqueous click modification as a supporting model study (b) UV-vis spectra of M1 (before click) and M1C (after click) in CHCl_3	73
Figure 3.23 $^1\text{H-NMR}$ spectrum of NVOC-PEG ₆₀ -OH (M1C) in CDCl_3	73
Figure 3.24 Intensity size distribution of non-cross-linked polymersomes before (PS2) and after click reaction (PS2C) and after photodeprotection (PS2D) at pH 8	74
Figure 3.25 (a) Reaction Scheme of RhB-NCS conjugation on PS1D polymersomes. (b) Monitoring RhB-NCS coupling to polymersomes through amino groups (PS1R) with UV-vis analysis during dialysis procedure. (c) UV-vis spectra of RhB-NCS containing polymersomes with (PS1R) and without (PS1) NH_2 groups to show the covalent conjugation of the dye. (d) cryo-TEM micrographs of PS1R polymersomes at pH 8.....	76
Figure 3.26 (a) UV-vis analysis to show sequential conjugation of cyclodextrin molecule to Rhodamine B NCS modified polymersomes (PS1R) by host-guest interaction. (b) UV-vis spectra of Cy7-CD containing polymersomes with (PS1H, PS1) and without (PS0) adamantane groups on their surface to show the conjugation triggered by host-guest interaction.	78
Figure 3.27 Reversible swelling-shrinking of (a) PS1C and (b) PS1D polymersomes upon changes in pH value.	79

Figure 4.1 Schematic overview of the Dox encapsulated polymersomes formation through pre-loading approach.	87
Figure 4.2 Intensity size distribution of Dox encapsulated polymersomes before (PS1-Dox) and after click reaction (PS1C-Dox) and after photocleavage (PS1D-Dox) at pH 7.4.	88
Figure 4.3 UV-vis spectra of Dox encapsulated polymersomes before and after dialysis of NVOC molecules and after subsequent irradiation process	88
Figure 4.4 In-vitro release of doxorubicin from (a) PS1C-Dox polymersomes and (b) PS1D-Dox polymersomes at 37 °C in different pH medium	89
Figure 4.5 Schematic overview of the polymersome/gold nanoparticle preparation through (a) pre-loading approach and (b) post-loading approach.....	90
Figure 4.6 UV-vis spectra of 5 nm sized-AuNP encapsulated polymersomes after HFF purification, (a) shows the whole spectra of the PS1-Au51 and PS1-Au54 polymersomes, (b) the enlarged area of the UV-Vis spectra showing the gold nanoparticle absorbance range.....	92
Figure 4.7 UV-vis spectra of 10 nm sized-AuNP encapsulated polymersomes after HFF purification, (a) shows the whole spectra of the PS1-Au101 and PS1-Au104 polymersomes, (b) the enlarged area of the UV-Vis spectra showing the gold nanoparticle absorbance range.....	93
Figure 4.8 Intensity size distribution of gold nanoparticle encapsulated polymersomes through pre-loading method, PS1-A54 and PS1-A104, at pH 8.....	93
Figure 4.9 The SPR monitoring with respect to time for only gold nanoparticles, AuNP-10nm at $\lambda_{max}=525$ nm, AuNP-5nm at $\lambda_{max}=522$ nm, and polymersome/gold nanoparticles assemblies, PS1-Au54 at $\lambda_{max}=522$ nm, PS1-Au104 at $\lambda_{max}=525$ nm	94
Figure 4.10 Scheme of the possible AuNP positions in polymersomes after the uptake process in which they can be located at the outer (1) or inner (3) hydrophilic part of the bilayer membrane, and are stuck/embedded within the hydrophobic region (2) and finally can be guided into the aqueous lumen (4).	96
Figure 4.11 cryo-TEM micrographs of PS1-Au104 polymersomes at pH 8. (a,b) AuNPs (~10 nm) were placed at the outer (1) or inner (3) hydrophilic part of the	

membrane and guided into the aqueous lumen (4). (c) AuNPs were placed at the interphase of shell and the hydrophilic corona. (d) This image shows the maximum number of AuNP incorporation into one single polymersome and exemplifies the embedded AuNPs at the hydrophobic membrane (2).97

Figure 4.12 cryo-TEM micrographs of PS1-Au54 polymersomes at pH 8. (a,b) AuNPs (~5 nm) were placed at the outer (1) or inner (3) hydrophilic part of the bilayer membrane and are stuck within the hydrophobic region of the membrane (2) as well as guided into the aqueous lumen (4).98

Figure 4.13 cryo-TEM micrographs of PS1-Au54P and PS1-Au104P polymersomes at pH 8. (a,b,c) AuNPs (~5 nm) were placed at the outer (1) or inner (3) hydrophilic part of the membrane and guided into the aqueous lumen (4). (d) AuNPs (~10 nm) were placed at the outer hydrophilic region of the membrane (1).99

Figure 4.14 Intensity size distribution of gold nanoparticle encapsulated polymersomes prepared with post-loading method, PS1-A54P and PS1-A104P, at pH 8.100

Figure 5.1 Schematic overview of the polymersome immobilization by adamantane- β -cyclodextrin host-guest complexation leading to spherical cap like shapes on the surface and further steps including tuned-adhesion properties, pH swellable surfaces and NIR induced photochemical reactions.106

Figure 5.2 Precoating steps to prepare β -cyclodextrin modified substrates (S2, S3) and further PEG passivation on S3 surface by postulated PEG threading into the cavity of cyclodextrin.107

Figure 5.3 Tapping-mode AFM height image of (a) the plasma activated silicon wafer, (b) 3-GPS SAMs layer, S1, (c) β -CD coated layer, S2.109

Figure 5.4 The illustrative scheme of the surface-immobilized polymersomes showing the chemical structure the used block copolymers in polymersome formation111

Figure 5.5 (a) Peak force tapping mode liquid-AFM height image of β -CD coated layer (S3) at pH 7.4. (b) small area of PS1-S2 polymersomes (PS1 on S2 surface) at pH 7.4, and (c) at pH 5 in swollen state. (d) small area of PS1-S3 polymersomes (PS1 on S3 surface) at pH 7.4112

Figure 5.6 Peak force tapping mode liquid AFM height image of PS1-S3 (a) and PS1-S2 (c) polymersomes at pH 7.4 condition, (b) 3D-image of the marked region of the

PS1-S3 polymersomes. Height vs diameter relationship for (d) PS1-S2 and (e) PS1-S3 polymersomes (inset schemes: 3D image of a single polymersome illustrating the shape variation due to the different adhering forces on S2 and S3 surfaces).....	114
Figure 5.7 (a) Peak force tapping mode liquid-AFM height image and (b) cryo TEM image of a single polymersome, (c) AFM and cryo-TEM measured particle analysis.	115
Figure 5.8 (a) Peak force tapping mode liquid AFM height image of PS1-S4 polymersomes at pH 7.4 condition (b) Height vs diameter relationship for PS1-S4 polymersomes (inset scheme: 3D image of a single polymersome illustrating the shape variation due to the different adhering forces on S4 surface).....	116
Figure 5.9 (a) Peak force tapping mode liquid AFM height image of PS0-S3 polymersomes (PS0 on S3 surface) without adamantane groups at pH 7.4 condition (b) Height vs diameter relationship for PS0-S3 polymersomes.	117
Figure 5.10 Peak force tapping mode liquid AFM height image of (a) PS1-S3 and (c) PS1-S2 polymersomes at pH 5 condition. (b) 3D-image of the marked region of the PS1-S3 polymersomes. Height vs diameter relationship for (d) PS1-S2 and (e) PS1-S3 polymersomes at pH 5 (inset schemes: representative shapes of polymersomes showing the distinct swelling ratios due to the different adhering forces on S2 and S3 surfaces as well as in different directions).....	119
Figure 5.11 (a) Schematic illustration of NVOC-cleavage on surface-immobilized polymersomes (1-2) and further reaction of ATTO 532 NHS ester with the freed amino functions (3) for the fabrication of fluorescent photopatterned structures under a liquid phase. (b) The chemical structures of NVOC-conjugated polymersomes indicating the cleavage leading to unprotected amines and further dye conjugation (c) Fluorescence microscopy images of lines photochemically written on substrates with immobilized PS3C polymersomes (PS3C on S3) at pH 8 condition after labelling with fluorescent dye.	120
Figure 5.12 Fluorescence microscopy images of lines photochemically written on substrates with immobilized PS1C polymersomes (PS1C on S3) at pH 8 condition after labeling with fluorescent dye.....	122

Figure 6.1 (a) Schematic illustration of the AFM indentation experiment: tip and vesicles are not in contact (1), first contact (2), indented (3). (b) Force vs separation curve of two different sized-polymersomes marked by blue and red arrow in the AFM height image at inset of the graph.	131
Figure 6.2 (a,b) Force vs indentation curves of corresponding polymersomes shown in the inset of force-separation graph (Figure 6.1b) to find membrane stiffness, k by linear fitting.	131
Figure 6.3 (a) Histogram of the Young's modulus and (b) bending modulus of the polymersomes.....	132
Figure 7.1 General overview of the main research developments within this work indicating the sub-divisions (1&2: chapter 3, 5: chapter 4, 3&4: chapter 5 and 6).	138
Figure 7.2 (a) Reversible swelling-shrinking of surface functionalized-polymersomes (PS1) upon changes in pH value. (b) pH-dependent diameter variation of the corresponding polymersomes (PS1).....	139
Figure 7.3 (a) Monitoring RhB-NCS coupling to polymersomes through amino groups with UV-vis analysis during dialysis procedure to finally obtain PS1R polymersomes (b) UV-vis analysis to show sequential conjugation of cyclodextrin molecule to Rhodamine B NCS modified polymersomes (PS1R) by host-guest interaction. (c) cryo-TEM micrographs of PS1D polymersomes at pH 8 and pH 5. (d) cryo-TEM micrographs of PS1R polymersomes at pH 8.....	140
Figure 7.4 In-vitro release of doxorubicin from (a) PS1C-Dox polymersomes (before photocleavage) and (b) PS1D-Dox polymersomes (after photocleavage) at 37 °C in different pH medium. (c-e) cryo-TEM micrographs of PS1-Au104 polymersomes at pH 8 (10 nm sized AuNP loaded).....	141
Figure 7.5 Immobilized spherical cap-shaped polymersomes and NIR induced selective photochemical reactions in which the released amino groups were conjugated with ATTO 532-NHS ester molecules for mimicking the biorecognition systems.	142
Figure 9.1 Dialysis of same amount of NVOC molecules without polymersomes for purification assesment (Diaysis duration=2 days with the 5 kDa MWCO membrane).....	162

Figure 9.2 Calibration curve of PS2C determined from absorbance values at $\lambda=345$ nm, measured in CHCl_3 , to calculate the relative NVOC functionalization degree of polymersomes (path length of the quartz cuvette =1 cm).....	164
Figure 9.3 Calibration curve of M1C determined from absorbance values at $\lambda=345$ nm, measured in CHCl_3 , to calculate the relative NVOC functionalization degree of polymersomes (path length of the quartz cuvette =1 cm).....	164
Figure 9.4 UV-vis spectra of freeze dried PS2C and PS2D in acidic water.....	165
Figure 9.5 Monitoring the cleavage of NVOC chromophore from 3 different batches of PS2C polymersomes to calculate the photocleavage efficiency.....	165
Figure 9.6 Calibration Curve of Rhodamine B NCS determined from absorbance values at $\lambda = 555$ nm, measured in polymersome solutions, to calculate the molar extinction coefficient (ϵ) of the corresponding dye (path length of the quartz cuvette =1 cm)	166
Figure 9.7 Calibration Curve of Cy7-labelled β -cyclodextrin determined from absorbance values at $\lambda = 775$ nm, measured in polymersome solutions, to calculate the molar extinction coefficient (ϵ) of the corresponding dye (path length of the quartz cuvette =1 cm)	167
Figure 9.8 Calibration curve of Doxorubicin at (a) pH 7.4 and (b) pH 5 determined from absorbance values at $\lambda = 480$ nm to calculate the cumulative release	169

List of Publications

Journal Articles

- 1) **Iyisan, B.;** Kluge, J.; Formanek, P.; Voit, B.; Appelhans, D. Multifunctional and Dual-Responsive Polymersomes as Robust Nanocontainers: Design, Formation by Sequential Post-Conjugations, and pH-Controlled Drug Release. *Chem. Mater.* **2016**, *28*, 1513-1525.
- 2) **Iyisan, B.;** Janke, A.; Reichenbach, P.; Eng, L. M.; Appelhans, D.; Voit, B. Immobilized Multifunctional Polymersomes on Solid Surfaces: Infrared Light-Induced Selective Photochemical Reactions, pH Responsive Behavior and Probing Mechanical Properties under Liquid Phase, *ACS Appl. Mater. Interfaces* **2016**, *8*, 15788-15801.

Among the above-mentioned articles, the first paper was partially adapted into chapter 3 and 4 whereas the second paper was adapted into chapter 5 and 6 of this thesis.

Conferences

- Lectures

- 1) **Iyisan, B.;** Janke, A.; Reichenbach, P.; Eng, L. M.; Appelhans, D.; Voit, B. Multifunctional Polymersomes as Smart Nanodevices for Biomedical Applications: Probing Responsive Behaviour and Mechanical Properties, IUPAC World Polymer Congress, 2016, Istanbul, Turkey.
- 2) **Iyisan, B.;** Appelhans, D.; Janke, A.; Formanek, P.; Voit, B. Smart Polymersomes with Multiple Functional Groups on their Surface for Biomedical applications, European Polymer Congress (EPF), 2015, Dresden, Germany.
- 3) **Iyisan, B.;** Appelhans, D.; Janke, A.; Voit, B. Multifunctional and Dual-Responsive Polymersomes as Smart Nanocontainers for Biomedical Applications, International Helmholtz Research School for Nanoelectronic Networks (IHRS Nanonet) Annual Workshop, 2015, Bastei, Germany.
- 4) **Iyisan, B.;** Reichenbach, P.; Georgi, U.; Appelhans, D.; Eng, L.; Voit, B. Metallnanopartikel als nichtlinear optische Antennen in photoaktiven Polymermatrizen: MNPs in Polymersomen und biomedizinische Anwendungsmöglichkeiten, SPP-1327 7. Workshop, 2014, Saarbrücken, Germany.

- 5) **Iyisan, B.;** Appelhans, D.; Voit, B. Functionalization of pH responsive polymersomes with photoactive moieties and adamantane groups for biomedical applications, IUPAC World Polymer Congress, 2014, Chaing Mai, Thailand.
 - 6) **Iyisan, B.;** Georgi, U.; Reichenbach, P.; Appelhans, D.; Eng, L.; Voit, B. Metallnanopartikel als nichtlinear optische Antennen in photoaktiven Polymermatrizen: MNPs in Polymersomen und biomedizinische Anwendungsmöglichkeiten, SPP-1327 6. Workshop, 2013, Bochum, Germany.
- Posters
- 1) **Iyisan, B.;** Appelhans, D.; Janke, A.; Voit, B. Multifunctional Polymersomes with Photoactive Moieties and Their Non-covalent Attachment onto Surfaces, International Helmholtz Research School for Nanoelectronic Networks (IHRS Nanonet) Annual Workshop, 2014, Bastei, Germany.
 - 2) **Iyisan, B.;** Appelhans, D.; Janke, A.; Voit B. Multifunctional Polymersomes with Photoactive Moieties and Their Non-covalent Attachment onto Surfaces, 8th ECNP International Conference on Nanostructured Polymers and Nanocomposites, 2014, Dresden, Germany.
 - 3) **Iyisan, B.;** Kluge, J.; Appelhans, D.; Voit, B. Functional Polymersomes Designed for Covalent and Non-covalent Conjugation, International Helmholtz Research School for Nanoelectronic Networks (IHRS Nanonet) Annual Workshop, 2013, Dresden-Rossendorf, Germany.
 - 4) **Iyisan, B.;** Kluge, J.; Yassin, M.; Appelhans, D.; Voit, B. Azide and Adamantane Functionalized Polymersomes Designed for Covalent and Non-covalent Conjugation, IUPAC 10th International Conference on Advanced Polymers via Macromolecular Engineering (APME), 2013, Durham, UK.
 - 5) Appelhans, D.; Yassin, M.; **Iyisan, B.;** Kluge, J.; Gaitzsch, J.; Formanek, P.; Voit, B. Polymeric Vesicles for Drug Delivery and Synthetic Biology: View on pH and Size-Controlled Diffusion Processes, 8th ECNP International Conference on Nanostructured Polymers and Nanocomposites, 2014, Dresden, Germany.

Versicherung

Hiermit versichere ich, dass ich die vorliegende Arbeit ohne unzulässige Hilfe Dritter und ohne Benutzung anderer als der angegebenen Hilfsmittel angefertigt habe; die aus fremden Quellen direkt oder indirekt übernommenen Gedanken sind als solche kenntlich gemacht. Die Arbeit wurde bisher weder im Inland noch im Ausland in gleicher oder ähnlicher Form einer anderen Prüfungsbehörde vorgelegt.

Die Dissertation wurde vom September 2012 bis August 2016 am Leibniz-Institut für Polymerforschung Dresden e.V. unter der wissenschaftlichen Betreuung von Prof. Dr. Brigitte Voit (TU Dresden) angefertigt.

Frühere erfolglose Promotionsverfahren haben nicht stattgefunden.

Hiermit erkenne ich die Promotionsordnung der Fakultät Mathematik und Naturwissenschaften der Technischen Universität Dresden vom 23.02.2011 an.

Banu Iyisan

Dresden,2016